Techno-economic and Environmental Multi-Objective Optimization of Concentrated Solar Power Hybridization with both Wind and Gas Turbines in Arid Region Climate

Mohammed S. Alfailakawi

A thesis submitted in fulfilment of the requirements for the degree of

Doctor of Philosophy

The University of Sheffield

Faculty of Engineering

Department of Mechanical Engineering

Energy 2050

March, 2024

DECLARATIONS

The candidate confirms that the work submitted is his own and that appropriate credit has been given where reference has been made to the work of others.

ACKNOWLEDGMENT

First and foremost, thanks to almighty Allah, creator of the heavens and earth, has taught man that which he knew not.

I am extremely grateful for my supervisors; Professors Mohamed Pourkashanian, Derek Ingham, Lin Ma, and Dr. Kevin Hughes for their unlimited support and guidance that were pivotal to the accomplishment of my PhD. In addition, I would like to thank Dr. Stavros Michailos for his support with several aspects of the modelling and documentation of the research and for providing very useful ideas and comments that helped in improving this work.

Furthermore, this research work would not have been possible without the valuable financial support provided by the Kuwait Ministry of Defense. Moreover, I would like to thank Kuwait Institute of Scientific Research (KISR) for providing the required data to this study for the inclusion in my PhD research work.

Finally, I would like to give special thanks to my lovely family, especially my parents, who admired me, invested and believed in me the most. Also, very special thanks to my wife Maryam, kids Abdalrahman & Lulu; the apples of my eyes, for their prayers, continuous care, encouragement and moral support throughout my study. I could not have done my PhD without their sacrifices, unconditional support and love.

Abstract

This work assesses a novel hybridization of concentrated solar power (CSP) with both wind and gas turbines for a remote arid region application. The CSP component is based on a solar power tower (SPT) which is considered as the main component of the proposed plant. The assessment is based on different ranges of Wind Turbine (WT) capacities, Natural Gas Combined Cycle (NGCC) capacitates and CSP's key design parameters such as Thermal Energy Storage (TES) and Solar Multiple (SM). The proposed plant performance assessment has been achieved through an observation of the key performance indicators of the Levelized Cost of Energy (LCOE), Capacity Factor (CF), CO_2 emissions and water consumption.

Prior to the entire proposed plant performance assessment, this work assesses the greatest two threats to the techno-economic feasibility of the main component of the plant (SPT) in arid regions, i.e. aerosols density and water scarcity. The aerosols effect on the SPT has been first assessed by an assembly of a site adapted typical aerosols year (TAY). Based on the assembled TAY, the performance of the SPT has been observed based on three different aerosols scenarios: no-aerosols, daily and yearly averaged aerosols representative values. Regarding the water consumption issue in arid regions, the work has assessed four different scenarios of SPT condenser, i.e. wet-cooled, air-cooled and two hybrid scenarios where trade-offs between the highest energy generation and water consumption have been assessed. The entire standalone SPT assessment has been carried out in the System Advisor Model (SAM) simulation tool.

Then, both the WT and the NGCC have been proposed as hybridization options with the SPT. Here, both these technologies' ability to enhance the performance of the SPT has been assessed in detail with regards to the above mentioned performance indicators. While both the solar and wind components have been separately simulated in the SAM, the performance of the NGCC has been simulated in Aspen Plus. Then, all the proposed hybrid plant's components have been imported into the SAM in order to simulate the performance of the entire proposed system with the assistance of an in-house developed algorithm. This has been carried out based on two different scenarios: a Carbon Capture and Storage (CCS) unit inclusion scenario in addition to the conventional scenario without a CCS. The novelty of this work emerges from the integration of the aerosols affected SPT with both WT and NGCC, i.e. a methodology that provides accurate SPT

assessment and uses both renewable and fossil fuel technologies to enhance the overall techno-economic performance of the plant.

Since these performance indicators are of a conflictive nature, the optimal configuration of the proposed hybrid system is elected through a multi-objective optimization technique where the previously assessed key performance indicators are assigned as objective functions for the optimization problem. In addition to the important performance indicators of LCOE and CF, this work prioritizes water consumption and assigns it as an objective function in the optimization problem; a typically left out metric in the literature. Also, the proposed methodology assesses the CO_2 for the entire lifetime of the proposed system through carrying out a full-scale life cycle assessment (LCA), then assigns the CO_2 emissions as an objective function among the other performance indicators which is essential as it considers all techno-economic and environmental aspects of a proposed plant. The work exposes both the advantages and the limitations of each component inclusion and eventually proposes sets of optimal configurations elected by an elitist evolutionary algorithm; the Genetic Algorithm (GA) with regards to the objective functions. Finally, a sensitivity study is carried out by assigning different weights to the objective functions of the elected set of optimal solutions according to their importance. This is achieved with the assistance of a multi criteria decision making tool (here the TOPSIS) which also enables the ranking of the optimal solutions from best to worst.

Research outputs

Publication in scientific journal articles

Chapter 2 contains the following publication:

- M. S. Alfailakawi, S. Michailos, D. Ingham, L. Ma, K.J. Hughes, and M. Pourkashanian, "**Multi-temporal resolution aerosol impacted techno-economic assessment of concentrated solar power in arid regions: case study of solar power tower in Kuwait**" *Sustainable Energy Technologies and Assessments*, vol. 52, Aug. 2022. https://doi.org/10.1016/j.seta.2022.102324.

Chapter 3 & 4 contain the following publications:

- M. S. Alfailakawi, S. Michailos, D. Ingham, L. Ma, K.J. Hughes, and M. Pourkashanian, "**Performance Improvement of Aerosols-affected Solar Power Tower in Arid Regions: Case study of Wind Turbines Hybridization with Different Condenser Types**" Under review *in Results in Engineering*.

- M. S. Alfailakawi, S. Michailos, Kh. Alzahrani, D. Ingham, L. Ma, K.J. Hughes, and M. Pourkashanian, "**Techno-Economic Assessment of a Solar Power Tower Hybridization with Wind Turbines in Arid Regions: Optimal Design through Multi-Objective Optimization**" will be submitted shortly *to the Thermal Science and Engineering Progress*.

- M. S. Alfailakawi, S. Michailos, D. Ingham, L. Ma, K.J. Hughes, and M. Pourkashanian, "**Environmental and Techno-Economic Multi-Objective Optimization of Concentrated Solar Power Hybridization with both Wind and Gas Turbines**" will be submitted shortly *to the Energy Conversion & Management*.

Publications in peer reviewed conference papers

- M. S. Alfailakawi, S. Michailos, D. Ingham, I. Al-Arfi, K.J. Hughes, L. Ma and M. Pourkashanian, "**Performance improvement of aerosols impacted concentrated solar power in arid regions: Case study pf solar power tower hybridization with wind turbines in Kuwait**" *14th International Conference on Applied Energy*, Aug. 2022. https://doi.org/10.46855/energy-proceedings-10201

- M. S. Alfailakawi, Kh. Alzahrani, D. Ingham, K.J. Hughes, L. Ma and M. Pourkashanian, "**Multi-Objective Optimization of Solar Power Tower Hybridization with Gas Turbine and Thermal Energy Storage Back Up**" *8th International Conference on Energy Research and Development*, Nov. 2023.
  (Yet to be available online)

- Al-Arfi, B. Shboul ,S. Michailos, M. S. Alfailakawi, G. Udeh, D. Ingham, L. Ma, K.J. Hughes and M. Pourkashanian, "**Multi-objective optimal sizing of a hybrid concentrated solar power-biogas for desalination and power generation**" *14th International Conference on Applied Energy*, Aug. 2022. https://doi.org/10.46855/energy-proceedings-10209

Nomenclature

Symbols

A	Attenuation percentage (%)
A_{hel}	Heliostats area (m^2)
$CDF_{m(di)}$	Short term cumulative distribution function (-)
$CDF_{y,m(di)}$	Long term cumulative distribution function (-)
CO_2	Carbon Dioxide (-)
E_{bn}	Broadband Direct Normal Irradiance (W/m^2)
E_{sc}	Solar constant (-)
h	Enthalpy (J/kg)
h_{tower}	Tower height (m)
N_{hel}	number of heliostats (-)
$\dot{m}_{HTF}$	Mass of the heat transfer fluid (kg/s)
$\dot{m}_{flue\ gas}$	Mass flow rate of the flue gas (kg/s)
n	Analysis period (year)
P_R	Wind rated power (MW)
$Q_{rec,cond}$	Thermal power loss due to conduction (kWh)
$Q_{rec,conv}$	Thermal power loss due to convection (kWh)
$Q_{rec,em}$	Thermal power loss due to emissivity (kWh)
Q_{Field}	Solar field incident thermal power (kWh)
Q_{HTF}	Thermal power transferred to the heat transfer fluid (kWh)
$Q_{rec,rad}$	Thermal power loss due to radiation (kWh)
Q_{rec}	Receiver incident thermal power (kWh)
Q_{TES}	Thermal power of thee thermal energy storage (kWh)
q_{pb}	Power block thermal power (kWh)
T_d	Dry bulb temperature (K)
V_{HTF}	Volume of the heat transfer fluid (m^3)
V_{TES}	Volume of the thermal energy storage tank (m^3)

v	Wind speed (m/s)
v_C	Cut-in speed (m/s)
v_O	Cut-out speed (m/s)
v_R	Rated wind speed (m/s)
$\dot{W}$	Work (J)
y_c	Aerosols post quantile mapping (-)
Z	Wind turbine height (m)

Subscripts

$comp$	Compressor
d	Dry bulb
$Field$	Solar field
GT	Gas Turbine
HTF	Heat Transfer Fluid
$m(di)$	Short term monthly behavior in the cumulative distribution function
pb	Power block
P_R	Wind rated power
rec	Receiver
TES	Thermal Energy Storage
Tur	Turbine
v_C	Cut-in speed
v_O	Cut-out speed
v_R	Rated wind speed
yc	Aerosols post quantile mapping
$y, m(di)$	Long term monthly behavior in the cumulative distribution function in year y

Acronyms

AEG	Annual energy generation (GWh/y)

AOD	Aerosols optical depth (-)
CAPEX	Capital expenditures ($)
CCS	Carbon Capture and Storage (-)
CF	Capacity Factor (%)
CSP	Concentrated solar power (-)
DNI	Direct normal irradiance (W/m^2)
FS	Finkelstein Shafer (-)
GA	Genetic Algorithm (-)
GHI	Global horizontal irradiance (W/m^2)
GT	Gas Turbine (-)
HTF	Heat transfer fluid (-)
KISR	Kuwait institute of scientific research (-)
LCA	Life Cycle Assessment (-)
LCOE	Levelized cost of energy (c/kWh)
LK	Language kit (-)
MBE	Mean Bias Error (-)
MCDMT	Multi Criteria Decision Making Tool
MENA	Middle East & North Africa (-)
MS	Molten Salt (-)
NSGA	Non Dominated Sorting Genetic Algorithm (-)
NGCC	Natural Gas Combined Cycle (-)
NPV	Net Present Value (-)
OPEX	Operation expenditures ($)
PTC	Parabolic trough collector (-)
RE	Renewable Energy (-)
RMSE	Root Mean Square Error (-)
RTM	Radiative transfer model (-)
SAM	System advisor model (-)
SM	Solar multiple (-)

SPT	Solar power tower (-)
SREP	Shagaya Renewable Energy Park (-)
ST	Steam Turbine (-)
TAY	Typical aerosol year (-)
TES	Thermal energy storage (h)
TMY	Typical metrological year (-)
TOPSIS	Technique for order preferences by similarity to the ideal solution (-)
WT	Wind Turbine (-)

Greek symbols

α	Power law exponent (-)
β	The Aerosols Optical Depth at 1 μm (-)
Δ	Change in quantity (-)
η_{at}	Attenuation loss (-)
η_{cos}	Cosine loss (-)
η_d	Dry cooled cycle efficiency (-)
η_{gen}^{el}	Electrical efficiency of the generator (-)
η_{Turb}^{mec}	Mechanical efficiency of the steam turbine (-)
η_{opt}	Solar field optical efficiency (-)
η_{rec}	Receiver efficiency (-)
η_{sp}	Spillage loss (-)
$\eta_{s\&b}$	Shadowing & blocking loss (-)
η_{TES}	Efficiency of the thermal energy storage (-)
η_w	Wet-cooled cycle efficiency (-)
ρ_{HTF}	Density of the heat transfer fluid (kg/m^3)
τ	Band average aerosols optical depth (-)
ϕ	Relative humidity (%)

Table of Contents

List of Figures

List of Tables

Chapter 1 – Introduction

1.1 Background

A good decent life is a must for all human beings on this planet. It happens to be that no decent life today may be without having day long available electricity. The population and their ambitions on our blue planet are on a steady rate of increase and so is the electricity requirement [1]. Such an increase requires an increase of electricity generation worldwide in order to fulfill people's daily needs on the domestic scale, for industry and for transportation. According to the International Energy Agency (IEA), the worldwide electricity demand is expected to increase by 150% by the year 2050 [2].

Since the last century, the use of fossil fuels has been our sanctuary solution for the production of electricity. For instance, more than 85% of the primary energy consumption was provided through burning conventional fossil fuels in 2018 [1]. Coal followed by natural gas lead the fuel global shares in electricity generation with shares of 38.1% and 23.2%, respectively [3]. This, however, has heavily affected nature and the atmosphere through a steady increase of greenhouse gases emissions and its prime component, i.e. Carbon Dioxide (CO_2) [4].

Usage of fossil fuel at the present rate will definitely cause a permanent and unfixable harm to the planet. The north and south poles for example, due to the increased greenhouse gases emissions as one important reason among others, are melting down and not freezing back up at the same rate at which they were used to do, which is causing a sea level rise worldwide in a process called Arctic Amplification [5]. Such a rise in the sea level, which is partially caused by such a usage of fossil fuel will probably affect the coastal cities and regions, and this is the home to about 50% of the world's population [6].

Action is immediately required, feasible and available, i.e. Renewable Energies (RE). The energy of the wind, geothermal, biomass, sun, hydro power, etc. are all readily available in the vast majority of world's countries and this can be harnessed to overcome the world's need for energy and theoretically with negligible negative impacts on the planet. The sun, for example, hits the earth with sufficient energy in just one hour of a day that the entire world actually consumes of electricity during an entire calendar year [7]. This, among other potential

sustainable resources, elects RE to majorly contribute in the worldwide energy demand scene in the near future as it is shown in Figure 1-1.

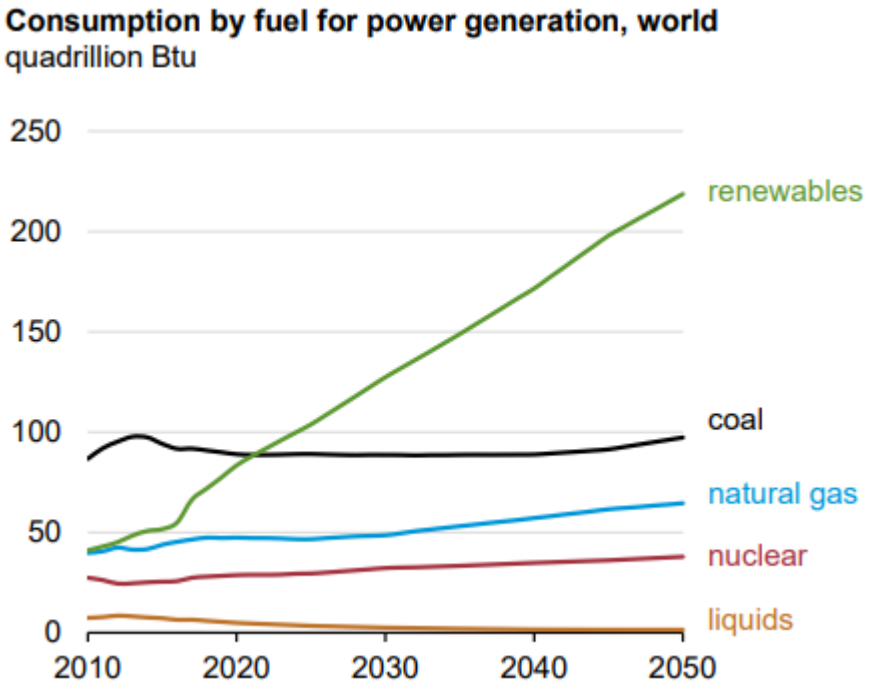

Fig. 1-1. Current and expected energy mix by fuel type [8].

Efforts have been gathered in the last fifty years in order to harness RE resources for the best cost-effective utilization. Wind Turbines and PV are two mature, efficient and relatively cheap technologies which can directly provide electricity to both on and off grid applications. Unfortunately, both technologies suffer from weather intermittency which requires storage batteries to store excess power and thus overcome periods with less resources. However, storage batteries are relatively expensive regarding installation costs, have less storage lifetime and less annual round trip storage efficiency [9].

1.2 Motivation

Nowadays, solar energy is considered as one of the most prevailing RE sources worldwide. This is because the amount of the yearly solar energy that is received by the earth is so abundant to the extent that it has been estimated to be equal to 120,000 TW [10], i.e. approximately 10 times of what the earth's reserve is worth in fossil and nuclear fuels [11]. From a purely

theoretical point of view based on solar resources abundancy and where energy storage and transportation are unconsidered, it is estimated that an area of 100 km by 100 km (10,000 sq km) in the Algerian Sahara desert is enough to supply the entire world need of electricity in case covered with solar panels [12].

Another advantage in the favor of solar energy is that the solar irradiance consists of different components, each of which is a key factor for specific solar technology. For example, the Global Horizontal Irradiance (GHI) is the solar resource component that PV technology is based on as the latter harnesses the photons from the sun creating a flow of electrons, thus a DC current. While on the other hand, the Concentrated Solar Power (CSP) works on concentrating the beam irradiance of the sun (the Direct Normal Irradiance (DNI)) in order to harness the sun thermal energy. CSP diverse technologies have received much of attention in the last 50 years, and this is mainly due to the high level of dispatchability it can offer among other RE technologies. Having the ability to store thermal energy (in a relatively cheap and more efficient manner surpassing electrical, chemical, mechanical energy storage technics [13]) is what mainly makes CSP to be dispatchable in overcoming periods at which the sun is absent or blocked.

In addition to the solar energy, wind energy also emerges as another potential RE resource with great outlook for energy generation. Wind energy has been successfully harnessed through Wind Turbines (WT) for quite some time now which makes the technology relatively mature when compared to other RE technologies. This has been projected in having loweredLCOE as a result of optimized capital costs, however, the technology suffers from the lack of a proper back up system which ends up by having lowered the Capacity Factors (the ability of energy generation in a year time) which falls in the ranges of 30-40% [14]. The difference of renewable resource nature between the solar and the wind energy can be a synergic solution of hybridization.

Finally, despite the many efforts for its elimination and limitation of usage, fossil fuel remains as the most reliable type of energy source worldwide. This is mainly because of its maturity and ability to constantly provide energy which meets demand’s requirements. The integration of fossil fuel backup systems within RE plants has gained much attention and even has been commercialized on a wide scale worldwide to overcome energy insufficiency that

originates from RE resources fluctuations. Also, the inclusion of reliable fossil fuel backup systems with the newly developed RE plants avoids to a great extent the skepticism and opposition of decision makers who are not in the favor of an extreme shift from fossil fuel-based energy system into a totally RE one.

This has recently been more adopted and backed up with the breakthrough of Carbon Capture and Storage (CCS) systems that have emerged as a viable solution to mitigate CO_2 emissions. CCS are expected to reduce global CO_2 emissions by 19% in the year 2050 according to the International Energy Agency (IEA) [15]. In addition, CCS is considered as one of the most effective decarbonization initiatives which can allow the economic growth in developing countries while commissioning newly employed fossil fuel plants without disruption [16]. Different CCS approaches have been reported to reach up to 96% by [17] and 100% in achieving net-zero CO_2 emissions [18]. However, this is paired with an energy consumption penalty as the latter is required for the process of carbon separation, compression, transportation and storage [17], which can reach up to 15-40% of less energy than what the plant without a CCS would have produced [19]. Also, the CO_2 emissions produced from power plants that includes a CCS has been reported to be higher than these without CCS as obviously energy needs to be used during the life cycle of the CCS itself. The CCS inclusion can be a great solution for fossil fuel rich and dependent regions as it can enable such countries to optimally exploit both of sustainable and fossil fuel resources while implementing a soft transitioning towards a total Carbon neutrality when RE technologies turns fully mature.

1.3 Local Exploitation & Incentive

The Middle East North Africa (MENA) region is situated in the so-called Sun Belt regions of the world, with the highest DNI received by the sun worldwide, which plays a major role in the thermo-economic feasibility and effectiveness of all CSP plants [20]. A minimum DNI value of 2000-2800 kW/h is found to be necessarily available for an effective CSP plant [21], which is densely attained in most countries of the MENA region throughout the year. In Kuwait for example, the annual DNI value is assumed to be equal to 2100 $kW/m^2/y$ in approximately most

of the country's land area [22]. A resources assessment has elected CSP as a high potential technology to be implemented in Kuwait [23].

Among the MENA region, the six Arabic gulf countries known as the Gulf Cooperation Council (GCC), have recently directed their energy production policies towards the adoption of RE in an attempt to limit their carbon emissions (all six gulf countries are considered among the highest fifteen carbon emitters in the world in 2009, in metric tons per capita [24]) in addition to committing to the international climate change protocols, as for the fact the implementation of the RE policy support has been already established in 146 countries worldwide by 2015 [25]. Figure 1-2 illustrates the high levels of emitted CO_2 by the GCC countries among MENA and other worldwide regions [26].

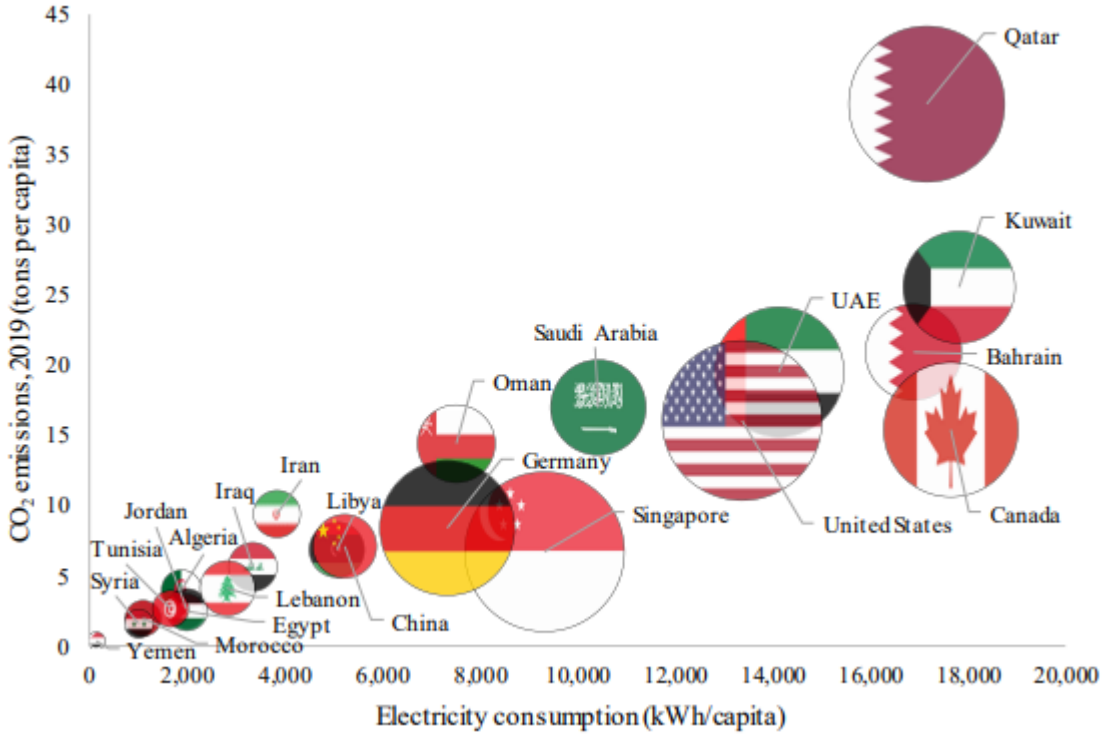

Fig. 1-2. Worldwide electricity consumption and CO_2 emissions in association with the GDP per capita (size of the sphere) [26].

The combined RE deployment of all the GCC countries only accounts for a total of 867 MW which represents less than 1% of the total installed power capacity in the region, i.e. 146 GW in 2018 [27]. However, some GCC countries have already been following some optimistic

first steps towards the achievement of influential visions these countries are seeking to accomplish in the near future. The United Arab Emirates, followed by the Kingdom of Saudi Arabia, are actually the leading GCC countries in the adoption race of RE, with a capacity of 589 MW for the former and 142 MW for the latter, mostly through PV and CSP. Kuwait follows with 79 MW between PV, CSP and WT which is equal to 0.4% of the country's total electricity capacity [27]. Being an oil producing/exporting country and consuming 16% of what is produced oil [28], Kuwait has a potential to raise its exports of oil, to where it is substantially needed and more valuable, as well as its share of locally consumed RE. Furthermore, although the substantial amount of natural gas in the country, it is non cost effective for many reasons to produce such a fuel in Kuwait, and this forces the importing of liquefied natural gas for power production plus other industrial needs [29].

A brave vision named "New Kuwait" counted on RE as one of its pillars to generate 2000 MW in the year of 2030, for an initial plan. The first phase of the plan was actualized through a 100% RE location called Shagaya Renewable Energy Park (SREP) which has WT, PV and Parabolic Trough Collectors (PTC) with a total capacity of 70 MW divided between the three technologies with shares of 10, 10 and 50 MW, respectively. The second and third phases were planned to add 930 and 1000 MW by year 2026 and 2030, respectively. However, due to an increasingly elevating demand of electricity in the country (Kuwait tops internationally in per-capita electricity consumption with an average of 40,100 kW a year for each house in the country [30]), the initial plan was recently modified with the integration of a fourth phase consisting of another 2300 MW. Thus the total capacity of RE share in Kuwait will be 4.3 GW, and this is planned to be reached by 2030, and projected to equal by then 15% of the country's total energy installed capacity [31], which was 18.3 GW in 2015 when the project of SREP was first commission [32] and has recorded a raise since then to 20.2 GW in 2022 [33]. As of yet, the renewable energy share in the country's mix does not surpass 1% as the published numbers of Kuwait Ministry of Water, Electricity and Renewable Energy suggests [33] and as it is illustrated in Figure 1-3.

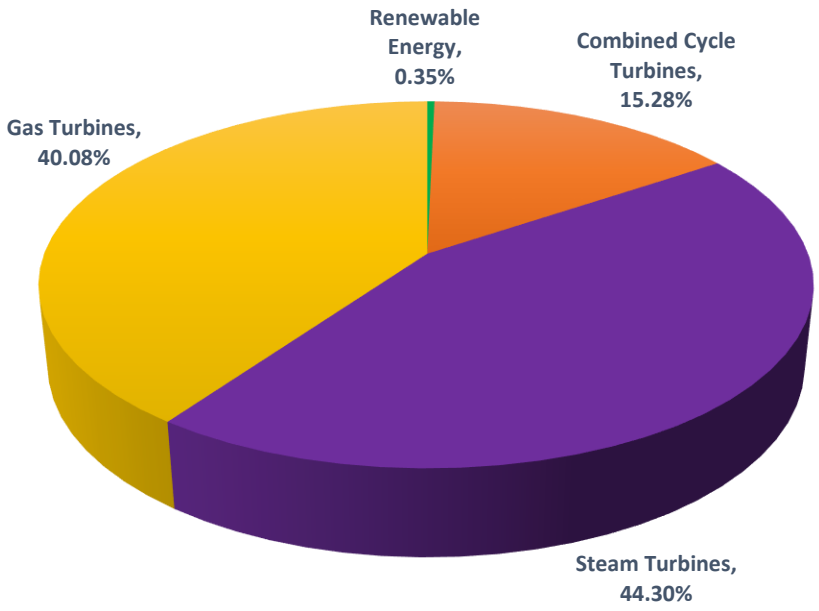

Fig. 1-3. Kuwait energy production mix by technology types (raw data acquired from [33]).

Research and planning of the SREP are entrusted to the Kuwait Institute for Scientific Research (KISR) which is a governmental research facility established in 1967 with the main role of the reinforcement of technology innovation and scientific research in the country. The institute has already announced the intention of building other CSP plants to be dedicated to the third and fourth phases in addition to the already operational 50 MW PTC at SREP. The total CSP share of the project will be 1.15 GW [31], and that includes PTC, SPT and Linear Fresnel (LFR) as it is approved by the plan of KISR [34]. The study is flexible to various plant capacities, as it was only agreed that the Thermal Energy Storage (TES) capacities are defined. Another study regarding the SREP ran a technology mix optimization and compromised a total of 1250 MW dedicated to CSP at the park [35].

1.4 Preface

The RE technologies discontinuity issue has been, to some extent, solved in CSP applications by the employment of the TES as back-up systems. CSP systems have managed to reach up to 74% Capacity Factor (CF) percentages thanks to the TES [36]. Despite being associated with higher costs, TES have very high efficiency rates (98% [37], [38]) and have been proven to drive down the overall relative initial costs to the unit of produced energy of CSP system, i.e.

Levelized Cost of Energy (LCOE). However, even TES-backed CSP systems remain with relatively high costs compared to fossil fuel systems or even more mature RE systems, e.g. WT.

All different CSP types have the common objective of optimizing the manner of capturing and reflecting sun rays, however, they vary in the technical achievement of this goal. Flat, parabolic or dish reflecting mirrors work on concentrating the sun rays on either a common line or point. At present, there are four main CSP types on the commercial scale. CSP types are divided into two different categories regarding each of their collector's manner of tracking the sun throughout the day. For instance, both the PTC and LFR track the sun with one axis (orientated on the north-south axis) [39]. While the other two, SPT and SPD track the sun within two axes (south-north and east -west) [40].

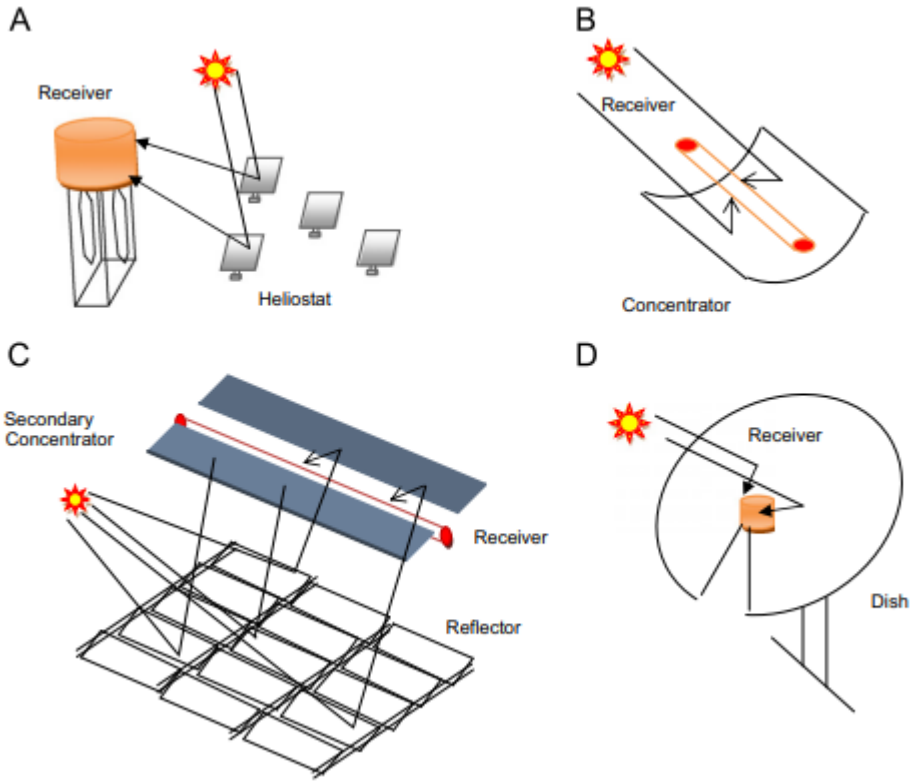

Fig. 1-4. Simplified schematic of the 4 CSP types: (a) SPT, (b) PTC, (c) LFR and (d) SPD [41].

All the CSP, each in their respective type, consists of a carrier which contains at it a Heat Transfer Fluid (HTF) which will be elevated in temperature and this is due to sun rays reflection and concentration at the carrier of the HTF, i.e. the receiver. The HTF afterwards is transferred

with the assistance of a pump into a heat exchanger, at which the heat of the HTF is transferred to a working fluid at a power block (e.g. water in a steam Rankine power cycle) in order to evaporate it, thus creating saturated or superheated steam at a high temperature and pressure. The steam is then driven to a turbine where the thermal energy is transferred into mechanical work through the expansion applied at the turbine. The turbine is connected to an electricity generator which has the ability to convert the mechanical work into electricity. Afterwards the steam is recovered with the assistance of a condenser that transfers the steam back to water in order for the latter to be sent to the heat exchanger again and hence repeat the process. A similar methodology takes place for the HTF in the solar field, as the cold HTF after the heat exchanger is resent to the focal point/line to repeat the process [42].

Today, the PTC is considered as the most mature CSP type as it is the most proven and hence operational at the commercial level. Spain leads the world with 42 PTC commercial plants. United States follows with 17 plants and these plants are out of a total number of 77 PTC plants worldwide [43]. Both countries dominate the global market by generating more than 4 GW combined only through CSP [44]. The SPT comes in second place in the CSP maturity. It is agreed that the SPT has a better potential outlook for improvement due to the higher concentration ratios (300-1000 compared to 25-100 for PTC), better solar to electricity annual efficiency (20-35% compared to 15% for the PTC) and a higher capacity factor (55% compared to 22-43% with and without the TES, respectively) [21].

Making a great use of TES and employment of the HTF, SPT emerged as one of the most promising CSP technologies due it is unmatched level of sun irradiance concentrations [45]. This enables such technology of using a HTF of an elevated thermal stability such as molten salt. In this case, molten salt can be used as both a HTF and a storage media, thus, bypassing the need of an extra heat exchanger between the storage media and the solar field as it is adopted in the most mature CSP technology, i.e. PTC. In addition, the high ability of SPT to elevate the HTF's temperatures translates into less size of storage media as the molten salt can store more thermal energy for less quantities of salt [46].

On the other hand, with the rapid growth in RE adoption as a potential solution of CO_2 emissions mitigation, some challenges emerge as a confrontation with the feasibility and reliability of such systems. This is mainly based on two issues: the relatively low techno-economic performance of the RE systems and secondly, the CO_2 emissions non-neutrality of these systems despite being total renewable. The first issue originates from multiple reasons such as efficiency and compatibility. Compared to fossil fuel-based technologies, most of the RE technologies are less techno-economic efficient due to immaturity. In addition, the availability of fossil fuels makes their ability to supply constant energy levels higher. This ensures energy provision continuity, in contrast to RE technologies which are subject to fluctuations as they are dependent on their intermittent resources. The second issue concerns the CO_2 emissions neutrality of these RE as in fact, during the manufacturing phase of the various components of most of RE technologies, fossil fuel is heavily used and thus CO_2 is emitted. This, for example, results in 41 and 14 grams of CO_2/kWh of the produced energy from solar and wind energy technologies, respectively [47].

One of the most threating risks to the efficiency of the CSP performance especially in arid regions is its sensitivity to aerosols. It is commonly agreed that in clear sky conditions, the aerosols are the most affecting factor in the probable attenuation process of the DNI [48]. Aerosols are best quantified by the Aerosols Optical Depth (AOD), which is known as the absorption of the light due to the existence of aerosols [49]. This is even expected to be more amplified in a SPT plant because the SPT is quite unique among other CSP types in having its common receiver placed on top of a tower. This results in having the distances between the reflectors in the solar field and the receiver to reach up to thousands of meters. In arid regions where dust storms are quite common, this might heavily affect the key design parameter of the CSP, the DNI.

Another issue of the SPT beyond it is high sensitivity to the aerosols density in arid regions, the SPT as well as all other CSP types, are known to have a relatively elevated LCOE compared to other more mature RE technologies. This fact has led many recent researchers to target the hybridization of CSP with other more mature technologies in order to return positive impact in case synergic solutions are found. For instance, the capital costs of WT are relatively low which enables the technology of having lowered LCOE. However, this lowered LCOE is usually paired

with a penalty on the AEG as the WT does not employ a backup system as the CSP does. A similar conflict is found when fossil fuel back-up systems are considered. Such systems ensure energy provision, however, majorly contribute in CO_2 emissions. Such a complex hybridization optimization problem requires to first assess the proposed system's performance with regards to the associated risks to its feasibility and properly assign objectives that fit the scope of the problem's background while ensuring the techno-economic competitiveness of the proposed plant.

1.4.1 Research Gaps

As seen from the literature, multiple research gaps can be identified and form the potential scope for an important and beneficial work for a wide range of researchers especially in arid regions. Herein, a list of the research gaps that have been found and will be addressed in this work:

- A lack of an accurate, inclusive and typical aerosols' behavior representation.
- A lack of a techno-economic assessment of a SPT that integrates the aerosols effect on its solar field reflected irradiance.
- A lack of an assessment of the aerosols temporal resolution variation's effect on different SPT configurations based on different ranges of TES-SM.
- A lack of a water consumption assessment of a CSP through a dynamic hybrid power cycle condenser cooling employment.
- A lack of a research that evaluates the backup system's ability to compensate the loss energy of the SPT sue to the aerosols density.
- A lack of a multi-objective optimization that assigns water consumption as one of its objective functions.
- A lack of a research that visualizes the environmental impact of a wide range of system's configurations.

1.5 Thesis Outline

1.5.1 Research Proposal

The main goal of the current work is to optimally exploit the existing natural resources through the application of a CSP-WT-fossil fuel hybrid system. This is carried out by quantifying the most important risks to such application, a detailed assessment of the proposed plant and lastly the promotion of an optimal configuration of the system. The objectives to reach this aim are listed as follows:

- To assess the aerosols density in the case study location by assembling an aerosols representative data set.
- To integrate this aerosols data set into an appropriate simulation tool.
- To validate a SPT base model against existing models in the literature.
- To assess the performance of the aerosols affected SPT.
- To validate both WT and NGCC against existing models in the literature.
- To integrate WT and NGCC with the aerosols affected SPT model.
- To perform a parametric analysis by varying SPT capacity, WT capacity, NGCC capacity, TES and SM over assigned ranges.
- To carry out a similar parametric analysis but with a CCS unit inclusion scenario.
- To perform a LCA for each system's component in regard to the global warming potential for each configuration.
- To conduct a techno-economic/environmental multi-objective optimization using the LCOE, CF, global warming potential and water consumption as objective functions.
- To vary the objective functions weights using a multi-criteria decision making tool.

1.5.2 Thesis Knowledge Contribution

Firstly, a novel methodology of aerosols representative integration within a RE simulation tool has been developed. The novelty emerges from the fact that a long-term aerosols data has been first site adapted with the assistance of short-term ground measured aerosols data. Then, the site adapted data has been used to assemble a typical year data set based on which the performance of the SPT has been tested with different temporal resolutions of aerosols. The

typical year assembly method that has been used here is usually used to assemble typical weather data files which describe the incoming irradiance among other important metrological parameters but not the aerosols effect on the reflected irradiance of the solar field, i.e. a typically addressed effect in this work. Also, aerosols temporal resolution variation effect has been evaluated with the assistance of an in-house developed algorithm.

Secondly, the aerosols affected SPT has been integrated with both WT and NGCC forming a novel RE-fossil fuel plant configuration. The proposed configuration has been presented and analyzed in three different aspects, i.e. technical, economic and environmental. This work is the first successful attempt to dynamically integrate and automate more than RE technology of the SAM simulation tool. This has been accomplished with the assistance of an in-house developed algorithm which also enabled this work of integrating a non-RE back-up system; a typically non existing feature in the conventional SAM set up.

Finally, the optimal sizing strategy of the proposed plant has been elected with the assistance of an evolutionary algorithm where the LCOE, water consumption, CF and the CO_2 emissions have been assigned as objective functions. One novel aspect of this methodology that the CO_2 emissions objective functions that has been used in the optimization algorithm is a product of a full life cycle assessment (LCA) which has been carried out for all possible configurations of the proposed plant based on the different variables ranges assigned of the optimization problem. This represents an integrated techno-economic/environmental study as the inclusion of the LCA outcomes within the multi-objective optimization qualifies the selection of the optimal configuration of the proposed hybrid plant in this work to be inclusive, rationale and coherent.

1.5.3 Thesis Structure

Chapter 1 – Introduction

This chapter sheds the light on the research problem and introduces the motivations behind the research. It also gives a glimpse of the thesis methodology reaching its aim by presenting the research objectives. Further, this chapter fairly clarifies how the novelty of the work distinguishes from the already existing knowledge and its ability to enhance related future research work.

Chapter 2 – Aerosols Affected SPT

In this chapter, a detailed and independent assessment of an aerosols affected SPT performance has been presented. This includes a comprehensive review of the existing literature and this research's approach to enhance the accuracy of such assessment. In addition, this chapter details the aerosols quantification methodology and finally exposes the results of the integration of aerosols in the SPT performance model.

Chapter 3 – Hybridization

Here, both WT and GT are presented as hybridization options with the aerosols affected SPT. Both of these components are firstly validated against their prospective data sets from both commercial and literature published references. Then, the hybridization technique of the entire proposed plant of SPT-WT-GT is presented in detail. Finally, the ability of different capacities of WT or/and the GT to compensate the energy loss of the SPT due to aerosols density is illustrated.

Chapter 4 – Multi-Objective Optimization

After assessing the entire system performance post the hybridization, the optimal sizing strategy of the system is carried out through a multi-objective optimization technique. Several system performance indicators are assigned as objective functions to the optimization problem. Seen the conflictive nature between the assigned objective functions, the optimization tool will only be able to elect a set of optimal solutions rather than one optimal solution. To address this, a multi criteria decision making tool is used to assign different importance weights to the objective functions and finally rank the individual solutions from best to worst.

Chapter 2 – Aerosols affected SPT

Abstract

This chapter evaluates the SPT performance in arid regions where elevated aerosols levels and water scarcity threaten solar applications feasibility. It conducts an aerosols aware modelling and techno-economic assessment by considering possible aerosols effects on the solar field's reflected irradiance; an effect that is typically ignored in the literature. Aerosols effect's inclusion modifies the thermal input to the solar field and this, in turn, provides a more accurate assessment. A parametric analysis has been performed using a 50 MW model by varying the TES and SM based on three aerosols temporal resolutions: a typical year's average, daily and no-aerosols schemes. Further, water consumption is examined over four different condenser scenarios: dry, wet and two hybrid set ups. The assessment performed in Kuwait reveals that the wet-cooled condenser scenario with a 16h of storage and a 3.2 solar multiple yields the lowest LCOE of 12.06 c/kWh when the no-aerosols scheme is considered. This increases to 12.87 c/kWh when the daily aerosols are considered as the generated energy decreases by 6.7%. Besides, both hybrid condenser scenarios offer a trade-off as they result in a 55.1-68.7% of water saving for only 2.1-2.3% less energy generation.

2.1 Introduction

Since the Gemasolar SPT became operational in 2015, an important milestone for the CSP has been successfully achieved as the plant coupled the elevated concentration of the technology and the large TES, resulting in the first CSP ever to generate electricity for 24 uninterrupted hours [50]. Also, Gemasolar was the first CSP ever to deploy molten salt as both the HTF and a storage media which avoided having a heat exchanger between the solar field and the storage tanks, thus saving the plant capital cost and heat losses [51] as it is illustrated in Figure 2-1.

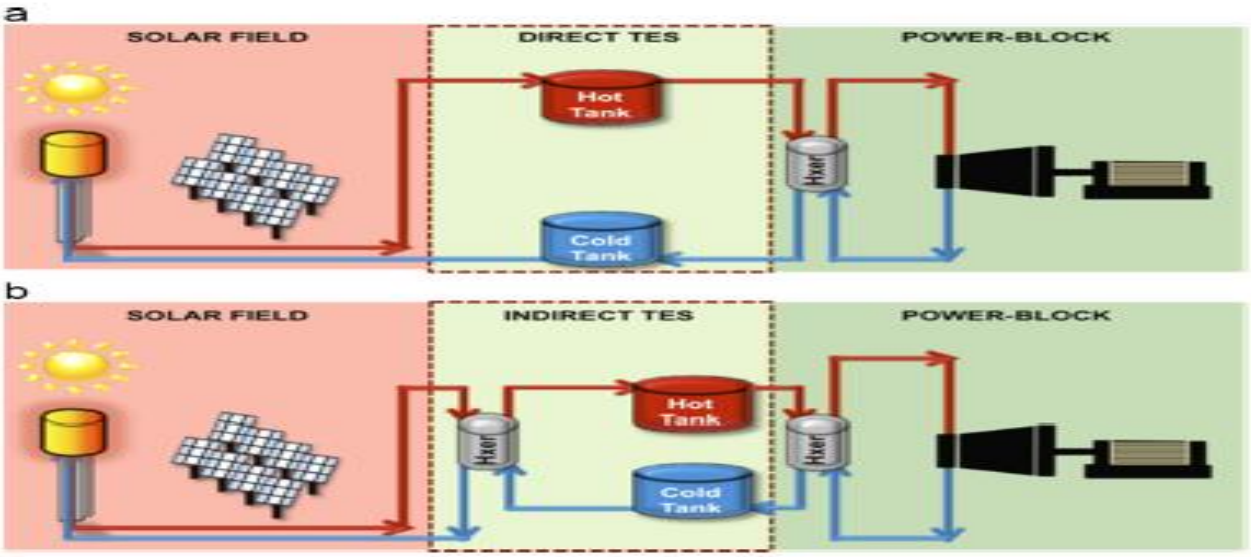

Fig. 2-1. The SPT plant in two different configurations: (a) direct and (b) indirect TES [51].

The plant has proven that the SPT technology can take a bigger share of the total CSP capacity worldwide which is dominated by the PTC (15.3% for SPT and 76.6% for PTC) [52]. The SPT is probably one of the most efficient types of the commercially proven CSP and this is due to its high levels of concentration and elevated temperatures of the working fluid that surpasses the PTC [21], [45], [53]. In the SPT technology, the solar field consists of hundreds or even thousands of mirrors, called heliostats, which work on reflecting the DNI of the sun at a common tower top mounted receiver [40].

In a typical prefeasibility research work, all CSP are observed under clear sky conditions, where the sky is cloud free and the CSP is expected to deliver its rated capacity with a focus on the DNI as it is the only solar irradiance component that can be concentrated, which qualifies it as the main design parameter for such technology [20]. However, in such sky conditions, aerosols followed by water vapor, are the most important factors that contribute to the attenuation of the DNI with a superiority of the former [48], [54], [55]. Other sun irradiance components, such as the GHI are affected by aerosols, however to a lesser extent [56]. In addition, in all CSP types, the attenuation of the DNI takes place twice, first during the transit of the sunrays towards the reflectors and secondly when the reflected rays transit towards the receiver which does not occur in other solar applications such as Photovoltaic (PV), as the sun light is harnessed once it reaches the solar panel. Aerosols extinction is best introduced by a dimensionless parameter, called the

Aerosols Optical Depth (AOD) which is referred to as being the most adequate compared to any of the other parameters (e.g. Metrological Optical Range) for the purpose of attenuation measurement [57].

In contrast to all other CSP types which all have their prospective receivers within a few meters from the reflector, the heliostats in the SPT are situated at hundreds, or even thousands, of meters from the receiver, where the slant range (the distance from each heliostat to the receiver), plays a major role in the attenuation process. Figure 2-2 illustrates how the existing CSP types differ in having different slant ranges [58]. In the meanwhile in arid regions, where dust storms are quite frequent, aerosols can mask off up to 70% of the sun light [59]. As regards to the reflected sun rays from the heliostats towards the receiver, some researchers have found that a loss of 12.7% of the total Annual Energy Generation (AEG) can be obtained when taking into account the effect of the aerosols on the reflected sun rays [60].

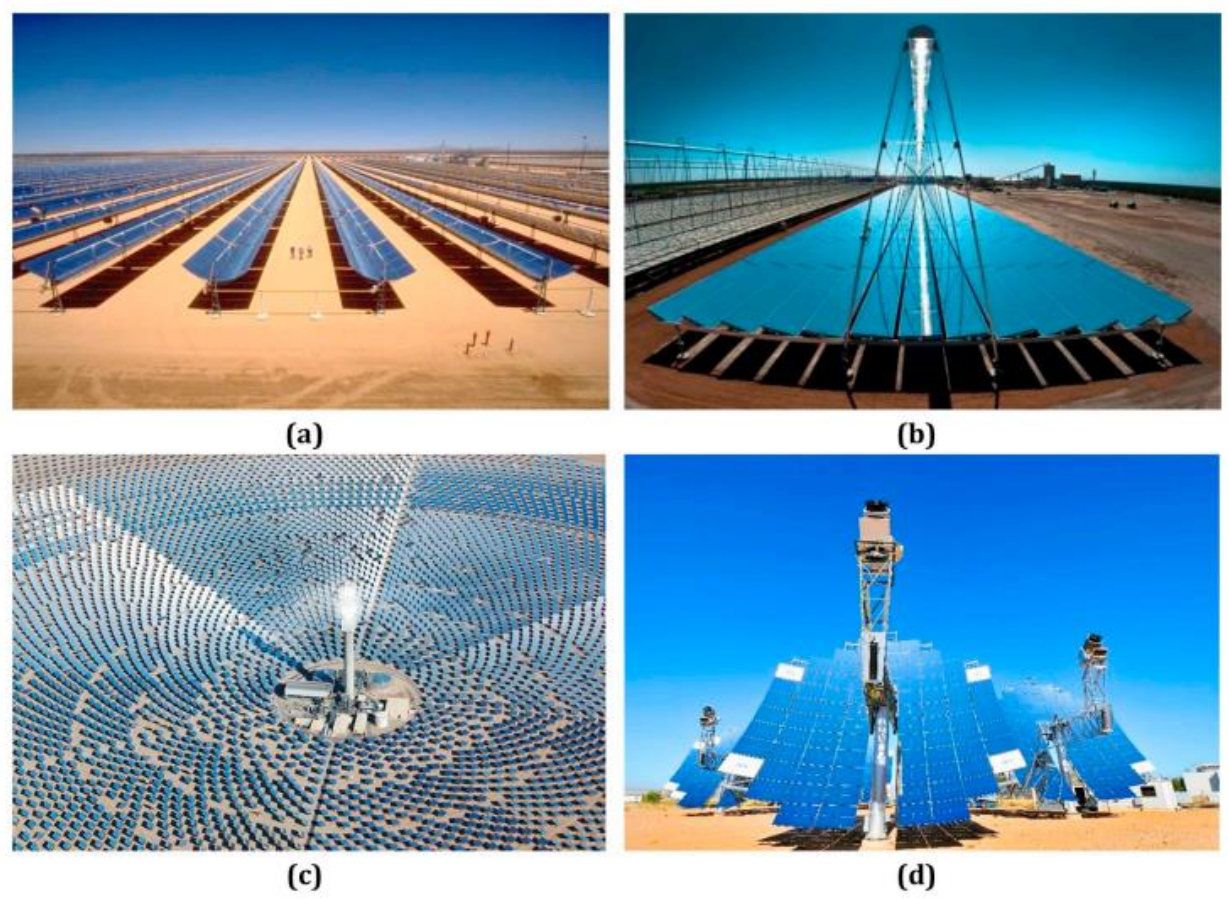

Fig. 2-2. Slant ranges difference between (a) PTC, (b) LFR, (c) SPT and (d) SPD [58].

2.1.1 Techno-Economics

Many researchers have already examined and simulated the performance of most of the CSP technologies in arid regions where solar applications are at multiple risks. Sultan et al. [61] examined the competiveness of a 50 MW PTC in Kuwait and compared its performance to a commercial operational plant in Spain. The PTC simulated in Kuwait yielded a better efficiency as the dumped thermal energy was less. Roubiah et al. [62] examined the SPT performance in different locations in Algeria while variating the TES capacity and the solar field size which resulted in different appropriate combination based on the location's DNI resource. Also, Boudaoud et al. [63] tried to find the optimal configuration of the TES and solar field size for a SPT in different locations in Algeria, however with a fossil fuel back-up. This hybridization offered the best techno-economic returns. In addition, research has been done on comparing the SPT performance to other CSP technologies. For instance, Mihoub et al. [64] examined the performance of both the SPT and PTC at 50 MW in Algeria. They simulated different scenarios, including a fossil fuel back-up and found that the SPT with 48% back-up and a TES of 8h is the most attractive scenario. Similarly, a comparison between the SPT and PTC has been carried out by Cekirge and Elhassan [65] in Saudi Arabia and they revealed that the SPT excels in higher efficiency and lower capital costs. Also, Hirbodi at al. [66] compared both the latter CSP types with different plant capacities, TES and solar field sizes.

Many other similar researches have been conducted in locations of interest around the world [67], [68], [69], [70], [71], however, there is no aerosols aware techno-economic assessment that exists in the literature. All previously mentioned techno-economic assessments did not consider the aerosols effect in the solar field attenuation especially that the latter can mask off up to 70% of the sun reflection towards the receiver as mentioned in the introduction. Most of the SPT techno-economic assessments are satisfied by finding an optimal combination of the key design parameters targeting the lowest Levelized Cost of Energy (LCOE) using a weather file that mainly describes the incoming irradiance but not the reflected ones towards the receiver. No techno-economic research has discussed both the effects of the aerosols on the total incoming irradiance at the solar field in addition to that effect on the reflected irradiance and the reliability of the optimal design parameter combinations in terms of the total absorbed

thermal power at the receiver and the AEG. The focus of this study is to perform an accurate techno-economic assessment with the awareness of the most threatening factor of such CSP type in arid regions, i.e. aerosols.

2.1.2 Attenuation Extension

The number of researches observing the effect of the aerosols on the reflected DNI at the SPT are constantly increasing, as more visions of Renewable Energy (RE) projects are becoming reality in the Sun Belt regions. More than six different mathematical models that describe the reflected DNI attenuation process in the SPT have been proposed in the literature. The models mainly differ in the Radiative Transfer Model (RTM) used, the plant capacity/configuration and the location used for the case study. However, only a few of these models have been validated against experimental data and have shown to produce acceptable results [72]. From these mathematical models, the Polo model [60] is one of the most widely used. This model can be coupled with the transient techno-economic RE simulation tools, which enable the user to observe the projection of the effect of aerosols on the techno-economic aspects of the SPT. Using the Polo model, the difference in the AEG of a SPT with different AOD temporal resolutions has been examined. The authors simulated two extreme values of AOD, one representing an aerosols-free sky and the other a hazy sky and found that the differences in the AEG are not negligible. Furthermore, using a year of ground measured AOD data, Polo et al. [49] compared the AOD temporal resolution variation effect on the AEG of two commercial SPT plants (Gemasolar and Crescent Dunes). A maximum difference of 20% has been observed in the AEG when employing daily AOD compared to the annually averaged AOD.

Further, Carra et al. [73] developed a more typical year of AOD data as they prepared a Typical Aerosol Year (TAY) in order to examine the attenuation extinction levels in Platforma Solar, Spain. This work has found that the attenuation extinction levels can reach up to 21.2% for a slant range of 2km even when performing the simulation based on a more inclusive aerosols behavior throughout the years rather than a one-year behavior which sometimes is subject to abnormalities. Although the preparation of a more typical time period, the work did not examine the SPT outputs based on the recommended temporal resolution in arid regions, i.e. sub two days [59] and was satisfied with the annual averaged AOD. The literature still lacks a study that

includes the typical behavior of aerosols, projects it at the SPT annually performance through a techno-economic assessment and eventually examine the outputs against a fine temporal resolution.

Little information exists in the literature regarding the attenuation effect of aerosols and this has been based on examining existing commercial scale SPT plants with fixed TES and SM values in different locations worldwide [49]. The work of Polo et al. [49] has greatly contributed in the confirmation of the aerosols effect on the reflected irradiance, however, the employed methodology assumes a fixed TES-SM configuration for different locations and this is not accurate as the optimal TES-SM depends on the DNI of the location. Thus, only a techno-economic assessment, as the one conducted herein, consisting of a parametric analysis with a variation of the main design parameters (here TES and SM) can give a much clearer understanding of how gradually a TES-SM configuration is sensitive to aerosols. In addition, the effect of the AEG reduction on the LCOE is assessed; an analysis that is missing in the literature.

2.1.3 Water consumption

Solar applications in arid regions raises another issue, namely the most suitable sites for the solar applications are situated in locations that lack water resources [74], [75]. Water is required for cleaning the reflectors from the accumulated dust, but mainly for the heat rejection process that takes place at the condenser of the power block as the latter consumes up to 90% of the water usage in the plant [76]. Air-cooled condensers have emerged as a potential option, however with multiple penalties on capital costs and efficiency. Such a type of condenser costs up to 3 times more than the wet-cooled [77] and can result in much lower performance in hot periods of times [78], which is quite common in arid regions. The wet-cooled condenser type remains the most efficient and cost effective [79], [80].

The majority of researchers have been observing both wet and dry cooled condensers in trials to find a tradeoff between the efficiency of the plant, represented by the AEG, and the economics represented by the water consumption. For instance, Marugan-Cruz et al. [75] noticed a 3.7% decrease in the AEG when deploying an air-cooled condenser compared to a wet-cooled one. Further, Qoaider and Liqreina [81] simulated an air-cooled 50 MW PTC in Jordan and reported a decrease of only 1.5% in the AEG and an increase of 2% in the LCOE when shifting

from a wet to air-cooled condenser. Fares and Abderafi [82] simulated the Noor 1 PTC plant in Morocco with an air-cooled condenser and compared the results with the existing wet one. In addition, many other researchers have examined both types from multiple prospective including exergetic analysis [83], techno-economic analysis with different types of HTFs [84], different plant capacities [66] and different locations [85]. However, much less attention has been made towards the hybrid condenser type in spite of the potential benefits that it can bring to the CSP plant, including Asfand et al. [86] who carried a thorough water consumption analysis but without a projection on the AEG or the LCOE. To the best of the author's knowledge, only a couple of researches have assessed the AEG using a hybrid condenser , i.e. Poullikkas et al. [77] and Wagner and Kutscher [78] and both have assumed fixed percentages of hybridization, i.e. 30 and 50%.

On the commercial scale, only a couple of SPT have been reported to use a hybrid condenser, i.e. Ivanpah solar electric [77] and the Platforma Solar de Almeria [86], both of which did not report any performance assessment as of yet. As for the literature, no techno-economic assessment that investigates the performance of a CSP in terms of the LCOE, AEG and water consumption with a dynamic hybrid condenser that is temperature dependent has been found. Switching between cooling sides of the hybrid condenser based on the ambient temperature would restrict water consumption to when it is needed.

2.1.4 Local Exploitation and Incentive

Among the MENA region and the Arabic gulf countries of the Gulf Cooperation Council (GCC), Kuwait has recently directed its energy production policies towards the adoption of RE in order to limit its carbon emissions. It should be noted that all six gulf countries are considered among the highest fifteen carbon emitters in the world in 2009, in metric tons per capita [24]. This work also assists in giving a clearer assessment as to whether the SPT technology is an appropriate technology to fulfill the country's vision of shifting 15% of its power production towards RE by the year 2030. Further, no similar technology has ever been tested either experimentally or by simulation, while an increase in aerosols levels has been detected in the country which probably leads to a decrease in the DNI [87].

Regarding the CSP being part of this vision, the annual DNI value is found to be equal to 2100 kW/m^2/y in approximately most of the Kuwait land area [22], which is known to be sufficient for such a technology [21], [20]. A resources assessment has elected CSP as a high potential technology to be implemented in Kuwait [23] based on the elevated levels of the DNI in the country, however, elevated levels of aerosols are also recognized and considered as a concern for such technology [88], [89]. The first phase of the vision has been already accomplished in the western part of the country at the SREP as mentioned in the introduction, with a further phase that includes SPT in a total CSP capacity of 1.15 GW, however with, as yet, no assigned capacities or configurations [35], [34].

2.1.5 Aim and Objectives

The main aim of this chapter is to assess the techno-economic feasibility of the SPT in such extreme weather conditions as that of the case study location. To accomplish this, firstly, all the possible effects of aerosols must be carefully observed and quantified. Then, the aerosols effect must be included with multi temporal resolutions into the techno-economic assessment (a wide range of TES-SM has been considered). This will assist in examining how gradual is the effect of aerosols over the increasing SM range and how is the role of the TES in the compensation of the AEG potential losses.

The techno-economic assessment essentiality emerges from the fact that some arid regions with elevated levels of aerosols might appear as inappropriate for such technology only because the aerosols effect is amplified when coupled with a large solar field. An aerosols impacted techno-economic assessment, as the one proposed in this chapter, would give an appropriate solar field size, larger than which the effect of aerosols will have a considerable amplified impact due to the too large slant ranges. Thus, a novel fully aerosols aware method of conducting a techno-economic assessment in arid regions is proposed in this work for the SPT technology. The method considers all possible effects of aerosols on such technology, namely, the total incoming irradiance on the solar field, the reflected irradiance in addition to the aerosols' temporal resolution variation effect. In addition, a water consumption analysis is carried out in this chapter that includes wet, dry and two hybrid condenser set ups. This is mainly realized through the following objectives:

- Assembly of a site adapted Typical Aerosols Year.
- A parametric analysis of the key design parameters that lead to the lowest LCOE for different types of power block condensers.
- An examination of different aerosols temporal resolutions employment effect on the outputs of the parametric analysis optimal design parameters combinations.

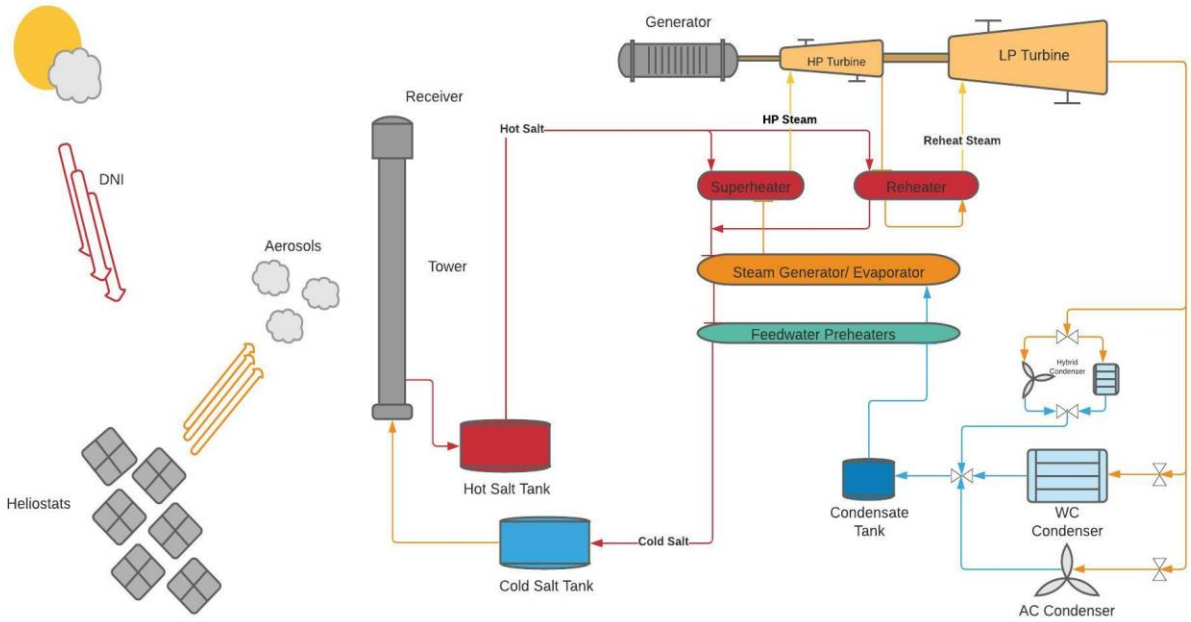

Fig. 2-3. Solar Power Tower diagram with 3 power block condenser scenarios.

2.2 Materials and Methods

2.2.1 Metrological data

2.2.1.1 Typical Metrological Year (TMY)

As part of the solar resources assessment in Kuwait, the KISR has managed to obtain at least one year of ground measured data at five potential sites in Kuwait [88]. Among the five locations, Shagaya has been found with the highest DNI values , which makes it the most interesting site as shown in Figure 2-4 (a). Shagaya has been already set with a TMY weather file that is based on site adapted satellite derived data acquired from SolarGIS [90]. The TMY is obtained based on typical values of the most important weather parameters in the period

between 1999 and 2016 and has been provided to the authors of this work by KISR. Figure 2-4 (b) illustrates the DNI levels in Kuwait including the Shagaya site.

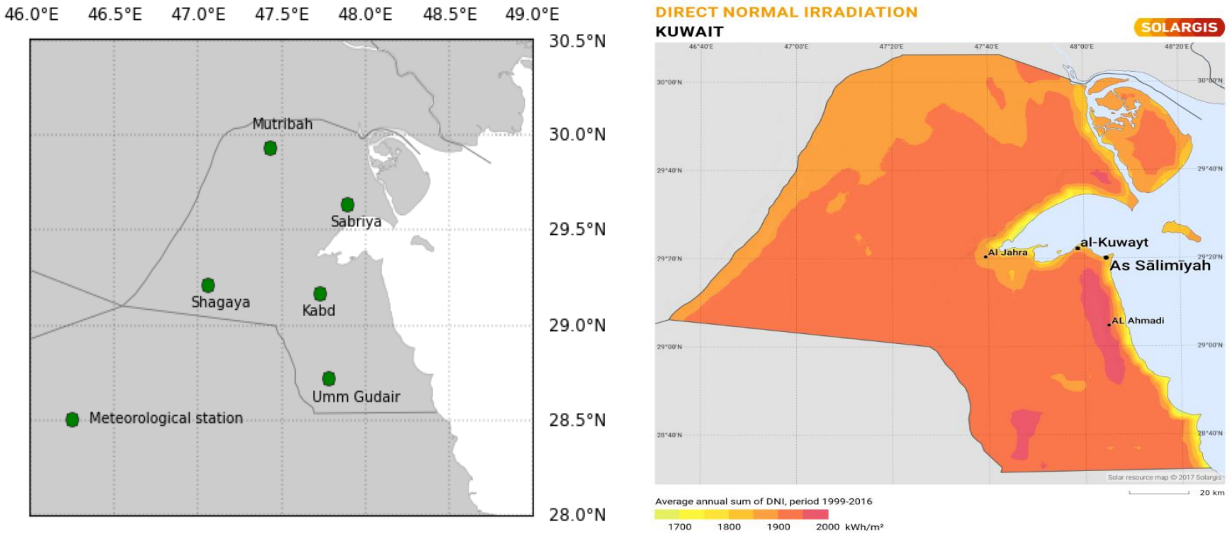

(a) (b)

Fig. 2-4. The geographic location of the case study location of Kuwait where (a) is illustrating the weather stations [88] and (b) is an illustration of the DNI levels in Kuwait [90].

Despite the promotion of the selected Shagaya site as the most appropriate geographic location for solar energy applications in Kuwait, it is worth mentioning that the site is situated in a remote area 60 km away from the nearest urban area. This exposes the site to be subject for dust storms which are quite frequent in the region. Figure 2-5 [91] confirms that the site of Shagaya witnesses high dust deposition rates that might affect the solar energy applications performance in the site.

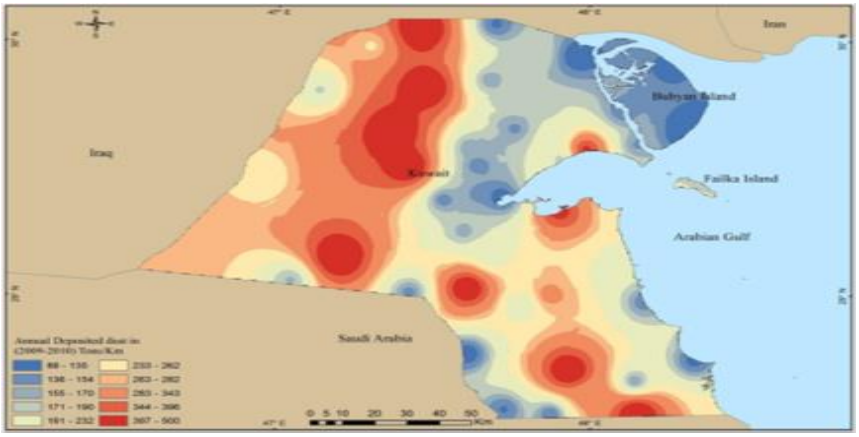

Fig. 2-5. Different dust deposition rates in Kuwait [91].

2.2.1.2 Typical Aerosols Year (TAY)

With the cooperation of NASA, KISR has also managed to set the site of Shagaya with an Aerosol Robotic Network (AERONET) station from which the short-term ground measured AOD data has been acquired. The latter data is for 289 days, a little longer than the minimum mandatory period for ground measured data in a site adaptation process, i.e. nine months [92], [93]. This data has been specifically chosen due to its high quality (level 2) which is known to be the most reliable data offered by AERONET as it is cloud screened, quality controlled and assured data [94]. In addition, the latter data lies in the same period as the TMY that has been provided by KISR, i.e. 2015-2016.

For a more typical aerosols behavior, the short-term ground measured AOD data from AERONET has been used in a site adaptation process with a long-term AOD data acquired from the reanalysis model of the Modern-Era Retrospective analysis for Research and Applications Version 2 (MERRA-2) which is highly referenced and widely used. The reanalysis model provides AOD data, besides several atmospheric parameters, through assimilation in a global forecast model, i.e. GEOS with a spatial accuracy of 0.625° x 0.5° and with a temporal resolution of 1-hourly [95]. The location of interest here is determined by a bounding box, which corresponds to the location of Shagaya, i.e. (47.060306°W/29.209889°S/47.160306°E/29.309889°N).

The site adaptation has been realized by the quantile mapping technique which insists on the establishment of a quantile dependent correction function that decreases the difference between both data sets, i.e. the cumulative distribution function of the modelled data (CDF_m) and it is matched to the one of the observed data (CDF_0) [96]. The technique is considered as reliable and widely used in the literature [97], [98], and has managed to reduce the existing bias between the ground measured data of AERONET and the corresponding data of MERRA-2 over the same period as the mean bias deviation has decreased from 0.1 to -0.0001 and the root mean square deviation decreased from 0.21 to 0.206. The slight improvement in the bias reduction is mainly due to the high-quality reanalysis model data of MERRA-2.

This technique uses the CDF as an operator that results in quantiles of data and in order to accomplish the latter, a vector of quantiles must be assigned for each data set through their

prospective CDFs, i.e. CDF_0 and CDF_m. The interpolation of the new corrected values (y_c) is obtained using the inverse of the CDF_0 as an operator as follows:

$$y_c = CDF_0^{-1}\,[CDF_m(x_m)] \tag{2-1}$$

This procedure has been carried out using five years of MERRA-2 data in the period between 2012 and 2016 which also intersects with the year of the ground measured data (2015-2016) of AERONET. The period of five years is sufficient for this purpose according to several researchers and has been used in [99] and [100]. The long-term data is for capturing the inter-annual and seasonal changes which are clearly seen in Figure 2-6 which also illustrates the ability of the one year of ground measured data of AERONET to positively affect the long term MERRA-2. This site adaptation process has successfully managed to reduce the 5 years long term data average from 0.429 to an average of 0.326.

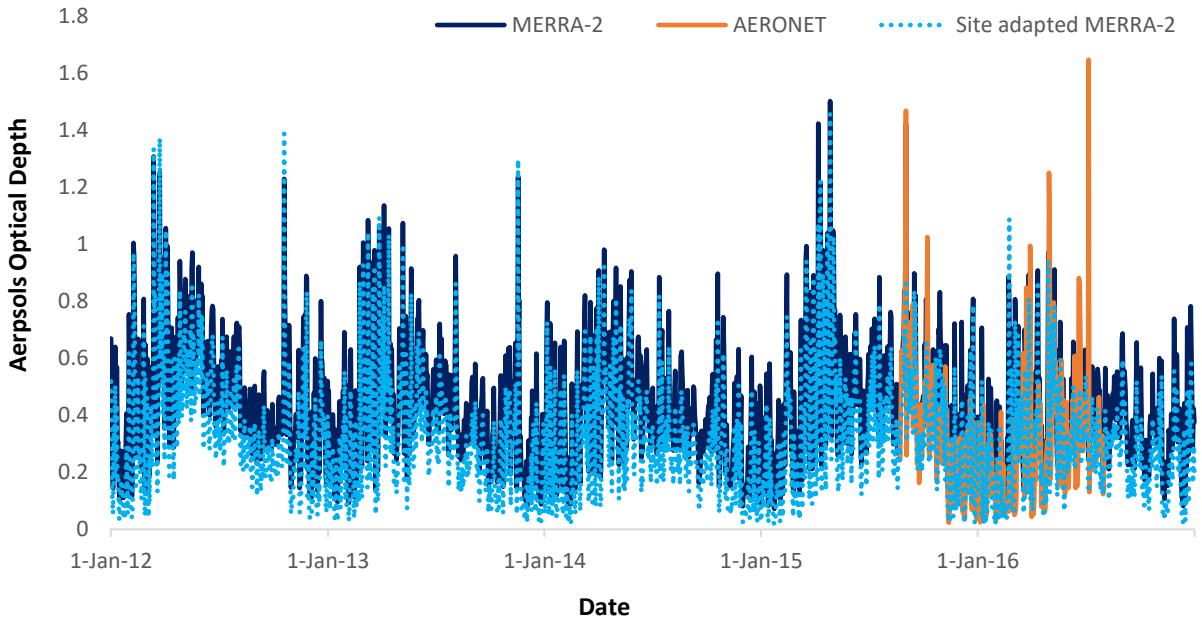

Fig. 2-6. The site adaptation of 5 years MERRA-2 AOF data with the assistance of 1 year ground measured data of AERONET.

These long-term data sets, whether ground or satellite measured, are converted into the most typical form of representation, i.e. TAY. For each accounted metrological parameter, each individual month from different years is compared to the long-term behavior of the parameter, and the closest month is selected as a candidate month, thus forming a typical year. The most common method in the literature is the Sandia Method [101] and this is followed by the NREL

method [102]. Both methods use the Finkelstein-Schafer statistics (FS) technique to measure the closeness of the short-term behavior (each individual month) to the long term one (every similar month along the entire data period). The FS is obtained as follows [73], [103]:

$$FS = \frac{1}{N}\sum_{i=1}^{N} |CDF_{m(di)} - CDF_{y,m(di)}| \quad (2\text{-}2)$$

where $CDF_{m(di)}$ is the cumulative distribution function of the long term of the indices (d_i) daily mean, $CDF_{y,m(di)}$ is the cumulative distribution function of the short term in month *m* and year *y* and *N* is the days number in the corresponding month (in order to normalize the FS for months with different number of days [104]).

Both CDFs are first calculated by taking the daily means of the hourly values in the entire study period for each of the indices. Then, the daily means are sorted in ascending order in order for the CDF to be calculated based on the rank *K(i), j(i)* of the specific unrepeated value *(i)* and the number of days in the corresponding month *N,* the number of days in any calendar month of the entire data set *n* as follows [105]:

$$CDF_{m(di)} = \frac{K(i)}{N+1} \quad (2\text{-}3)$$

$$CDF_{y,m(di)} = \frac{j(i)}{n+1} \quad (2\text{-}4)$$

Consequently, the month that returns the lowest FS value is considered the closest to the long term trend and thus its prospective AOD average value is chosen as the most typical month as it is shown in Table 2-1.

Table 2-1. The monthly AOD averages with the closest FS to the long-term trend.

month	year				
	2012	**2013**	**2014**	**2015**	**2016**
January	**0.1950**	0.2211	0.2461	0.1449	0.1721
February	0.3154	**0.2254**	0.1812	0.2650	0.1892
March	0.4822	**0.4596**	0.3470	0.3557	0.3382
April	0.4976	0.3938	**0.4193**	0.6251	0.2762
May	0.5839	**0.4281**	0.4061	0.4308	0.3639

June	0.4486	**0.3880**	0.3312	0.3479	0.3207
July	0.3990	**0.3534**	0.3237	0.3991	0.2780
August	**0.3216**	0.2684	0.2877	0.3936	0.2947
September	0.2437	0.2445	0.2212	0.4248	**0.2604**
October	**0.3228**	0.2161	0.3135	0.3923	0.2147
November	0.2848	0.3002	0.1724	0.2236	**0.2192**
December	0.2439	0.1646	0.1278	**0.2437**	0.2638

As a result, the typical year is constructed by typical months from different years, e.g. January from the year 2012 and February from 2013.

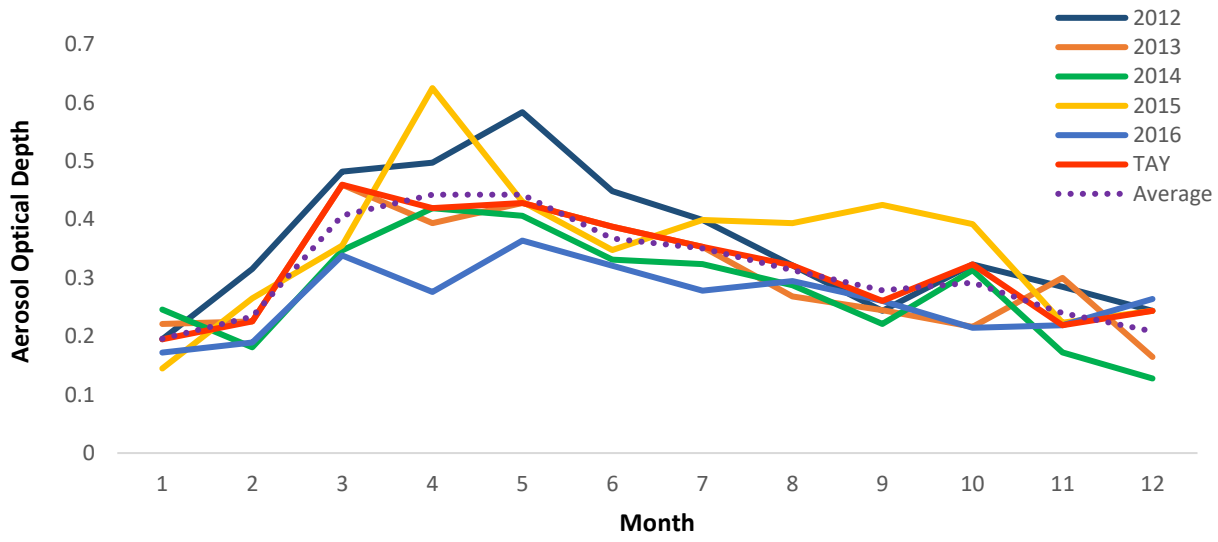

Fig. 2-7. AOD month selection for the TAY assembly according to the Sandia Method.

Further, once the TAY is assembled according to the Sandia Method, the selected months from different years are concatenated in a daily AOD basis in order to test the temporal resolution variation effect on the plant's outputs. However, the yearly averaged AOD value of the assembled TAY is still of importance for the preliminary evaluations of the parametric analysis

which targets the optimal TES-SM combinations based on the lowest LCOE. Here, the annual averaged AOD value based on the site adapted TAY is equal to (0.3205) as it is illustrated in Figure 2-8.

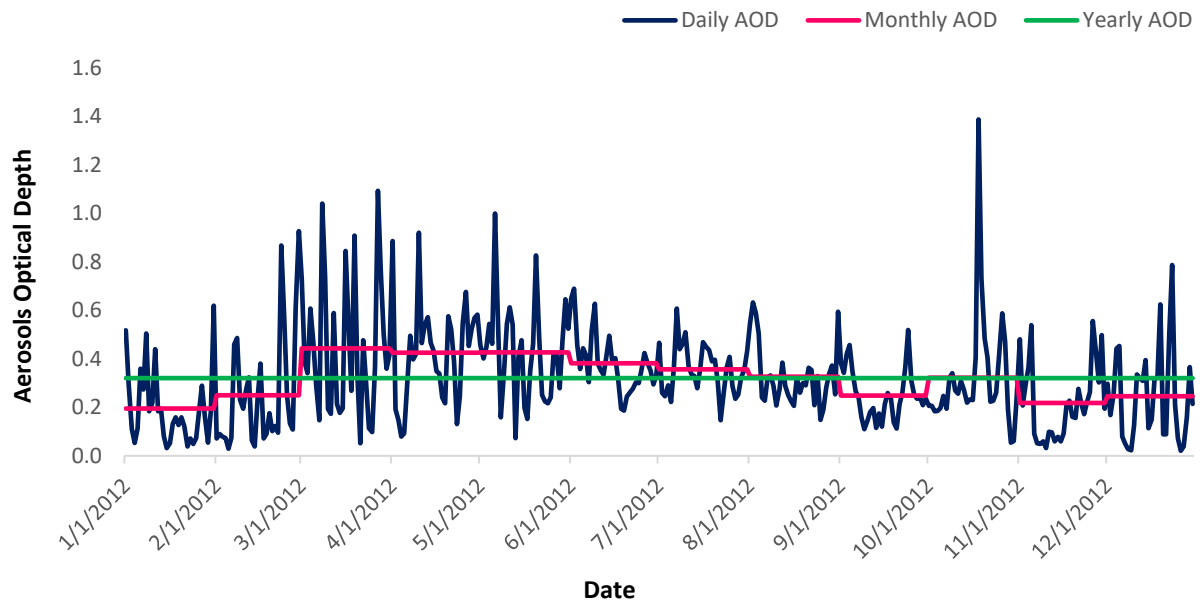

Fig. 2-8. The assembled TAY based on daily, monthly and yearly AOD resolutions.

2.2.2 Solar Power Tower Performance

2.2.2.1 Aerosols and Direct Normal Irradiance

This section generally describes how any solar irradiance can be affected by aerosols. Whether the incoming irradiance from the atmosphere or the reflected irradiance in the solar field, these are all subject to attenuation due to aerosols density. There is a nonlinear relation between the AOD and the DNI and this is given as follows [56]:

$$E_{bn} = S\, E_{sc}\, T_a\, \Pi T_i \tag{2-5}$$

where E_{bn} is the broadband DNI, S is a correction factor of the sun-earth distance, E_{sc} is the solar constant, T_a is the transmittance of the broadband aerosol and ΠT_i is a product of all the other extinction processes transmittance (Rayleigh scattering, ozone absorption, water vapor etc.). Each band of the aerosol transmittance is obtained as follows [106]:

$$T_a = \exp(-m\,\tau_\alpha) \quad (2\text{-}6)$$

where m is the air mass and τ_a is the band average AOD. While a simplification of the Angstrom law [107] gives the following:

$$\tau_\alpha = \beta\,\lambda_e^{-\alpha} \quad (2\text{-}7)$$

where β is the AOD at 1 μm (represents the amount of aerosols in the vertical direction), λ_e is the effective wavelength and α is Angstrom exponent which is related to the aerosol size distribution [73], [108]. For the sake of clarification, an AOD value of 0.05 for instance, is considered as a value for a clear sky and a maximum visibility, while an AOD value of 1 refers to hazy conditions. AOD values of 2 and 3 indicate very heavy aerosols content. However, no absolute maximum value of the AOD exists [109].

2.2.2.2 The System Advisor Model

The System Advisor Model (SAM) is a simulation tool developed by the National Renewable Energy Laboratory (NREL) and supported by the United States Department of Energy (DOE) [110]. SAM, which is freely available, includes a SPT performance model among multiple RE models, e.g. PTC, Linear Fresnel Reflectors, Solar Power Dish, wind and PV [111]. The SPT model in SAM is only available with one possible configuration that the user may employ, i.e. the Molten Salt (MS), previous versions of SAM used to have the Direct Steam Generation (DSG) configuration too. Another advantage offered by the SAM is that it incorporates not only the technical aspects of the simulated plant performance but also the financial aspects.

The tool is capable of performing a series of steady state solutions at hourly intervals that can approximate a transient system over the course of a year, and this can assist the user to observe the evolution of both the technical and economic parameters on an hourly resolution of the entire year. SAM works on the reading and processing the user inputs and specified weather file data, finds iterative solutions of the system and finally converges [112]. The dynamism of the tool is based on finding solutions for the time varying HTF flow and heat transfer variables in addition to constant inputs at each time step of the hourly weather file of the TMY (i.e. 8760 hours). For that, the tool implicitly runs multiple steady state iterative simulations, which are proper to the actual time step. Once the convergence is reached for a given time step, the

solution of the actual time step becomes the previous time step solution for the next time step. Such a simulation process is necessary in order to examine the parameters evolution over time, which is essential for an accurate solar radiation simulation. It is worth mentioning that in addition to the DNI values (which are essential for a CSP performance model), the tool calculates the sun position based on the location's coordinates existing at the weather file and thus the solar rays directions and the solar field optical efficiency.

2.2.2.2.1 Solar Field

Further, SAM incorporates multiple specific tools that automatically optimize key design parameters in the plant once enabled by the user. For instance, the SAM's SPT performance model integrates a separate tool which assists in the tower and receiver characterization process, ray tracing and heliostats positioning, i.e. SolarPILOT, which has also been developed by NREL and can be used as a stand-alone tool [113]. The tool calculates the incident thermal energy of the solar field as follows [114]:

$$Q_{Field} = N_{hel} \cdot A_{hel} \cdot DNI \tag{2-8}$$

where N_{hel} is the number of heliostats and A_{hel} is the area of a single heliostat. In addition, the tool consists of a weather attenuation loss evaluation function (the only one among all other CSP models), and this includes the attenuation effect in the solar field efficiency calculation as follows:

$$\eta_{opt} = \eta_{cos} \cdot \eta_{at} \cdot \eta_{sp} \cdot \eta_{s\&b} \tag{2-9}$$

where η_{cos} is the cosine loss, η_{at} is the attenuation loss, η_{sp} is the spillage loss, $\eta_{s\&b}$ are the losses due to the shadowing and blocking [115], [116]. This results in the incident thermal energy at the receiver being affected by the solar field optical efficiency as follows [117]:

$$Q_{rec} = A_{hel} \cdot N_{hel} \cdot DNI \cdot \eta_{opt} \tag{2-10}$$

Due to the reasons mentioned earlier in the introduction concerning the attenuation extinction of the SPT, SAM deploys a unique weather attenuation loss evaluation function and this is in the SPT performance model. The function is in the form of a third order polynomial with regards to the slant range (S), i.e.:

$$A(\%) = aS^3 + bS^2 + cS + d \quad (2\text{-}11)$$

Where *A* is the attenuation percentage. The four coefficients in the polynomial are unique functions of the slant range and the (x,y) positions of each heliostat in accordance with the tower and the receiver as follows:

$$S = \sqrt{h_x^2 + h_y^2 + h_{Tower}^2} \quad (2\text{-}12)$$

This can lead to the incorrect estimation of the model performance because of two aspects: first, no aerosols effect is included despite its potential influence. Second, the aerosols have a very high degree of spatiotemporal variability [118] and cannot be accurately described by an annual attenuation function. Thus, the introduction of the aerosols effect, in addition to the effect of the distance with the recommended temporal resolution on the attenuation function of the solar field must be much better understood.

2.2.2.2.2 Polo Model

Among the very few other researchers that have developed a solar field attenuation model, Polo et al. [60] has used a RTM, namely the Libradtran, in order to develop an AOD dependent attenuation model. This enables the accurate determination of the four coefficients in the third order polynomial for the heliostats field's weather attenuation function used in SAM. This model is reportedly referred to as very promising extinction model for SPT plants [72] and with the assistance of this model, an integrated effect of both the slant range and aerosols is obtained in the solar field weather attenuation function. The model is uniquely appropriate to AOD wavelengths of 550nm and slant ranges up to 3km. These coefficients are given as follows:

$$\begin{aligned} a &= 3.13\,AOD^3 - 1.9\,AOD^2 + 1.6\,AOD - 0.133 \\ b &= -14.74\,AOD^3 + 2.49\,AOD^2 - 11.85\,AOD + 0.544 \\ c &= 28.32\,AOD^3 - 7.57\,AOD^2 + 48.74\,AOD + 0.371 \\ d &= -2.61\,AOD^3 + 3.70\,AOD^2 - 2.64\,AOD + 0.179 \end{aligned} \quad (2\text{-}13)$$

2.2.2.2.3 Receiver, Tower & TES

As a consequence of sorting the incident thermal energy on the receiver (Q_{rec}) post the solar field losses, the thermal energy transferred to the HTF is calculated. However, the latter is obtained after multiple energy losses at the receiver. The receiver suffers from losses due to

emittance ($Q_{rec,em}$), reflectivity ($Q_{rec,ref}$), convection ($Q_{rec,conv}$), conduction ($Q_{rec,cond}$) and radiation ($Q_{rec,rad}$). Thus, the total thermal energy transferred from the receiver to the HTF can be obtained as follows [71], [115]:

$$Q_{HTF} = Q_{rec} - Q_{rec,em} - Q_{rec,ref} - Q_{rec,conv} - Q_{rec,cond} - Q_{rec,rad} \quad (2\text{-}14)$$

Consequently, based on both the Q_{HTF} and the desired full load hours of TES (t_s), the required thermal energy of the TES (Q_{TES}) gets defined as follows:

$$Q_{TES} = Q_{HTF} * t_s \quad (2\text{-}15)$$

Also, in order for the TES tanks to store the HTF volume that is able to deliver the required thermal energy of the TES (Q_{TES}), the mass of the HTF can be defined as follows [119]:

$$m_{HTF} = \frac{Q_{TES}}{C_P*(T_{hot}-T_{cold})} = \frac{Q_{HTF} * t_s}{C_P*(T_{hot}-T_{cold})} \quad (2\text{-}16)$$

where C_P is specific heat of the HTF, T_{hot} and T_{cold} are the hot and cold tanks temperatures, respectively. Thus the volume of the HTF (V_{HTF}) is defined as follows:

$$V_{HTF} = \frac{m_{HTF}}{\rho_{HTF}} \quad (2\text{-}17)$$

where ρ_{HTF} is the density of the HTF. Lastly, the TES tank size (V_{TES}) is obtained as follows [120]:

$$V_{TES} = \frac{V_{HTF}}{\eta_{TES}} \quad (2\text{-}18)$$

In addition, the SM of each configuration is a ratio between the solar field incident thermal energy (Q_{Field}) and the thermal energy required at the power block to meet the rated capacity which can be obtained as follows [121]:

$$SM = \frac{Q_{Field}}{Q_{pb}} \quad (2\text{-}19)$$

where Q_{pb} is the thermal power required at the power block for nominal conditions operation. Also, a variation of the SM is projected at the tower height and thus, a variation of the slant range. The relation between the SM and the tower height can be expressed as follows [122]:

$$h_{SM} = h * \sqrt{SM} \quad (2\text{-}20)$$

where the h is the tower height for a SM = 1 while the h_{SM} is the tower height at any other specific SM value.

The SM is also directly related to the water consumption of the SPT plant. This is because there is only minimum water consumption in the chosen power cycle's condenser type for arid region, i.e. air-cooled condenser. These minimal quantities are to make up the evaporated water

in the power cycle, while most of the water consumption is dedicated for the heliostats washing process.

2.2.2.3 Parametric Analysis

In addition, SAM incorporates a scripting language, namely (LK), which enables the user to run more advanced customized simulations, i.e. input automation based on user developed scripts. Parametric analyses can be carried out based on multiple runs with a user specified step size and number of iterations. This gives the user a better insight of the parameters variation effect on the performance of the simulated technology with ease and much savings in time. SAM also employs another scripting tool, namely the Software Development Kit (SDK) which permits the user to develop scripts and take over the performance model out of the SAM simulation core using other languages, e.g. C/C++, JAVA, Python [123].

A parametric analysis has been carried out for two key design parameters: TES and the SM in order to observe the variation effect of such parameters on the important plant outputs. The analysis targets the lowest LCOE as an indication of an optimal TES-SM combination. The TES is where all the excess heat of the solar field is stored and it is varied from 0h to 18h with a step size of 1h. The SM is the ratio of the thermal power produced by a specific solar field size at the design point to the power required at the power cycle block at nominal conditions. In other words, a SM of 1 basically represents a solar field size with which the plant will deliver its full power directly to the power block with no excess power (dedicated to co-generation or TES for example). While a SM of 2 can provide the full power required at the power block as well as an equivalent amount of power to the TES for later usage as it is illustrated in Figure 2-9 [51].

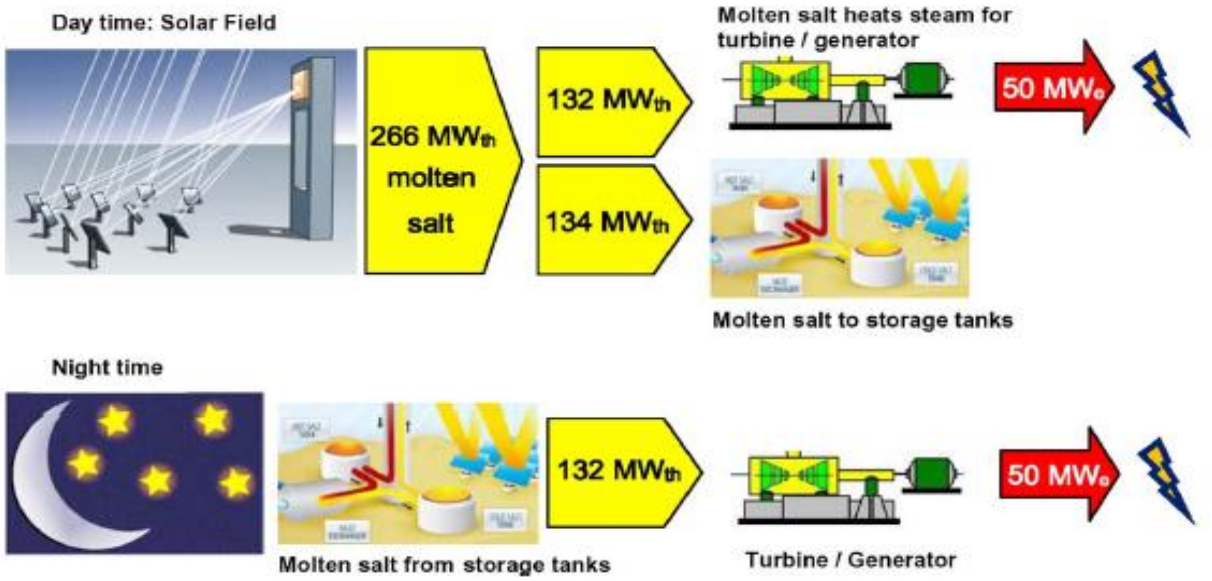

Fig. 2-9. Day and night operation of a SPT plant with a SM of 2 [51].

Here, the SM ranges from 1 to 4 with a step size of 0.2. A total of 304 simulations have been performed for each type of condenser using the inputs shown in Table 2-2. This range is commonly used in the literature as a SM of 1 is the minimum possible, while a SM of 4 is usually found a bit too big, however, is necessary to observe the performance indicators behavior at such a solar field size. Regarding the step size, a finer step size of 0.1 has been found unnecessary as it imposes expensive computational effort while the results are very close by. Bigger step sizes risk of missing out the accurate evolution of indicators and thus are avoided.

Table 2-2. SPT technical parameters.

	parameter	description
System Design	Solar multiple	1 to 4 (with a step of 0.2)
	Irradiation at design	700 W/m^2
	HTF hot temperature	574 °C
	HTF cold temperature	290 °C
	Full load hours of storage	0-18 (with a step of 1 h)
Tower and Receiver	Tower height	Obtained from optimization (SolarPILOT)
	Receiver diameter	Obtained from optimization (SolarPILOT)
	HTF type	Molten Salt (60% $NaNO_3$ + 40% KNO_3)

	Receiver flow pattern	Configuration 2
Heliostats Field	Layout configuration	Always optimize
	Heliostats length	12.2 m
	Heliostats width	12.2 m
	Water usage per wash	0.7 L/m^2
Atmospheric attenuation	Annual averaged AOD	0.3205
	Polynomial coefficient 0	-0.0037298
	Polynomial coefficient 1	0.154
	Polynomial coefficient 2	-0.0348
	Polynomial coefficient 3	0.0028768
Power Cycle	Condenser type	Air-cooled, wet-cooled and Hybrid
	Ambient temperature at design	31.6 °C for the air-cooled and hybrid condensers 14.3 °C for the wet-cooled condenser
Thermal Energy Storage	Storage type	Two tanks
	Tank height	20 m

Due to the limitations in the published technical data of CSP in Kuwait, the examined SPT plant is assumed a capacity of 50 MW in order for it to be comparable to the only operating CSP plant in Kuwait, i.e. Shagaya 50 MW PTC. This capacity has been revealed as a potential standardized CSP capacity [124], [125].

2.2.2.4 Power Block Condenser Scenario

In addition to the better heat rejection that wet-cooled condenser can import to the steam Rankine cycle compared to the air-cooled condenser due to the higher heat capacity [126], [127], the latter type is usually of higher initial costs [77]. However, the scarcity of water in arid regions forces the users to limit their usage of water to the lowest necessary quantities. A small water requirement in the case of CSP is used for the mirror washing (1.4%). This cannot be replaced (air cleaning is less effective and is not available in the SAM), while the biggest amount of water is for the heat rejection at the condenser (90%) [128] and can be replaced by using an air-cooled condenser which uses air for heat rejection despite not being as great conductor [129]. A hybrid condenser option including both wet and dry condensers mounted in parallel can take

the advantage of the wet-cooled side's better heat rejection as well as the lower water consumption of the air-cooled side.

In a conventional Rankine cycle based on a dry cooled condenser, the only variable that has an effect on the cycle performance is the dry bulb temperature (T_d). The efficiency of the dry cooled cycle is shown as follows [130]:

$$\eta_d = -0.1468\, T_d + 22.526 \tag{2-21}$$

In addition, as the difference between the wet and dry bulb temperatures depends on the humidity in the air (wet and dry bulb temperature are equal at 100% humidity [131]), in the wet-cooled condenser cycle, both dry bulb temperature and the relative humidity are of importance and considered in the wet-cooled cycle as follows:

$$\eta_w = a(\phi) T_d + b(\phi) \tag{2-22}$$

Where ϕ is the relative humidity, a and b which are the wet efficiency coefficients can be obtained as follows [130]:

$$a(\phi) = -0.102\, \phi - 0.0684 \tag{2-23}$$

$$b(\phi) = -0.305\, \phi + 24.26 \tag{2-24}$$

The SAM enables the user assigning the temperature at which the power cycle is supposed to operate at its rated efficiency, i.e. the ambient temperature at design. The latter must be a dry bulb temperature in the case of air-cooled condenser, and a wet bulb temperature in the case of wet-cooled condenser [130], [132]. In this work, the design temperatures shown in Table 2-2 are the average wet/dry bulb temperatures from March to September and they are taken from the weather file as it is the period at which CSP are expected to deliver its highest production [75].

Several researchers have observed an efficiency drop in the power block with air-cooled condenser at temperatures above 32 °C and a serious efficiency drop at temperatures above 37 °C [76]. Thus, here the hourly scheduling set up in the SAM system control has been automated in accordance with the monthly averaged dry bulb temperature of the weather file. As in the case when the temperature is below 32°C (or 37 °C), the air-cooled side of the hybrid condenser is activated, while in the case when the temperature is higher than 32°C (or 37 °C), the wet-cooled side is activated. Two different scenarios have been initially considered based on the latter

reference temperatures, i.e. wet-cooled side activated in months with average temperatures equal or above 32 °C and wet-cooled side activated in months with average temperatures equal or above 37 °C.

The hot arid climate of Kuwait resulted in only two months (July and August) having a monthly average temperature higher than 37 °C, which represents 17% of the year time. The second scenario is based on activating the wet-cooled side of the condenser in case the monthly temperature averages are higher than 32 °C and this has been found in five months (May to September) which represent 42% of the year. However, the inclusion of the entire month is misleading as some temperatures drop over the night of the above-mentioned months have been observed, and this is shown in Figure 2-10.

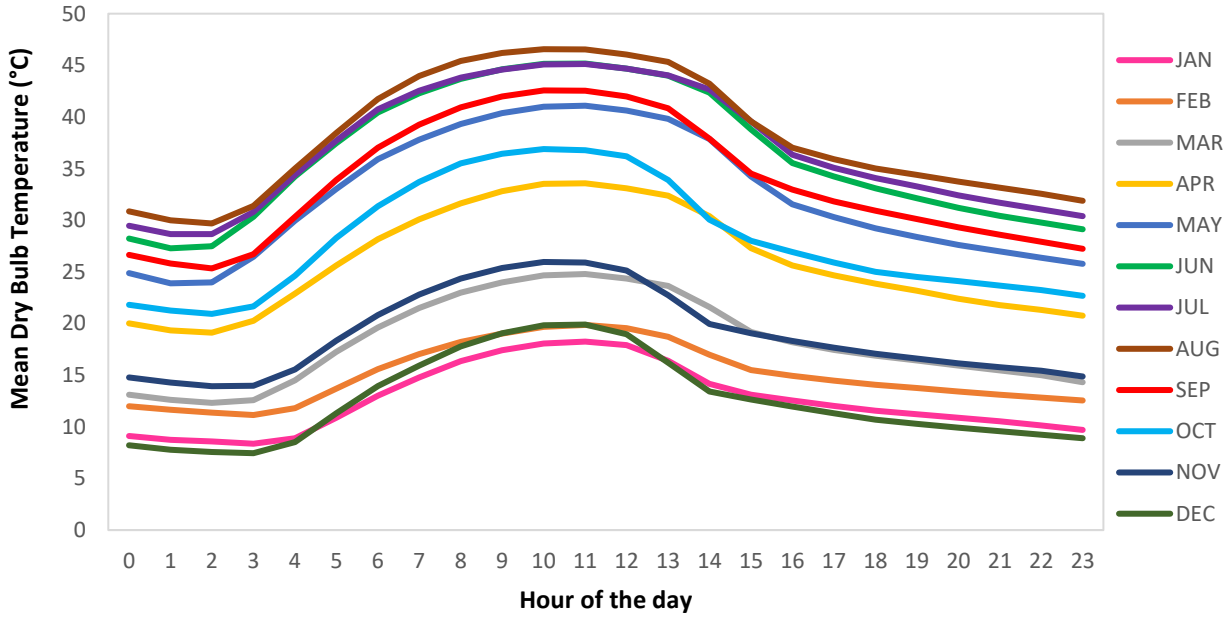

Fig. 2-10. Monthly averaged dry bulb temperature at Shagaya, Kuwait.

Thus, for a more accurate simulation, the system control has been set based on each hourly averaged temperature for each month and this is shown in Figure 2-11, which results in having only 19% of the temperatures above 37 °C while 30% are higher than 32 °C, hence the hybrid scenarios are named accordingly. In Figure 2-11, the digit 1 indicates when the wet-cooled side activation, while the digit 2 indicates the activation of the air-cooled side of the hybrid condenser.

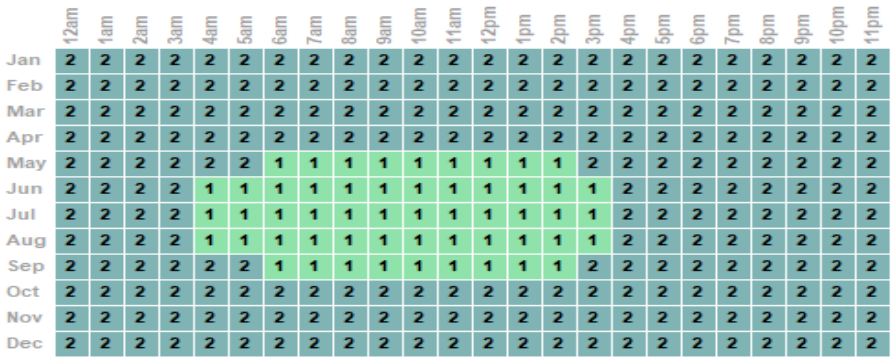

(a)

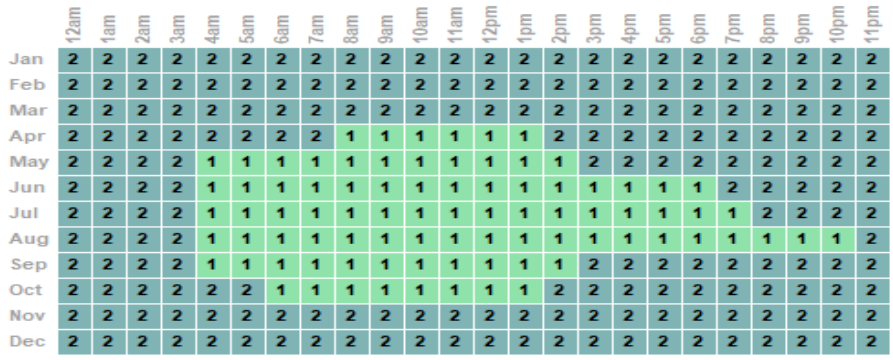

(b)

Fig. 2-11. The SAM hybrid condenser system control for (a) the 19% hybrid scenario and (b) the 30% scenario.

2.2.2.5 AOD Temporal Resolution Variation

Despite the integration of the aerosols effect in the solar field mentioned in the SAM atmospheric attenuation section, the polynomial coefficients are still based on a yearly averaged AOD value. This is because it is the conventional set up in the SAM, as well as all other RE simulation tools and this is not the temporal resolution that has been recommended by lead researchers, i.e. sub two days [59], in order to avoid the effect of the high spatiotemporal variability of the aerosols, especially for arid regions. This has led Polo et al. [49] to use the Polo model (equation 2-13) but with an automation applied on the SAM. The authors performed the automation with the assist of the SDK tool, which is offered by the SAM, and this enabled the simulations to be performed based on the number of AOD values, i.e. 12 and 365 (for monthly and daily AOD resolutions). This process creates 12-365 polynomials, hence a similar number of

solar field attenuation scenarios for the same solar field. The current research has followed a similar methodology but with an automation performed by the LK scripting language rather than the SDK. The former permits the user of automating the SAM from the inside of the SAM simulation core and this has been chosen because of the variety of the already built in functions that it contains in addition to the pre-defined variables that the user can output and comment upon.

The LK script enabled the SAM to be operated with daily AOD values from the assembled TAY, as presented in the Section 3.1.2, in order to evaluate the effect of the temporal resolution variation of the AOD on the SPT performance. To this extent, no finer resolution than daily is considered here. As it is demonstrated in [59], an AOD resolution of up to two days is acceptable to be taken into account in arid regions such as that of Kuwait, in order to avoid any possible over/underestimation ambiguity that occurs when coarser temporal resolutions are adopted. For instance, hourly resolution is excluded here as it has not been proven to have a significant effect on the attenuation; on top of this, it comes with a significant computational penalty (in terms of time). Hence, 365 runs have been carried out for each of the 19 optimal TES-SM combinations, i.e. 6935 for each condenser type.

It is worth mentioning that the script does not change the nature of the simulation in the SAM (yearly simulation) but runs a number of simulations to the desired temporal resolution, i.e. 365. The total outcome is basically 365 years of simulation, each of which has been run with a daily value of the AOD as obtained from the TAY. The script considers an AODi and this corresponds to day = i from the TAY and used for the SAM simulation to produce a daily outcome of an entire year (O_{year_i}). The total AEG of the script is a summation of the daily outcomes of each corresponding day i in each O_{year_i} from each simulation. For instance, day 1 of the AOD data in the TAY is automated to generate a first yearly simulation (O_{year_1}), from which the first day's energy generation is counted as the first day's outcome (O_{day_1}) of the daily AOD based script. Then the second day's energy generation of the second yearly simulation (O_{year_2}) is counted as the next daily outcome (O_{day_2}) of the daily AOD script thus forming a yearly outcome of the daily basis ($\sum O_{day\_i}$) based on the i number of the AOD values as it is illustrated in the flowchart of Figure 2-12.

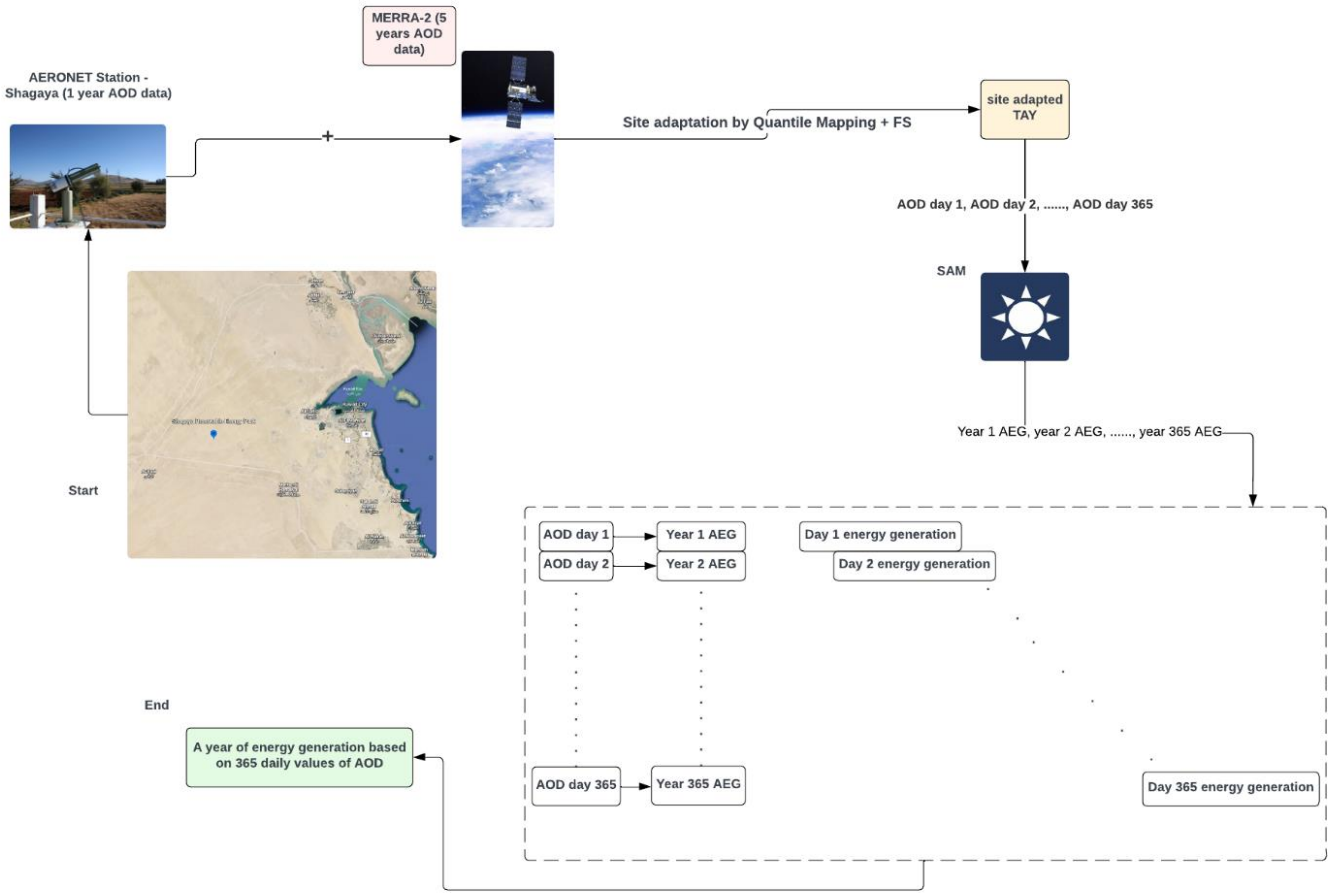

Fig. 2-12. AOD temporal variation methodology.

2.3 Results & Discussion

2.3.1 SPT Model Validation

Initially, the 50 MW SPT model used in this work has been validated. The validation process has been accomplished using the data derived from Soomro et al. [133] as it is one of the few published data of a similar model and capacity. The results have been compared against the air-cooled scenario in two locations and they produce a maximum deviation of 8.8% (found in the LCOE) and this is most probably due to the differences in the weather files and the possible differences in the financial assumptions used in the simulations processes. Table 2-3 illustrates the comparison of both simulations.

Table 2-3. The validation process of the SPT model against [133] in Quetta and Peshawar.

Parameters	Quetta [133]	Our model results for Quetta	Deviation (%)	Peshawar [133]	Our model results for Peshawar	Deviation (%)
Annual Energy Generation (GWh)	209.80	214.03	+ 2.1	124.09	131.12	+ 5.66
Capacity Factor (%)	53.2 %	54.3	+ 2.06	31.5	33.3	+ 5.71
Cooling water requirements (m^3/year)	38,273	39,837	+ 4.8	32,241	34,158	+ 5.94
LCOE (¢/kWh)	11.43	10.78	- 5.68	19.06	17.38	- 8.81

The validation process has been limited to being performed only based on simulated data as no commercial scale SPT published data of the same capacity is available in the literature. The validation against the data of Soomro et al. [133] has been carried out at the same locations that they have examined, i.e. Quetta and Peshawar. In addition, a further step in the validation has been accomplished in order to further assess the tool's suitability. This second step of validation has been performed against the official published data of the 19.9 MW Gemasolar SPT in Spain [134] and this produced a maximum deviation of 5.1% as shown in Table 2-4.

Table 2-4. The validation of Gemasolar SPT.

	Our model results for Gemasolar	Reported data [134]	NREL validation [36]	Deviation (%)
Annual Energy Generation (GWh)	107.4	110	107.4	-2.4
Capacity factor (%)	70.4	74	70.4	-5.1
Cooling water requirements (m^3/year)	365,312	-	368,347	-
LCOE (¢/kWh)	18.48	-	-	-

In addition, the Polo model [60] has been validated in terms of the linearity with an increasing range of AOD values (Appendix A). The objectives of this work can be conducted with confidence as in despite of the different weather data, the deviation between the obtained results of this work against both commercial scale and published simulated data does not exceed 5.9% for the technical outputs which falls into the acceptable range as illustrated in [61].

2.3.2 Preliminary Performance and Techno-Economic Assessment

By conducting a TES-SM parametric analysis, an optimal SM value is located for each TES capacity over the designated range (0-18h) based on the lowest LCOE value and that is for each power block configuration based on different scenarios in the condenser types. The LCOE is an economic evaluation indicator that decision makers take into consideration in order to compare the plant economic performance with other similar RE, or even fossil fuel plants, as it is simply the cost of each produced kWh, and it is considered as a figure of merit for the economic viability of a plant [135].

Three power block condenser types are investigated: water-cooled, air-cooled and hybrid condensers, with the latter being examined under two different set ups: a hybridization by 30% and 19% wet cooling. It should be noted that the SAM's only set up for the hybrid condenser option is in a parallel arrangement with which the user has the ability to set up which side of the condenser is activated on an hourly schedule basis for the entire year [132]. This advantage has been used in this research based on the dry bulb temperature of the used weather file.

2.3.2.1 AEG results

In order to observe the integrated effect of the solar field size and TES capacity variation effect on the various techno-economic outputs of the plant, the SM has been varied from 1 to 4 and that is for each TES capacity from 0h to 18h. The variation effect is illustrated on the AEG, the water consumption and the LCOE in Figures 2-13, 2-14 and 2-15.

As for the AEG, the increase of the SM implies an increased quantity of the collected sun irradiance, thus more generated energy as shown in Figure 2-13. The difference in the generated energy is minimal at zero storage capacity and this is only very clear as the TES increases. This is because an oversized solar field is limited in the case where no or very small TES is adopted. The

proportional relation between the SM and the generated energy continues until the plant is operated at its rated capacity, after which the generated energy flattens out. It is worth noting that at higher values of SM (3.4-3.8), the generated energy is not very different. This indicates that the plant's solar field cannot be bigger as the resource irradiance will not be able to increase the generated energy accordingly. On the other hand, the Capital Expenditures (CAPEX) keeps increasing linearly as the solar field and the receiver increase in size, thus also the LCOE increases.

The variation of the TES capacity for lower values of SM has a limited effect on the AEG as seen in Figure 2-13. The SM of 1 scenario actually should not be effected by the increase in the TES capacity as a SM of 1 is only supposed at best to drive the plant at its rated capacity with zero excess heat. As the SM values increases, larger are the TES capacities and this starts to have an impact on the generated energy. The effect reaches a saturation-like trend at higher capacities of the TES due to the solar irradiance limitation.

As for the cooling option, the wet-cooled condenser is supposed to easily yield the highest AEG because of the better heat rejection at the power block, however this is not exactly the case here. The SAM evaluates each configuration's ability to achieve the rated capacity of the plant (50 MW in this investigation) at each hour and hence optimizes the solar field. Since the cycle efficiency in the air-cooled scenario is lower, the air-cooled condenser scenario needs a bigger solar field for the same TES and SM compared to the wet-cooled scenario. This shrinks the gap in the AEG between both scenarios; however, the wet-cooled scenario remains with a higher AEG by 6.7% compared to the air-cooled scenario.

In addition, it is also worth mentioning that the SAM considers the hybrid condenser mainly as an air-cooled scenario as the air-cooled side of the hybrid condenser is bigger than the wet-cooled side. Thus, the solar fields of the hybrid scenarios are very similar to the air-cooled ones at the same TES and SM. Consequently, the hybrid scenarios have both the advantages of a bigger solar field and a water heat rejection in the most critical operation times of the year, thus interestingly overcomes the AEG of the air-cooled scenario by 4.6% in the 30% hybrid scenario and by 4.4% in the 19% hybrid scenario.

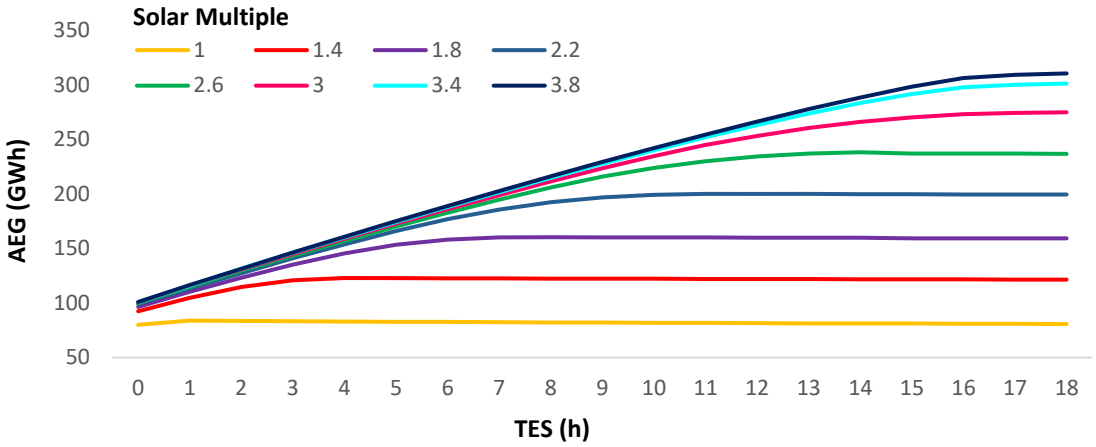
Solar Multiple
1
1.4
1.8
2.2
2.6
3
3.4
3.8
AEG (GWh)
350
300
250
200
150
100
50
0 1 2 3 4 5 6 7 8 9 10 11 12 13 14 15 16 17 18
TES (h)

(a)

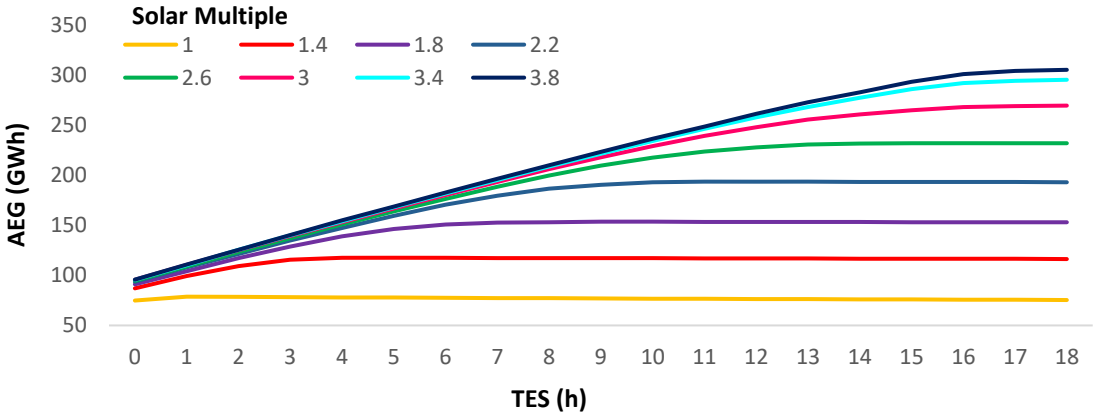
Solar Multiple
1
1.4
1.8
2.2
2.6
3
3.4
3.8
AEG (GWh)
350
300
250
200
150
100
50
0 1 2 3 4 5 6 7 8 9 10 11 12 13 14 15 16 17 18
TES (h)

(b)

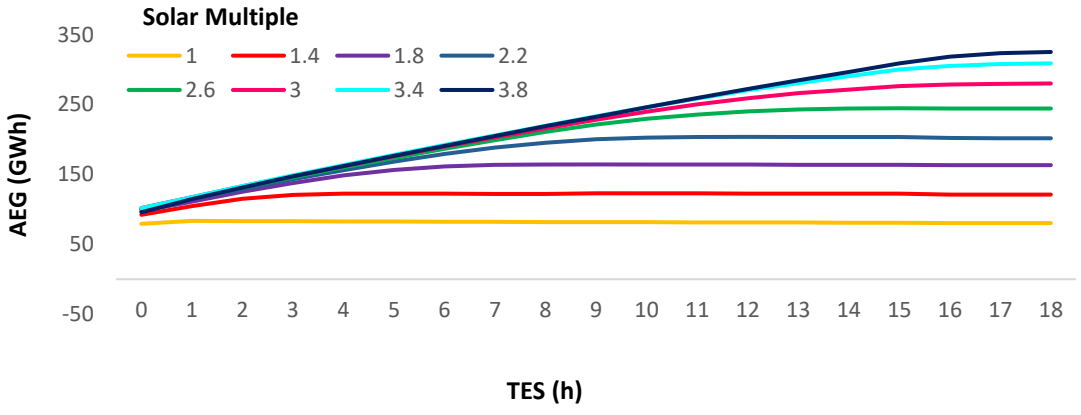
Solar Multiple
1
1.4
1.8
2.2
2.6
3
3.4
3.8
AEG (GWh)
350
250
150
50
-50
0 1 2 3 4 5 6 7 8 9 10 11 12 13 14 15 16 17 18
TES (h)

(c)

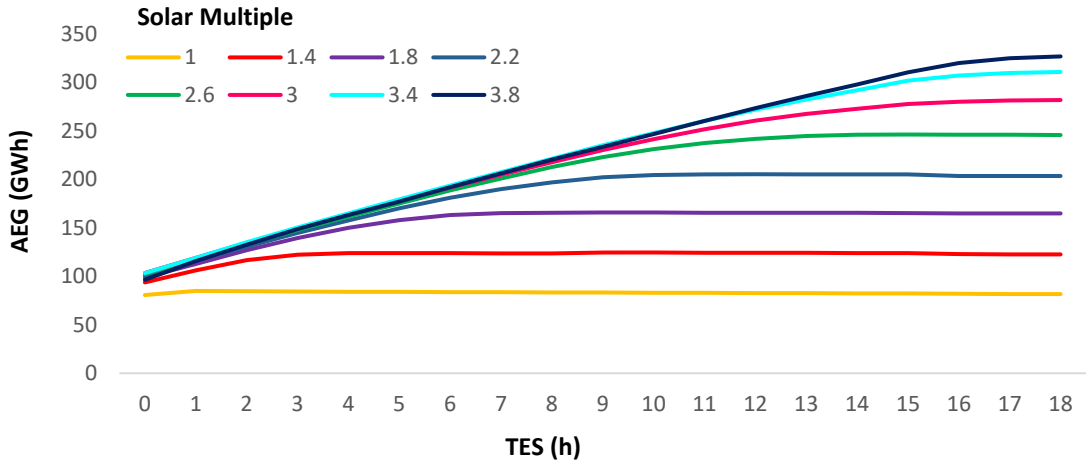

(d)

Fig. 2-13. The annual energy generation variation for the range of TES-SM of (a) wet-cooled condenser, (b) air-cooled condenser, (c) 19% hybrid condenser and (d) 30% hybrid condenser.

2.3.2.2 Water Consumption

The evolution of the water consumption is totally different as some scenarios use much less water than others. For instance, the gap in the water consumption between the different values of SM starts as being minimal and increases rapidly as the TES capacity increases in all the scenarios that involves the usage of water. Clearly, this is because at small TES capacities, the collected thermal energy of all the oversized SM values are wasted as no or too small TES is available. This means that less energy is transferred to the power block, hence there is less need of water for heat rejection. On the other hand, as the TES capacity increases, then bigger solar fields are of more use, and thus more thermal energy is transferred to the power block, which leads to more water consumption. This confirms the findings in the literature of the small percentage of the water being consumed in washing the solar field compared to that consumed at the power block. This is obvious in the air-cooled scenario shown in Figure 2-14 (b) as all the values of the water consumption in this scenario are of an almost fixed value as it is only for washing the solar field reflectors and the latter are of fixed areas for a single SM value no matter how large is the TES.

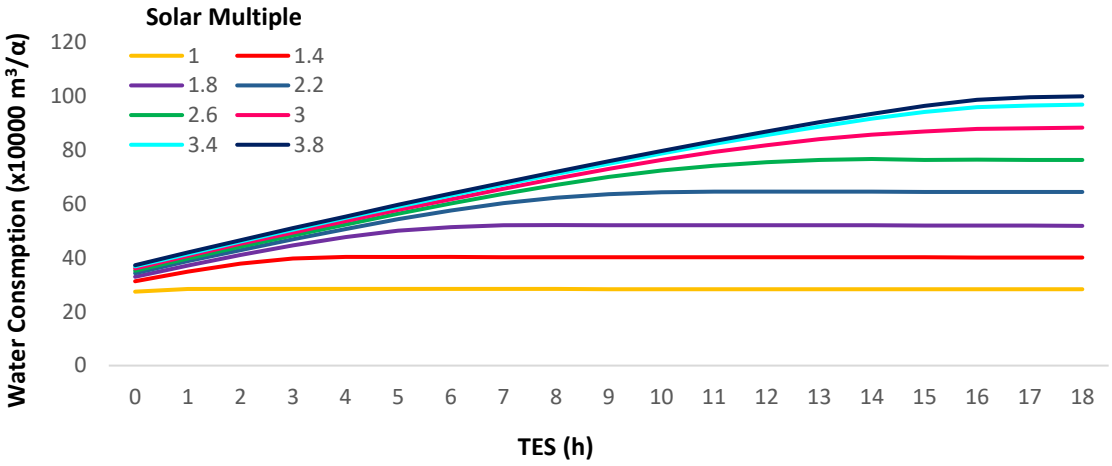
Solar Multiple
1
1.4
1.8
2.2
2.6
3
3.4
3.8
Water Consmption (x10000 m³/α)
120
100
80
60
40
20
0
0 1 2 3 4 5 6 7 8 9 10 11 12 13 14 15 16 17 18
TES (h)

(a)

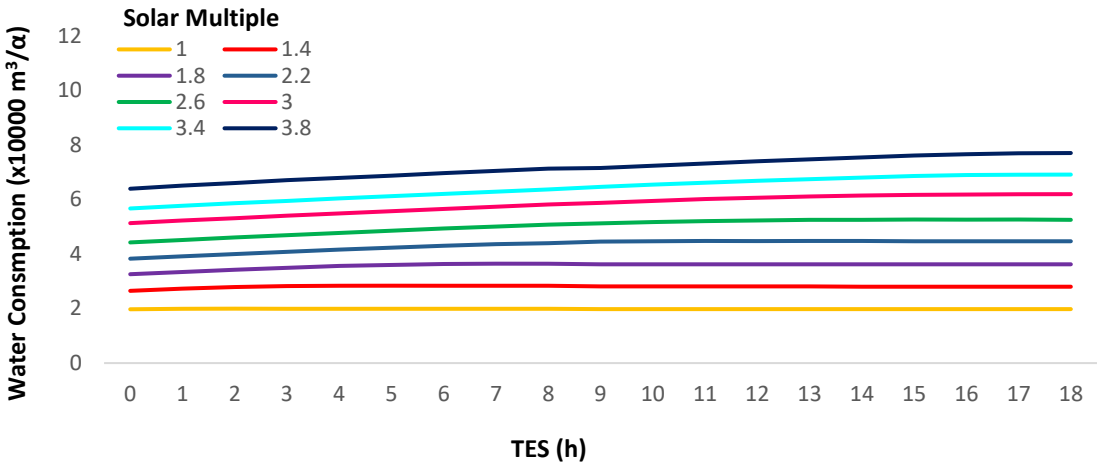
Solar Multiple
1
1.4
1.8
2.2
2.6
3
3.4
3.8
Water Consmption (x10000 m³/α)
12
10
8
6
4
2
0
0 1 2 3 4 5 6 7 8 9 10 11 12 13 14 15 16 17 18
TES (h)

(b)

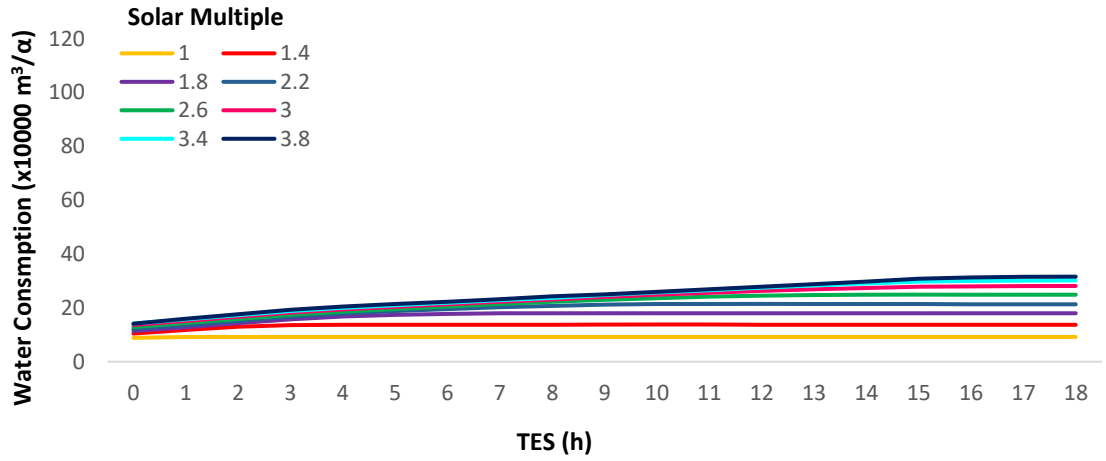

(c)

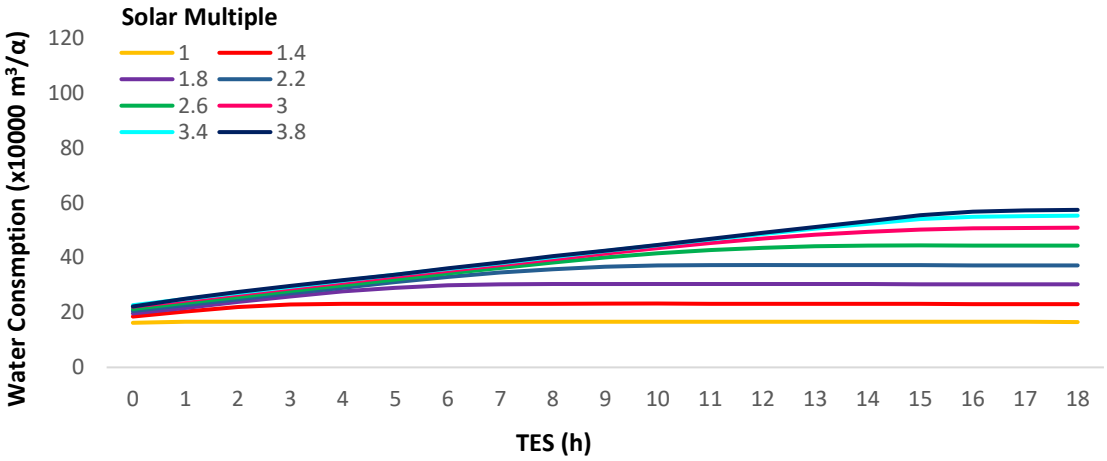

(d)

Fig. 2-14. The Water Consumption variation over the TES-SM ranges of (a) wet-cooled condenser, (b) air-cooled condenser, (c) 19% hybrid condenser and (d) 30% hybrid condenser.

However, the variation of the TES capacity has less effect on the water consumption as the latter is related to both TES and SM rather than to only one of them. For example, for smaller SM values, the water consumption is steady no matter how large the TES reaches. While for larger SM values, the water consumption appears to have a proportional relation with the TES. This is obvious in the wet-cooled condenser, as the latter is the most generating configuration due to the better heat rejection, hence the highest water consuming. In addition, this applies to the two other hybrid condenser configurations, however to a lesser extent. On the other hand,

the air-cooled configuration is almost unaffected by the variation of the TES capacity. This can be explained by the fact that although as much energy may be generated but there is no usage of water in the power block, which consumes 90% of the water at such plants. The water is only for heliostats washing.

The superiority in the AEG obtained in the wet-cooled scenario over the air-cooled scenario is impaired with an elevated water consumption of 92.8% as shown in Figure 8. This can be critical as the water transport to an arid region can sometimes be logistically very difficult. However, it cannot be entirely eliminated as the plant still needs water for other purposes, which makes the hybrid scenario an interesting consideration as it presents a trade-off between the AEG and the water consumption. To this extent, the 30% hybrid scenario resulted in a decrease of 55.1% in the water consumption compared to the wet-cooled scenario, while the 19% hybrid scenario achieved a further decrease reaching 68.7%. Here, for a fair comparison between the four different configurations, the 15h scenario has been taken as the reference point for comparison as it yielded a similar value of SM for all configurations, i.e. 3.2.

Table 2-5. 50 MW SPT four power block condenser types performance comparison.

	Condenser Type			
	Wet-Cooled	Air-Cooled	30% Hybrid	19% Hybrid
Annual Energy Generation (GWh)	281.4	262.6	275.4	274.8
Deviation (%)	N/A	- 6.7	- 2.1	- 2.3
Water Consumption (m^3/a)	909,147	65,270	401,719	284,339
Deviation (%)	N/A	- 92.8	- 55.1	- 68.7

2.3.2.3 LCOE results

Similar to the AEG, the LCOE results show a similar trend for all the scenarios as depicted in Figure 2-15. The trend found in all scenarios shows that the LCOE for small values of SM begins at its minimal values and increases rapidly with the increase of the TES. Conversely, the higher values of SM begin at their highest LCOE and then decreases, reaching their minimal values at

higher TES capacities. Some values in the middle of the SM range start with a decrease, however they end up by increasing again at the highest TES capacities. This trend occurs because for high values of TES and SM, the plant stores all the potential irradiance as excess heat in the TES, which is used at night and this reflects in the higher generated energy and lower LCOE. However, a further increase in the TES capacity (beyond 16-17h for instance) is useless as the solar field size required in order to store the excess heat for 18 full load hours would be too big to be economical. This explains the rise of the LCOE after a certain point for the same SM value.

In general, lower values of LCOE are obtained in the wet-cooled scenario as the latter is of higher generation and lower capital costs compared to the air-cooled situation. This applies to the hybrid scenarios, however to a lesser extent as the lower LCOE values obtained in these two configurations are also a result of a better heat rejection, hence more energy generation in addition to the smaller air-cooled side in the hybrid configuration (compared to a fully sized air-cooled condenser).

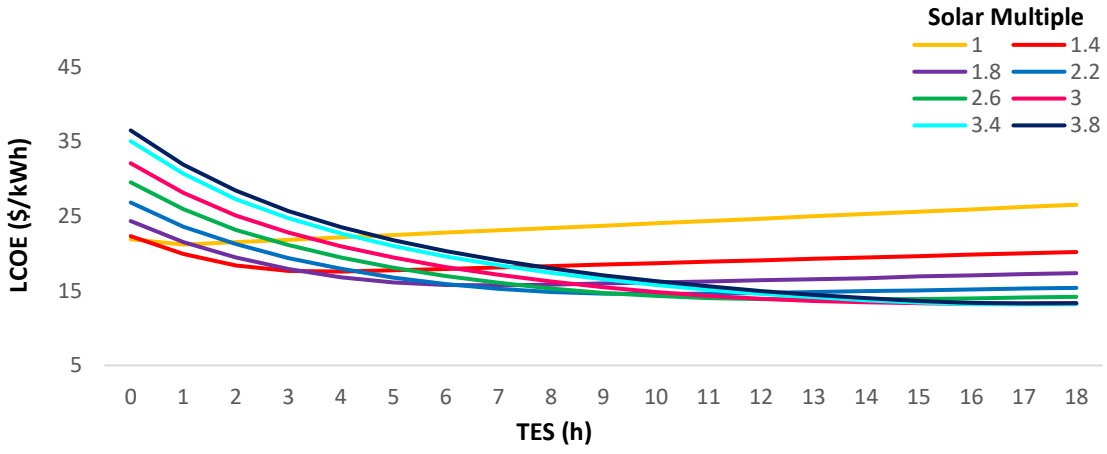

(a)

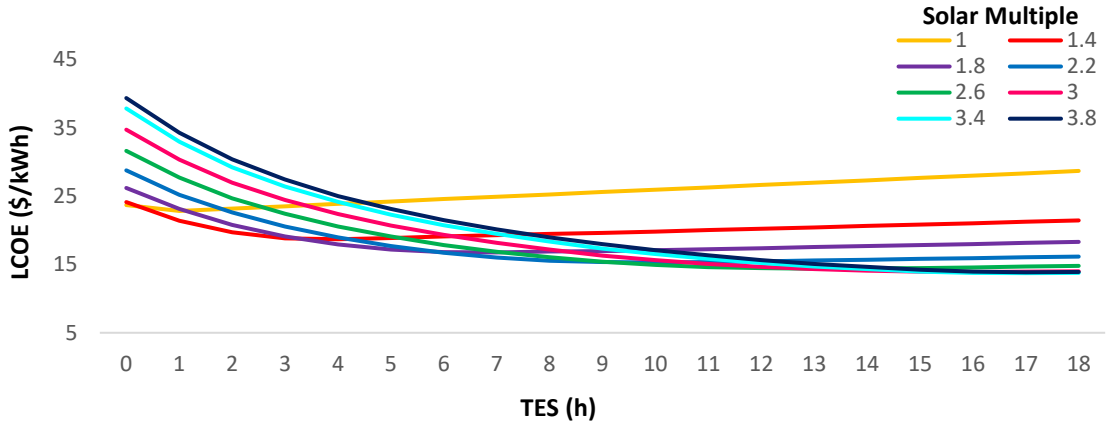

(b)

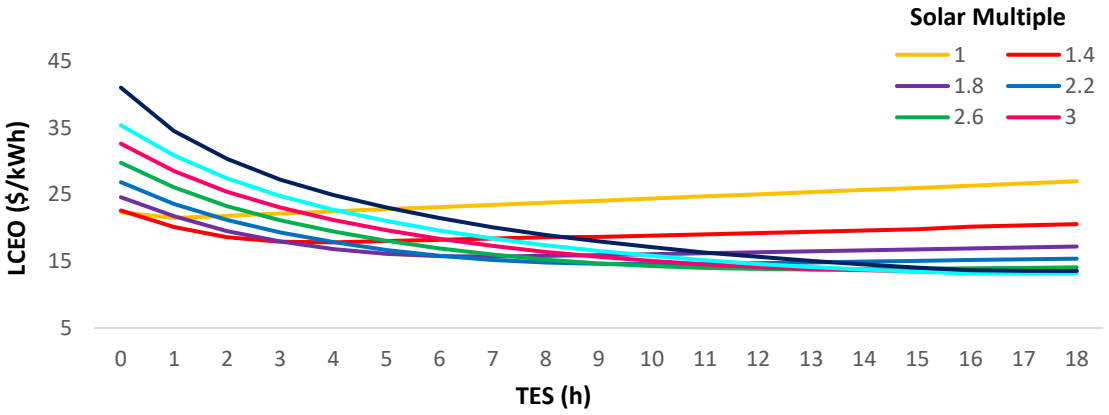

(c)

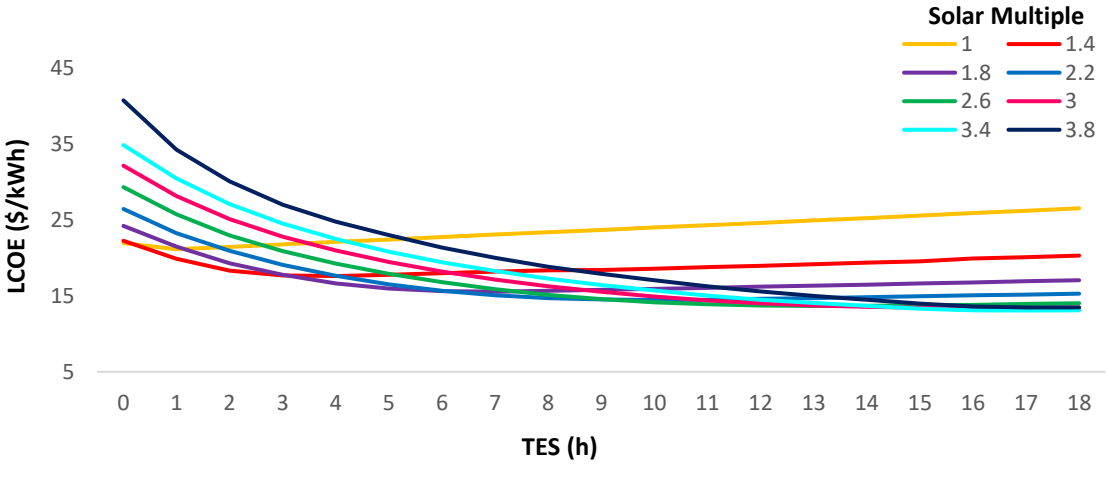

(d)

Fig. 2-15. The LCOE variation over the ranges of TES and SM for (a) wet-cooled condenser, (b) air-cooled condenser, (c) 19% hybrid condenser and (d) 30% hybrid condenser.

This finding can be an indication for not having to further increase both the TES and SM. The relation between the LCOE, CAPEX, Operational Expenditures (OPEX) and the AEG is given as follows [136]:

$$LCOE = \frac{CAPEX_0 + \sum_{t=1}^{N} \frac{OPEX_t}{(1+\mathrm{i})t}}{\sum_{t=1}^{N} \frac{Production_t}{(1+\mathrm{i})t}} \quad (2\text{-}25)$$

where $Production_t$ is the plant production in year t (AEG). Some of the results in the literature have shown that there are more critical outputs as the LCOE increases sharply after reaching its minimum value with the continuous increase of TES and SM [61], [66], [137]. In this case, an increase in TES and SM is not recommended. However, the findings in this work indicates that the increase in TES and SM is left to the decision makers based on whether it is acceptable to increase the CAPEX for a minor increase in the power generation at the same/slightly higher LCOE levels. Here, the most optimal TES-SM combination has been found at the wet condenser configuration with a LCOE of 12.78 (¢/kWh) with a TES of 16h and a SM of 3.2.

2.3.3 AOD Temporal Resolution Variation Effect

This section examines the difference in the SPT outputs based on the conventional set up of the SAM compared to the recommended AOD temporal resolution in arid regions, i.e. the daily AOD. A water consumption analysis is excluded here as the SAM is limited to the output of the annual water consumption value, thus the concatenated daily outputs summation method presented in AOD Temporal Resolution Variation Section of the Methodology cannot be adopted in this section.

The outputs of the preliminary parametric analysis carried out in the Preliminary Performance and Techno-Economic Assessment Section has resulted in the optimal SM values for each TES capacity based on the lowest LCOE and that is for the four different condensers scenarios. For all four scenarios, all these optimal SM values are found in the range from 1.2 to 3.4. An increase in the SM values is actually an addition of new heliostats in the solar field. These new heliostats will all be placed at the outer circumference of the existing ones, which means that all newly added heliostats have an even larger slant range, thus are subject to a larger attenuation effect applied on the reflected sun irradiance that they are supposed to focus on the

receiver. This effect, alongside with the larger daily values of AOD (compared to the annual averaged value, i.e. 0.3205) can theoretically mask off a considerable portion of the reflected irradiance.

2.3.3.1 AOD Variation Effect on the Solar Field and the AEG

A very similar pattern can be found in all the four observed SPT configurations in terms of the effect of the daily AOD temporal resolution on: receiver incident thermal power, estimated receiver thermal power to the HTF and AEG. It has been found that the employment of the daily AOD results in a minor difference in the thermal power from the solar field (this does not exceed 1.1% and this is shown in Appendix B) in all the SM values over the designated range. Despite the gradual increase in the slant range, as a result of increasing the SM value, no substantial increase in the deviation of the thermal power from the solar field has been found. A linearity has been found in the latter range as the deviation increases gradually, however, close to the conventional solar field thermal power based on the annually averaged AOD value (0.3205). It has been found that no matter how large is the increase in the slant range for this specific plant's capacity in this case study location, the AEG is not substantially affected, which is most probably due to the other factors in the equation being not very important, e.g. the AOD intensity and/or AOD temporal variability.

Despite the limited effect of the daily AOD temporal resolution adoption, it would still be very critical in the case when such an investigation has not been done in such a region. That is why a comparison between both the annually averaged and daily AOD temporal resolutions has been carried out against the no aerosols scenario. Figure 2-16 (a) illustrates the latter effect uniquely on the daily energy generation for the optimal (lowest LCOE) wet-cooled configuration of 16h at SM of 3.2. In addition, it is also worth mentioning that this work has considered that the large TES capacity might play a role in the mitigation of the temporal resolution's variation effect, thus a similar examination has been carried out at the optimal TES-SM combination with a TES of 0h, as shown in Figure 2-16 (b).

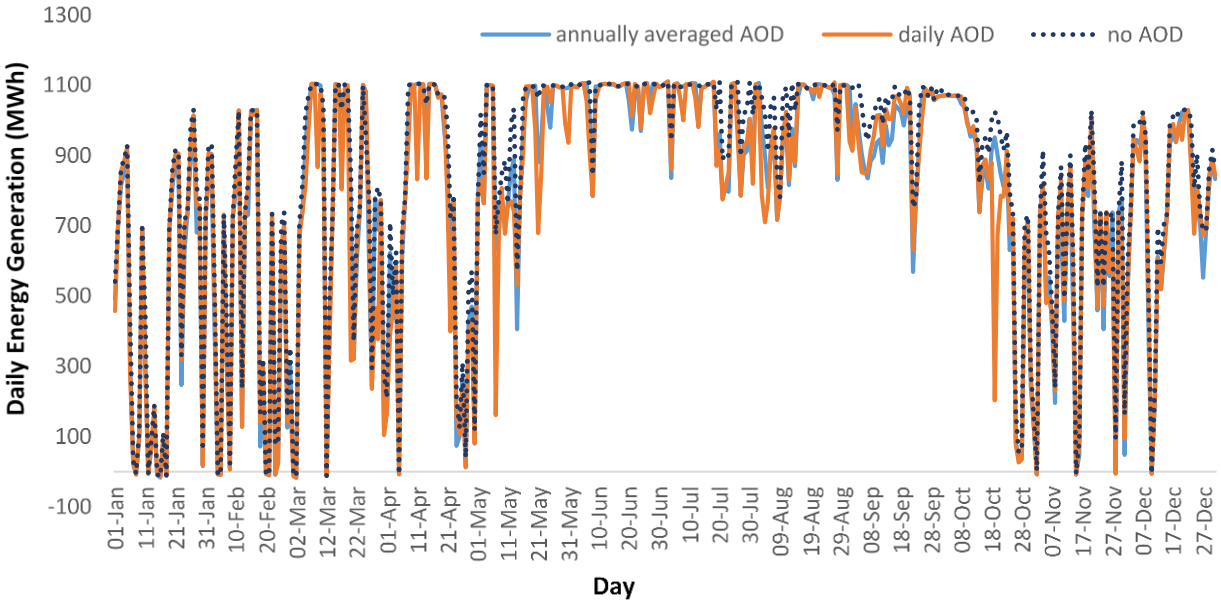

(a)

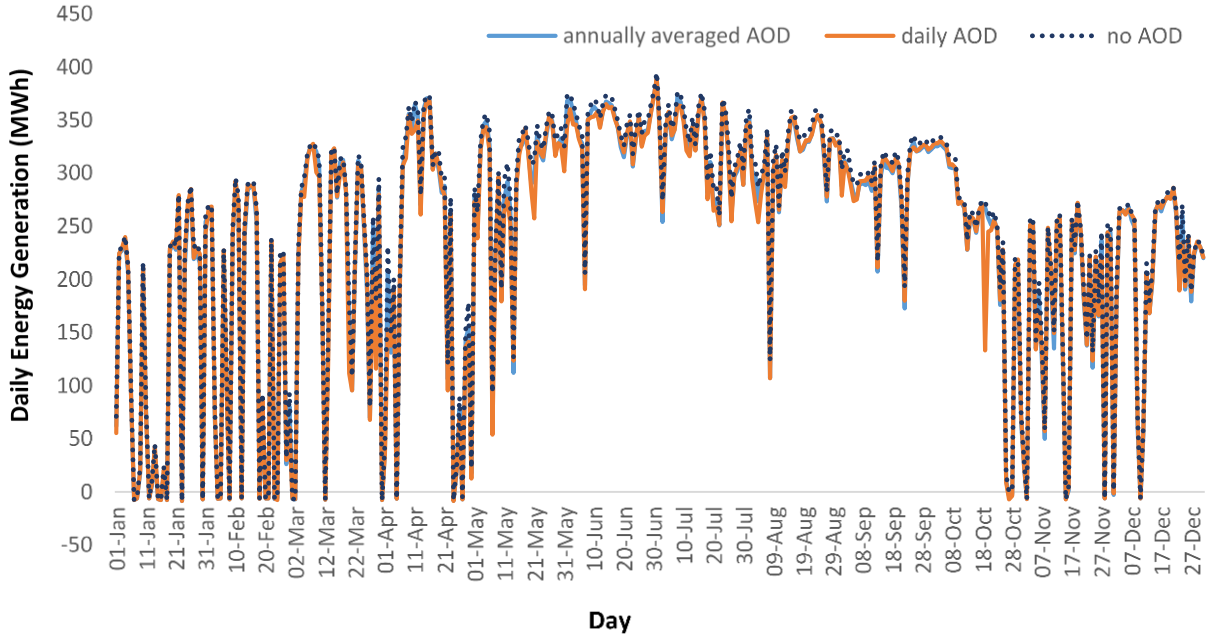

(b)

Fig. 2-16. The AOD temporal resolution variation effect on the daily energy generation for (a) 16h of TES and (b) 0h of TES.

In the 0 h TES scenario, the daily AOD temporal resolution resulted in a decrease of 0.6% in the AEG compared to the annually averaged AOD (0.3205) and a decrease of 3.7% compared to the no aerosols scenario. As for the 16h TES scenario, the daily AOD resolution yielded a

decrease of 1% compared to the annually averaged case, while a decrease of 6.7% has been obtained between the former and the no aerosols scenario. Clearly, it is seen that having a bigger solar field results in an elevated attenuation extinction, even in the case of having a large TES capacity such as the case examined here, i.e. 16h. Larger plants capacities, which have larger solar fields, will most probably have an amplified effect of aerosols even in the case when large TES are adopted.

Table 2-6 illustrates the effect of the aerosols inclusion in the SPT solar field and its consequences that are projected to the AEG and thus the LCOE for the wet-cooled scenario. From what is shown in the table, it is obvious that the effect is firstly detected in the shape of less thermal power from the solar, this effect also reaches the thermal energy that is absorbed at the receiver. The loss is also carried to final AEG which gives less values for all configurations and affects the LCOE which shows higher numbers as a result. Similar results for the three other condenser scenarios can be found in Appendix D.

Table 2-6. 50 MW wet-cooled condenser SPT technical outputs for each optimal SM over the TES range based on different aerosols scenarios.

TES (h)	LCOE ($/kWh)			SM (-)	Gross to net conversion factor (%)	CF (%)	No. of heliostats	Aperture Area (m^2)	Total power incident on the SF (MWh_{th})	Thermal power from SF (MWh_{th})		Total absorbed energy (MWh_{th})		Thermal energy to the PB (MWh_{th})	Thermal energy into the TES (MWh_{th})	Total water consumption (m^3/α)	AEG (kWh)			Overall efficiency (%)
	No aerosols	Annually averaged AOD	Daily AOD							Annually averaged AOD	Daily AOD	Annually averaged AOD	Daily AOD				No aerosols	Annually averaged AOD	Daily AOD	
0	20.49	21.14	21.24	1.2	90.5	22.3	2667	385,047.6	641,695.1	293,773.3	292,368.3	277,417.3	272,226.9	261,985.4	0	298,454	90,588,080	87,748,264	87,227,470.9	13.7
1	18.4	19.17	19.3	1.2	90.6	24.8	2674	386,058.2	643,649.9	320,744.5	318,729.8	277,970.8	275,633	288,192.4	31,905.03	326,793	102,100,600	97,901,864	97,123,566.6	15.2
2	17.21	17.85	17.95	1.4	90.8	29	3101	447,706.3	746,714.7	369,391.6	367,242.9	324,825.4	322,042.1	331,977.7	66,333.82	378,967	118,796,864	114,488,208	113,682,961.2	15.3
3	16.45	17.03	17.15	1.6	91	33.1	3623	523,069.9	872,522	414,098.6	411,283.3	370,803.8	367,286.9	373,993.1	102,013	429,835	135,158,960	130,451,536	129,350,985.9	15
4	15.52	16.32	16.41	1.6	91.1	34.8	3618	522,348	871,280.1	431,812.3	429,529.9	370,648.9	367,192.3	391,717.2	121,684.8	449,877	144,455,072	137,194,496	136,284,768.9	15.7
5	14.96	15.64	15.72	1.8	91.2	39.1	3990	576,055.5	960,545.4	484,745.2	482,417.2	420,618.1	416,663.9	436,958.1	168,890.2	503,441	161,345,376	154,147,136	153,194,705.1	16
6	14.57	15.18	15.29	2	91.3	43.1	4477	646,366	1,078,546	528,859.8	524,670.4	466,192.3	460,911.8	478,314.5	200,478.8	553,111	177,124,160	169,794,224	168,244,315.3	15.7
7	14.27	14.85	14.95	2.2	91.3	47	4950	714,655.5	1,192,865	574,210.3	570,023.7	512,793.8	507,101.6	519,743.9	239,160.1	602,930	192,934,480	185,301,056	183,734,792.7	15.5
8	13.74	14.44	14.52	2.2	91.4	48.7	4955	715,377.1	1,194,189	592,194.9	588,433.7	513,020.9	507,583.1	537,571.5	258,037.4	623,198	202,270,160	192,112,624	190,691,644.8	16.1
9	13.49	14.13	14.2	2.4	91.3	52.8	5386	777,602.7	1,297,274	640,579.6	636,678.7	561,507.4	555,343.9	580,740.9	299,490.9	674,518	218,324,816	208,152,688	206,726,982.7	16
10	13.08	13.84	13.91	2.4	91.3	54.1	5352	772,693.9	1,289,721	653,897.2	649,995.7	561,164.2	554,825.9	594,049.3	313,606.4	689,391	225,763,936	213,090,528	211,656,469.3	16.5
11	12.91	13.61	13.69	2.6	91.2	58.2	5790	835,930.1	1,395,102	704,547.8	700,006.7	609,450.5	602,322.2	638,718.4	356,842.5	742,462	242,377,712	229,577,840	227,666,453.5	16.5
12	12.72	13.36	13.45	2.8	91.2	62.1	6193	894,113.1	1,492,446	749,472.1	744,124.6	655,693.6	647,505.4	680,190.4	397,281.6	791,599	257,807,072	244,975,680	242,724,818.3	16.4
13	12.47	13.23	13.33	2.8	91.3	63.5	6256	903,208.7	1,507,698	764,096.4	759,244.8	656,482	648,621.8	694,425	411,908.3	808,277	266,038,496	250,473,440	247,960,235.2	16.6
14	12.34	13.04	13.13	3	91.1	67.4	6659	961,391.8	1,604,822	809,247.4	803,371.1	701,849.6	292,901.6	735,913.3	452,804.5	857,748	281,159,776	265,576,208	262,996,526.3	16.5
15	12.22	12.91	13	3.2	91.1	71.4	7224	1,042,963.6	1,741,283	852,480.5	846,273.1	747,044.8	737,653.4	778,019.9	493,873.4	909,147	297,750,400	281,368,416	278,655,503.8	16.2
16	12.06	12.78	12.87	3.2	91.3	73.1	7223	1,042,819/2	1,740,274	866,384.7	861,100.9	750,737.3	741,529.5	788,652.3	505,039.9	926,835	305,831,616	288,012,320	285,203,004.7	16.5
17	12.16	12.83	12.92	3.4	91.3	76.1	7760	1,120,348.4	1,871,022	897,231.7	891,215.1	795,572.2	785,182.4	818,105.8	533,241.3	966,321	317,011,488	300,073,536	297,232,372	16
18	12.19	12.86	12.96	3.4	91.3	76.4	7764	1,120,925.9	1,871,903	899,819.4	894,583.1	795,693.5	785,303.4	820,257.8	535,694.6	969,583	318,202,208	301,133,696	298,104,762.3	16.1

Another very important finding is that despite the limited percentage of AEG decrease after examining the plant under the daily AOD resolution, the plant still has a considerable percentage of deviation in the daily energy generation on specific days as the solar field is affected substantially on some aerosols peak days. Figure 2-17 illustrates how the solar fields of the two configurations presented in Figure 2-16 are affected on specific days based on different aerosols scenarios.

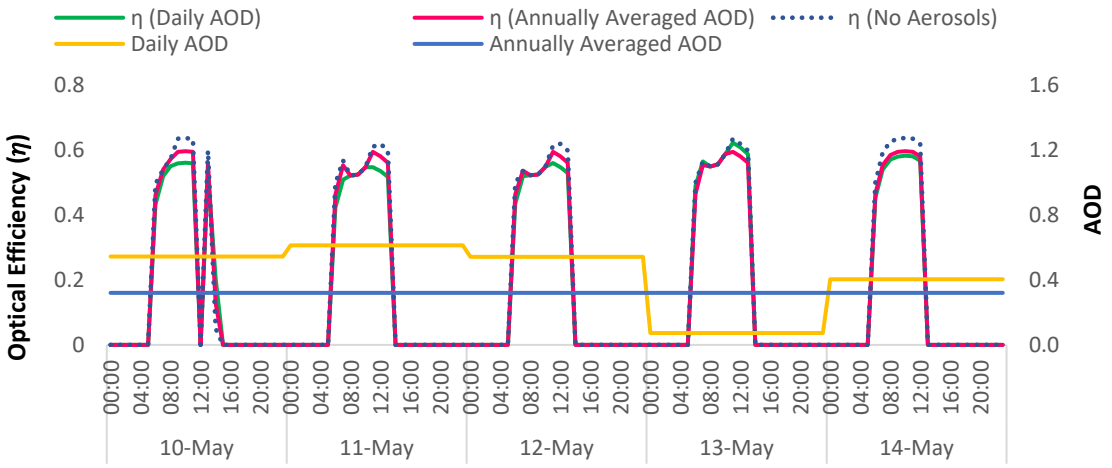

(a)

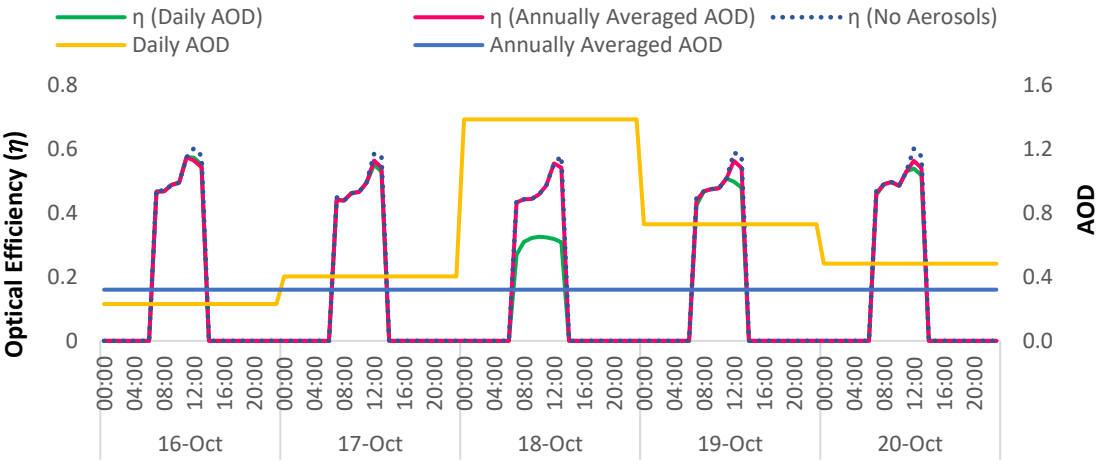

(b)

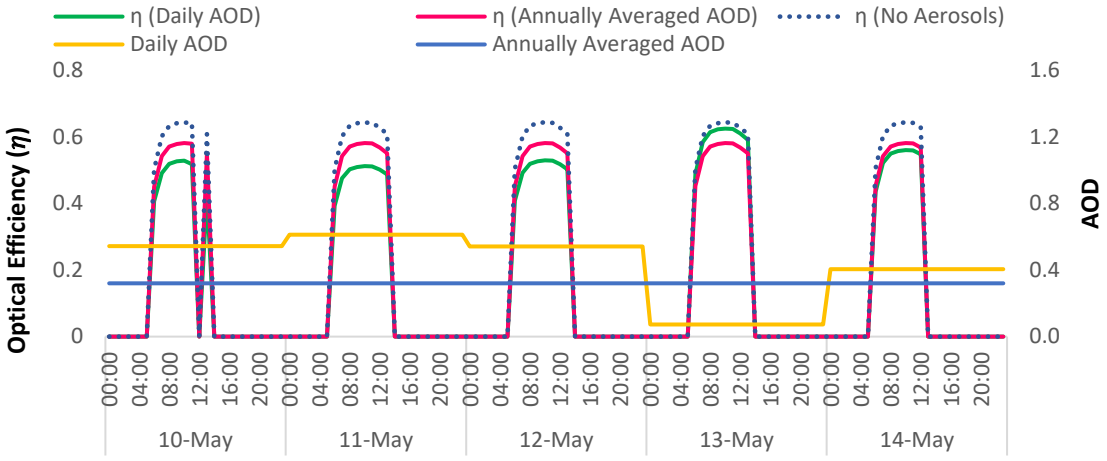

(c)

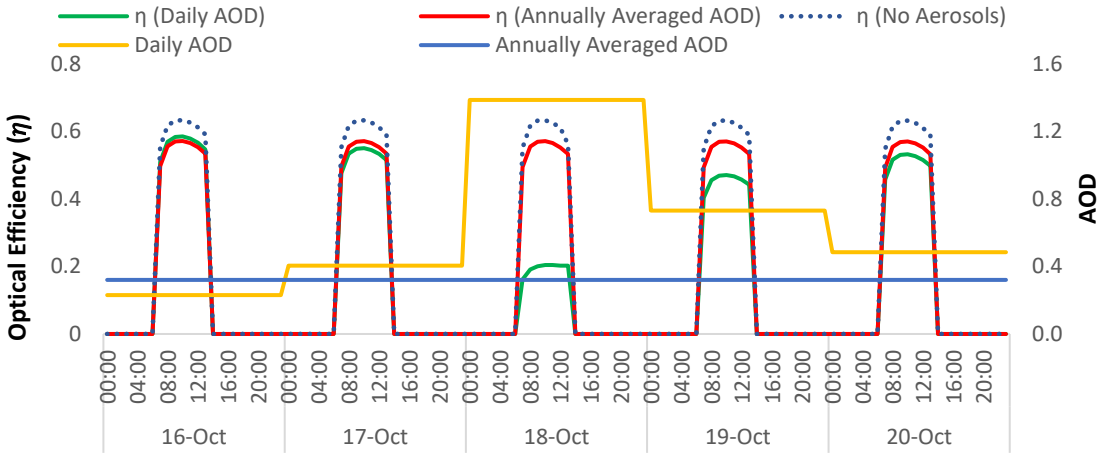

(d)

Fig. 2-17. The solar field optical efficiency based on different scenarios for (a) and (b) the 0h TES and the 16h TES in (c) and (d).

Due to some abnormally elevated AOD daily values, which are most likely caused by dust storms, the daily energy generation on some days of the year witnesses a more considerable deviation. Depending on the TES-SM scenario, the daily energy generation of an aerosols dense day (18th of October on a 16h and SM 3.2 wet-cooled configuration for instance) can be overestimated by 77.8% as the annually averaged AOD simulation results in 912.1 kW, while based on the daily AOD, the same simulation only gives 202.1 kW. This signifies how the daily AOD case can give a better estimation of the daily generated energy, thus better estimation of the SPT' daily energy delivery commitment to the grid. This finding is very important for the grid control purposes as it can be used for the plant daily energy generation forecast work.

2.3.3.2 AOD Effect on the LCOE

The deviation of the solar field thermal output due to the adoption of different temporal resolutions translates into a deviation in the absorbed thermal energy to the HTF and finally to a deviation also in the AEG as seen in the last section. This will of course influence the LCOE as the latter is directly related to the AEG, as shown in equation 2-25. However, since the deviation in the AEG has been insignificant, the same trend is expected for the LCOE. Each optimal SM value is located for each TES capacity based on the lowest value of the LCOE and this presented in Table 2-7, which initially illustrates the evolution of the AEG, capacity factor and the LCOE based on the annually averaged AOD value (0.3205), and then compares these outputs against those of the no aerosols and daily AOD scenarios.

Table 2-7. The 50 MW SPT optimal TES-SM outputs based on the annually averaged AOD and compared to different aerosols temporal resolutions: No aerosols[1] and daily AOD[2].

Condenser Type	Wet				Dry			
TES (h)	Optimal SM (-)	LCOE (¢/kWh)	AEG (GWh)	CF (%)	Optimal SM (-)	LCOE (¢/kWh)	AEG (GWh)	CF (%)
0	1.2	20.49[1]	90.6[1]	22.3	1.2	23.15[1]	80.7[1]	19.8
		21.14	87.7			23.94	77.9	
		21.24[2]	87.2[2]			24.07[2]	77.5[2]	
3	1.6	16.45[1]	135.2[1]	33.1	1.6	18.32[1]	122.5[1]	30
		17.03	130.5			18.97	118.2	
		17.15[2]	129.4[2]			19.09[2]	117.3[2]	
6	2	14.57[1]	177.1[1]	43.1	2	16.2[1]	162.4[1]	39.4
		15.18	169.8			16.9	155.4	
		15.29[2]	168.2[2]			17[2]	154.3[2]	
9	2.4	13.49[1]	218.3[1]	52.8	2.2	14.75[1]	192.7[1]	45.8
		14.13	208.2			15.72	180.6	
		14.2[2]	206.7[2]			15.81[2]	179.2[2]	

[1] No Aerosols
[2] Daily AOD

12	2.8	12.72[1]	257.8[1]	62.1	2.8	14[1]	239.6[1]	57.6
		13.36	244.9			14.75	226.9	
		13.45[2]	242.7[2]			14.85[2]	224.9[2]	
15	3.2	12.22[1]	297.8[1]	71.4	3.2	13.41[1]	278.5[1]	66.6
		12.91	281.4			14.2	262.6	
		13[2]	278.7[2]			14.3[2]	260.2[2]	
18	3.4	12.19[1]	318.2[1]	76.4	3.2	13.23[1]	285.9[1]	68
		12.86	301.1			14.08	268.2	
		12.96[2]	298.1[2]			14.2[2]	265.2[2]	

Condenser Type	30% Hybrid				19% Hybrid			
TES (h)	Optimal SM (-)	LCOE (¢/kWh)	AEG (GWh)	CF (%)	Optimal SM (-)	LCOE (¢/kWh)	AEG (GWh)	CF (%)
0	1.2	21.56[1]	87.1[1]	21.3	1.2	21.68[1]	86.6[1]	21.2
		22.3	84.5			22.43	83.7	
		22.42[2]	83.6[2]			22.55[2]	83.1[2]	
3	1.6	17.17[1]	131.2[1]	32	1.6	17.35[1]	130.3[1]	31.9
		17.78	126.6			17.97	125.7	
		17.89[2]	125.6[2]			18.08[2]	124.8[2]	
6	2	15.2[1]	172.5[1]	41.8	2	15.3[1]	171.5[1]	41.6
		15.87	164.9			15.97	164.1	
		15.96[2]	163.8[2]			16.06[2]	162.9[2]	
9	2.4	14.08[1]	213.1[1]	51.3	2.4	14.17[1]	211.8[1]	51.2
		14.76	203.1			14.86	201.8	
		14.85[2]	201.5[2]			14.95[2]	200.2[2]	
12	2.8	13.35[1]	251.8[1]	60.5	2.8	13.44[1]	251.3[1]	60.5
		14.03	239.2			14.14	238.6	
		14.13[2]	236.9[2]			14.24[2]	236.3[2]	

15	3.2	12.82[1]	291.2[1]	69.9	3.2	12.83[1]	290.9[1]	69.7
		13.54	275.2			13.56	274.8	
		13.64[2]	272.5[2]			13.65[2]	272.2[2]	
18	3.2	12.77[1]	310.4[1]	71.7	3.4	12.8[1]	308.8[1]	74.1
		13.47	293.7			13.5	292.2	
		13.58[2]	290.6[2]			13.6[2]	289.3[2]	

A maximum increase of 6.8% has been observed in the LCOE when the daily AOD is adopted compared to the no-aerosols scenario. This in turn qualifies the SPT technology to be suitable in this specific location and the 50 MW plant capacity. The aerosols are one of the most important factors that threats the success of such a technology and the estimated small effect on both the AEG and the LCOE suggest that there exist good prospects for potential future applications. Further, the techno-economic outputs of multiple commercial and simulated CSP plants of the same capacity have been compared against the results of the daily aerosols scenario of this work as shown in Table 2-8.

Table 2-8. Comparison of the modelled results in this work with both commercial and modelled 50 MW CSP plants.

Project Name/ Publication	**Location**	**Site Annual DNI (kWh/m²)**	**CSP Type**	**Condenser Type**	**TES capacity (h)**	**Capacity Factor (%)**	**LCOE (¢/kWh)**	**AEG (GWh)**
Termesol 50 [138]	Spain	2097	PTC	Wet Cooling	7.5	40	-	175
Andasol 3 [43]	Spain	2200	PTC	Wet Cooling	7.5	40	-	175
La Africana [43]	Spain	1950	PTC	Wet Cooling	7.5	39	-	170
Hirbodi et al. [66]	Iran	-	PTC	Wet Cooling	15	73.9	14.6	320.4
				Air Cooling	15	73.5	15.2	318.6
			SPT	Wet Cooling	15	86.6	12.3	375.5
				Air Cooling	15	85.7	12.6	371.5
Sultan et al. [61]	Kuwait	1857	PTC	Air Cooling	16	60.4	15.07	238.2
Dersch et al. [139]	Spain	2111	SPT	-	7.5	40	-	161.1
Li et al. [140]	China	-	SPT	-	10	-	-	208.2
Chen et al. [71]	China	2752	SPT	-	15	-	13.77	361.1

Ouali and Richert [141]	Morocco	1989.9	SPT	-	7	-	-	159.07
Mihoub et al. [64]	Algeria	2008.4	SPT	-	8	45	23.57	193
Soomro et al. [133]	Pakistan	1992.9	SPT	Wet cooling	12	57.6	10.98	233.23
This work	Kuwait	2241	SPT	Wet Cooling	16	73.1	12.87	285.2
				Air Cooling	16	67.9	14.1	264.9
				30% Hybrid	17	74.2	13.48	289.9
				19% Hybrid	17	73.9	13.56	288.6

Despite the deviation imposed by the application of the daily AOD resolution on the AEG and the LCOE, the 50 MW SPT model simulated in this work shows some very promising and competitive results when compared with other similar operational and simulated CSP plants of the same plant capacity. In addition, it is very encouraging that the lowest LCOE of these TES-SM ranges in all aerosols scenarios is lower than the average actual cost of electricity in the conventional fossil fuel plants in Kuwait, i.e. 14 ¢/kWh [142], [143]. This is a sign of the reliability of the SPT, as the effect of the aerosols on the AEG appears to be relatively low. In addition, the daily aerosols adoption emerged as a realistic methodology in such regions and this reduces the chance of inaccuracies in the techno-economic assessments and gives better estimation of the annually as well as the daily energy generation. This finding signifies the importance of the normalization of this process in the prefeasibility stage for such a technology, especially because other similar arid regions have been proven to have an amplified effect of aerosols on the solar field while having close annual averaged AOD values to the one in this work. That is because both the aerosols level and the slant range play major roles in the attenuation percentage of the solar field as it is illustrated in [60]. Further, it should be borne in mind that for bigger capacities consisting of bigger solar field of the same technology and in the same location might result in bigger deviations in the AEG when daily aerosols values are adopted. This has been clearly seen in the daily AOD adoption when applied on two different TES-SM scenarios, i.e. the first with no TES and a small solar field, while the second is with a large TES (16h) and a large solar field. It is very interesting to note that the deviation in the AEG of the larger solar field scenario is affected more than that of the smaller solar field and that is despite having a large TES that should have mitigated the attenuation effect. This is obviously because the aerosols density affects the thermal energy

of the solar field first before being transferred to the HTF and the power cycle. While on the other hand, the TES is at the end of the cycle as it is supposed to store the energy excess for later usage, which means that the energy reaching the TES is already mitigated because of the aerosols density.

2.4 Conclusions

This chapter has proposed a new multiple temporal resolutions aerosols techno-economic assessment of a SPT in arid regions. This is extremely important for solar applications in arid regions, especially CSP which is majorly reliant on the reflection of the DNI, i.e. its main design parameter. The latter is a very sensitive sun irradiance component to aerosols, which can mask off up to 100 % of it in dust storms, i.e. a quite frequent occurring phenomena in arid regions.

The general metrological condition that is described by the TMY of the case study location at SREP confirms that the case study location has a great potential for a CSP application as the DNI values of the TMY file are found to be higher than the threshold of minimum required DNI for CSP. In addition, the preliminary assessment of the raw aerosols data acquired from the AERONET aerosols ground measured data and the MERRA-2 reanalysis model data reveals that the aerosols levels are found in the medium-low ranges and not as high as other arid regions such as Tamanrasset in Algeria for example. These two preliminary findings paved the way to carrying out this techno-economic assessment with more confidence.

The proposed multi-temporal aware techno-economic assessment has been carried out by the most accurate possible manner. This is because a one year long ground measured aerosols data has been used to site adapt a five years long reanalysis aerosols data prior the assembly of the TAY. There could be one more accurate way to conduct this methodology and that is in case longer ground measured data is available, which is not the case with the data from the AERONET station at the SREP. Hence, the TAY has been assembled based on the months with the closest behavior to the long term aerosols behavior, and from there, both daily and annually AOD averages have obtained and use in the techno-economic assessment.

The inclusion of the aerosols effect on the reflected such irradiance of the SPT's solar field resulted in the biggest deviation of reflected irradiance, absorbed thermal energy by the HTF at the receiver and thus, the AEG. This has been found to be 6.7% at most and of course, had its effect on the LCOE. The latter has also increased 6.7% as a result of the decreased captured in the AEG. This has been observed on the wet-cooled condenser scenario, which has not shown a massive outperformance in the AEG compared to the air-cooled scenario. Similar results were also found at the two hybrid condenser scenarios as no big significance of employing such scenarios has been found compared to the huge amount of water they require. As a consequence and in order to save computational time and effort, it has been decided that only the air-cooled condenser scenario will be assessed from now onwards.

Although being able to reveal how sensitive the solar field is to the adoption of aerosols over a wide range of TES-SM for a 50 MW SPT, higher SPT plant capacities are expected to have higher reductions in the AEG when aerosols effects are included, as they consist of larger slant ranges (due to the addition of the new heliostats at the outer circumference of the already existing heliostats). Therefore, as future research, the examination of higher plant capacities is highly recommended. In addition, the results show an elevated LCOE numbers compared to more mature RE and fossil fuel technologies. This can be potentially improved by the employment of a fossil fuel back up or by the hybridization with another RE technology that is able to decrease the LCOE.

Chapter 3 – Hybridization

Abstract

The work in this chapter is firstly, an extension of the work carried out in the previous chapter in what concerns the aerosols effect on the SPT solar field. This extension is mainly based on testing the aerosols effect on higher SPT capacities reaching up to 100 MW of standalone SPT. The results for the aerosols effects on the higher SPT capacities increases as expected and reaches up to 9.1 % of the AEG. Secondly, this work proposed both a RE and a fossil fuel technologies as hybridization options with the SPT, i.e. WT and NGCC in order to improve the SPT performance. After being individually simulated and validated, both of these two technologies have been evaluated in terms of their ability to compensate the energy losses of the SPT due to the aerosols density. Then, the WT and NGCC have been integrated with the SPT model in the SAM with the assistance of an in-house developed algorithm. This work has been able to automate the hybrid configuration of RE and fossil fuel technologies due to the developed algorithm, i.e. a typically unavailable option in the conventional SAM set up, which has permitted to observe the different RE technologies performance when these are hybridized as well as the exploration of benefits that the fossil fuel can bring to the hybridization. The water consumption and the CF have been observed as technical parameters, while the LCOE gave an idea of the economic performance and lastly the Global Warming Potential (GWP) gave the environmental aspect of the system. These parameters have been observed based on two different scenarios, i.e. a Carbon Capture & Storage (CCS) scenario and a no CCS scenario.

3.1 Introduction

3.1.1 Background

In addition to being able to quantify and assess the effect of the aerosols on the SPT, the feasibility of the latter is still a concern as it genuinely suffers from another main issue. This issue is that in order for the SPT to reach these unmatched sun irradiance concentrations, it requires that the SPT deploys a relatively very large solar field. As a result, the total initial costs of the SPT sharply rises compared to other CSP types as the solar field of the SPT can alone cost up to 50 % of its entire CAPEX [144]. The very high CAPEX of the SPT' solar field leads to another issue with the solar field sizing strategy as the solar field size cannot be

ultimately increased with the consideration that this will result in an increased AEG and will eventually pay off the CAPEX by driving the LCOE down. The solar field oversizing is a very delicate process because it imposes the resizing of a series of components in the SPT, e.g. the receiver and the tower. The problem with the steady increase of the solar field size from the receiver perspective is that the latter has a thermal limit. Consequently, CSP with oversized solar field are forced sometimes to defocus their reflectors in order not to overheat and damage their perspective receivers, or otherwise a bigger receiver must be adopted. The more are the solar field's reflectors defocused, the more dumped energy the CSP will suffer and the less efficient the CSP becomes.

The CSP sizing strategy is based on the SM of the solar field which represents the solar field size that is able to deliver the required thermal energy appropriate to the assigned rated power cycle capacity with accordance to the solar resource [51] as explained in the previous chapter. The number of reflectors with which this condition is achieved, is assigned a SM value of 1. The SM value is also related to a design DNI value which is the sun irradiance that is able to achieve the CSP rated capacity. For example, a solar field of a 100 MW SPT with a DNI design value of 700 W/m^2 is able to deliver the SPT capacity with 4558 heliostats (Figure 3-1 (a)), thus this number of reflectors is assigned a SM value of 1. In contrast, for a similar SPT capacity, another SPT plant which is situated in a location with higher DNI, can be designed at 900 W/m^2 and thus would only need 3453 heliostats (Figure 3-1 (b), which is also assigned a SM value of 1) in order for it to achieve its rated capacity.

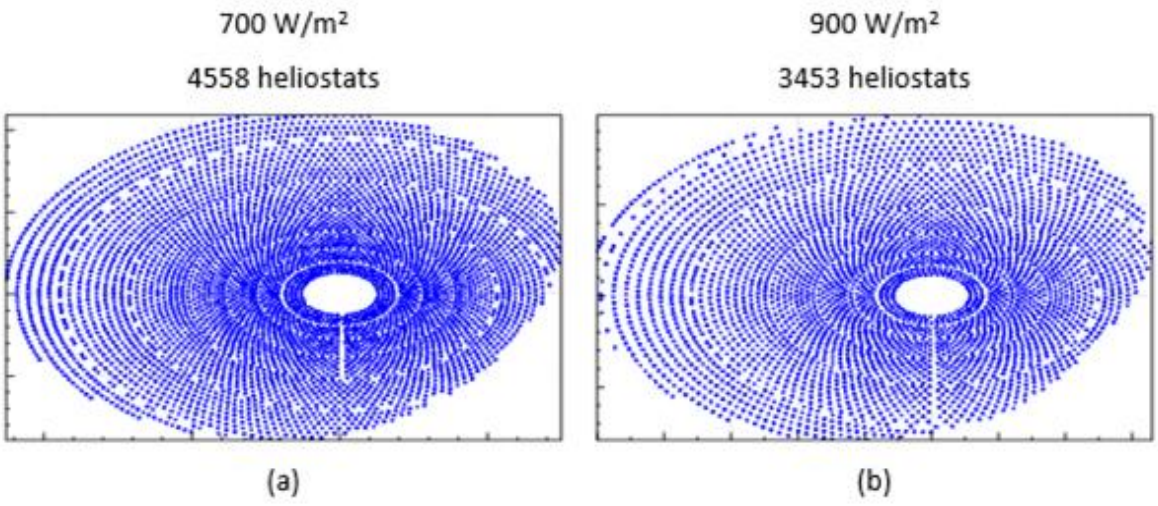

Fig. 3-1. The difference of heliostats number based on different design DNI values (similar scales have been used for (a) and (b).

However, a SM of 1 will only deliver the rated capacity in day time and in clear sky and as a result, most of the CSP plants adopt an oversized solar field which is represented by a SM value that is greater than 1. This is in order for the solar field to be able to deliver the sufficient thermal energy directly to the power cycle to be operated at its rated capacity in addition to another amount of thermal energy dedicated to the TES for later usage. Thus, the CSP plant can make up the hours with lower sun irradiance than the system's rated capacity at design. With CSP plants that have a SM greater than 1, defocusing is inevitable as during the year there must be some days with sun irradiance that is greater than that of the design point. This is avoided to the maximum by setting a DNI design point at the most frequent DNI values which is represented by the DNI probability cumulative function (PDF) and the cumulative distribution function (CDF), but never completely avoided. Figure 3-2 illustrates the DNI CDF of the case study location of SREP with the DNI value of 750 W/m^2 as the chosen value as the design DNI point.

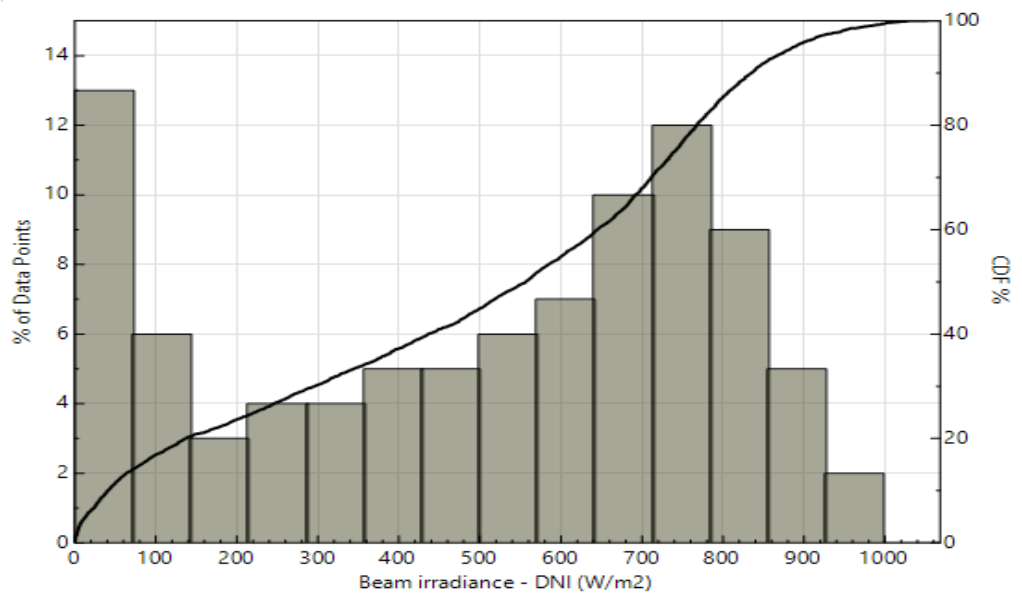

Fig. 3-2. The PDF/CDF graph as per the case study location's weather file DNI values (zeros are excluded).

As per the PDF alone of the DNI illustrated in Figure 3-2, the most appropriate DNI design value is in the range of 710-790 W/m^2 as the highest PDF percentage is located in this range (about 12.8% of the total number of points). However, when incorporating the CDF with the PDF, the intersection of the CDF with the highest column of the PDF falls at the DNI values around 750 W/m^2, which projects at 80% of CDF. This means that in this case 750 W/m^2 is chosen as a design DNI value, and the SAM solar field algorithm will size the solar field as it

would dumb 20% of the of the DNI and these are the values greater than 750 W/m^2. This value has been chosen as the design DNI value for optimal operation of the power cycle despite the fact that other higher values will result in lower dumped energy, however these higher values will also result in poor operation of the power cycle as the latter will never reach its rated capacity.

As a result of the non-linearity of the relation between the SM and the AEG, most of the standalone CSP techno-economic studies have been found with saturated like AEG levels when energy generation is analyzed over a range of TES and SM. This is mainly due to the fact that the unlimited solar field oversizing ends up by requiring a too large receiver and tower which is not techno-economic efficient. Thus, optimization tool and algorithms stops oversizing the receiver at this point while the user continues to increase the SM value. This ends up by the new added solar reflectors being defocused without having any energy addition to the plant's output. This can be clearly seen in case LCOE is simultaneously analyzed along with the AEG as the former starts decreasing as the AEG increases at the beginning of the TES-SM range, however when the AEG attains this saturation-like state, the LCOE starts increasing as it is found in [61], [145] and this furtherly confirmed in the previous chapter.

3.1.2 Motivation

To step up beyond this limitation, the hybridization concept of the CSP with other more mature technologies emerges as a viable solution especially because it is expected to have a great positive impact on the AEG and LCOE. Technologies such as PV and/or WT for instance are known to have lower CAPEX due to their continuous advances in technology which leads to an improved performance and thus lower costs [146], [147]. Current estimations ranges the LCOE of PV systems at 1.92 to 3.51 c/kWh, while the LCOE of WT is located between 3.94 and 8.29 c/kWh [148]. These LCOE ranges are very unlikely achievable numbers for the standalone CSP even at locations with very elevated solar resources. Further, it is worth mentioning that these technologies are hardly coupled with an appropriate back-up system for them, e.g. battery, and this is because the latter comes with high costs [149]. This promotes WT integration with CSP as this type of hybridization first, has a great potential of having both high AEG and low LCOE. Secondly, the fact that the wind resource is of a different nature than that is of solar can form a synergic solution with CSP especially this occurs in the case study location of SREP which has been reported with a great potential for

wind energy applications by multiple previous studies [150], [151] and furtherly confirmed by the reported actual performance of the already operational 10 MW WT in the SREP that sometimes exceeded what has been expected [152], [153]. Figure 3-3 illustrates the topography of Kuwait where the western part is obviously the most elevated, thus the most appropriate region for wind energy applications [154].

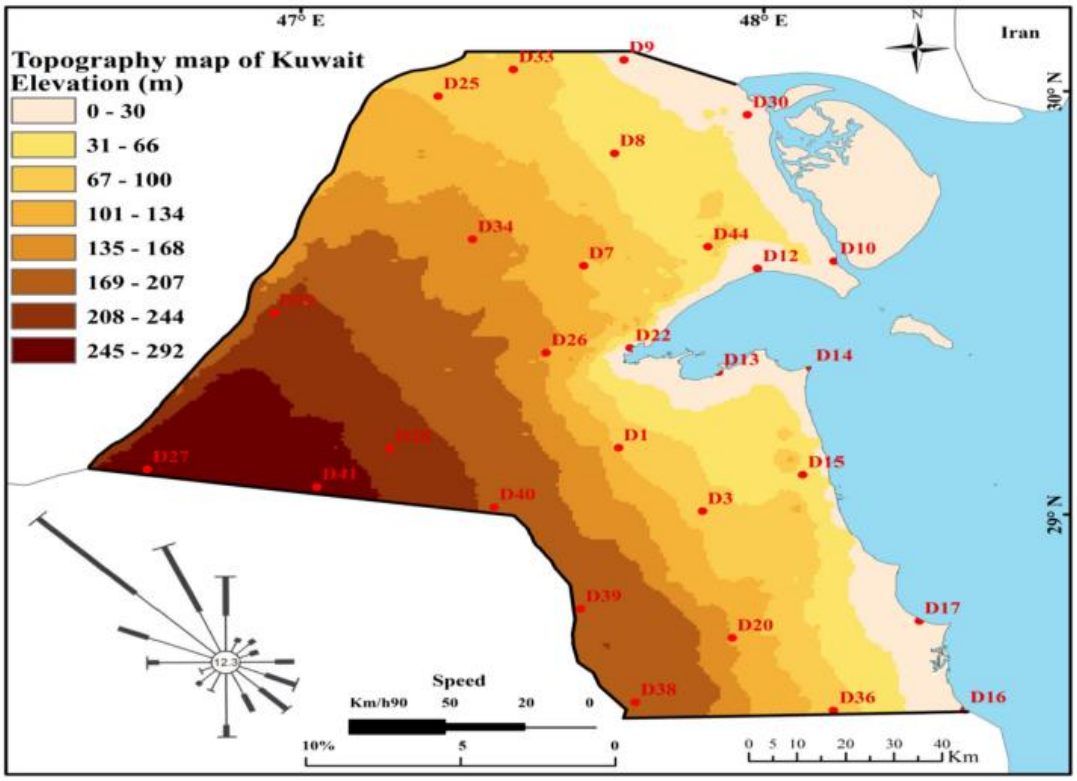

Fig. 3-3. Topography map of the state **of** Kuwait [154].

Thus far, CSP-WT hybridization has been thoroughly studied, for example, Kost et al. [155] examined the performance of standalone CSP against that of CSP-WT and concluded that the latter has less costs than the standalone. Also, Sioshansi and Denholm [156] illustrated the benefits of collocating CSP-WT with different percentages for each technology's capacity while fixing the CSP solar field at a SM of 1. Vick and Moss [157] also varied the percentages of each of the CSP and WT capacities, however, with fixing the TES of the CSP at 6 hours. It has been found that the configuration with two thirds WT and one third CSP performs the best.

Also, Sahin [158] simulated different capacities of solar and wind after defining the correlation of each of the technology's potential in the Arabian Peninsula. Similarly, Kost et al. [155] examined different CSP-WT capacities in the MENA region and concluded that the

hybrid configuration comes with a lower cost compared to the standalone CSP. Sioshansi and Denholm [156] examined different percentage shares of CSP-WT hybridization fixing the solar field represented by a SM at 1 and varied both the technologies' capacities. The study concluded that a minimum of 67% share of CSP is required for the hybrid configuration to be economically beneficial. Further, Vick and Moss [157] simulated a 100 MW hybrid model with an alternation of 33% and 67% of the CSP-WT shares while fixing the CSP's TES to 6h. They have found that the wind farm with 67 MW and the CSP with 33 MW delivers the best techno-economic outputs. These contradicting findings confirm that the RE technologies are strongly dependent on the location resources. However, a true judgement requires less restrictions on the boundaries of the optimal sizing strategy criteria such as the SM value and the TES capacity.

3.1.3 Preface

Despite the large amount of CSP-WT work that exists, the literature still lacks work that gradually varies both the solar field size and the TES for different plant capacities along with different capacities of WT. Most of the previous work has focused on the variation of each technology's capacity share disregarding the key design parameters of the CSP, i.e. TES and SM; it is necessary to first optimize these parameters to fully exploit the solar resources by the deployment of a TES. Only then, an optimization of the CSP-WT capacity share can be more accurate and provide more meaningful results. This can be accomplished through a parametric analysis that varies the solar field size paired with a variation of the TES along with the WT hybridization. The importance of such a study lies in the potential of locating a resized solar field-TES configuration for different numbers of WT. The latter has a great potential to drive the LCOE down, while keeping a threshold for both the CSP capacity and the TES size will ensure that both the AEG and the CF remain at high values.

On the other hand, the integration of WT with the CSP base model jeopardizes what distinguishes the CSP in the first place, i.e. high CF percentages. It has been reported that WT integration with CSP had a positive effect on the LCOE and the AEG, however, with a non-negligible penalty on the CF which drastically decreases as found in [159]. To address the risk of having lowered CF percentages, the integration of fossil fuel back-up for the RE systems is a very viable solution. This is because fossil fuel back-ups are known for their reliability of continuous energy provision, thus high CF (usually 85% [160], [161]). This has gained an

increased attention in the last two decades as most of the RE technologies still fail to have its breakthrough in storage and are still very expensive [162].

This proposed RE-fossil fuel configuration can potentially harness the sustainable energy sources without a complete disregard of the fossil fuel resources that happens to co-exist in the same region. In several parts of the MENA region, both fossil and renewable natural resources are abundantly collocated, e.g. the Arabian Gulf, Iran, Egypt and Algeria. Fossil fuel integration as back-up systems for the RE systems and represent a viable solution in the soft shift towards renewables adoption. However, fossil fuel usage has a major contribution in the CO_2 emissions and with the emerging climate change, all these countries have pledged to adopt more RE in their energy mix. Fossil fuel usage as a back-up system in RE systems has been limited in the legislation of such technologies in worldwide pioneering countries, e.g. 15% of the total CSP capacity in Spain can be generated by natural gas [163].

In this context, natural gas prevails as one of the cleanest fossil fuel types that can be used as a backup system for RE. This is because natural gas causes relatively lower environmental damage than other fossil fuel types such as diesel and coal [164], [165]. As a result, CSP-GT hybrid plants have recently gained increased interest in the literature. In this context, one of the best ways to capture a newly proposed energy generation plant's environmental impact is to run a LCA assessment which can quantify CO_2 emissions among other specific environmental categories over the entire life span of the plant, i.e. from cradle to grave. The LCA of CSP hybridization with fossil fuel backup systems has gained an increased attention recently due to the outstanding performance of such hybridization, but also the negative environmental impact that it could cause. For example, Adeoye et al. [166] compared two different TES materials while being hybridized with a natural gas heater in a 80 MW PTC plant. The study revealed that the configurations with the fossil fuel backup had the biggest environmental impact. Also, Corona et al. [167] examined the LCA of a 180 MW SPT of a SPT-GT hybridization for multiple geographic locations. The authors reported significant differences depending on the location. In addition, Corona et al. [168] varied the natural gas contribution from 0 to 35% in a 50 MW PTC plant with 7.5 h of TES. Also, Ameri and Mohammadzadah [169] proposed an integrated solar combined cycle based on PTC and performed a LCA for it.

Recent researches have also examined the environmental impact of the standalone CSP technologies to assess how the subcomponents of such system contribute in the CO_2 emissions. For example, Batuecas et al. [170] compared the environmental impact of using two different HTFs in a PTC plant. Pelay at al. [171] performed a LCA for a SPT and found that the solar field is the most environmental impacting component of the SPT. Gasa et al. [172] carried out a LCA for a SPT with different capacities of TES, i.e. 3, 6, 9 and 17.5 h. Interestingly, the authors revealed that the most environmentally efficient plant configuration is the one with 9 h of TES and not necessarily the one with the smallest TES capacity. It is confirmed that even the 100 % RE systems contribute in CO_2 emissions as well as other environmental impacts as these require resources, energy and materials in order for them to be manufactured, constructed, operated and eventually decommissioned. Figure 3-4 illustrates a general overview of the LCA of a typical CSP plant.

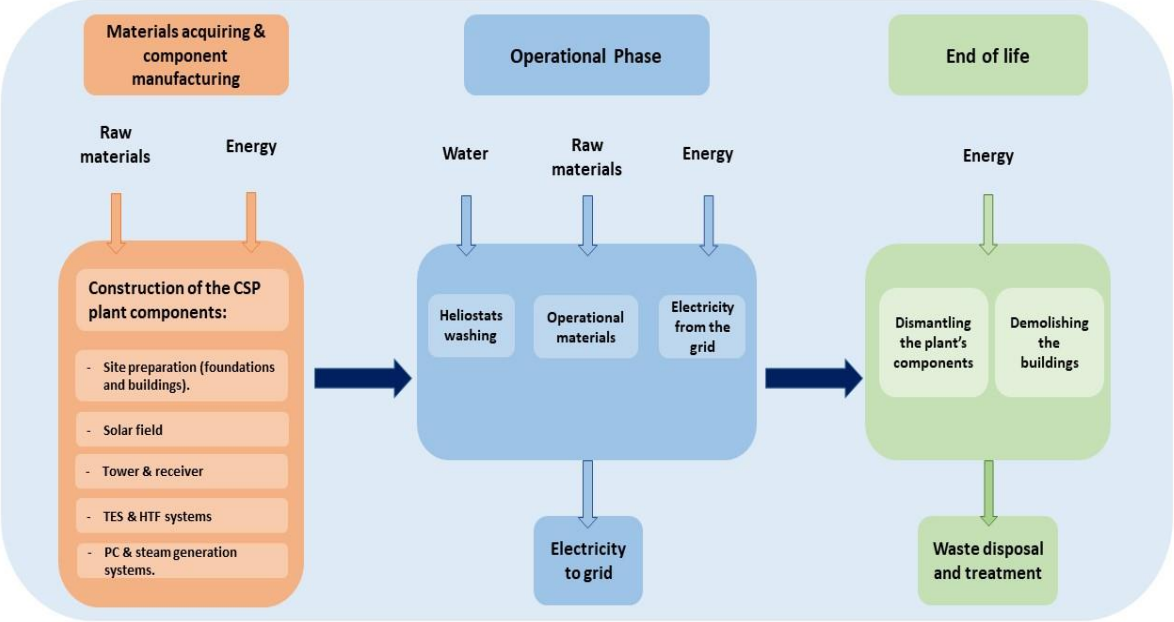

Fig. 3-4. A typical LCA by phases for a CSP.

3.1.4 Problem formulation

Despite the distinguished performance of the CSP in the case study location, which is represented by having high AEG and CF values, the LCOE of the CSP has been found to be very high (see previous chapter for details) compared to the average LCOE of other technologies such as WT and fossil-fuel based technologies worldwide. Also, since arid regions are scarce in water, this is considered as another downside for the CSP application in such region as a

considerable amount of water is required for multiple reason, e.g. power cycle heat rejection and solar field reflectors washing process. On the other hand, WT indeed possess low values of LCOE, however, suffers from lowered CF percentages compared to a CSP plant which has an advantage of a TES. Lastly, the fossil fuel back-up manages to secure energy for extended periods of time outperforming both the CSP and WT, on the other hand, it contributes to emitting non negligible amount of CO_2 to the atmosphere. This contradiction in the key performance indicators leads to a sizing strategy issue where no single sub component can have an overwhelming share of the proposed system at the expense of others.

Thus far, the literature still lacks research that includes both techno-economic and environmental impacts of a CSP hybridization with fossil and/or non-fossil fuel systems. The techno-economic assessment can be carried out by running a parametric analysis with all the possible configurations of the proposed plant, while the environmental assessment of the study can be realized by carrying out a LCA for these possible configurations where all system's subcomponents environmental impact is observed from cradle to grave. The parametric analysis variation considers all the possible configurations of the chosen key design parameters of each technology of the system. The proposed natural gas cycle here is an independent Natural Gas Combined Cycle (NGCC) that can be operated as a standalone with no restrictions related to either the SPT or/and the WT. The NGCC is chosen over a natural gas burner and a steam turbine because the NGCC is simply higher in thermal efficiency than both of the former [173]. This also simplifies the operation mode of the system's subcomponents as each of these can operate independently. In addition, maintenance of the system's subcomponents can be optimally scheduled as for example the WT can be stopped for maintenance in summer when it is expected to deliver its lower energy levels while maintenance work for the CSP can be scheduled during winter.

3.1.5 System Description

The entire idea of the proposed system is to exploit the region's available resources of both solar, wind as well as fossil fuel resources. The MENA region is an ideal case study location for such a system, however, some other regions that share the same factors are also a subject of a perfect fit to this system, e.g. the west and mid-west states in the USA. The backbone of the system is the SPT as it is considered as the baseload energy provider. This is because the SPT has shown a great ability to provide steady levels of energy due to the TES

that it employs. In addition, WT is included as it is able to provide energy for relatively low costs. This can drive down the LCOE of the hybrid system in addition to the exploitation of another type of resource. Lastly, an independent medium sized NGCC is chosen to be integrated with the system as a fossil fuel back-up system. The NGCC first admits the Natural Gas (NG) in addition to the compressed air in the combustor. The air/NG mixture is then sent to the Gas Turbine (GT) where the energy from the combustion is recuperated and sent to the grid. At the exit of the GT, the high temperature flue gases are admitted to an extra Steam Turbine (ST) in order to avoid going to waste. This takes place by admitting the flue exhaust gases to a Heat Recovery Steam Generator (HRSG) which has water running on its other side. The water gets heated due to the flue gases high temperature and then runs the ST, thus generating an extra amount of energy that is also sent to the grid. After passing through the turbine, the water becomes condensed before repeating the cycle as it is shown in Figure 3-5.

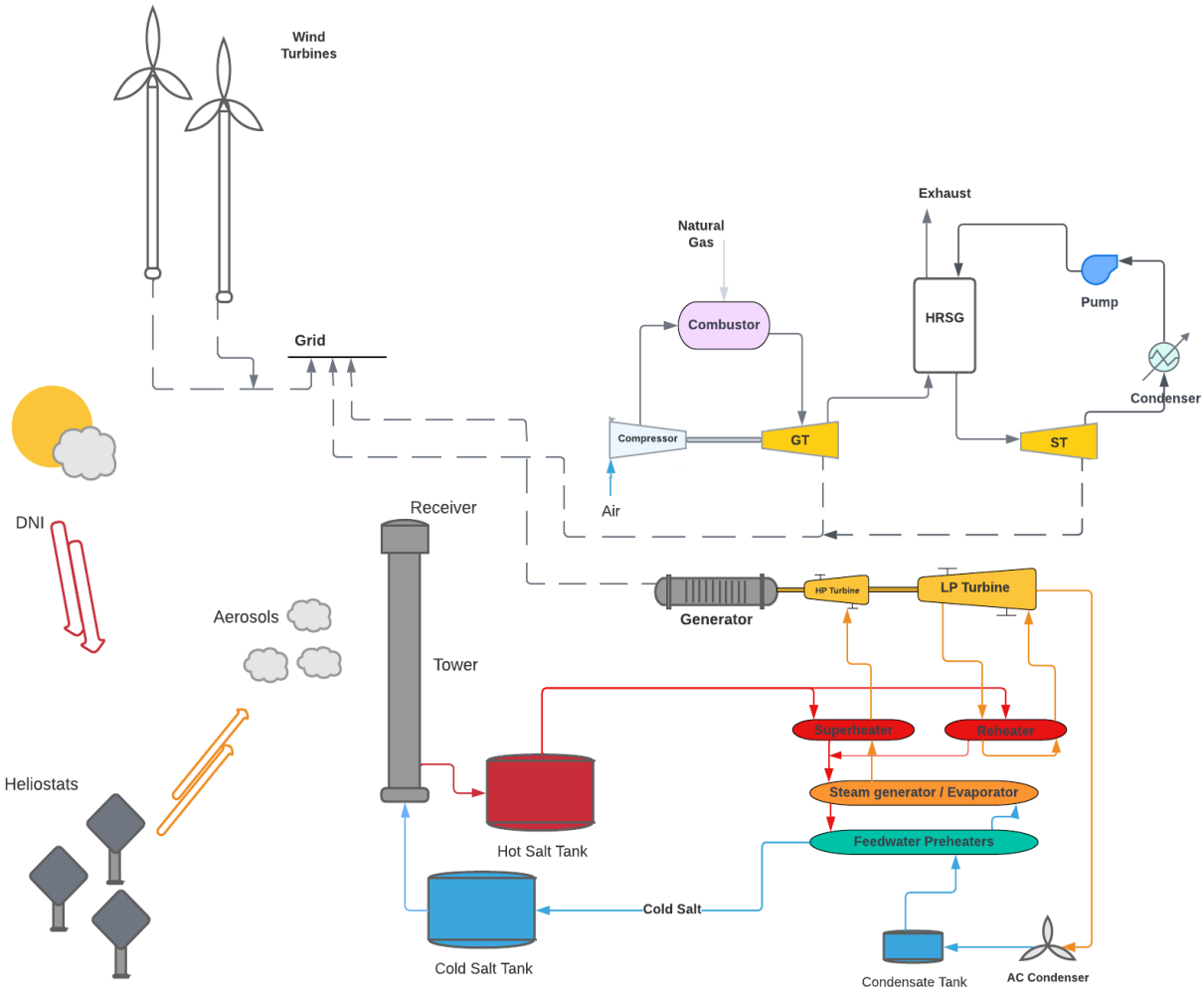

Fig. 3-5. A schematic of the SPT-WT-NGCC proposed system.

3.2 Materials and Methods

Despite the differences observed in the AEG and the LCOE of the SPT as a result of the AOD temporal resolution variation in the previous chapter, from here on, the effect of the aerosols on the SPT solar field will only be included as an annually averaged value of the assembled TAY. This is in order to avoid the immense computational time that is required to apply the daily AOD temporal resolution. Also, it is true that the hybrid condenser scenarios that have been tested in the previous chapter have both managed to reduce the water consumption of the SPT compared to a wet-cooled scenario simultaneously with being able to outperform the AEG of the air-cooled condenser, however, this AEG outperformance is negligible. Thus, from here on, this work will uniquely focus on the air-cooled condenser type of the SPT.

Also, unlike what has been observed in the previous chapter in terms of fixed capacity for the SPT model at 50 MW, from here on, the tested capacity of the SPT varies from 50 MW up to 100 MW. This is important as larger SPT capacities require larger solar fields and these larger solar fields are most probably more affected by the aerosols inclusion that has been proven in the 50 MW SPT base model.

3.2.1 System Components Validation

Since the base model validation of the SPT has been illustrated in the previous chapter, this chapter only illustrates the validation of the two remaining system's components, i.e. the WT and the NGCC.

3.2.1.1 Wind Turbines Model

The WT model used in this work is based on the commercially available WT of Siemens-Gamesa G97, i.e. an identical model to the one used in the pilot plant in the case study location at the SREP. The power estimation of this type of WT can be obtained as follows [174]:

$$P_{WT}(t) = \begin{cases} \frac{v^k - v_C^k}{v_R^k - v_C^k} \cdot P_R & v_C \leq v \leq v_R \\ P_R & v_R \leq v \leq v_O \\ 0 & v \leq v_C \ and \ v \geq v_O \end{cases} \quad (3\text{-}1)$$

where v is the location's wind speed (m/s) is, v_C is the cut-in wind speed, v_O is the cut-out speed, v_R is the rated wind speed P_R is the rated power of the WT (W) and k is the Weibull shape factor. In a similar procedure to the ST model validation, the WT of this work has been

validated against the actual performance of the 10 MW WT plant in the SREP available in [175].

Also, since the 5 WT of the 10 MW pilot plant are positioned in the north eastern part of the SREP rectangular shape, this work has simulated the first 5 WT in the exact same position as that in the pilot plant. Further, different numbers of WT have been simulated on the extension of the inclined upper border line of the SREP using the SAM's wind farm position import feature along with the approximate geometries of Figure 3-6 (a). Other WT positioning and alignment scenarios have been simulated (see the supplementary materials), however, none of which has been generated as good as the one implemented in reality in the SREP.

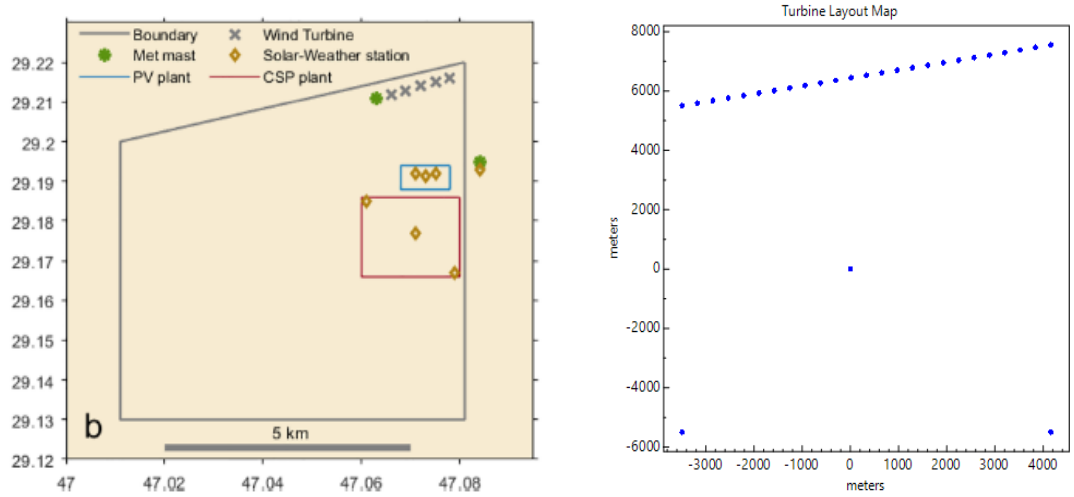

(a) (b)

Fig. 3-6. (a) WT pilot plant in SREP [175] and (b) a total of 25 WT represented in the same location.

In addition, since the weather file is obtained from a freely available reanalysis model (PVGIS [176]) in the form of a TMY, the wind speed is calculated at 10m of height. This hub height does not suit the simulation of the WT in this work as the WT in SREP are of 78m hub height. This can be resolved by interpolating the wind speed using the following correlation of the power law exponent as a function of the wind velocity and height [177]:

$$\alpha = \frac{0.37 - 0.088 \ln(U_{ref})}{1 - 0.088 \ln(\frac{Z_{ref}}{10})} \quad (3\text{-}2)$$

where U_{ref} is the mean wind speed at the reference height Z_{ref}. Thus, the wind speed at the desired height U_Z can be obtained as follows:

$$\frac{U_Z}{U_{Z_{ref}}} = \left(\frac{Z}{Z_{ref}}\right)^{\alpha} \quad (3\text{-}3)$$

Table 3-1 lists the inputs to the WT model in SAM:

Table 3-1
Technical characteristics of the 10 MW wind turbines in SREP (adopted from [175]).

Parameter	Details
Turbine make and model	Siemens_Gamesa G97
Rated power per turbine (MW)	2
Number of turbines	5
Hub height (m)	78.98
Rotor diameter (m)	97
Swept area (m²)	7,390
Wind cut-in speed (m/s)	3
Wind rated speed (m/s)	11
Wind cut-off speed (m/s)	25
Distance between wind turbines (m)	330

3.2.1.2 Natural Gas Combined Cycle Model

The case study location of SREP is situated in the western part of the country in a remote region where no oil and gas fields exist. This represents a logistical issue of the feasibility of the proposed plant, i.e. the lack of a main natural gas supply pipeline from the gas fields to the SREP from what appears in Figure 3-7 [178], which is one of the few reliable sources that has been found in the literature. However, it is not definitive that the oil and gas pipelines network does not reach the SREP (or the SREP approximates). This is because the already operational gas turbine and combined cycle units in the country are situated in locations that are not connected to the major gas pipeline illustrated in Figure 3-7. These locations include the Doha power station (south), Shuwaikh station (Kuwait City) and Az-Zour station (south) [33]. Thus, this work neglected the techno-economic assessment and the LCA

inventory of the hypothetical pipeline to the SREP. This is also because since it is a fossil fuel based technology and not RE, the location is less important. The NGCC can typically be built where it is most suitable (near the already existing NG stations for example) as long as its outputs are integrated with the proposed configuration in SREP.

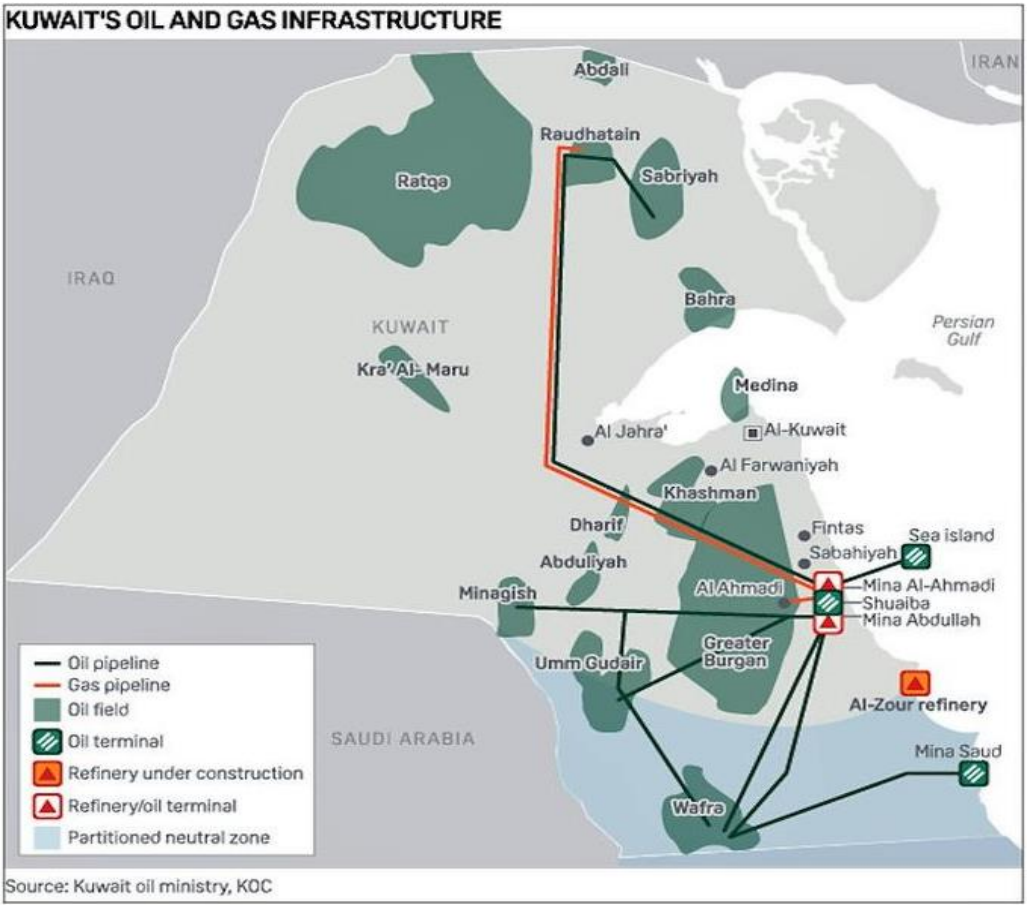

Fig. 3-7. Kuwait oil and gas fields and pipelines [178].

As for the NGCC expected energy generation, this energy is primarily obtained through the energy generation from the GT cycle. In addition, an additive amount of energy is also obtained through the passage of the recuperated flue gas from the GT through the ST. For the GT, the electrical power ($\dot{W}_{GT}^{el}$) can be obtained as follows:

$$\dot{W}_{GT}^{el} = \eta_{gen}^{el} \left(\dot{W}_{Turb}^{mec} - \dot{W}_{Comp}^{mec}\right) \quad (3\text{-}4)$$

where η_{gen}^{el} is the efficiency of the generator, $\dot{W}_{Turb}^{mec}$ is the mechanical work of the turbine and $\dot{W}_{Comp}^{mec}$is the mechanical work of the compressor. As for the ST, the electrical power ($\dot{W}_{ST}^{el}$) is obtained as follows:

$$\dot{W}_{ST}^{el} = \eta_{Turb}^{mec} \cdot \dot{m}_{flue\ gas} \cdot \Delta h \quad (3\text{-}5)$$

Where η_{Turb}^{ec} is the efficiency of the ST, $\dot{m}_{flue\ gas}$ is the mass flow rate of the flue gas after passing through the heat recovery system and Δh is the difference between the inlet and outlet enthalpies of the expansion process [162].

Despite the various advantages of the main simulation tool of this work, the SAM does not consider any non-renewable systems in their late versions. Thus, another robust simulation tool has been used in order to simulate the hourly performance of the NGCC as a fossil fuel back-up system, i.e. Aspen Plus. The tool offer a great deal of flexibility to construct various component systems that is eventually governed by a heat and mass balance. In this work, three different NGCC configurations are simulated with the assistance of Aspen Plus and the technical data published by the manufacturer. The inputs data in accordance with the technical data of the manufacturer [179] are listed in Table 3-2.

Table 3-2

NGCC technical parameters inputs adopted from [179].

Config. 1	GT		ST		Total
	Power output (MW)	5.1	Max power output (MW)	3.5	8.6
	Exhaust mass flow rate (kg/s)	19.5	Inlet steam pressure (bar)	63	N/A
	Exhaust T (C)	544	Inlet steam T (C)	482	N/A
Config. 2	**GT**		**ST**		**Total**
	Power output (MW)	10.4	Max power output (MW)	3.5	13.9
	Exhaust mass flow rate (kg/s)	34.2	Inlet steam pressure (bar)	49	N/A
	Exhaust T (C)	510	Inlet steam T (C)	440	N/A
Config. 3	**GT**		**ST**		**Total**
	Power output (MW)	14.3	Max power output (MW)	3.5	17.8
	Exhaust mass flow rate (kg/s)	44.5	Inlet steam pressure (bar)	49	N/A
	Exhaust T (C)	529	Inlet steam T (C)	440	N/A

The major components of these NGCC three different configurations have been selected among other available in the literature in order to get an ascending total generated power from configuration 1 to 3 with respect of the exhaust/inlet temperatures of the GT and ST, respectively.

As for the amounts of CO_2 emitted by these different configurations of NGCC, these values have been calculated based on the system heat rate (ϕ_{hr}) of each configuration which can be obtained as follows:

$$\phi_{hr} = {}^{H}/_{E} \tag{3-6}$$

Where H is the heat that is supplied to the system and E is the energy output of the NGCC [180]. Also, since the natural gas is majorly composed from methane (up to 96% [181]), it has been assumed that the natural gas is entirely composed of methane for the simplification of the calculations. Thus, the H can be calculated as follows:

$$H = total_{fuel} \,.\, C_{v\ methane} \tag{3-7}$$

Where $total_{fuel}$ is the hourly total fuel usage of the system and $C_{v\ methane}$ is the methane calorific value (here, the lower calorific value of 50 MJ/kg is considered [182]). Thus, for the yearly fuel consumption, $total_{fuel}$ is multiplied by the hours of the year with a consideration of the 85% CF of the NGCC. Finally, the CO_2 emitted from the different NGCC configurations is obtained in MMBTU/y for each kWh generated by the system under the assumption that the natural gas emits 52.91 kg of CO_2 per MMBTU [183]. Unit conversions and full calculations of the CO_2 emissions for all three NGCC configurations are found in details the Appendix H.

3.2.2 System's Performance Indicators

In this work, some important performance indicators have been elected to optimally observe the system's performance and test its compatibility among its counterpart in the literature and the commercial scale. These elected performance indicators are objectively selected as they must fit the general and specific aim of this work. For example, the LCOE is the economic performance indicator that has been chosen for this evaluation. Also, the CF has been chosen over the absolute AEG as the former is more inclusive than the latter and gives a visualization of the system's ability to fulfill its rated capacity. In addition, the GWP is the environmental indicator that is observed in this work through the LCA as it describes the amounts of CO_2 emissions of the system as well as other greenhouse gases. Lastly, since the system is proposed in an arid region, water consumption stands as one of the most important figures to be observed and controlled.

Unlike the water consumption and the CF which can be easily calculated for the system, the LCOE and the GWP calculations are more complex. With regards to the GWP, it is true that

the NGCC is the component that is most associated with the CO_2 emissions in the proposed system, however, this does not mean that both of the other components (SPT and WT) are carbon neutral. The SPT and WT contribute in emitting CO_2 during their entire life cycle as their corresponding sub-components require energy consumption over their life span, e.g. raw materials extraction, manufacturing, etc. A fossil fuel plant type usually surpasses the RE plants by far in regards to the CO_2 emissions, which may give a prejudged decision on how the system negative impact on the environment. However, since the majority of the newly installed NGCC are already or expected to be equipped with CCS units, the system behaviors is less predictable with regards to the CO_2 emissions. This uncertainty still exists with fossil fuel-based plants that include a CCS that is able to capture 100 % of the CO_2 emissions. This is because there are non-negligible CO_2 emissions that are emitted during the manufacturing and disposal processes of the raw materials that are used in the installation/ decommissioning phases of the plant lifetime which can be optimally captured through a LCA.

These four performance indicators for each hybrid configuration will assist later in the thesis to assess all configurations' performances and thus elect the optimal system configuration. This can be achieved by a multi-objective optimization technique in which multiple proposed solutions will be optimal and represent a tradeoff between the four objective functions. It could be argued that there are many important performance indicators that must be taken into account in the optimization process beyond the selected four, however, due to the nature of the multi-objective optimization that can only assess up to four objective functions at a time, this work has only elected LCOE, CF, water consumption and GWP. Otherwise, it would be very difficult in terms of representation and analysis.

3.2.2.1 Global Warming Potential through Life Cycle Assessment

The LCA of the entire proposed system is carried out according to the standardized framework of ISO 14040 and 14044 [184]. This approach assigns four main steps of the LCA: objective and scope definition, inventory analysis, environmental impact determination and lastly the interpretation of the results. The chosen method is the ReciPe 2016 as it contains 18 midpoint environmental impact indicators, among which the GWP is the one of interest for this work. ReciPe2016 is available in the SimaPro V.9.3.0.3 LCA simulation tool which also has multiple built-in data bases and has been used in this work's LCA.

3.2.2.1.1 Objective & Scope

The main goal of the LCA here is to allocate and control the environmental impact of the entire proposed system with regards to the CO_2 emissions. The LCA process is restricted in the way that it is able to observe the entire life cycle of each of the main components of the three technologies in the proposed system. This will enable this work to allocate specific environmental impact indicators (i.e. the CO_2 emissions here) to each technology in the hybrid configuration. Then, the various possible system configurations will each be assigned CO_2 emissions value that will be included in the multi-objective optimization process as an objective function which is to be minimized. Also, since the final product of this entire proposed system is energy, this LCA is assigned a functional unit on an energy basis, i.e. kg CO_2 eq. / kWh.

3.2.2.1.2 LCA Inventory

This stage is where the data collection is carried out and it is divided into two primary sources: first, the literature derived data which is either of the materials weight as in the SPT model or otherwise, normalized per unit of energy production as in the WT and the NGCC models. Regarding the SPT model, it is quite commonly known in the CSP assessment works that key design parameters, such as TES and SM, have a great effect on the technology's performance. This encouraged many researchers to examine the CSP performance over wide ranges of such design parameters. The issue is that the LCA inventories are not widely available and this is mostly due to confidentiality, which limits the vast majority of the literature to only rely on the few available data inventory in their LCA, apply a minor change in the system and calculate the new LCA for the newly configured system. For example, Gasa et al. [185] carried out a LCA based on the 120.8 MW Abengoa SPT available data which has a TES of 17.5h. The authors examined the TES effect on the LCA of the SPT by entirely excluding the TES and recalculating the new amount of CO_2 eq. / kWh of the SPT.

Due to the scarcity of SPT inventory materials, the scaling approach has been more acceptable recently. For instance, Gasa et al. [172] carried out a LCA of a SPT for different TES capacity based on scaling. Similarly, Klein et al. [186] did a linear regression to calculate the material inventory of the TES of a PTC plant. This work has followed a similar approach in order to interpolate the corresponding values of the SPT subcomponents inventory materials that are illustrated in Figure 3-8.

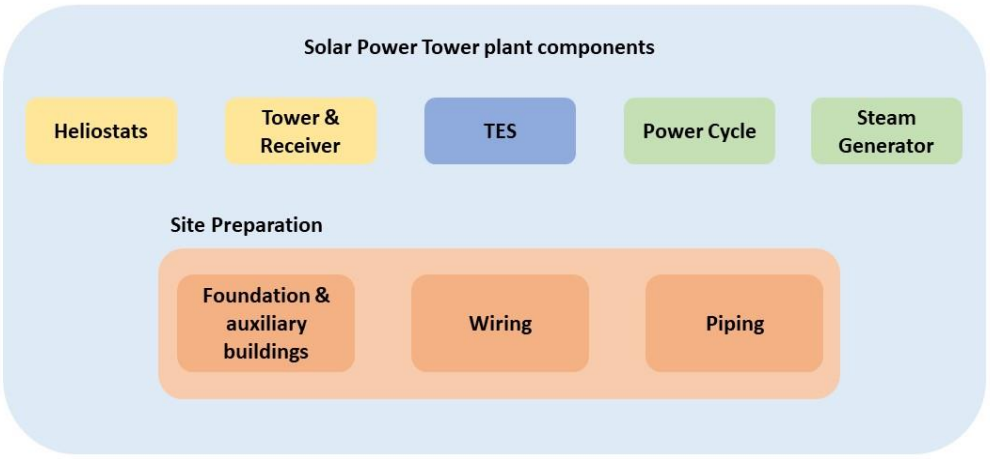

Fig. 3-8. The SPT subcomponents that are considered in the LCA.

Since one of the main aims of this work is to provide a realistic estimation of the environmental impacts of the various different SPT system configurations, this work has tackled this issue by scaling the LCA inventories of three of the most reliable data bases of three different SPT: Gemasolar [37], [187], [188], [189] 115 MW [190], and 220 MW [191] SPT which are commercial scale plants for which the LCA inventory can be found in the Appendices and the main technical parameters are illustrated in Table 3-3.

Table 3-3
The technical parameters of the three SPT plants used in LCA of this work.

	Gemasolar [36]	115 MW SPT [190]	220 MW SPT [191]
Gross capacity (MW)	19.9	115	220
Total land area (m^2)	1,850,000	7,903,511	22,028,145
Total solar field aperture area (m^2)	304,750	1,289,000	3,592,616
Single heliostat area (m^2)	115	148.8	19.03
Number of heliostats (-)	2650	8662	188,787

Receiver total area (m^2)	126.4	360.6	632.5
Tower height (m)	140	203	260
Annual water consumption (m^3)	368,347	124,000	-
PC thermal cycle efficiency (%)	40	40	40
AEG (GWh/y)	110	539.7	783.5
TES full load hours (h)	15	10	6
TES thermal capacity (MWhth)	670	1552.5	4055

3.2.2.1.3 LCA Impact Assessment

The impact of the LCA is assessed through the GWP by using the hierarchal ReciPe 2016 midpoint impact assessment (H) mainly due to its ability to calculate the GWP for a period of 100 years [192].

Since the prime energy provider of this proposed system is the SPT, the latter has been thoroughly observed based on the LCA inventory data of the three SPT references of Table 3-3. Both the WT and NGCC corresponding GWP values are normalized based on the literature averaged values mainly for two reasons: first, because both of these technologies are more mature than the SPT, thus GWP normalized values are quite reliable and commonly used. Secondly, the exact amount of materials used on the LCA inventory is usually classified as a confidential information, thus not readily available even for academic purposes. The United Nations Economic Commission for Europe [193] averaged the GWP of the onshore WT at 11.9 g CO_2 eq. / kWh, the NGCC without a CCS unit at 258.65 g CO_2 eq. / kWh and the NGCC with CCS at 156.5 g CO_2 eq. / kWh. However, in this work, the emission factors for all NGCC configurations have been calculated and presented in detail in the results section of this chapter.

3.2.3 Hybridization

The main simulation tool of this work (SAM) has offered many advantages to this work thus far as seen in the previous chapter. One of the greatest advantages lies in its economic model integrity compared to other in house developed economic models. Also, the flexibility offered to the user through multiple automations tools. Despite these aforementioned advantages, the SAM is limited with regards to different RE model hybridization. In addition, the SAM only has got the RE models and does not possess any fossil fuel options.

Also, since the overall performance assessment in this work is yearly based, performance indicators of interest such as the AEG, CF and water consumption can be obtained through simple aggregations of these corresponding values from each of the three main technologies in the hybrid SPT-WT-NGCC. On the other hand, more complex performance indicators such as the LCOE cannot be simply obtained similarly. This is because the LCOE calculations involves multiple nonlinear economic inputs that are subject to inflation and depreciation over the entire analysis period of the plant and this is shown as follows:

$$LCOE = \frac{-C_0 - \frac{\sum_{n=1}^{N} C_n}{(1+d_{nominal})^n}}{\frac{\sum_{n=1}^{N} Q_n}{(1+d_{real})^n}} \quad (3\text{-}8)$$

where Q_n is the Net Present Value (NPV) of the AEG over the entire analysis period N of the assumed plant life, C_0 is the project equity, C_n is the NPV of the annual costs of the project, d_{real} is the discount rate, $d_{nominal}$ is the nominal discount rate and n is the analysis year [159].

In order to calculate the LCOE of the entire system, the calculation steps of the LCOE shown in Equation 3-8 must be broken down to the points where the involved inputs of each of the three technologies of the system (SPT, WT and NGCC) are added together. The LCOE calculation break down procedure starts by the calculation of the NPV of the AEG which can be obtained as follows:

$$\mathrm{Q_n} = \frac{AEG_n}{(1+d_{real})^n} \quad (3\text{-}9)$$

The AEG of the entire system is the sum of all technologies energy generation:

$$AEG_n = AEG_{SPT_n} + AEG_{WT_n} + AEG_{NGCC_n} \quad (3\text{-}10)$$

Similarly, the NPV of the annual costs is obtained as follows [194]:

$$C_\mathrm{n} = \frac{Annual\ Costs_n}{(1+d_{nominal})^n} \quad (3\text{-}11)$$

The plant annual costs is the main economic parameter in the LCOE calculation as it involves all the considered economic inputs of the three technologies and it is calculated as follows [195]:

$$Annual\ Costs_n = federal\ tax\ benefit_n + state\ tax\ benefit_n - total\ expenses_n - working\ capital\ reserve\ funding_n - working\ capital\ reserve\ realease\ of\ funds_n - debt\ service\ reserve\ funding_n - debt\ service\ reserve\ release\ of\ funds_n - debt\ interest\ payement_n - debt\ principal\ payement_n + interest\ on\ reserve_n \quad (3\text{-}12)$$

In accordance with the SAM inputs, a federal tax of 17% has been considered for the case study location of Kuwait. This is because the Kuwaiti taxation code compels 15% as a corporate tax and 1% for Islamic compulsory charity (Zakat 1%) as well as another 1% for the Kuwait Foundation for the Advancement of Sciences (KFAS) [196]. The total tax benefit is calculated as follows:

$$total\ tax\ benefit_n = \ total\ taxable\ income_n * tax\ rate_{\ corporate\ +Zakat+KFAS} \quad (3\text{-}13)$$

Thus, the total taxable income can be obtained as follows [195]:

$$total\ taxable\ income_n = \ EBITDA_n + interest\ on\ reserve_n - debt\ interest\ payement_n \quad (3\text{-}14)$$

where EBITDA is the Earnings before Interest, Taxes, Depreciation and Amortization and is calculated as follows [197]:

$$EBITDA_n = total\ revenue_n - total\ expenses_n \quad (3\text{-}15)$$

As for the interest on the reserve and the debt interest payment, these are calculated as follows:

$$interest\ on\ reserve_{n+1} = total\ reserve_n * reserve\ interest \quad (3\text{-}16)$$

$$debt\ interest\ payement_n = debt\ ending\ balance_{n-1} - term\ interest\ rate_n \quad (3\text{-}17)$$

The total expenses of the plant are calculated as follows [195]:

$$total\ expenses_n = insurance_n + electricity\ purchase_n + \ O\&M\ production\ based\ expenses_n + O\&M\ production\ capacity\ expenses_n + Fuel\ expenses_n \quad (3\text{-}18)$$

where the electricity purchase represents the rate at which the electricity is purchased from the grid in case it is needed. Since the SPT requires to keep the TES at it lower permissible temperature of 290 °C in the cold TES tank when there is not enough solar resource, the SPT has to acquire electricity from the grid. However in this work, both the WT and the NGCC do not need any electricity from the grid and whatever needed electricity for the SPT can be supplied by the WT or/and the NGCC. Thus, the electricity purchase is excluded from the total expenses here.

The fuel expenses is uniquely attributed to the fossil fuel consumed in the NGCC and is obtained as follows:

$$Fuel\ expenses_n = \left(Fuel\ costs * Annual\ fuel\ consumption * \left(1 + \frac{fuel\ cost\ escalation}{inflation\ rate}\right)\right)^{n-1} \quad (3\text{-}19)$$

Also, selling the electricity to the grid is based on the Power Purchase Agreement price (PPA). The PPA contributes in the calculation of the total revenue as a function of the AEG as follows:

$$total\ revenue_n = AEG_{SPT+WT+NGCC} * PPA_{SPT+WT+NGCC} \quad (3\text{-}20)$$

It is worth mentioning that the literature lacks the price details for combined systems. Thus, the PPA in this work has been calculated based on the aggregation of each relative technology PPA price as follows:

$$PPA_{SPT+WT+NGCC} = PPA_{SPT} * \frac{Capacity_{SPT}}{Capacity_{SPT+WT+NGCC}} + PPA_{WT} * \frac{Capacity_{WT}}{Capacity_{SPT+WT+NGCC}} + PPA_{NGCC} * \frac{Capacity_{NGCC}}{Capacity_{SPT+WT+NGCC}} \quad (3\text{-}21)$$

Also, as part of the total expenses, the O&M capacity based expenses of the entire plant is calculated similarly as follows:

$$O\&M\ capacity_{SPT+WT+NGCC} = Fixed\ Costs_{SPT} * \frac{Capacity_{SPT}}{Capacity_{SPT+WT+NGCC}} + Fixed\ Costs_{WT} * \frac{Capacity_{WT}}{Capacity_{SPT+WT+NGCC}} + Fixed\ Costs_{NGCC} * \frac{Capacity_{NGCC}}{Capacity_{SPT+WT+NGCC}} \quad (3\text{-}22)$$

The O&M production based expenses is uniquely a factor of both the SPT and NGCC variable expenses as the variable costs of the WT are equal to zero:

$$O\&M\ production_{SPT+WT+NGCC} = (Variable\ Costs_{SPT} * AEG_{SPT}) + (Variable\ Costs_{NGCC} * AEG_{NGCC}) \quad (3\text{-}23)$$

The lifetime of the project is 25 years and the main economic assumptions and parameters are shown in Table 3-4.

Table 3-4
LCOE calculation inputs.

	Parameter	Details	Description
SPT	**Capacity**	40 - 110 MW (gross)	-
	AEG	Case dependent	Calculated and called from SAM
	O&M fixed costs	66 $/kW-y	NREL [198]
	O&M variable costs	3.5 $/MWh	
	PPA price	85 ¢/kWh	
	Total installed cost	Case dependent	Calculated and called from SAM
	Net capital cost	Case dependent	
WT	**Capacity**	0 – 12 MW (net)	-

	AEG	Case dependent	Calculated and called from SAM
	O&M fixed costs	42 $/kW-y	NREL [199]
	O&M variable costs	0 $/MWh	
	PPA price	4 ¢/kWh	
	Total installed cost	Case dependent	Calculated and called from SAM
	Net capital cost	Case dependent	
NGCC (with no CCS)	**Capacity**	8.6 - 13.9 – 17.8 (gross)	-
	AEG	Case dependent	Calculated in Aspen Plus and imported to SAM
	O&M fixed costs	3.6 $/kW-y	NETL [161]
	O&M variable costs	1.7 $/MWh	
	PPA price	5 ¢/kWh	
	Total installed cost	Case dependent (780 $/kw)	NETL [161] + CEPCI then imported to SAM
	Net capital cost	Case dependent	
NGCC (with CCS)	**Capacity**	8.6 - 13.9 – 17.8 (gross)	-
	AEG	Case dependent	Calculated in Aspen Plus and imported to SAM
	O&M fixed costs	7.6 $/kW-y	NETL [161]
	O&M variable costs	4.1 $/MWh	
	PPA price	5 ¢/kWh	
	Total installed cost	Case dependent (1727 $/kw)	NETL [161] + CEPCI then imported to SAM
	Net capital cost	Case dependent	
Entire system	**Inflation rate**	2.4 %/year	For Kuwait [200]
	Real discount rate	3.5 %/year	For Kuwait [201]
	Nominal discount rate	5.98 %/year	Calculated and called from SAM
	Annual interest rate	4 %	For Kuwait [202]
	Federal tax	17 %	Kuwait Corporate, Zakat and KFAS tax [196]
	State tax	0 %	-
	Fuel costs	4.42 $/MMBTU	NETL [161]
	Fuel costs escalation rate	1 %	
	Term tenor	18 years	
	Debt size	50 % of total installed cost	
	Debt upfront fee	450000 $	Default values in SAM
	Debt closing fee	2.75 % Of debt	
	Interest on reserves	1.75 %/year	
	Insurance rate	0.5 % of total installed cost	

It is worth mentioning that the economic inputs that are listed in Table 3-4, and that has been used here, slightly differs from what has been used in the previous chapter as these in Table 3-4 are the most recent.

3.3 Results & Discussion

3.3.1 Aerosols Impact Results

Unlike that which has been presented in the previous chapter, which uniquely examined the aerosols effect on the 50 MW SPT base model, this section extends the examination of the aerosols reaching a SPT capacity of up to 100 MW. In this regards, it is critical to select a specific point to assess the solar field performance as both the TES-SM are expected to majorly contribute in the definition of the aerosols effect on the AEG. Thus, for simplicity, the TES and SM configurations with the probable best techno-economic outputs (18h and 3.4 of SM) has been chosen as the reference point at which the AEG is observed. In addition, the configuration with the same SM value but with no TES inclusion is examined in Figure 3-9, which illustrates the assessment of both the SPT 50 MW and 100 MW capacities.

As it is commonly known and widely found in the literature, an increase in the TES capacity results in an increase in the AEG. However, as it can be seen in Figure 3-9, the effect of the aerosols on the TES scenario is greater than that of the no TES scenario. This is due to the fact that in the case where there is no TES included, a limited amount of thermal energy is reflected on the receiver and thus attenuated by the aerosols. The limitation is set by the small SM of the solar field which is only enough to run the power cycle at its rated capacity without any excess energy. On the other hand, in the case where a TES is included, a large value of SM is required to fully exploit the TES besides running the power cycle at its rated capacity, hence more thermal energy from the solar field is used and bigger aerosols effect is found.

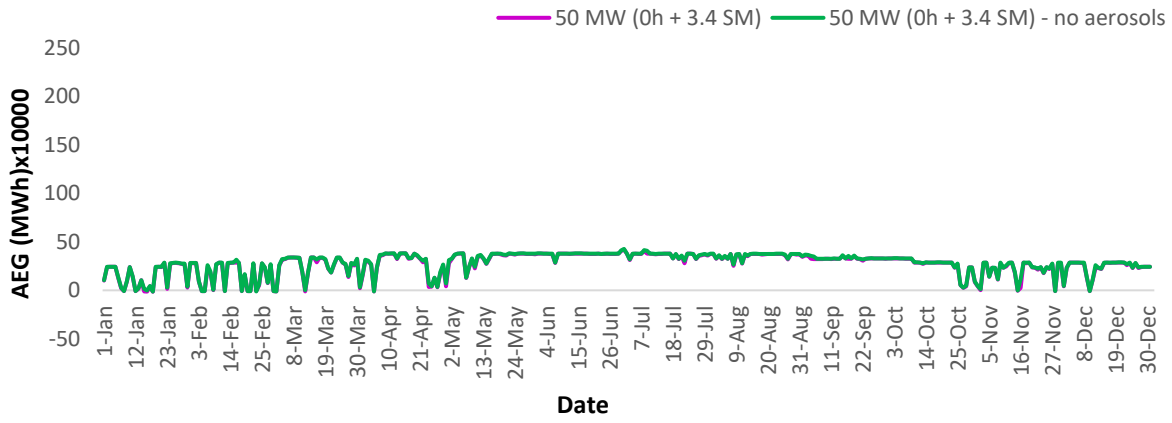
50 MW (0h + 3.4 SM)
50 MW (0h + 3.4 SM) - no aerosols
AEG (MWh)x10000
250
200
150
100
50
0
-50
1-Jan
12-Jan
23-Jan
3-Feb
14-Feb
25-Feb
8-Mar
19-Mar
30-Mar
10-Apr
21-Apr
2-May
13-May
24-May
4-Jun
15-Jun
26-Jun
7-Jul
18-Jul
29-Jul
9-Aug
20-Aug
31-Aug
11-Sep
22-Sep
3-Oct
14-Oct
25-Oct
5-Nov
16-Nov
27-Nov
8-Dec
19-Dec
30-Dec
Date

(a)

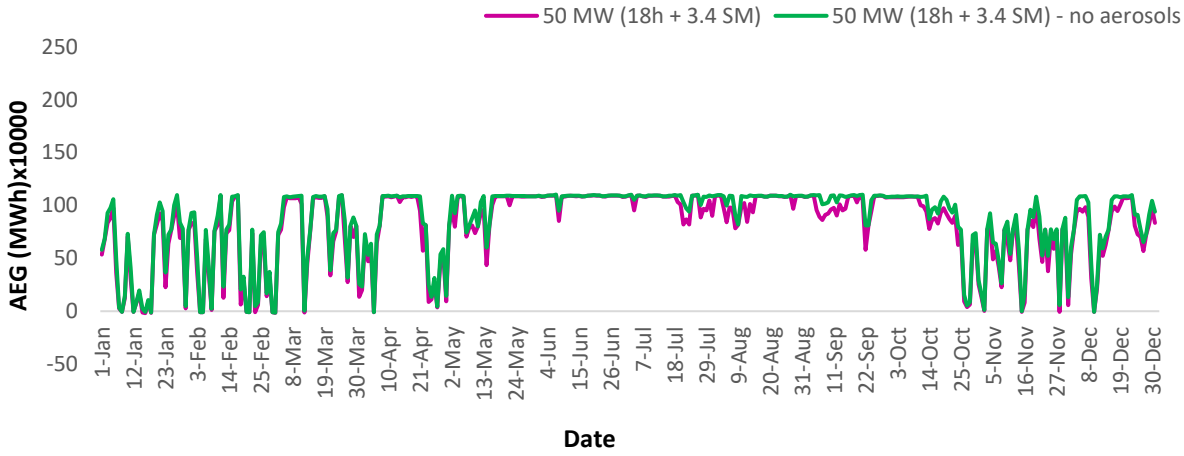
50 MW (18h + 3.4 SM)
50 MW (18h + 3.4 SM) - no aerosols
AEG (MWh)x10000
250
200
150
100
50
0
-50
1-Jan
12-Jan
23-Jan
3-Feb
14-Feb
25-Feb
8-Mar
19-Mar
30-Mar
10-Apr
21-Apr
2-May
13-May
24-May
4-Jun
15-Jun
26-Jun
7-Jul
18-Jul
29-Jul
9-Aug
20-Aug
31-Aug
11-Sep
22-Sep
3-Oct
14-Oct
25-Oct
5-Nov
16-Nov
27-Nov
8-Dec
19-Dec
30-Dec
Date

(b)

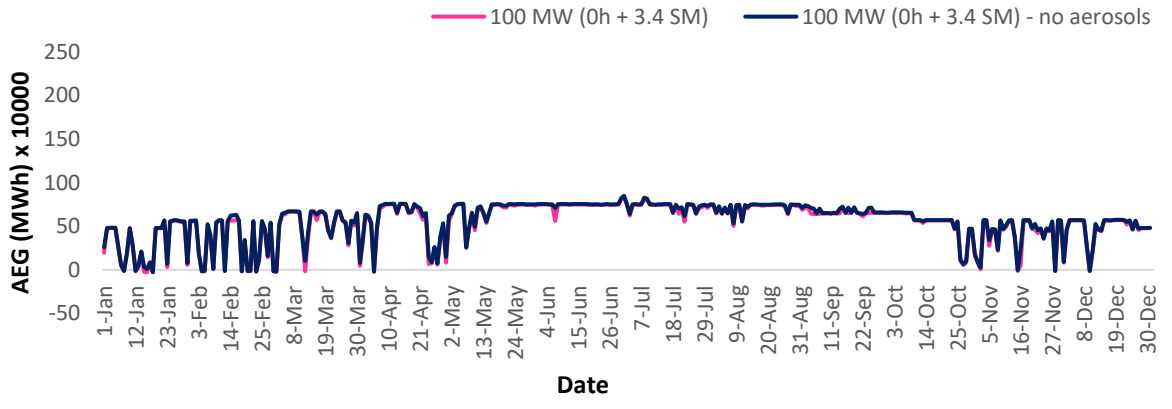
100 MW (0h + 3.4 SM)
100 MW (0h + 3.4 SM) - no aerosols
AEG (MWh) x 10000
250
200
150
100
50
0
-50
1-Jan
12-Jan
23-Jan
3-Feb
14-Feb
25-Feb
8-Mar
19-Mar
30-Mar
10-Apr
21-Apr
2-May
13-May
24-May
4-Jun
15-Jun
26-Jun
7-Jul
18-Jul
29-Jul
9-Aug
20-Aug
31-Aug
11-Sep
22-Sep
3-Oct
14-Oct
25-Oct
5-Nov
16-Nov
27-Nov
8-Dec
19-Dec
30-Dec
Date

(c)

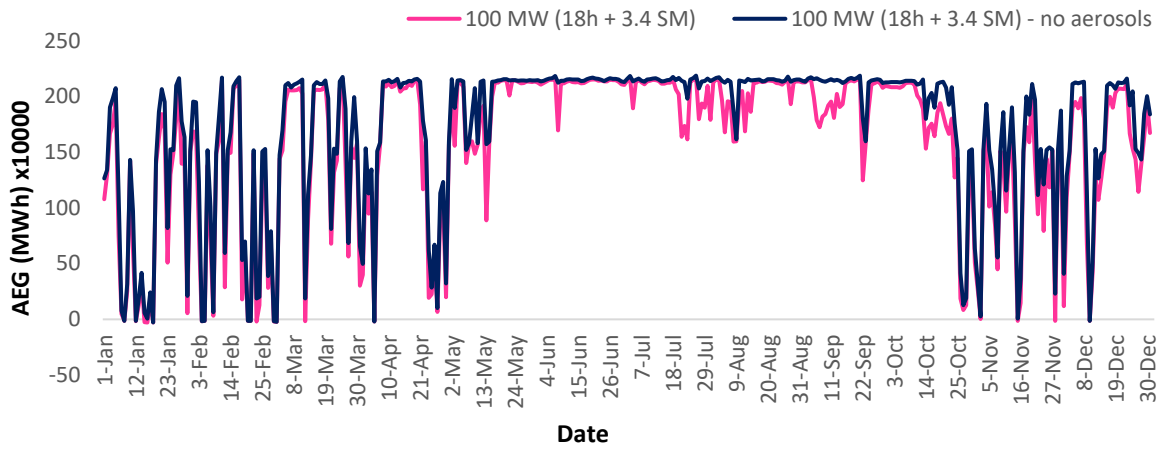

(d)

Fig. 3-9. Aerosols inclusion effect on the standalone SPT for (a) 50 MW with 0 h TES, (b) 50 MW with 18 h TES, (c) 100 MW with 0 h TES and (d) 100 MW with 18 h TES.

Since the SM represents the solar field size relative to the plant capacity, a similar value of SM does not represent the same solar field size, thus the solar field sizes in Figure 3-9 are not of the same size. For instance, the solar field of the 100 MW standalone SPT is larger than that of the 50 MW standalone SPT despite having a similar value of SM (here 3.4). In addition, regarding the reflectors shading effect, the reflectors, in the case of the SM is to increase, are added at the outer circumference of the existing ones. As a result, larger slant ranges from larger solar fields are produced which theoretically should amplify the effect of the aerosols on the reflected irradiance. The latter is indeed what is found in this work, however, not with a sharp amplitude. For example, the difference found between the AEG of the 50 MW SPT that is impacted by aerosols and that of the no aerosols scenario of the same capacity (and the same 18h TES and 3.4 SM) is found to be 5.8% and the difference in the AEG of the same cases but for the 100 MW SPT is found in this work to be 9.1%.

As depicted in Table 3-5, the deviations in the AEG due to aerosols inclusion result in deviations in the LCOE. The deviation in the AEG is first captured in the form of less reflected thermal energy from the solar field to the receiver. As a consequence, less thermal energy is transferred from the receiver to the HTF and thus, less thermal to electrical energy conversion. This affects the LCOE as the latter is deviated as a result of the AEG deviation. For the 50 MW capacity, the LCOE of the no aerosols scenario is found to be 5.9% less than that of the annually averaged AOD scenario. As for the 100 MW capacity, the LCOE of the no

aerosols scenario is found to be 9% less than that of the annually averaged AOD scenario (both at 18h of TES and 3.4 SM).

Table 3-5

The 50 and 100 MW standalone SPT optimal TES-SM outputs based on the annually averaged AOD and compared to the no aerosols scenario.

50 MW									
TES (h)	Optimal SM (-)	Thermal power from SF (MW_{th})		Total absorbed energy (MW_{th})		AEG (GW)		LCOE (¢/kWh)	
		Annually averaged AOD	No aerosols	Annually averaged AOD	No aerosols	Annually averaged AOD	No aerosols	Annually averaged AOD	No aerosols
0	1.4	291.7	297.6	273.8	279.4	91.8	94	19.2	18.6
3	1.8	400.8	434.9	378.7	412.4	134.9	138.1	15.6	15.2
6	2.2	507.8	563.9	479.2	534.7	175.4	180.2	14.1	13.6
9	2.6	606.1	680.4	574.7	648.2	212.1	219.4	13.2	12.8
12	2.6	660.3	734.4	628.6	702.1	227.9	243.3	12.7	11.9
15	3	763.7	860.1	725.1	820.7	265.8	284.1	12.3	11.5
18	3.4	843.7	963.2	799	917.3	300	317.8	12.1	11.4
100 MW									
TES (h)	Optimal SM (-)	Thermal power from SF (MW_{th})		Total absorbed energy (MW_{th})		AEG (GW)		LCOE (¢/kWh)	
		Annually averaged AOD	No aerosols	Annually averaged AOD	No aerosols	Annually averaged AOD	No aerosols	Annually averaged AOD	No aerosols
0	1	507.6	531.7	482.4	506.3	157.1	166.5	18.6	17.6
3	1.4	717.8	793.8	683.9	759.1	236.6	254.2	15.3	14.3
6	1.8	922.3	103,8.9	878	993.5	311.2	335.5	14	13
9	2.2	1,116.3	1,272.6	1,063.1	1,217.8	380.8	411.6	13.3	12.3
12	2.6	1,324.3	1,534.7	1,254.7	1,462.9	456.9	494	12.7	11.8
15	3	1,517	1,778.7	1,438.8	1,697.9	527.6	570.5	12.4	11.5
18	3.4	1,659.5	1,979.2	1,573.7	1,890.3	574.2	630.2	18.1	16.6

3.3.2 WT & NGCC Validation Results

Since the proposed plant is novel in terms of the configuration, it is complex to validate the entire system against another existing system as there were none that have

exactly the same configurations that have been found in the literature. Thus, the validation process of this work has been realized through a sub-system approach, i.e. validation of each of the individual components of SPT, WT and the NGCC.

3.3.2.1 WT Validation

The WT modelling results have been compared with the pilot plant data (over two years) from SREP that is available in [175]. As depicted in Table 3-6, the modelling results are in good agreement with the pilot data:

Table 3-6
The WT validation against the reported data in [175].

	Present work	Reported data for the 1st year	Reported data for the 2nd year	Contractor guarantee
AEG (GW/y)	34.1	39.6	36.9	35.2
Capacity Factor (%)	38.9	45.2	42.1	-

The deviation of this work's results compared to the first year of operation of the WT plant is found to be equal to -13.9%. This improves in the second year to -7.59%. Interestingly, the contracting company had assured a 35.2 GW/y, which is only -3.13% from the modelled AEG in this work. The differences can be attributed to the weather file that has been used in this work. This is a TMY file that describes the metrological conditions over an extended period of time and it is expected to give more accurate results when compared to the long-term operational data. It is worth mentioning that the validation revealed a LCOE of 3.9 c/kWh which is considered as the only reported LCOE value for this location.

3.3.2.2 NGCC Validation

The validation of the different configurations on the NGCC is illustrated in Figure 3-10. Here, the entire simulation process has been carried out based on an air-cooled condenser for the steam out of the ST. This is in order to minimize the consumption water which does not exist in abundant quantities in the case study location or arid regions in general. Also, a similar simulation based on water cooled condenser has been carried out and illustrated in the Appendix G in details. From here on, all NGCC simulations will only include an air-cooled

condenser as the water cooled condenser model has yielded huge amounts of consumed water which is to be avoided.

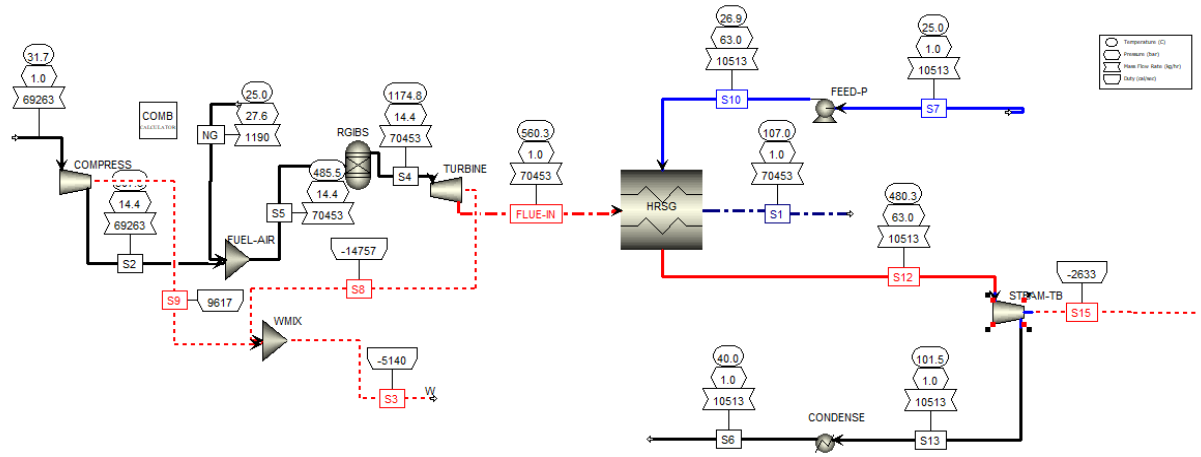

(a)

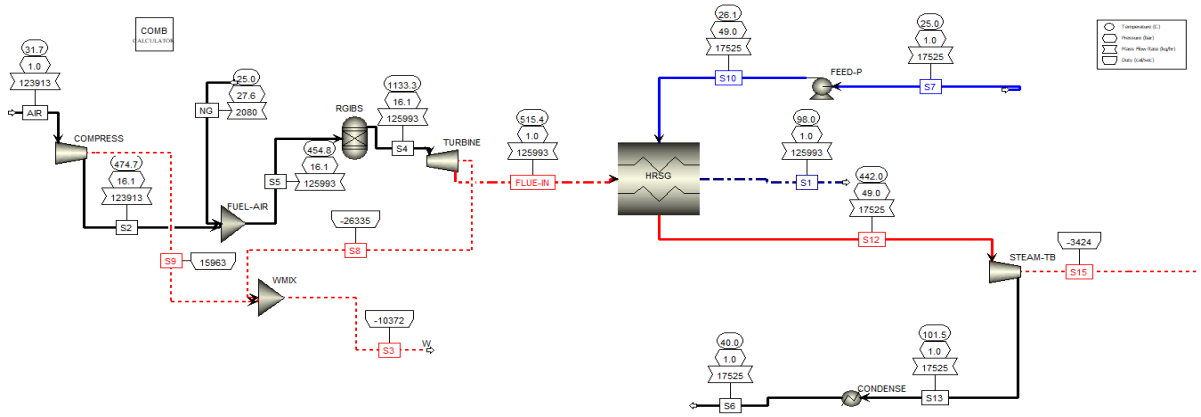

(b)

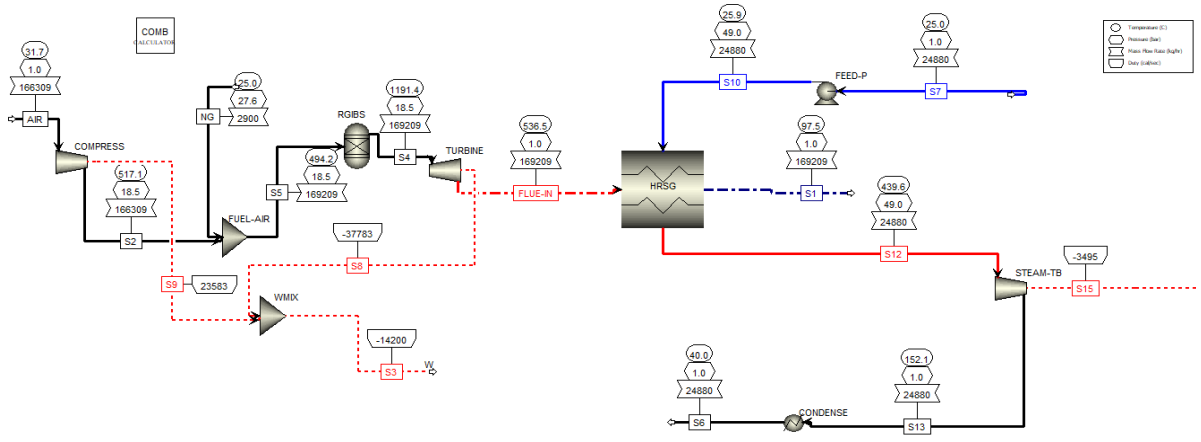

(c)

Fig. 3-10. Aspen Plus models for: (a) 8.6 MW, (b) 13.9 MW and 17.8 MW NGCC scenarios.

The results shown in Figure 3-10 reveal an acceptable deviation from the data acquired from the manufacturer data sheet [179]. In addition, the model set up in the Aspen Plus environment has considered similar metrological conditions as those considered in the SPT, e.g. the NGCC has been assigned an air inlet temperature of 31.65 °C which is a similar temperature of that assigned to the air-cooled condenser of the SPT in the case study location. Also, a ratio of air to fuel has been calculated in order to be used as an input to the mixer before the RGIBS reactor. The air quantity that is supposed to go into the mixer equals 17.118 kg air/kg CH_4 * 3.4 times the quantity of the fuel. This is calculated based on the stoichiometric air to fuel ratio as follows:

$$CH_4 + 2\,(O_2 + 3.76\,N_2) \rightarrow CO_2 + 2\,H_2O + 7.52\,N_2 \qquad (3\text{-}24)$$

Also, compared to the manufacturer data sheets, results of the Aspen models for all three NGCC scenarios are with minor deviations and this is shown in Table 3-7:

Table 3-7
The validation of the scenarios of NGCC.

		NGCC					
		8.5 MW		13.9 MW		17.8 MW	
		Manufacturer data sheet	Aspen Model	Manufacturer data sheet	Aspen Model	Manufacturer data sheet	Aspen Model
GT	Power output (MW)	5.1	5.1	10.4	10.4	14.3	14.2
	Exhaust mass flow rate (kg/s)	19.5	19.6	34.2	34.9	44.5	47
	Exhaust Temperature (C°)	544	560.3	510	515.4	529	536.5
ST	Inlet steam pressure (bar)	63	63	49	49	49	49
	Inlet steam temperature (C°)	482	480.3	440	442	440	439.6
	Max power output (MW)	3.5	2.6	3.5	3.4	3.5	3.5

The AEG for these three scenarios is subject to 85% CF as mentioned in the Materials & Methods section as this percentage considers maintenance and emergency stoppages. Regarding the CO_2 that is emitted by the NGCC different configurations, it differs from one configuration to another as it is a function of system heat rate and quantity of fuel consumed by the system. Table 3-8 lists the different annual emitted CO_2 quantities for the different NGCC configurations. It is worth mentioning that these CO_2 emissions correspond to a no CCS scenario as the latter is illustrated later on in the results. Also, full calculations including conversion rates are found in Appendix H.

Table 3-8
The CO_2 emissions for all three NGCC scenarios.

	NGCC		
	8.5 MW	**13.9 MW**	**17.8 MW**
System's Hourly fuel consumption (kg/h)	1190	2080	2900
The natural gas heat input to the system (BTU/h)	56,395,290	98,573,280	137,433,900
Hourly electricity generation (kW)	7,773	13,796	17,695
System heat rate (MMBTU/y)	419,613.7	733,456.6	1,022,434.1
Yearly net CO_2 emissions (kg/y)	22,201,760.9	38,807,188.7	54,096,988.2
CO_2 emission factor (g/kWh)	383.6	377.8	410.6

3.3.3 Individual Components & Aerosols Effects

In this section, each of the WT and the NGCC individual ability to compensate the loss

of the SPT due to aerosols inclusion are tested separately. This is important in order to understand how these individual components of the system contribute in the energy provision on a daily basis throughout the year. First, different SPT-WT configurations are examined under the condition that the hybrid configuration is always 100 MW. All observed SPT-WT configurations are compared to a theoretical optimally performing plant, which is represented by the no-aerosols 100 MW standalone SPT at the same TES-SM configuration, as this is expected to generate the highest AEG among all the other configurations of the SPT and/or SPT-WT as illustrated in Figure 3-11.

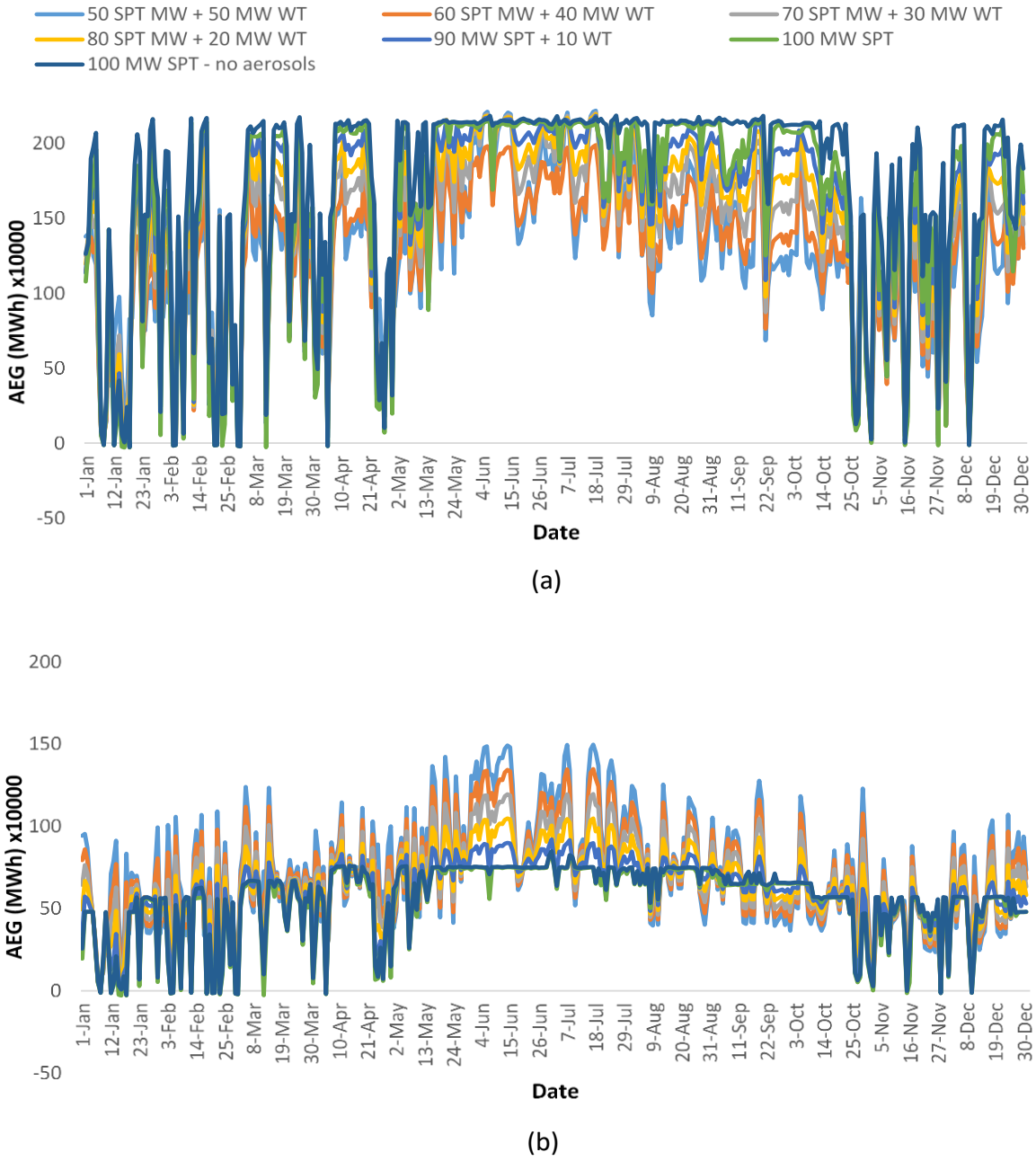

Fig. 3-11. The performance of a 100 MW hybrid SPT-WT model with different shares of both technologies compared to the 100 MW standalone SPT with and without considered aerosols for (a) 18h of TES and (b) 0h of TES.

Despite the inclusion of the aerosols effect on the solar field, the standalone aerosols impacted 100 MW SPT outperforms all other SPT-WT configurations as the WT integration fails to fully compensate the loss of the AEG caused by the aerosols density. The configurations with a major share of WT outperforms those of the major shares of SPT only for a few days over the entire year, e.g. first and mid-July. This is mainly due to the lack of energy storage for the WT. The latter finding is also obvious in the AEG of the configurations with a major SPT share as these assure an almost steady energy supply over the entire summer season. Interestingly, in the case of TES exclusion, which is illustrated in Figure 3-11 (b), the configurations with the major share of WT outperform those of the major SPT share. This agrees with previous studies findings, thus confirming that the intensity of the wind resource for this case study location has a great potential. Also, only from the AEG prospective, this proves that the SPT is much less valuable without a TES deployment as the large solar field is dumbing all the excessive thermal energy.

As for the NGCC hybridization with the SPT, the capacity share is less straight forward as the NGCC different capacities are restrained by the capacities that been found in the manufacturer data sheet and thus assigned for the NGCC different configurations. Hence, in order to run a reasonable comparison, the SPT share in the SPT-NGCC hybrid configurations has been assigned a capacity value that is equal to 100 MW when aggregated with the corresponding previously assigned capacity of the NGCC and this is shown in Figure 3-12.

The SPT- NGCC hybridization results in having a better energy provision compared to the WT when the TES is included. All three NGCC scenarios slightly outperform the standalone aerosols affected SPT, however, none reach the AEG level of the theoretical no aerosols SPT scenario. Due to the continuous energy provision and less fluctuations, these NGCC scenarios remain dominant even when the TES is excluded (Figure 3-12 (b)), however, never reach the levels of AEG that the SPT-WT provide when the TES is excluded (Figure 3-11 (b)). This further confirms the fact that the SPT is less appealing when the TES is excluded. In addition, despite the fluctuations in the energy levels with the SPT-WT configurations, the WT proves once again its compatibility for application at this location.

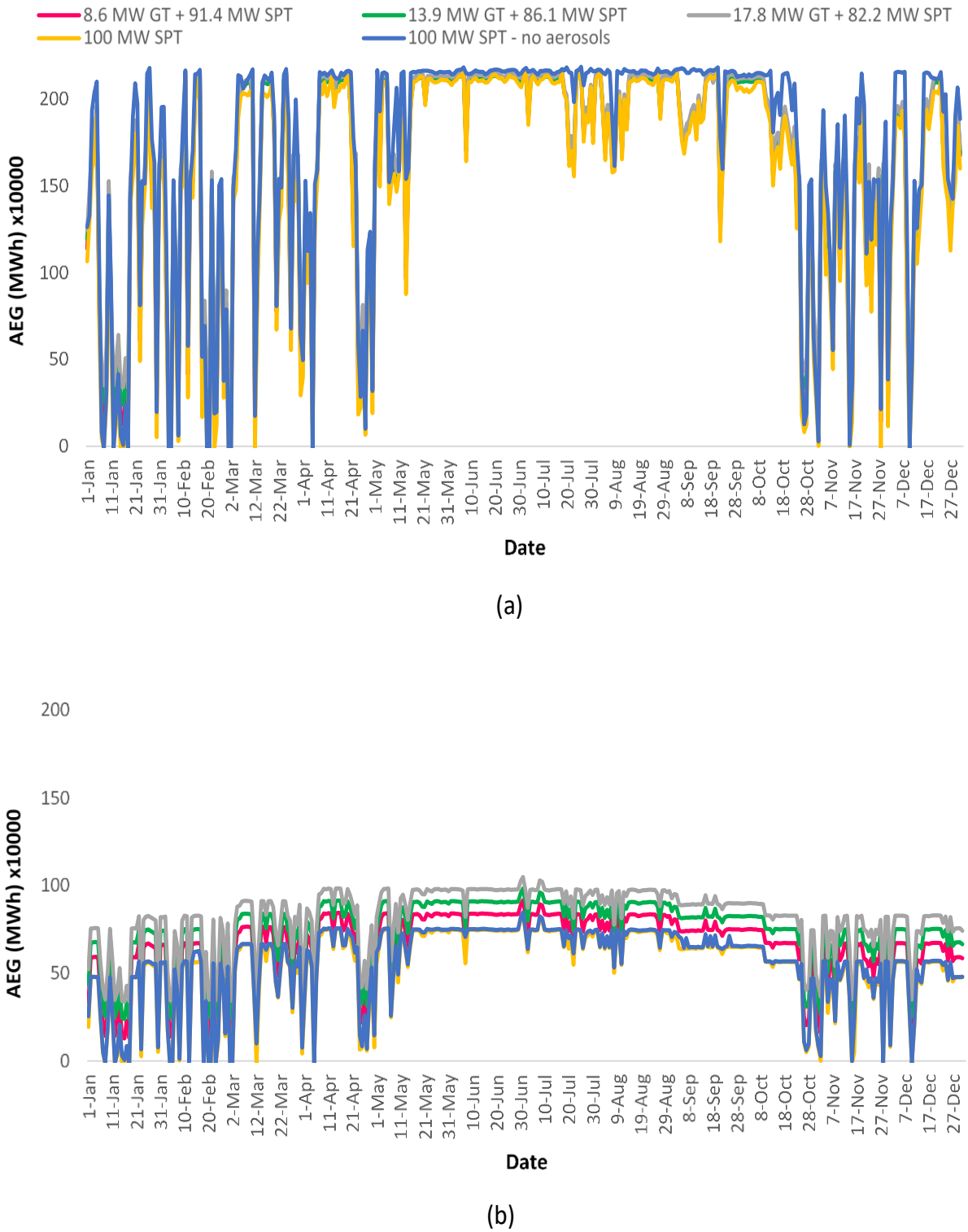

Fig. 3-12. The performance of a 100 MW hybrid SPT-NGCC model with different shares of both technologies compared to the 100 MW standalone SPT with and without considered aerosols for (a) 18h of TES and (b) 0h of TES.

3.3.4 System's Preliminary Performance

In order to understand the system's performance with respect to each individual component's effect on the entire system, this section illustrates the key performance

indicators behavior with a coarse variation of the key design parameters of all the system's components. The first two key performance indicators that are chosen to be illustrated are the GWP and the AEG because first, the GWP is normalized by the amount of produced energy thus directly related to the AEG. Secondly, the AEG variation projects at both the CF and LCOE, i.e. both are considered as performance indicators of interest in this work and are discussed right after the AEG and the GWP.

3.3.4.1 Global Warming Potential (GWP)

Regarding the GWP, the total value of each kg of CO_2 /kWh produced by the system is a simple aggregation of the corresponding GWP values of each system subcomponent, i.e. SPT, WT and NGCC. Since both WT and NGCC are considered as alternative/back-up components in the proposed hybrid plant and since they are relatively mature technologies compared to the CSP, both of these technologies' GWP are assumed averaged values from the literature as previously mentioned in section 3.2.2.1.3.

In contrast, the SPT is considered as the base model of this hybrid configuration and its main components are subject of examination in this work and its corresponding GWP is not assumed by an averaged value. Rather, it is calculated based on a sub-system evaluation approach where each main sub-system contribution of the GWP is evaluated separately before being aggregated to other SPT components' GWP to form the total GWP of each SPT configuration.

With the assistance of the inventory data of the three referenced SPT plants mentioned in Table 3-3, this work has been able to output the corresponding GWP values of the different SPT's subcomponents by a scaling technique. Figure 3-13 illustrates the scaling of the SPT subcomponents GWP in with accordance to each SPT relative AEG.

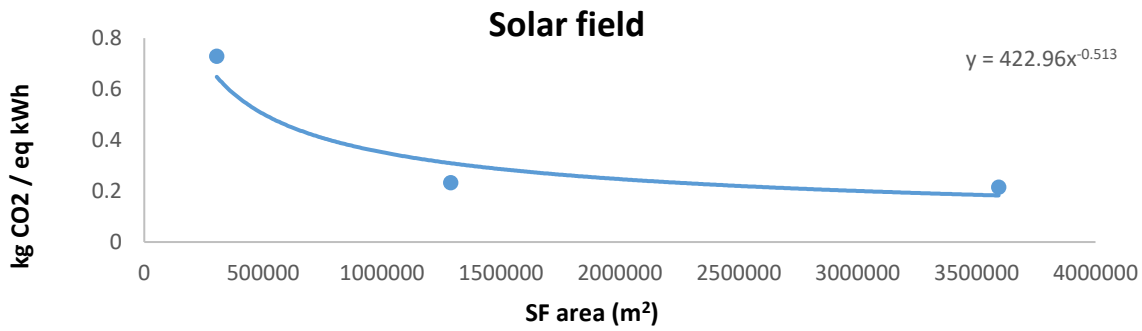
Solar field
y = 422.96x-0.513
kg CO2 / eq kWh
0.8
0.6
0.4
0.2
0
0
500000
1000000
1500000
2000000
2500000
3000000
3500000
4000000
SF area (m²)

(a)

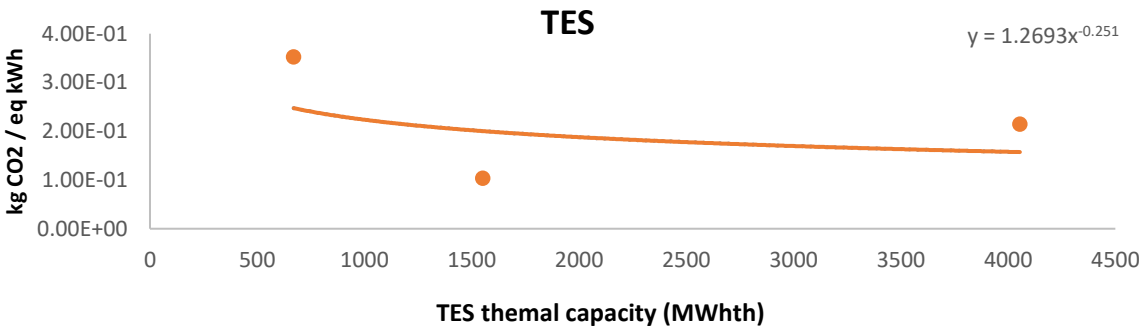
TES
y = 1.2693x-0.251
kg CO2 / eq kWh
4.00E-01
3.00E-01
2.00E-01
1.00E-01
0.00E+00
0
500
1000
1500
2000
2500
3000
3500
4000
4500
TES themal capacity (MWhth)

(b)

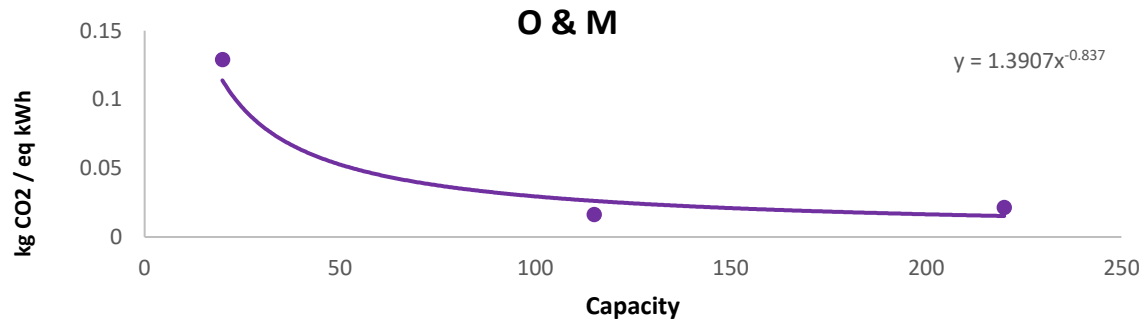
O & M
y = 1.3907x-0.837
kg CO2 / eq kWh
0.15
0.1
0.05
0
0
50
100
150
200
250
Capacity

(c)

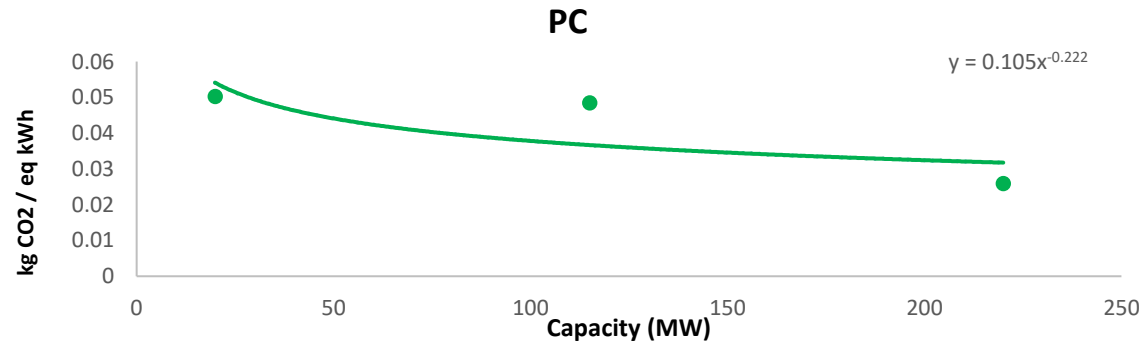
PC
y = 0.105x-0.222
kg CO2 / eq kWh
0.06
0.05
0.04
0.03
0.02
0.01
0
0
50
100
150
200
250
Capacity (MW)

(d)

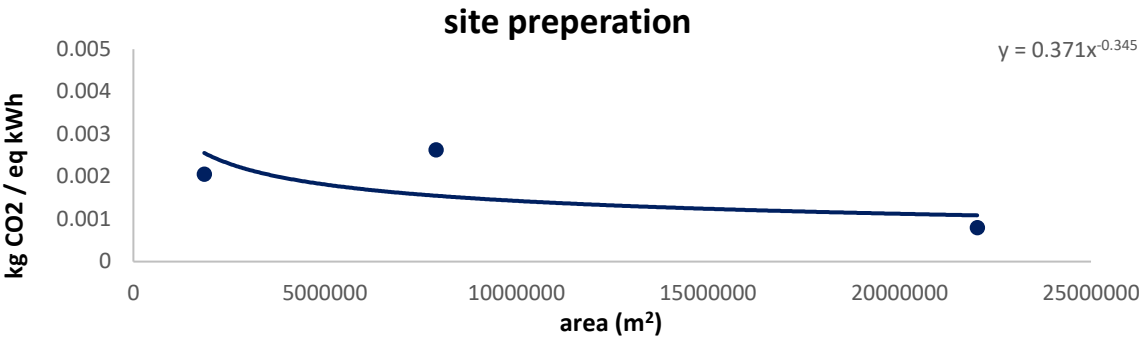

(e)

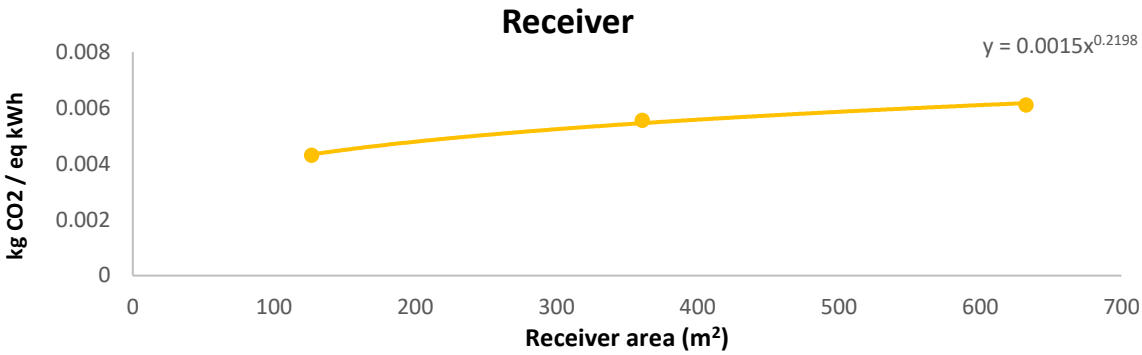

(f)

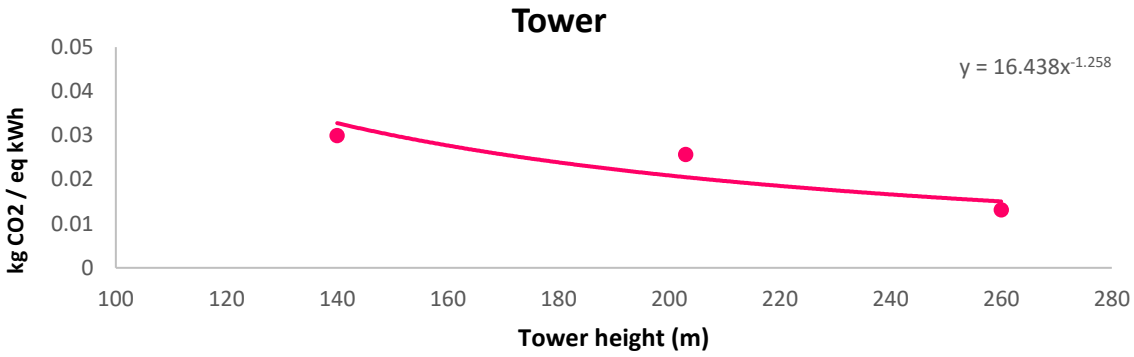

(g)

Fig. 3-13. The LCA inventory scaling for the SPT sub components based on the three SPT: Gemasolar, 115 MW and 220 MW.

The scaling of the SPT subcomponents GWP illustrated in Figure 3-13 is carried out in accordance to each SPT relative AEG during the entire lifetime of each corresponding plant, i.e. 25 years. Also, since some key design parameters such as the TES and the SM are considered as some of the variables in this work's optimization, the GWP scaling in this work is not uniquely associated with the SPT capacity. Rather, each sub component resulted GWP

is associated with its relevant parameter illustrated in Table 3-3. For instance, the GWP of the tower is normalized by its height, while the GWP of the receiver is normalized by its total area. Thus, these values can be calculated for each corresponding SPT configuration in the SAM and then plugged into the slope equation of the GWP in Figure 3-13. It is worth mentioning that some of the parameters can only be associated with the SPT capacity, e.g. Power Cycle and the O & M.

It is clear from Figure 3-13 that despite emitting more absolute quantities of CO_2 with a bigger employed solar field for instance, the GWP is on a downtrend as larger the solar field size becomes. This is because a larger solar field majorly contributes in increasing the AEG which makes the normalized value of kg CO_2 eq. / kWh becomes lower. This signifies the fact that the higher the AEG gets, the better from a GWP prospective. The only exception to this trend is found in the receiver which shows a slightly uptrend as its total area becomes larger, however, this does not majorly affect the GWP as the receiver contribution in the total GWP from the SPT has been found to be negligible for all three referenced SPTs as it is illustrated in Figure 3-14.

In this regard, it has been noticed that both the solar field followed by the TES top the GWP contribution with a quite noticeable difference compared to the other SPT subcomponents which agrees with what is found in the literature [167], [185]. Both of these subcomponents together present over 83-91% of the entire GWP of the reference SPT plants and this is illustrated in Figure 3-14. This justifies the reason of choosing these two specific key design parameters as variables in this work and that is in addition to the fact that the variation of these two components actually force all the other components of the SPT to adapt accordingly.

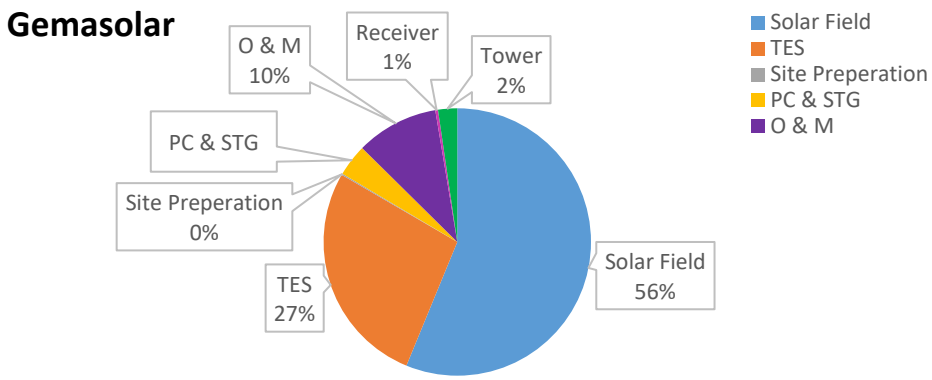

(a)

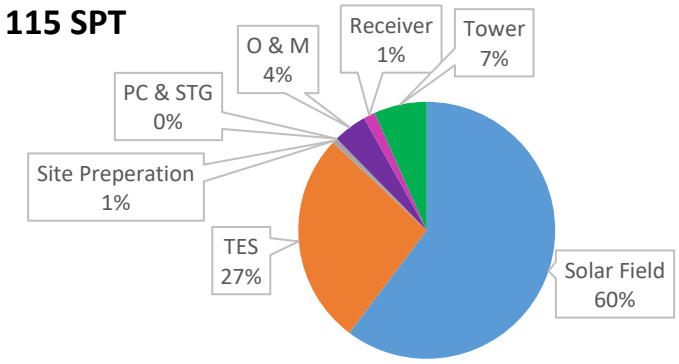

(b)

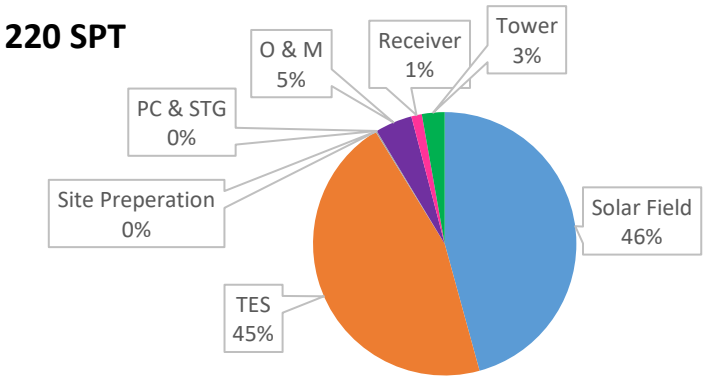

(c)

Fig. 3-14. The three reference SPT subcomponents contribution in the GWP.

3.3.4.2 Annual Energy Generation (AEG)

Once the GWP of the SPT is calculated, both the averaged values of WT and NGCC GWP are added to that of the SPT based on the entire system's configuration. Then, since the GWP is normalized by the system AEG per kWh, these two performance indicators are represented together in Figure 3-15 which illustrates the variation of the AEG for different SPT capacities when integrated along with and without WT for all the NGCC scenarios.

It is clear from Figure 3-15 that the addition of each of the WT and the NGCC increases the AEG, however, this increase is more noticeable in the 50 MW SPT rather than the 100 MW SPT. This is most probably because of the AEG that reaches the saturation-like state when both the TES and SM keep increasing. This limitation is expected as an excessive increase in the solar field size as a result of increasing the capacity of the SPT to capacities near the 100 MW is always paired with excessive increases in the receiver area, TES and the tower height, all of which are necessary in order to make use of the increased collected thermal energy form the solar field yet avoidable by the optimizer in the SAM as found in [145], [159]. The latter is set in order to only increase the size and capacity of the necessary SPT components when it is techno-economic efficient with accordance of the case study location resource.

In regards to the addition of the WT, a relatively minor increase in the AEG has been obtained due to the addition of the WT and that is seen in Figure 3-15 (b) compared to Figure 3-15 (a) for example. As for the effect of having higher SPT capacities, it is clear from Figures 3-15 (c) and (d) which correspond to a 100 MW SPT, that higher SPT capacities drastically increase the AEG. On the other hand, this is paired with positive returns on the emissions factor as the latter decreases compared to the 50 MW scenario.

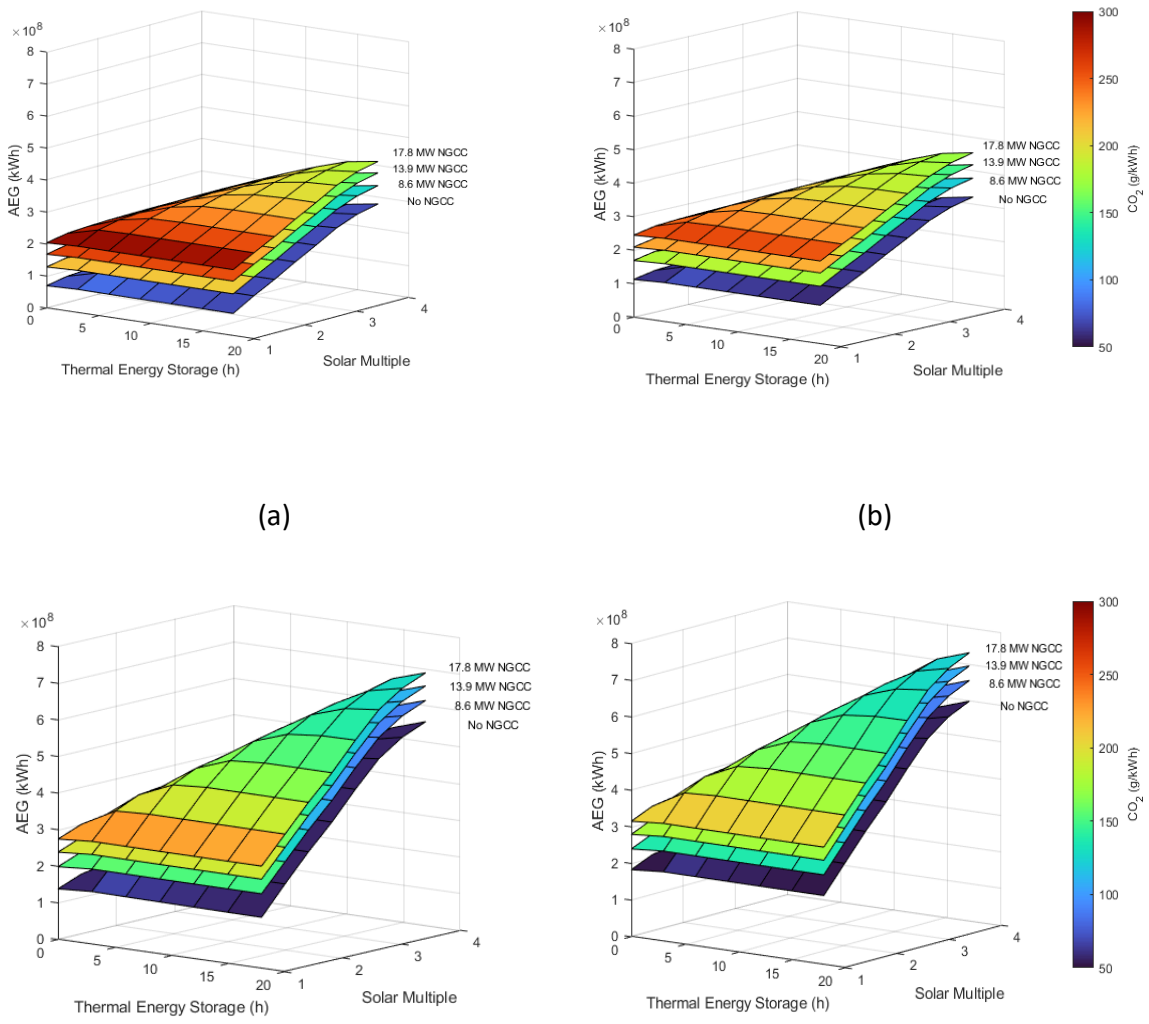

Fig. 3-15. The AEG and the emission factor (g CO_2 eq./kWh) based on different scenarios without a CCS unit: (a) 50 MW SPT + 0 WT, (b) 50 MW SPT + 6 WT, (c) 100 MW SPT + 0 WT and (d) 100 MW SPT + 6 WT.

From the color contour in Figure 3-15, it is clear that the NGCC integration dominates all the other components in the CO_2 emissions as the larger the NGCC is adopted, the larger emissions are obtained. In contrast, the WT integration has a positive impact on the CO_2 emissions, however, this impact is relatively small. On the other hand, the SPT capacity has a little more positive effect on the CO_2 emissions as the larger ranges of SM majorly contribute in increasing the AEG. This increase is crucial in decreasing the equivalent amount of CO_2 emissions grams per each produced kWh.

Regarding the CCS inclusion scenario, the used CCS model in this work is acquired from [203] and is able to capture 99% of the total CO_2 that is emitted by the NGCC. This high level of capture has been accomplished with amine post-combustion capture while focusing on multiple process variables such as lean loading, liquid to gas ratio and intercooling. In return, there is an energy penalty for such CO_2 capture, i.e. 3.7 MJ/kg of captured CO_2 (thermal to electrical energy conversion rate and calculations are found in Appendix K). Table 3-9 lists the results of energy penalty resulting from the CO_2 emissions capture for each year of the NGCC lifetime where the quantity of captured CO_2 is based on the net CO_2 emissions quantities illustrated in Table 3-8.

Table 3-9
The Annual energy penalty of the CO_2 capture process for all three NGCC scenarios.

	NGCC		
	8.5 MW	**13.9 MW**	**17.8 MW**
The quantity of captured CO_2 (kg/s)	0.7	1.23	1.72
The Energy Penalty (MW)	0.66	1.15	1.61
Percentage of the energy penalty from the total energy of the NGCC (%)	7.62	8.29	9

As seen form Table 3-9, the energy penalty that is a result of the CO_2 capture process ranges from 7.62-9% for the three different NGCC configurations. This finding agrees with what has been found in the literature as [204] has reported that a post combustion CCS for a NGCC has an energy penalty of 8.9%, while [205] has reported a AEG penalty of 15.5%.

Thus, the AEG ends up by being reduced as it is clear from Figure 3-16 which also confirms that the CCS has drastically managed to decrease the CO_2 emissions that is produced from the different NGCC configurations. On the other hand, it is also clear that the emitted CO_2 from the LCA of the NGCC is proportional to the capacity of the NGCC as it slightly

increases with the increase in the NGCC capacity. The acquired CCS from [203] is further illustrated in the Appendices.

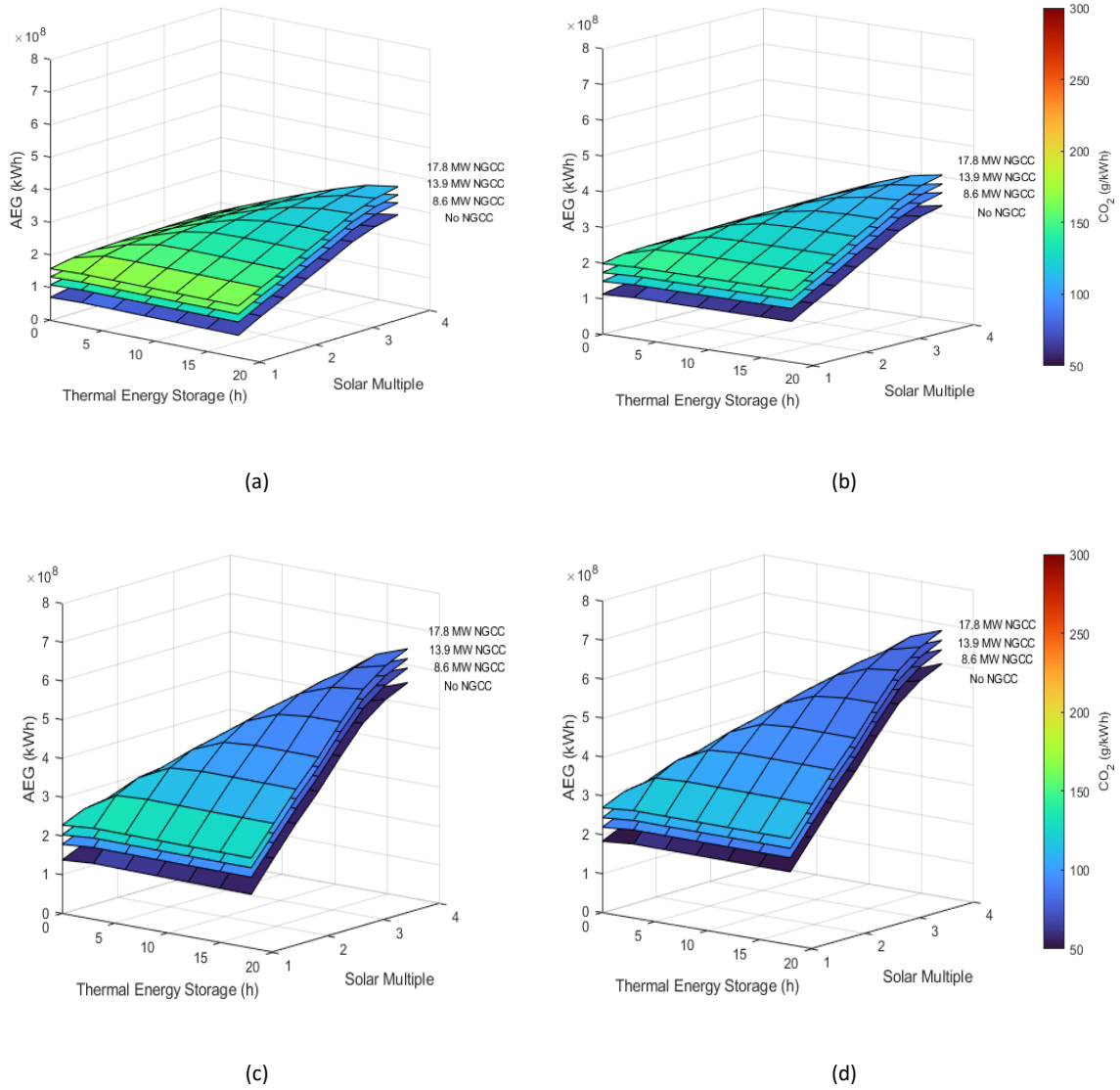

Fig. 3-16. The AEG and the emission factor (g CO_2 eq./kWh) variation based on different scenarios with a CCS unit: (a) 50 MW SPT + 0 WT, (b) 50 MW SPT + 6 WT, (c) 100 MW SPT + 0 WT and (d) 100 MW SPT + 6 WT.

3.3.4.3 Capacity Factor (CF)

The AEG penalty due to the CCS inclusion is clearly seen in Figure 3-16 as the contribution of the different NGCC configurations in increasing the AEG is not as big as it is in the no-CCS scenario (Figure 3-15). Also, the penalty in the AEG due to the CCS employment is

projected at the CF as expected as the latter is a function of the AEG and this is shown in Equation 3-25 which illustrates the CF of the entire hybrid system:

$$CF = \frac{AEG_{SPT+WT+NGCC}}{8760 * nameplate\ capacity} \quad (3\text{-}25)$$

The integration of the NGCC has greatly enhanced the performance of the proposed plant in terms of the CF as the configurations of 50 MW SPT with no WT can reach up to 95% of CF as illustrated in Figure 3-17 (a). On the other hand, despite the contribution of the WT in increasing the absolute values of the AEG, the WT inclusion scenarios are with lower CF as the increase in the AEG cannot make up the increase in the capacity of the hybrid plant which results in having lower CF values as illustrated in Equation 3-25. This WT's disability of increasing the AEG to the point where the CF is also increased is due to the lack of a back-up system which can store excess energy for later usage. This is unlike the SPT which has the TES, thus has the ability to provide energy for extended periods of time. Also, when the SPT capacity is larger, the NGCC ability to increase the CF becomes more limited compared to the case where the SPT is lower, e.g. 50 MW. This is normal as each capacity of the three adopted scenarios of the NGCC represent a bigger percentage of an alternative energy source for a 50 MW SPT plant compared to a 100 MW SPT plant.

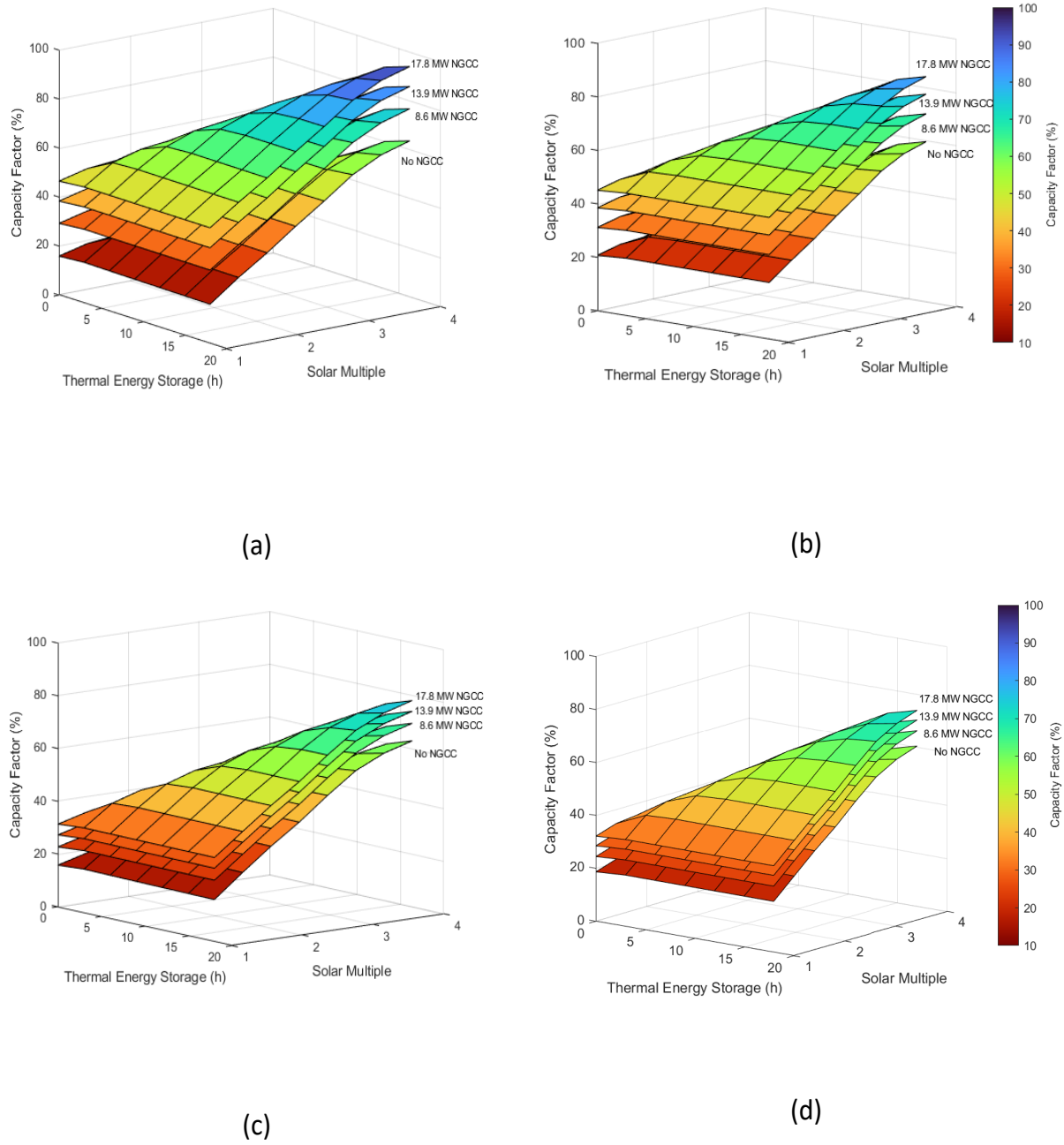

Fig. 3-17. The CF performance based on different scenarios: (a) 50 MW SPT + 0 WT, (b) 50 MW SPT + 6 WT, (c) 100 MW SPT + 0 WT and (d) 100 MW SPT + 6 WT.

It is worth mentioning that this preliminary parametric analysis is only necessary for a better understanding of the performance indicators behavior based on the plant different components and the optimal sizing strategy applies realistic boundaries on the optimization technique in order for it to only elect realistic solutions that fit the promoted county's plan in line with world leading renewable energy countries strategies.

As for the configurations with the CCS unit, where a penalty on the AEG exists due to the CCS unit needing to capture the CO_2, the CF is affected as a result. Figure 3-18 illustrates

the extent of this inclusion on the CF. The penalty on the AEG is also seen in the addition of different NGCC capacities when compared to Figure 3-17, the CF surfaces of the different NGCC scenarios are closer to each other's in having a similar trend as the one obtained in the AEG. This proves that the addition of larger NGCC capacities in the CCS scenario yields positive returns in terms of higher CF, however, these returns are lower than those of the no CCS scenario.

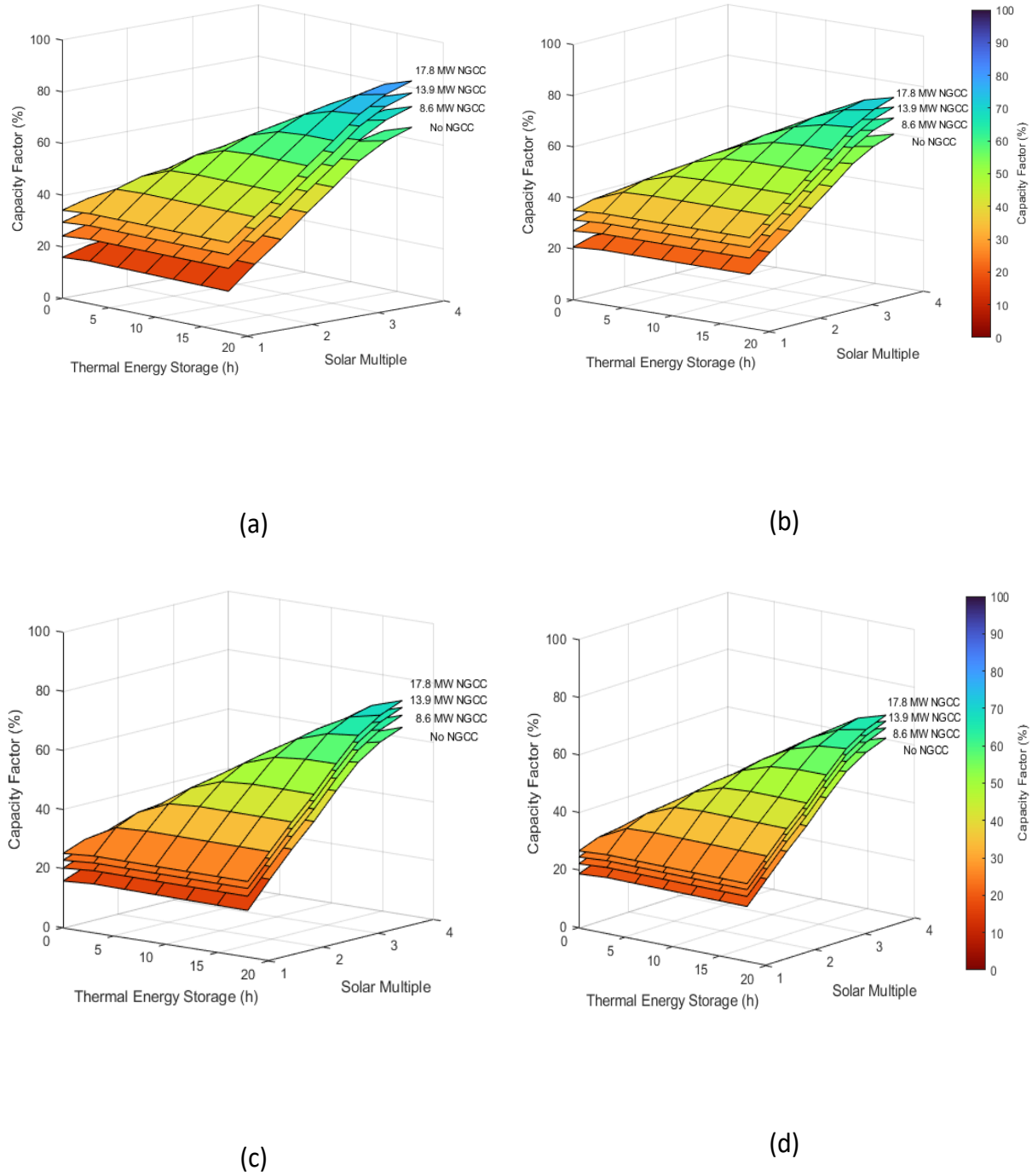

Fig. 3-18. The CF performance with a CCS unit based on different scenarios: (a) 50 MW SPT + 0 WT, (b) 50 MW SPT + 6 WT, (c) 100 MW SPT + 0 WT and (d) 100 MW SPT + 6 WT.

3.3.4.4 Levelized Cost Of Energy (LCOE)

In addition to the effect of the AEG variation on the CF, the variation of the AEG causes a variation of the LCOE. This is because the AEG is a major parameter in the calculation of the LCOE and this is illustrated in Equation 3-8. Figure 3-19 illustrates these variations for different SPT-WT capacities and the SM-TES of the no-CCS scenario.

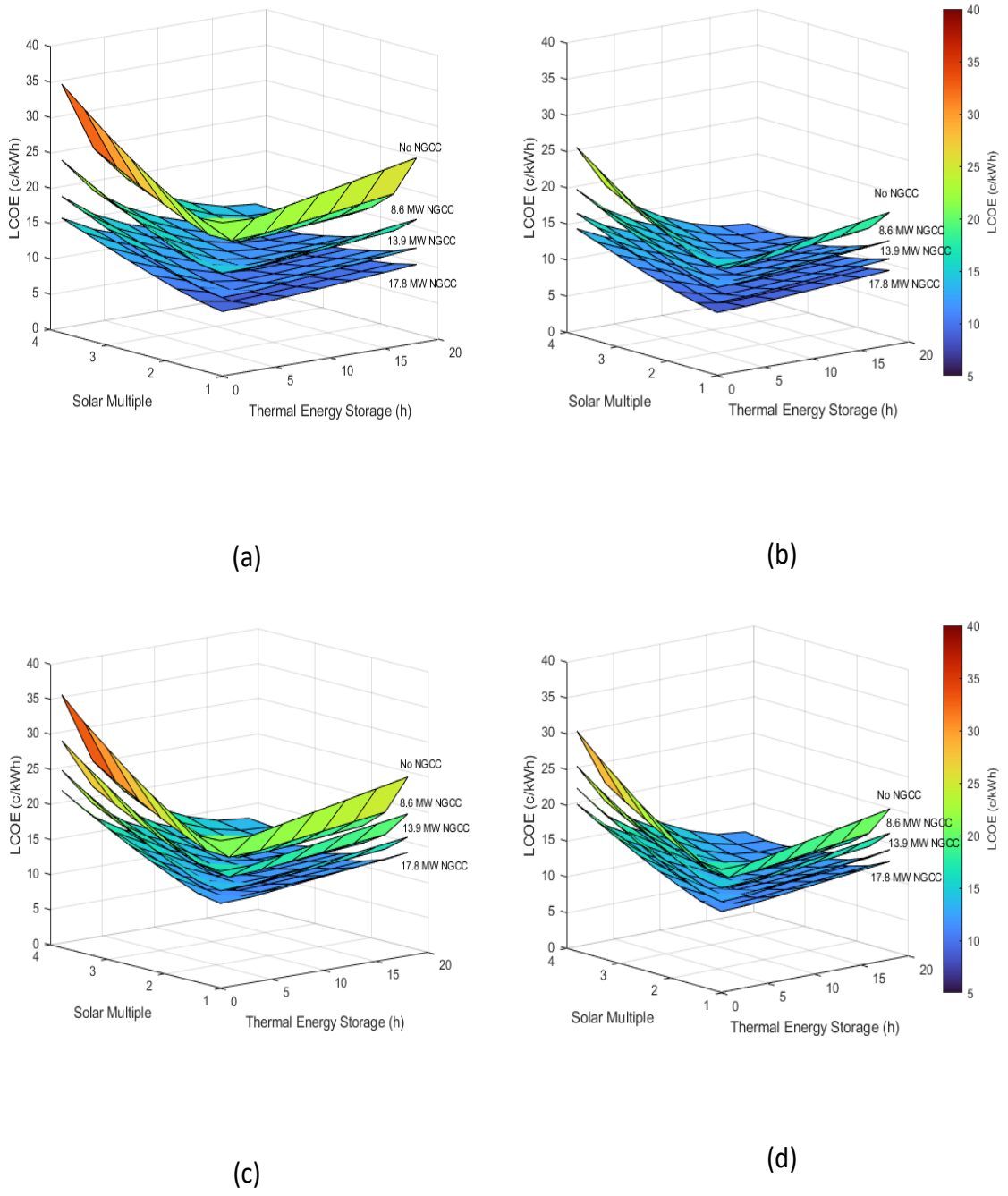

Fig. 3-19. The LCOE performance based on different cases for the no-CCS scenario: (a) 50 MW SPT + 0 WT, (b) 50 MW SPT + 6 WT, (c) 100 MW SPT + 0 WT and (d) 100 MW SPT + 6 WT.

It is clear from Figure 3-19 that the integration of NGCC can positively affect the LCOE as the larger the capacity of the NGCC gets, the lower the obtained LCOE. Also, it can be noticed that in the no WT scenarios (Figure 3-19 (a) and (c)), the LCOE is lowered relatively the most when the smallest NGCC is adopted. When the NGCC capacity becomes larger, the LCOE is further decreased, however, not to the same degree as in the smallest capacity of NGCC. On the other hand, this effect is less clear when the WT are adopted (Figure 3-19 (b) and (d)). This is most probably because the scenarios with the WT inclusion are already characterized by lower LCOE due to the lower CAPEX of the WT. This is also confirmed as the Figures 3-19 (b) and (d) generally exposes lower LCOE.

As for the CCS scenario, the variation of the LCOE takes an interesting turn. This is because, in the case seen from a generic point of view, the LCOE variation for both the CCS and no-CCS scenario do not differ much from each other's. However, a close look at Figure 3-20 (b) reveals that the NGCC inclusion has a greater positive effect on the LCOE for the CCS scenario compared to that of the no-CCS scenario. This is clear due to the total exploitation of the produced AEG in contrast to the CCS scenario where some energy is used during the carbon capture and storing process of the CCS. Overall, since the difference in the LCOE for the two scenarios are not very significant, this signifies a very positive sign for the CCS scenario as this scenario drastically reduces one of the performance indicators in this work, i.e. CO_2 emissions as seen in Figure 3-16 without having a major negative impact of the LCOE.

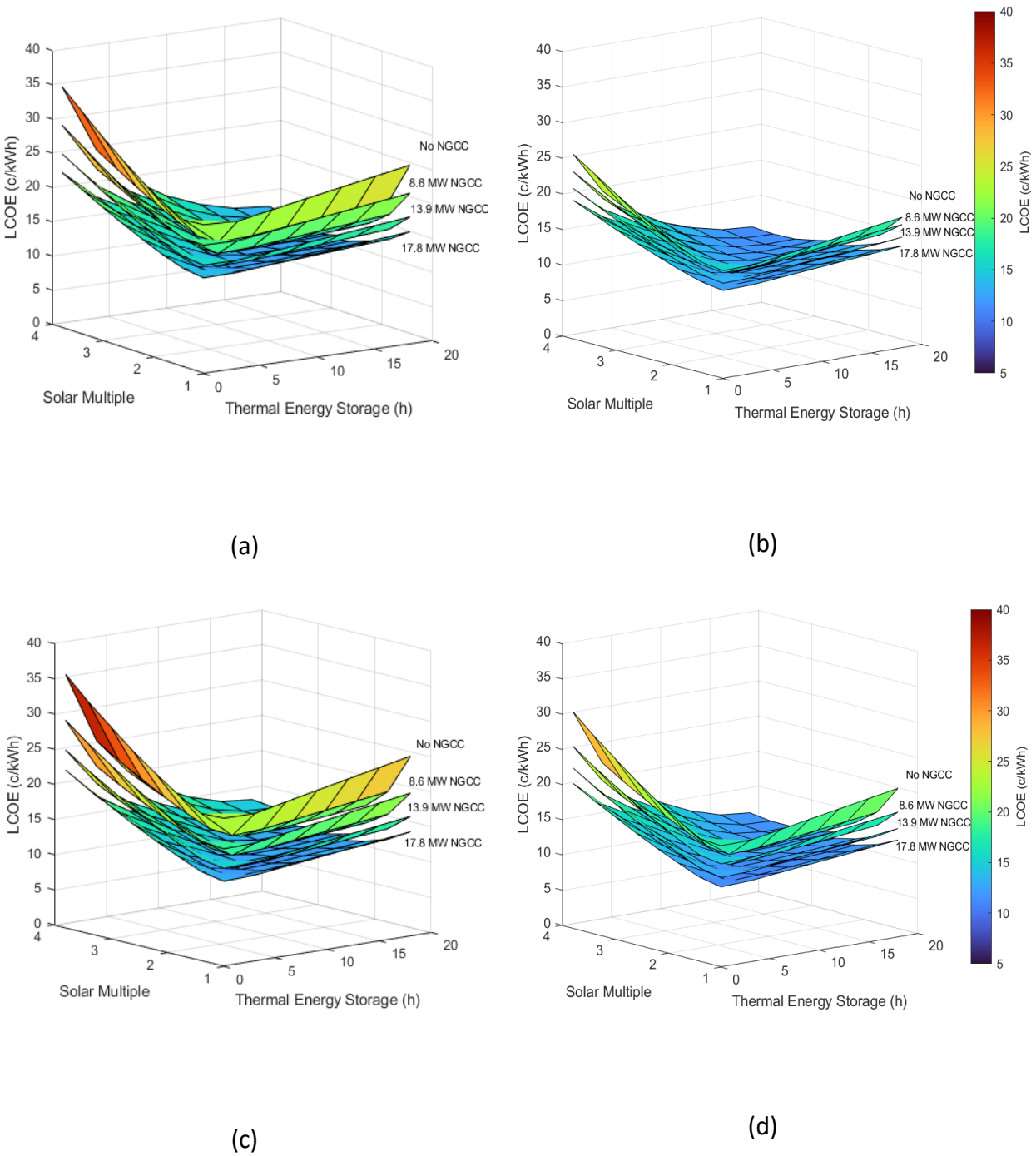

Fig. 3-20. The LCOE performance based on different cases for the CCS scenario: (a) 50 MW SPT + 0 WT, (b) 50 MW SPT + 6 WT, (c) 100 MW SPT + 0 WT and (d) 100 MW SPT + 6 WT.

3.3.4.5 Water Consumption

Since the case study location of this study is arid regions, this work has made a maximum effort to minimize the water consumption. For instance, the condensation process that takes place in the power cycle of both the NGCC and the SPT is based on air-cooled condenser where no water is used. In addition, this work promotes WT which does not

require any water to be fully functional (except for minor quantities for cleaning and washing off accumulated dust). However, the solar field reflectors of the SPT still need to consume water for washing off the accumulated dust particles as these can contribute in a soiling process and thus disturb the solar irradiance reflection. Thus, the reflectors washing is the only process that is considered in the water consumption and thus it is uniquely a function of the solar field size. The latter varies as a function of different SM values as well as different SPT capacities which both majorly contribute in the AEG production. Thus, for a simple illustration, Figure 3-21 shows the variation of the water consumption as a function of the AEG. This is because different SPT capacity values impose different solar field sizes even if the SM value are identical, which can make the illustration of the water consumption based on the SPT capacity a bit misleading.

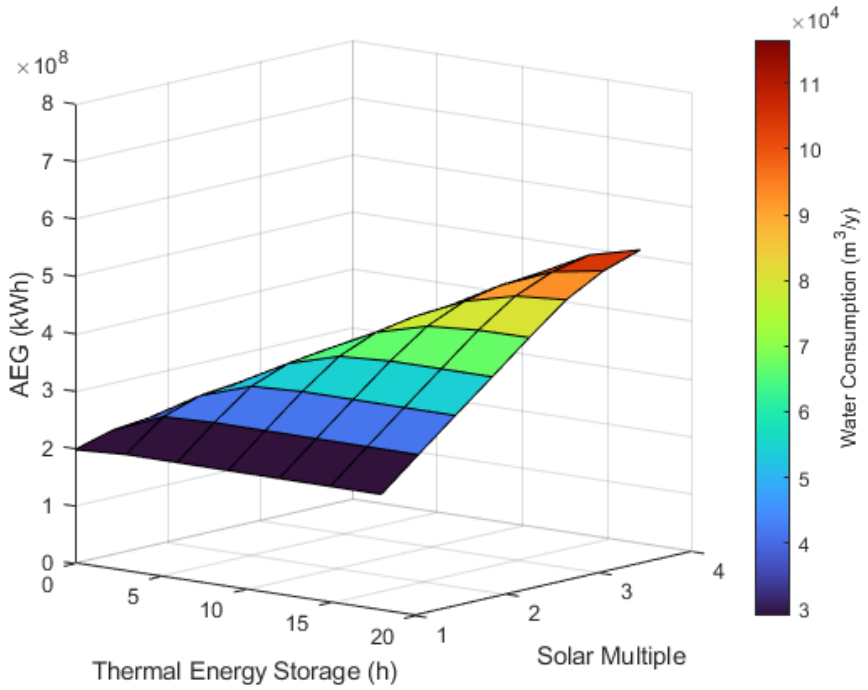

Fig. 3-21. The water consumption variation of the SPT as a function of the AEG.

The AEG illustrated in Figure 3-21 corresponds to the entire SPT capacity range of 40-110 MW. It is clearly seen in Figure 3-21 that the larger the SM gets, the larger the solar field gets and thus the larger amount of water is consumed. As previously mentioned, the water consumption is only affected by the solar field size and not the TES.

3.4 Conclusions

This chapter started off by testing the aerosols effect on the SPT solar field to reach capacities up to 100 MW, which is an extension of the previous chapter where the effect of aerosols on the SPT has only been tested on the baseload capacity of 50 MW. The results show an increasing effect of the aerosols density on the SPT solar field and the AEG as the losses of the latter reach up to 9.1%. With the increasing SPT capacity range, the obtained results of the aerosols effect on the solar field show an almost linear trend. This is most probably because of the methodology used by the simulation tool's strategy in the process of new heliostats addition in the solar field which adds new heliostats at the outer circumference of the already existing ones at each time a larger solar field is adopted. Also, this has been found to be projected at the LCOE, which also is deviated by 9% compared to the LCOE of the no aerosols scenario.

In addition to the SPT performance assessment, this chapter has also evaluated the potential of other renewable energy technologies application, i.e. WT. The preliminary evaluation of the WT performance has been based on a validation work of the already operational WT at the case study location in SREP. The validation work has revealed lowered LCOE value of 3.9 c/kWh which is the first LCOE reported value in the literature for this case study location to the best of the author's knowledge. This LCOE value indicates a great potential of wind energy applications and furtherly confirms what has been previously found in the wind assessment studies found in the literature. In addition, this justifies the proposed concept of this work which relies on the WT to lower the hybrid configuration's total LCOE value.

With the assistance of the in-house developed algorithm, this work has been able to automate the hybridized configuration of both the SPT and WT performance models that exist in SAM. As a consequence, this work has managed to assess the ability of WT to make up for the lost energy in the SPT due to aerosols density. The WT has shown a great ability to do so, however, only when smaller TES are adopted in the SPT. Also, a NGCC has been included as a fossil fuel back up system along with the SPT and the WT. This has also been realized with the assistance of the in-house developed algorithm despite not being included as an option in SAM. In a similar manner of for the WT, the ability of the NGCC to make up for the energy losses of the SPT has been assessed and found to be very efficient.

Once the hybrid configuration of SPT-WT-NGCC is set up, the algorithm has been used to run a parametric analysis where the key design parameters of each technology in the hybridization is varied over a designated range. This has been carried out to evaluate the performance of the hybridization through the illustrative performance indicators of LCOE, CF, CO_2 emissions and water consumption. The preliminary results of the system depict some positive, yet contradicting results. For instance, the WT majorly contributes in the decrease of the LCOE, however, limits the increase in the CF. Similarly, it has been noticed that the hybrid configuration with larger NGCC capacity results in an increased AEG and thus the CF, which reaches up to 95%. On the other hand, this inclusion of larger NGCC capacities drastically increases the CO_2 emissions in the no CCS scenario. This has been avoided in the CCS scenario, however, the latter comes with a penalty on the AEG as energy is needed in the CCS process. This energy penalty is typically projected at the LCOE, which is furtherly affected by the CAPEX of the CCS unit. Lastly, the WT has a positive effect on the LCOE because of its low CAPEX. Also, the WT has typically no effect on the CO_2 emissions compared to the SPT and the NGCC.

From the assessed performance indicators in this work, it can be concluded that the proposed plant of SPT-WT-NGCC has a great potential to optimally exploit both the RE and fossil fuel natural resources that the case study location and multiple other similar locations around the world possess. However, as a result of the contradicting nature between the performance indicators of the proposed hybrid system, it is difficult to elect an optimal configuration that maximizes the techno-economic characteristics of the system while limiting the environmental threats of the same system. Therefore, this complex problem must be solved through a multi-objective optimization approach which is able to evaluate each system's configuration by its corresponding performance indicators and thus, offer an optimal configuration of the SPT-WT-NGCC that equally satisfy these performance indicators to the best of its ability.

Chapter 4 – Optimal Sizing

Abstract

In this chapter, the optimal configuration of the proposed system is targeted. This has been mainly carried out based on the performance indicators that have been assessed in the previous chapter as a result of the hybridization process of the SPT, the WT and the NGCC with and without CCS. A performance map has been created based on the interpolation of each of the performance indicators of LCOE, CF, CO_2 emissions and water consumption through the assistance of an in-house developed surrogate model. The latter has been able to interpolate the corresponding values within a finer step size for each of the previously assigned variables reaching 76,608 possible configurations of the proposed system with precision, ease and short time. Then, the performance map is transferred to the optimization tool box in Matlab where each performance indicator is assigned as an objective function in the multi-objective optimization. The optimization function manages to elect a set of optimal solutions for each scenario, i.e. the CCS and the no-CCS scenarios. Also, the sets of the optimal solutions are ranked from best to worst with the assistance of a multi criteria decision making tool (MCDMT) which also helps in assigning different importance weights to the different objective functions.

4.1 Introduction

4.1.1 Background

Despite being able to improve the system's performance according to certain performance indicators, the hybridization of each the WT and the NGCC had limited the system's performance with regards to other aspects. This has been illustrated in the previous chapter as for instance, the addition of the WT has positively decreased the LCOE, however, limited the CF to low values. Similarly, the addition of the NGCC has increased both the AEG and the CF, on the other hand, it has drastically increased the CO_2 emissions. With multiple performance indicators that are essentially considered, it is complex to manually choose a system's optimal configuration especially when these performance indicators are of a contradicting nature as in the case in this work. In addition, for an inclusive insight, the most important design parameters of the main components in the hybrid configuration must be tested according to assigned ranges. This variation of parameters creates a massive number

of configurations and solutions, which is more detailed and inclusive than the preliminary parametric analysis that has been carried out in the previous chapter and usually exists in the vast majority of studies of the literature.

4.1.2 Preface

Most of the techno-economic studies that are found in the literature are of single objective optimizations origin which only target the lowest LCOE as an indication of the best techno-economic performing plant configuration. However, a single objective optimization study can be too subjective and discard other important factors in the performance and viability of the proposed plant. This is very critical as the optimization outcome risks of being too simplified and thus unrealistic [206]. Factors such as AEG, CF, CAPEX, and most importantly for arid regions, water consumption must be taken into account in the optimization process. The determination of multiple optimal solutions presented by a tradeoff surface for the conflicting objectives is a much more useful judgement methodology for decision makers.

This type of complex problems with multiple variables and objectives is optimally carried out by a multi-objective optimization technique. Such techniques can include all objectives of interest while also varying all the key design parameters, e.g. capacity, TES and SM. This is very important because it is commonly known that the standalone CSP optimal configuration is based on its key design parameters of TES and SM that produce the lowest LCOE value. However, when CSP is hybridized with other technologies such as WT, this is not valid anymore as the lowest LCOE of CSP-WT is always associated with the CSP-WT with bigger WT share as the latter majorly contribute in decreasing the LCOE. Including other objectives in the optimization process in addition to the LCOE will most probably prevent the extreme bias favoring the variable that decreases the LCOE, i.e. WT or/and fossil fuel inclusion

To this extent, recent research has redirected their focus towards the multi-objective optimization techniques. For instance, Allouhi et al. [207] applied a multi-objective optimization technique in order to find a tradeoff between the CF and the site improvement costs for a dish Sterling based CSP for two different sites in Morocco and Spain. Spelling et al. [208] attempted to minimize both total investment costs and the LCOE by varying the receiver area and the TES size of a SPT model. Similarly, Guedez el al. [209] targeted the minimization

of both LCOE and capital costs of a SPT modelled in Spain. Awan et al. [210] used a multi-objective optimization technique to locate an optimal tower height, SM and TES capacity for a 100 MW SPT and compared the results to a commercial scale SPT configuration.

4.1.3 Multi-Objective Optimization

Recently, the selection of an optimal sizing strategy issue for RE systems has been increasingly tackled by evolutionary algorithms. Algorithms such as Artificial Bee Colony, Ant Colony Algorithm, Particle Swarm Algorithm, Biogeography Based Optimization have been successfully used for such optimization problems [211]. In addition, Artificial Neural Networks [212] and Fuzzy Logic [213] have also been reported to be used for such problems. The Genetic Algorithm (GA) has recently emerged as one of the most reliable mimetic algorithms. The GA been chosen to be used in this work's multi-objective optimization because it is known by its ability of handling complex optimization problems with both linear and non-linear functions [214] and has been cited as one of the most practical multi-objective optimization tools for hybrid RE systems [215].

Also, there has been a vast diversity of the objective functions of interest that have been assigned by researchers as the most important factors in the optimal sizing strategy of a RE system. In this regard, the economic performance is arguably one of the most indicative performance indicators and has almost never been left unassessed. Whether an inclusive economic indicator such as the LCOE [174], [216], [217], [218] or more specific one such as net present value [219], land use [220], site improvements [207] and total costs [221], [222] almost all researchers agree on the economic part essentiality in any optimization problem.

On the other hand, while the LCOE can sufficiently describe the economic competitiveness of the proposed plant, the absolute AEG alone cannot describe the technical superiority of such a plant. This is because it is irrelevant to the rated capacity (the energy demand in other means). Thus, a few number of researchers have been motivated to include the CF as an important objective in the optimization process [223], [224]. It is true that some researchers who have been able to obtain certain demand loads in certain case study locations, tried to adhere to this demand by assigning the demand load follow ability as an objective function [225] or minimizing peak load [226]. In contrast, others did not have certain demand load, however, presumed a needed capacity, calculated the plant's ability to achieve

this capacity and thus assigned the capacity factor as an objective function [207], [217]. Other factors such as loss of power supply probability has also been found in the literature [174], [227] but more for off-grid applications.

Among the many multi-objective optimization studies in the literature, to the best of my knowledge, there is no study that has weighed the importance of the water consumption within a multi-objective optimization approach along with other important parameters. Water consumption assessments are given in numbers which can be complex to be interpreted by the decision makers. Also, it is worth mentioning that water consumption is typically not included in the LCOE calculations. This is crucial to be included in the optimization as the water production, purchase and transport costs can have a significant impact on the techno-economic feasibility of the proposed plant especially in arid regions where no water access is available.

In addition, in regards to the mitigation of CO_2 emissions, the literature is mainly based on LCA assessment that is carried out for already fixed CSP configurations as previously seen in Section 3.1.3, while the variation of the CSP's key design parameters such as the TES and the solar field can drastically vary the LCA outcome of the CSP. Thus, it is ideal for a study to assess the LCA of a variety of CSP possible configurations and then use the assistance of multi-objective optimization by including the LCA as one of the objective functions of the optimization in addition to these of techno-economic performance, e.g. LCOE, AEG and CF.

Also, It has been noticed that the vast majority of multi-objective optimization studies has been limited only to two objective functions [149], [228], [229], [230]. This discards other important performance indicators and this has been recently addressed by the inclusion of up to three different objective functions as in [231], [223], [232]. This work's aim is to assess and elect an optimal configuration of a SPT-WT-NGCC plant that is techno-economic efficient, with least environmental harm and with controlled water consumption. This can be achieved by assigning the following performance indicators as objective functions in the optimization problem: the LCOE, water consumption, the CF and the CO_2 emissions. The existing conflict between the aforementioned performance indicators can be optimally addressed by the GA where the SPT, WT, NGCC capacities, SM and TES are assigned as decision variables.

4.2 Materials and Methods

4.2.1 Objective Functions & Variables

To address the conflict between the various objective functions, the multi-objective optimization technique through the GA is chosen. The GA relies on an extensive parametric analysis of the optimization problem's variables as a primary input. Then, the GA observes the configurations associated with the best solutions. The best solutions are considered as such based on their ability to satisfy the user's assigned objective functions. Thus, the optimization problem of this work is defined based on four different conflicting functions and is formulated as follows:

Min.$f_1(\chi)$ = *Water Consumption* ($\vec{x}$),

Min.$f_2(\chi)$ = *LCOE* ($\vec{x}$),

Min.$f_3(\chi)$ = *CO_2 Emissions* ($\vec{x}$),

Max.$f_4(\chi)$ = *Capacity Factor* ($\vec{x}$),

In order to restrict the optimal solution space, the above mentioned objective functions are subject to the lower (χ_j^L) and upper (χ_j^U) boundaries of the selected decision variables. For instance, a general optimization problem constraint can be carried out as follows:

Min.$f_1(\chi)$ = *Water Consumption* ($\vec{x}$),

Subject to C_i ($\vec{x}$) = 0, I = 1, … m

$(\chi_j^L) \leq x \leq (\chi_j^U)$

where C_i ($\vec{x}$) is the equality constraint and m is the number of constraints [233]. The decision variables are SPT capacity, the SM, the TES capacity, the number of WT and the NGCC capacity. The boundaries of these variables are shown in Table 4-1:

Table 4-1
The upper and lower bounds for the decision variables.

Parameter	Lower bound	Upper bound
$SPT_{capacity\ (MW)}$	50	100
$SM_{(-)}$	1	3.8
TES $_{(h)}$	0	18

WT_n	0	6
$NGCC_{capacity\ (MW)}$	0	17.8

The objective functions that have been assigned for this optimization problem are a function of these decision variables with both linear and non-linear natures. For example, the water consumption depends on the washing process of the solar field reflectors; which are functions of the SPT capacity and the SM. The WT does not consume any water, thus it is excluded from any water consumption contribution. As for the LCOE, all the designated decision variables contribute in the calculation of the LCOE as they impose different CAPEX and OPEX. Also, all the decision variables contribute in the calculation of the AEG as their variation represents higher/lower AEG and the latter has a major contribution in the calculation of the LCOE. The AEG also contributes as an input in the CF calculations, in addition to each capacity of the system component, i.e. the SPT, the WT and the NGCC. The decision variables' contribution in the objective functions is simplified in the logic diagram illustrated in Figure 4-1.

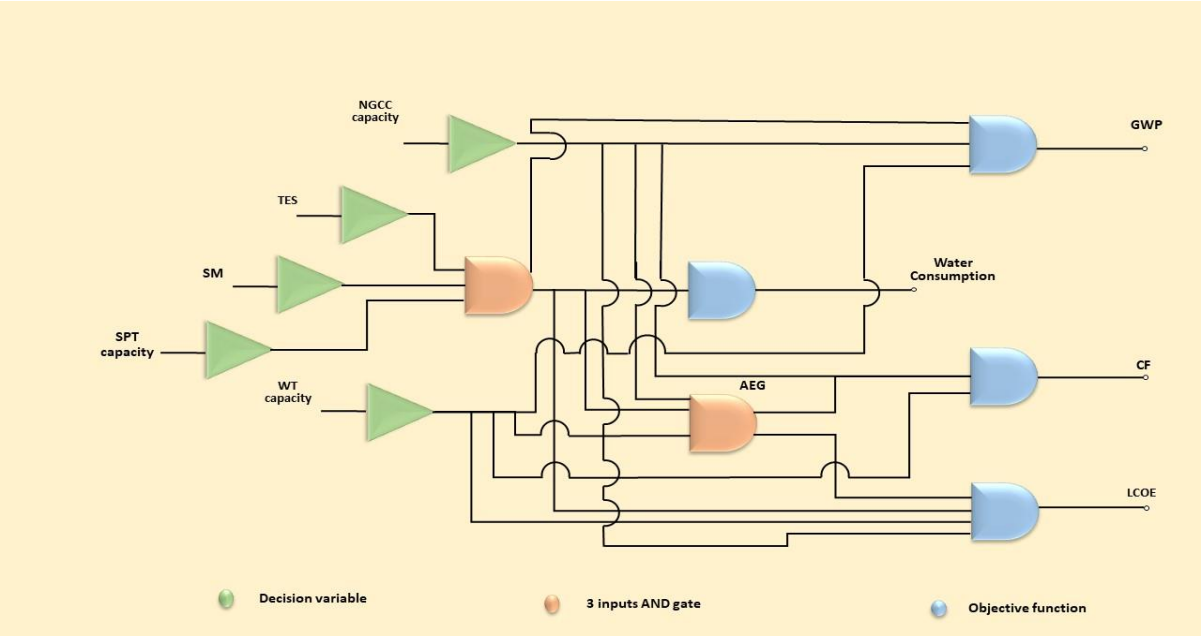

Fig. 4-1. A logic diagram of the contribution of each decision variable in the calculation of each objective functions.

4.2.2 Surrogate Model

The optimization's specific objective functions are obtained with the assistance of the in-house developed algorithm as it is illustrated in the previous chapter. Since the SPT performance model in the SAM has its own integrated optimization tools, the developed algorithm is designed to run these optimization tools prior to the hybridization process. This initiates an issue with regards to time consumption in case the step sizes mentioned in Table 4-1 are alternated to smaller step sizes which is required in order to create the performance map of the system for the GA. To overcome this issue, a surrogate model has been created in Matlab as such model can efficiently interpolate the required data based on finer step sizes than those that have been assigned for the in-house developed algorithm. This results in an acceleration and a better exploration of the performance of the system and thus, faster, more inclusive and deeper insight of the optimization [234], [235]. On the other hand, the surrogate model is mainly based on interpolation, which makes it subject to deviations from the original data that the developed algorithm would have calculated [207], [223], thus it has to be validated. A brief idea of the surrogate model ability to predict the system behavior is illustrated in Figure 4-2 where the red points represent the simulated (or measured in case of an experiment) indicators and the blue surface is the interpolated behavior of the system by the surrogate model [234].

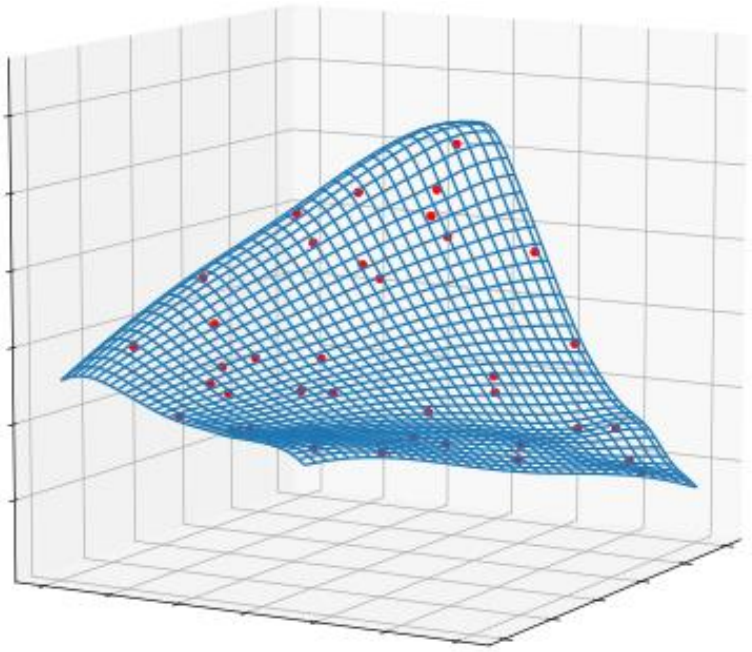

Fig. 4-2. Surrogate model interpolation [234].

Thus, the newly adopted upper and lower bounds due to the adoption of the surrogate model are listed in Table 4-2.

Table 4-2
The newly adopted upper and lower bounds for the decision variables compared to the initial ones.

	Parametric analysis			**Surrogate model**		
	Lower bound	**step size**	**Upper bound**	**Lower bound**	**step size**	**Upper bound**
$SPT_{capacity\ (MW)}$	50	10	100	40	5	110
$SM_{(-)}$	1	0.4	3.8	1	0.4	3.8
TES $_{(h)}$	0	3	18	0	1	18
WT_n	0	2	6	0	1	8
$NGCC_{capacity\ (MW)}$	0	N/A	17.8	0	N/A	17.8

The performance map that the surrogate receives as an input is typically the output of the parametric analysis that has been carried out in SAM in the previous chapter. This results in having 5376 possible configurations. With the assistance of the surrogate model which is based on the new step sizes in Table 4-2, this increases to 76,608 configurations due to both having smaller step sizes and broader lower and upper bounds. The broader upper and lower bounds are adopted to enhance the surrogate model's ability of interpolation and only applied where it is applicable.

The interpolation of the desired objective functions from the surrogate model is realized through the ***griddedInteropolant*** built in interpolation function in Matlab. In addition, the surrogate model is validated in this work through the following steps:

- 10 % of the total surrogate model outputs.
- Elimination of SAM original outputs.
- Figuring out the variables that correspond to the 10 % outputs.
- Simulation based on these variables in SAM.
- Comparison with the surrogate model outputs based on: maximum deviation percentage, MBE and RMSE.

4.2.3 Genetic Algorithm

Once a surrogate model is built for each of the conflicting objective functions, these are passed into the Matlab built in optimization application by the GA. The GA has the ability to handle complex optimization problems through the election of a non-dominated Pareto frontier (or surfaces) sort of solutions to the user in a fast and efficient manner, which makes such a technique widely used in this research area [236], [237]. The GA is capable of dealing with a high number of variables which makes it very inclusive. Also, the GA manages to save a lot of computational time.

Inspired by natural selection, the GA relies on the genetic operators of selection, crossover and mutation [238]. The pseudocode of the GA includes multiple aspects that starts by a random initialization of individuals, i.e. where both size of population and number of generations are determined. Here, gens are selected to be reproduced from the population, i.e. Selection [239]. Secondly, transformation of possible solutions via an encoding scheme that gives the individuals specific representation. Then, the problem's objective functions for each individual are evaluated to map their fitness where those of higher fitness have more chance of survival. Only then, a crossover is used for the creation of the new offspring. Finally, maintenance of the genetic diversity from one population to the next one is preserved by the mutation phase. The entire GA process is presented in Figure 4-3.

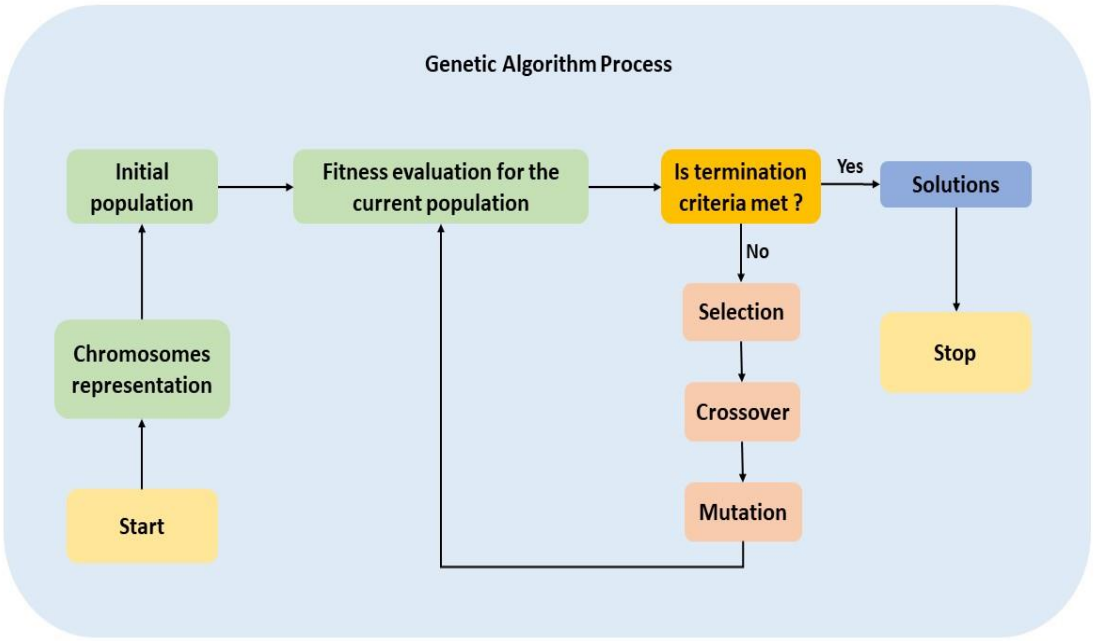

Fig. 4-3. The Genetic Algorithm working process.

Among the multiple available variations of the GA, the Non-Dominated Sorting Genetic Algorithm II (NSGA-II) is used in this work. This variation of GA combines both parent and offspring populations and gathers them in non-dominated classes. Then, the fittest individuals in each class are populated on the Pareto front (or surface in case on more than two objective functions are included). This method only focuses on the non-dominated optimal solutions while at the same time it ensures the preservation of the population's diversity [240]. The GA inputs of this work (listed in Table 4-3) are primarily acquired from [241] and adapted accordingly.

Table 4-3
GA operator specifications.

Parameter	Value
Population size	200
Maximum Generation	1000
Pareto Fraction	0.5
Crossover operator	Intermediate
Crossover fraction	0.8

Prior to running the GA, the set of solutions of the multi-objective optimization is constrained by some necessary boundary conditions. First, the outputs of the optimization are limited to integer variables values in order to avoid illogical variables selection by the GA. Also, the SPT is considered as a baseload energy generation source and has been assigned a minimum capacity of 50 MW; a potential standardized CSP size [124], on the other hand, the maximum capacity for the hybrid plant is 100 MW. As for the WT, an upper bound is set to 6 WT because this is the maximum WT number per planned SPT as proposed in the master plan of the SREP [34]. In addition, a total area of 3,260,000 m^2 has been set as a constraint on the GA as this area has been approximated from the dedicated area for the SPT in the SREP plan and this is illustrated in Figure 4-4 (b) while the operational PTC is illustrated by the satellite image in Figure 4-4 (a).

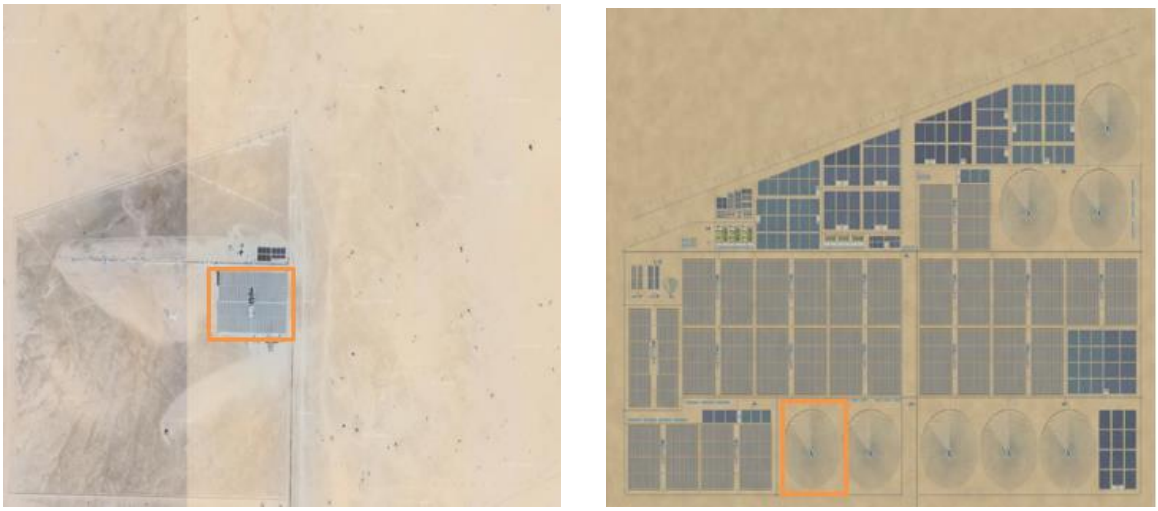

(a) (b)

Fig. 4-4. SREP in both (a) actual (PTC illustrated) and (b) future planned appearances (SPT illustrated, adopted from [34]).

Since the GA elects a series of optimal trade-off solutions among the conflicting objective functions, the elected optimal solutions satisfy the objective functions differently. For example, some of the GA optimal solutions lean more towards the lowest LCOE than other objective functions, however, without a total dissatisfaction of these objectives. In contrast, other solutions lean towards the lowest water consumption more than other objectives. The GA has not got the ability of ranking the individual solutions according to their ability to equally satisfy all the objective functions. Hence, there is a necessity to deploy a multi-criteria decision making tool (MCDMT) which is able to rank the individual solutions from best to worst over the set of the optimal solutions.

4.2.4 Decision Making Tool

Despite the NSGA's ability to elect a set of optimal solutions after eliminating all dominated solutions, however, even this set of optimal solutions can be a bit confusing for decision makers. Unspecialized concerned decision makers might prefer to have a ranking of the set of optimal solutions and here appears the importance of the MCDMT. In addition, there must be an importance weighting criteria that the decision makers rely on where an objective function is more valuable to be satisfied than other or all other objective functions. These two very important features can be crucial for the plant's configuration selection process and can be provided by the MCDMT.

A variety of MCDMT exists in the literature, each of which has its advantages and limitations. Table 4-4 lists some of the frequently used MCDMT by researchers in the literature.

Table 4-4
A general overview of different MCDMT.

MCDMT	Advantages	Limitations	Reference
Analytic Hierarchy Process (AHP)	• Simplicity of computation process. • Short calculation time.	• Possible inaccuracy and hazardous results because of interdependence of objectives and alternatives. • Final results require further verification.	[242]
Best-Worst Method (BWM)	• Minimization of comparisons.	• Lack of consistency.	[243]
Preference Ranking Organization METHod for Enrichment of Evaluations (PROMETHEE)	• Consideration of criteria's interdependency.	• Complexity of application. • High computational requirements.	[244]
Technique for Order Preference by Similarity to Ideal Solution (TOPSIS)	• Simplicity of computation process. • Short calculation time.	• Only suitable when the alternatives indicators don't vary much. • No consideration of negative and positive values difference.	[245], [246]
Weighted Sum Method (WSM)	• Simplicity of computation process.	• Basic estimations. • Only one preference criteria allowed.	[247]

In this work, the TOPSIS decision making tool has been used in order to rank the individual solutions from the set of optimal solutions elected by the GA despite the downsides

that the tool is known for. This is because these disadvantages of the TOPSIS listed in Table 4-4 do not present any fundamental ambiguity for the aim of this work and have been addressed in this work and thus, the ranking of optimal set of solutions for the optimization problem has been achieved with ease and short time.

The TOPSIS starts by an evaluation matrix creation based on the design points (D_1, D_2, …, D_m which are placed vertically) and the objective functions (C_1, C_2, …, C_n which are placed horizontally) as follows [207]:

	C_1	C_2	C_3	…	C_n
D_1	x_{11}	x_{12}	x_{13}	…	x_{1n}
D_2	x_{21}	x_{22}	x_{23}	…	x_{2n}
…	…	…	…	…	…
D_m	x_{m1}	x_{m2}	x_{m3}	…	x_{mn}

(4-1)

Then, since the different objective functions are measured differently, all the objective functions must go through a non-dimensionalization process. This can be accomplished by the division of design options (i) as well as the evaluation criteria (j) by the norm vector as follows:

$$x_{ij}^{n} = \frac{x_{ij}}{\sqrt{\sum_{i=1}^{m}(x_{ij})^2}} \tag{4-2}$$

Then, in the case where all objective functions have similar importance, no different weights are given to each of them. Conversely, in the case where some objective functions are more important than others, different weights (w_j) are given to the objective functions, thus the weighted normalized values are obtained as follows [207]:

$$x_{ij}^{wn} = w_j \,.\, x_{ij}^{n} \tag{4-3}$$

Once normalization and weighting have been performed, the TOPSIS defines two ideal points, one positive (*A +*) and one negative (*A -*):

$$A+ = \{a_1^+, a_2^+, \dots, a_n^+\} = \{best\ x_{i1}^{wn}, best\ x_{i2}^{wn}, \dots, best\ x_{in}^{wn}\} \,/\, i = 1 \dots m \tag{4-4}$$

$$A- = \{a_1^-, a_2^-, \dots, a_n^-\} = \{worst\ x_{i1}^{wn}, worst\ x_{i2}^{wn}, \dots, worst\ x_{in}^{wn}\} \,/\, i = 1 \dots m \tag{4-5}$$

Only then, both distances of the positive (d_i^+) and negative (d_i^-) ideal solutions from each solution (i) can be calculated as follows [174]:

$$d_i^+ = \sqrt{\sum_{j=1}^{n}\left(x_{ij}^{wn} - a_1^+\right)^2}\ \ i = 1 \dots m \tag{4-6}$$

$$d_i^- = \sqrt{\sum_{j=1}^{n}\left(x_{ij}^{wn} - a_1^-\right)^2} \quad i = 1 \dots m \tag{4-7}$$

Finally, the best solution among the elected optimal solutions is the solution with the highest relative closeness (*RC*) which can be calculated as follows:

$$RC_i = \frac{d_i^-}{d_i^+ + d_i^-} \quad i = 1 \dots m \tag{4-8}$$

This technique is simple while being able to handle large numbers of solutions as well as objectives [246], [248], which makes it suitable for this work purpose and this can be confirmed by its wide use in similar RE research [174], [216], [249], [250], [251], [252]. In addition, the ability of the weighting of different objective functions with the TOPSIS based on their relative importance is a robust feature that enables this work to prioritize objective functions that are more important in arid regions applications over others, e.g. water consumption. Figure 4-5 illustrates the methodology of the entire work where every data

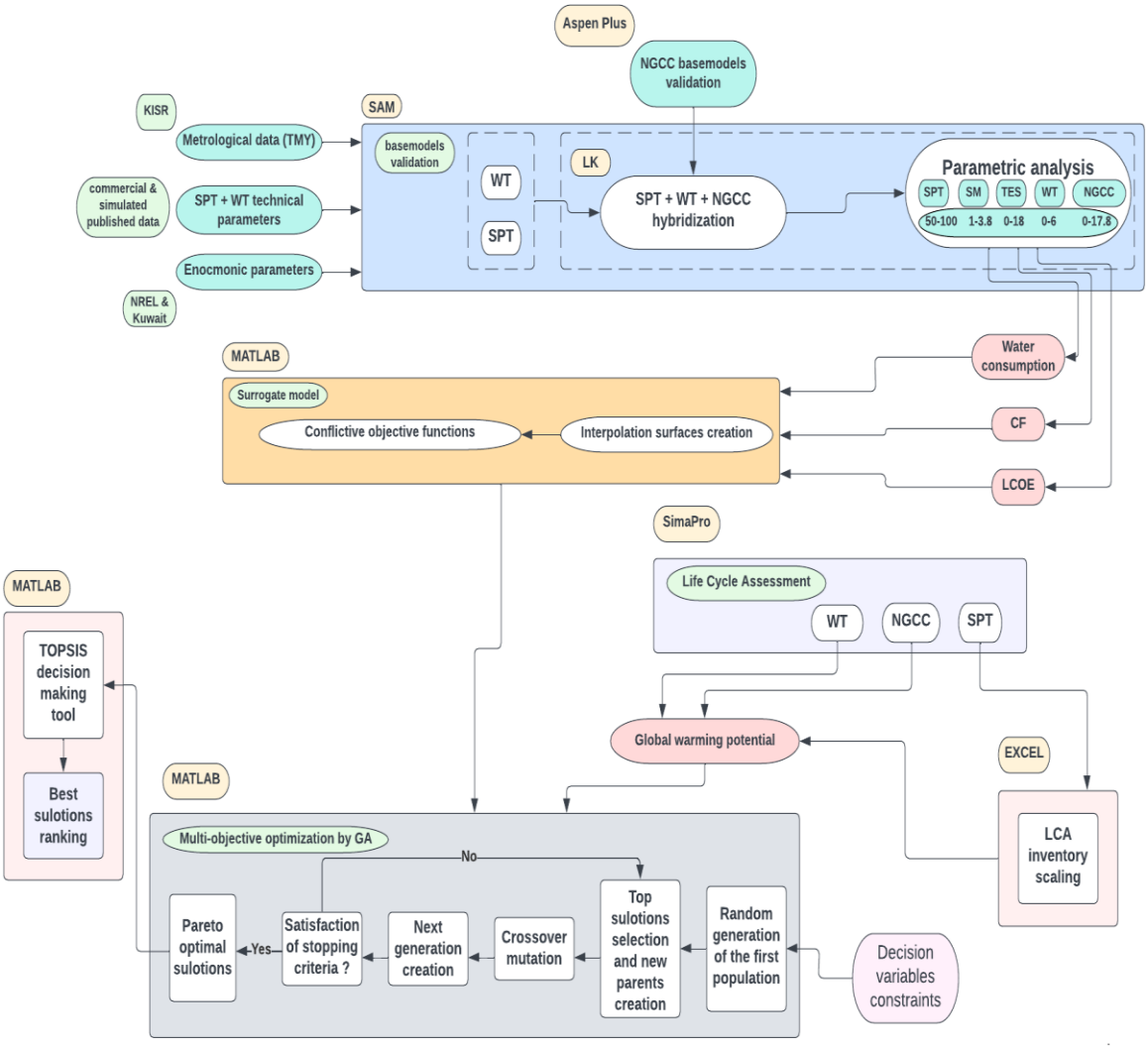

Fig. 4-5. A flowchart of this work's methodology.

set's acquisition, quality and verification have been clarified in the respective section of the thesis. Similarly, the validation process of the SPT, WT and NGCC models has been thoroughly illustrated in each respective section of the thesis.

4.3 Results & Discussion

4.3.1 Surrogate Model Validation

As previously seen in Section 4.2.2, each surrogate model for each objective function has to be validated. Thus, three surrogate models have been created, one for each of the following objective functions: LCOE, water consumption and the CF, i.e. the objective functions that have been initially calculated in the SAM. No surrogate model has been created for the GWP as this objective function has been calculated in the SimaPro tool and then with the assistance of Excel. The validation results of these three surrogate models are shown in Figure 4-6 where good results have been obtained with very limited and acceptable deviations compared to their counterpart values simulated in the SAM.

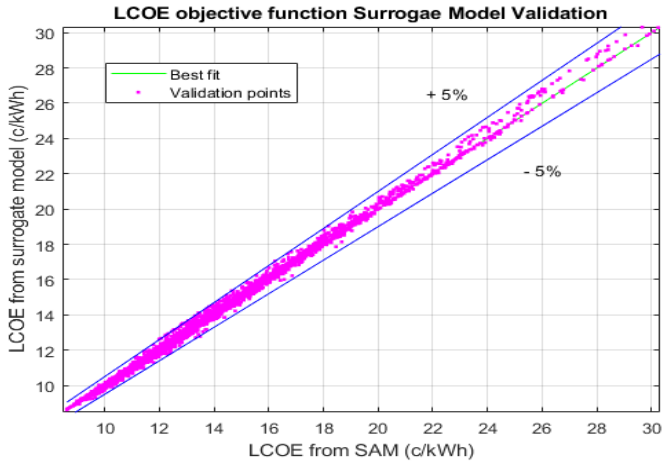

(a)

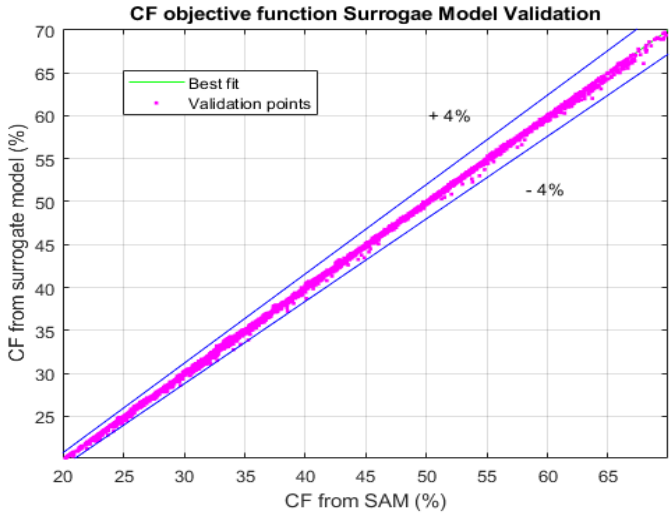

(b)

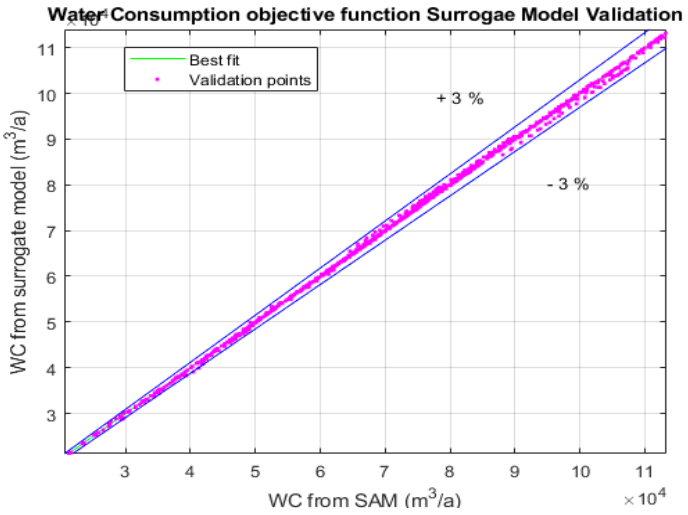

Fig. 4-6. The surrogate model validation process of the: (a) LCOE, (b) CF and (c) water consumption.

It is clear from Figure 4-6 that the surrogate model of the LCOE has the biggest deviations among all the other surrogate models. This is typically because of the non-linearity that the LCOE calculation imposes compared to other objective functions as these have more linear calculations. Further, the surrogate models have been validated according to multiple validation techniques as shown in Table 4-5 and have shown great accuracy compared to similar models in the literature [207], [228]:

Table 4-5
The surrogate models validation techniques.

		Validation techniques		
		Maximum percentage deviation (%)	**Mean bias error**	**Root mean square error**
Objective function	**LCOE**	± 5%	0.048	0.166
	Water consumption	± 3%	-0.0011	0.0007
	CF	± 4%	-0.093	0.223

4.3.2 Optimal Solutions

After sorting out the newly adopted variables' step sizes with the assistance of the surrogate model, the objective functions of LCOE, water consumption and CF are passed to the GA in Matlab to carry out the multi-objective optimization. Also, the GWP results for each SPT-WT-NGCC corresponding configuration are directly sent from Excel to Matlab as these do not require a surrogate model. In Matlab where the multi-objective optimization is carried out, the GA work on the presentation of a trade-off that satisfies all the objective functions through a set of optimal solutions to the optimization problem.

The initial results of the first scenario where no CCS is included depict that there is a dominance of the medium CO_2 emitting configurations in the range of 100-250 g of CO_2 /kWh. A very small number of solutions with CO_2 emissions higher than 250 g. eq CO_2 / kWh has been elected by the GA. It has also been noticed that the solutions that possess the highest CF percentages are associated with the largest amount of consumed water. This is clearly

because these solutions refer to the SPT configuration with both large TES and large solar fields. Lastly, the vast majority of solutions are placed in the 12-14 c/kWh range, while just a few managed to be located below the 12 c/kWh. In accordance with the results previously shown in Figure 3-13, the set of optimal solutions here in Figure 4-7 are uniquely of the 8.6 MW and the 17.8 MW NGCC scenarios as the solutions of the 13.9 MW NGCC scenario are entirely dominated.

Regarding, the inclusion of a CCS unit does not greatly divers the GA's strategy in finding the optimal solutions as the surface of the set of the dominant optimal solutions appears in a similar manner as its counterpart of the no CCS scenario as it is illustrated in Figure 4-7 (b). However, the energy penalty due to the inclusion of the CCS is projected at the LCOE and is clearly shown in Figure 4-7 (b) where the vast majority of the optimal solutions situate in the 14-16 c/kWh range and with no solutions lower value than 12 c/kWh at all.

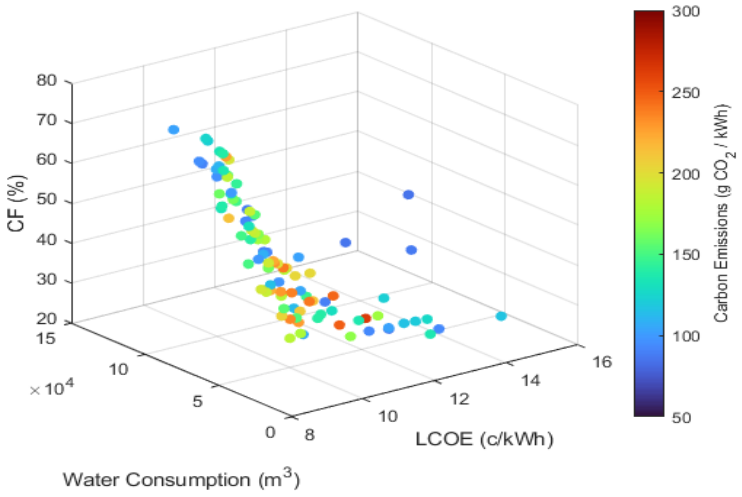

(a)

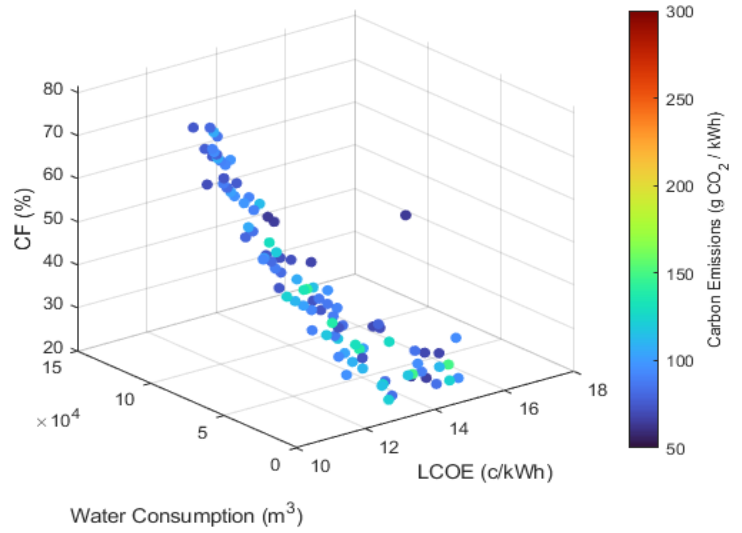

(b)

Fig. 4-7. The multi-objective optimization Pareto surfaces of the different scenarios: (a) no CCS scenario and (b) CCS scenario.

It is worth mentioning that almost all the optimal solutions of the both CCS and no-CCS scenarios include a NGCC component in their prospective configurations which promotes the great benefits of integrating such a component. On the other hand, the inclusion of high WT capacities in within the optimal solutions is found, however, not as consistent as that of the NGCC. This is because the WT participate in having a lower LCOE due to the decreased

CAPEX that it possess, however with no proportional AEG that furtherly decrease the LCOE and increase the CF which clearly because of the lack of the energy storage system for the WT.

As seen from two sets of optimal solutions that have been elected by the GA for the CCS inclusion/exclusion scenarios, it is delicate to compare different scenarios of the multi-objective optimization as these scenarios fundamentally changes the relation between the objective functions and variables in the optimization process. For example, in the CCS scenario, the CO_2 emissions of the NGCC is not considered as an obstacle that would prevent the GA of choosing configurations with a NGCC component with the intention of avoiding CO_2 emissions as these are captured. For that, it is essential to understand the relation between each decision variable and objective function based on the different scenarios of CCS. Figure 4-8 illustrates how correlated the objective functions based on the decision variables which gives a simplistic overview of how the GA sets the preference criteria among all the possible solutions. It is worth mentioning that the correlations illustrated in Figure 4-8 correspond to the two sets of optimal solutions and not the entire data set prior to the optimization as the latter can also be assessed, however, would require extensive time and computational efforts (76,608 solutions).

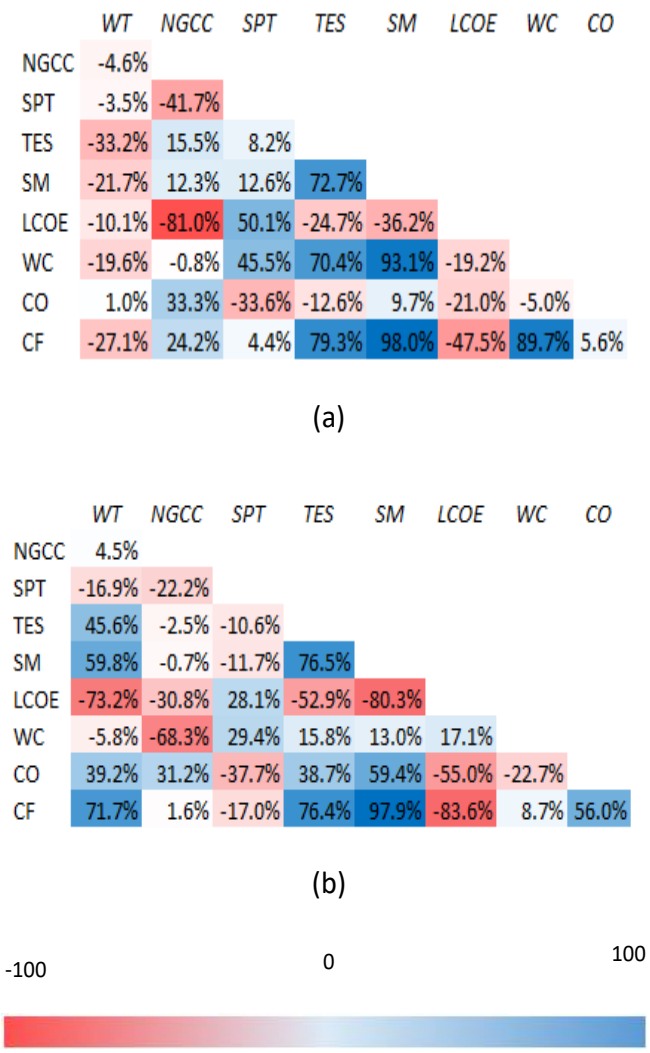

Fig. 4-8. The multi-objective optimized configurations' outputs and variables correlation of the different scenarios: (a) no CC scenario and (b) CC scenario.

It can be clearly seen that relation between the objective functions and the problem's variables is affected by the CCS inclusion/exclusion. This is mostly seen in the NGCC inclusion effect on the LCOE as the former contribute to up to 81% decrease in the LCOE when the CCS is not included. On the other hand, when the CCS is included, the LCOE also shows a decrease, however only for 30.8%. This is clearly because, when the CCS is included, a part of the produced AEG is dedicated to the process of CO_2 capture in the CCS, thus less energy that contributes in the calculation of the LCOE. In addition, it can be seen that the effect of the WT inclusion drastically differs between the two scenarios. This is most probably because in the case where no CCS is included, the LCOE is already at low values and thus it is difficult to furtherly lower it. In contrast, the LCOE increases because of the CCS inclusion because of less energy and higher CAPEX, thus it is easier to lower the LCOE through the inclusion of the WT.

A similar trend is observed with the SM and the TES. Seen the complexity of the relation between the decision variables and the objective functions in addition to the need of ranking the optimal solutions, it is a must that the optimal sets of solutions are evaluated by the MCDMT.

4.3.3 Decision Making Tool (TOPSIS)

Despite the fact that the GA has successfully elected a set of optimal solutions that satisfies all objective functions of the optimization problem, decision makers might remain misled by the variety of solutions in the set of optimal solutions. Thus the need for ranking these solutions from best to worst. In addition, with the assistance of the chosen MCDMT of this work, this work has been able to weight the importance of each objective function with accordance to multiple considerations, e.g. regions resources of water and fossil fuel.

Table 4-6 illustrates some selected indicative solutions of the total 200 optimal solutions that the GA generated for both CCS scenarios (for a simplified assessment, the GA has been set to populate 100 solutions per CCS scenario). These sets of solutions represent the optimal trade-off between the conflicting objective functions; in this case, each objective function is by default given an equivalent importance weight. The optimal 100 solutions of each scenario can be found in detail in the Appendices. Further, for the sake of comparison, Table 4-6 depicts the results for different standalone SPT that have been simulated in the SAM with the same capacity as the elected hybrid configuration's total capacity by the GA.

Table 4-6

Multi-objective optimization set of optimal solutions of both the CCS and no-CCS scenarios.

		Objective Functions (for the optimal GA elected SPT-WT-NGCC)					Decision Variables for the hybrid scenario					Objective Functions (for the standalone SPT capacity identical to the hybrid configuration)			
Solution	**TOPSIS rank**	**LCOE (c/kWh)**	**WC (m^3/y)**	**CF (%)**	**CO_2 (g / kWh)**	**CCS scenario**	**SPT_{CAP} (MW)**	**TES (h)**	**SM (-)**	**WT_{CAP} (MW)**	**$NGCC_{CAP}$ (MW)**	**LCOE (c/kWh)**	**WC (m^3/y)**	**CF (%)**	**CO_2 (g / kWh)**
1	72nd	13.7	17506	25	129.9	Yes	50	6	1	6	17.8	22.4	28360	18	77.5
2	51st	21.7	12973	16.2	68.4	Yes	50	1	1	0	0	20.9	19308	18.7	95
3	196th	11.4	74686	62.9	54	Yes	75	18	3	2	17.8	13.5	119157	63.4	60.3
4	85th	14.5	17501	25.4	151.4	Yes	50	12	1	6	17.8	24.2	28354	17.8	75.7
5	130th	10.4	60771	71.1	77.1	Yes	50	15	3	12	17.8	13.4	90235	61.7	65.3
6	170th	10.8	74843	80.3	99.8	Yes	50	17	3.8	12	17.8	13.7	124397	72.5	62
7	171st	10.9	74506	79.2	108.1	Yes	50	16	3.8	12	17.8	13.7	123975	71.4	62.1
8	135th	10.6	60111	68.9	110.6	Yes	50	13	3	12	17.8	13.7	97125	59.6	64.1
9	58th	14.4	15578	22.2	109.4	Yes	50	11	1	4	17.8	23.5	30581	18.2	74.3
50	25th	17.3	19432	23.4	66.8	Yes	50	5	1	8	17.8	21.9	28099	18.2	78.7
.															
.															
100	10th	14.1	19423	31.8	82.8	Yes	50	16	1	12	17.8	25.1	29921	17.9	74.4
101	178th	9.1	75181	71.5	195.6	No	50	18	3.8	0	17.8	13.4	105136	73.7	65
.															
.															
141	**1st**	**8.9**	**19436**	**35.6**	**68.5**	**No**	**50**	**3**	**1**	**12**	**17.8**	**21.1**	**30598**	**18.6**	**77.9**
150	117th	9.1	52047	58.5	116.9	No	50	18	2.6	0	17.8	14.2	71358	54.7	59
.															
.															
199	15th	8.9	27499	40.5	65.7	No	70	4	1.4	8	17.8	17.1	53733	27.4	69.2
200	67th	8.7	35274	45.4	63.1	No	50	9	1.8	12	17.8	15.6	57744	36.9	68.9

First, it has been noticed that the GA has greatly been in favor of the election of solution that are assigned a SPT capacity of 50 MW as this capacity dominated the set of optimal solutions for both the CCS and no-CCs scenarios. A total of 183 solutions out of 200 optimal ones have been found with a SPT capacity of 50 MW. This furtherly confirms what has been promoted in the literature as this capacity is the where CSP is most efficient and thus is the most adopted capacity worldwide [124], [125]. Another possible explanation here is that both the WT and the NGCC bring a lot of benefits to the hybrid configuration, thus, the GA is somehow forced to include them on the account of having a bigger SPT capacity than 50 MW with the consideration that the total maximum allowed capacity is not to surpass 100 MW (a constraint applied to the optimization). Table 4-6 also reveals that the proposed hybrid system is very competitive with the standalone SPT. For instance, the best elected solution, i.e. solution 141 which is ranked 1st by the TOPSIS is outperforming its counterpart in SPT standalone configuration in all aspects; the LCOE, water consumption, the CF and the CO_2 emissions. This also has occurred among the worst ranked solutions as the solution 3 which is ranked 196th by the TOPSIS still excelled in all aspects compared to its counterpart in standalone SPT configuration.

In contrast, it is very critical for a newly proposed plant to be assigned as a best ranked solution of those elected by the GA while it is associated with a much lowered CF, i.e. what is typically obtained in solution 141 in Table 4-6. Such a lowered CF discredits the proposed configuration's ability to satisfy all the objective functions especially that this solution has similar CF as a standalone WT would be delivering while the latter can actually deliver this with a way lowered LCOE (see previous chapter for details) and even zero water consumption. This much lowered CF is the result of having both lowered TES and SM values. This is understandable since the TES and SM are the only variables that contribute in the water consumption (see Figure 4-1), the GA only way to satisfy the objective function of having low water consumption levels is to avoid large TES and SM values. On the other hand, it is true that avoiding high TES-SM will negatively affect the AEG and thus the CF, however, these figures can be compensated by the GA through the election of the configurations with large capacities of NGCC for instance. This behavior of the GA can be avoided by applying an additional constraint to the optimization problem where a minimum value of TES or/and SM

is applied. However, this might be considered as an undesirable gesture of forcing results and thus not adopted in this work.

4.3.4 Objective Functions Weights Sensitivity Analysis

Despite having stressed the importance of water consumption quite enough in arid regions applications, the GA has been found with great sensitivity to this particular objective function which greatly affects other objective functions and hence the ranking made by the MCDMT as seen in the previous section. A variation of the objective functions' importance weights emerges as a potential way to correct this amplified sensitivity to water consumption imposed by the GA. This can be carried out with the assistance of the chosen MCDMT in this work, i.e. the TOPSIS. This is very important because through this technique the objective functions can be assigned the appropriate importance weights according to the decision makers' preference and that is without any of the objective function being completely discarded.

Here, a sensitivity analysis is carried out by alternating the importance weight of each objective function in the optimization process. The definitions of each relative intensity of importance is adopted from [253] and illustrated in Table 4-7.

Table 4-7
Objective function weights assigning ranges.

Objective function intensity of important	**Definition**
1	Equal importance
3	Moderate importance
5	Strong importance
7	Demonstrated importance
9	Extreme importance
2, 4, 6 and 8	Intermediate range

Consequently, a decision matrix has been created with the new relative weights for each objective function of the optimization and this is shown in Table 4-8 where the LCOE is still given the most important weight. Then, instead of prioritizing the water consumption as it is an arid region application, this work has chosen CF to be assigned the second most

important weight. This is because, firstly, the CF is a very important figure as it describes the plant's ability to meet the energy demand. Secondly, because of the amplified sensitivity of the GA towards the water consumption that has been illustrated in Section 4.3.2. Lastly, the CO_2 emissions and the water consumption are given close by importance weights with a slight priority of the former over the latter.

Table 4-8
The Decision matrix of all the objective functions.

	LCOE	CO_2 emissions	CF	Water consumption
LCOE	1	1 / 5	1 / 7	1 / 3
CO_2 emissions	5	1	2	1/2
CF	7	1/2	1	1/4
Water consumption	3	2	4	1

According to the newly weighted objective functions, the TOPSIS majorly changes the ranking of the 200 elected solutions (see the Appendices for more details). The 1st ranked solution shifts from the solution number 141 (a LCOE of 8.9 c/kWh, a water consumption of 19,436 m^3/y, 68.5 g of CO_2 eq. / kWh and a CF of 35.6 %) to solution number 5, which has a LCOE of 10.4 c/kWh, a water consumption of 60,771m^3/y, 77.1 g of CO_2 eq. / kWh and a CF of 71.2 %. The new second top ranked solution, which corresponds to a 50-12-17.8 SPT-WT-NGCC configuration, 14h of TES and a SM of 3, and among all the other optimal solutions for all scenarios post weight variation, is tabled in the Appendices.

Despite assigning the greatest importance weight to the LCOE, the top ranked solution has had a higher value of LCOE by approximately 18.2 % compared to the base case in which all objectives have the same importance weight. This is because this solution has much better results in both the CF and the CO_2 emissions. In fact, assigning the second most important weight to the CF has raised its value from 35.6 % to 71.2 %, i.e. an increase of 100 %. In addition, the CO_2 emission factor decreased despite being assigned a lower importance weight. This is despite having a bigger solar field and a bigger TES which both contribute in the CO_2 emissions in their respective LCA as seen in the previous chapter. However, these two

key design parameters also majorly contribute in the increase of the AEG and this in turn makes the equivalent value of kg of CO_2 eq. / kWh lower.

On the other hand, these improvements obtained on both objective functions of CF and the CO_2 emissions were on the account of assigning a lower importance weight to the last objective function, i.e. the water consumption. The latter showed a non-negligible increase by approximately 214.1 % which seems critical for the case study location as it is an arid region with limited access to water. However, it is genuinely believed that this can still be acceptable as first, the water consumption has not been completely disregarded from the optimization problem as in the vast majority of studies in the literature. Secondly, even with an increase of over 200%, this quantity of water consumption will not impose an infrastructural or logistical issue to the feasibility of the proposed plant since there is an already operational PTC plant with a wet-cooled condenser at the case study location of SREP. In conclusion, the ability of weighting objective functions differently demonstrates how beneficial and influential the MCDMT can be to the optimization problem.

4.3.5 Optimal Solutions Compatibility

In order to showcase the effectiveness of the employed optimization approach, a comparison is presented herein, between the hybrid elected optimal solutions against the results of different standalone CSP (SPT and PTC) technologies from the literature. This has been carried out with the standalone SPT and PTC due to the lack of hybrid configurations in the literature that assesses similar objective functions. Seen the complexity of finding a total capacity match between these standalone SPT + PTC from the literature and those elected solutions from the GA of this work, it has been decided that the comparison will be carried out based capacities close by or equal to the 100 MW mark for the GA elected solutions and this is because this capacity is abundantly chosen by the authors in the literature. In addition, in order for the comparison to be fairly performed, it has been realized with the assistance of the TOPSIS decision making tool as this can ensure that all objective functions of interest are given the weights that have been already presented in Table 4-8. Table 4-9 presents the results of these comparisons; it should be noted that the selected studies from the literature have considered the same objective functions of LCOE, CF and water consumption. The CO_2

emissions objective function is almost an impossible figure to get for such a comparison, thus it has been excluded from this analysis.

Since the objective functions employed in this work are very specific, it has been delicate to compare the solutions of this work to that presented in the literature; for the sake of carrying out consistent comparisons, the studied work deals with similar plants' capacities and assess identical objective functions. As such, only 8 solutions (acquired from multiple sources, i.e. [66], [81], [85], [137] and [254]) that have been proposed by the literature could have been used in this comparison. Table 4-9 lists the top ranked solutions chosen by the GA in this work for both the CCS and the no-CCS scenarios compared to the 8 solutions from the literature. With the newly adopted weighting criteria, the solutions that have been elected by the GA has shown an absolute dominance of the top ranked places among the optimal values of previous studies from the literature. This is firstly evident in the LCOE (which has been given the greatest weight among all the other objective functions), as the latter attains slightly lower values for the scenarios developed in the present study compared to what is found in the literature. These lower values of LCOE are most probably a result of the WT and/or NGCC integration. Out of a total of 208 solutions (200 from the GA + 8 from literature) the GA solutions have dominated the ranking and take over all the places between the 1st and 126th places. The best solution form the literature [254] is found in the 127th overall ranking as it is seen in Table 4-9.

Table 4-9

Comparison between the optimal hybrid solutions against standalone CSP technologies of 100 MW capacity from [66], [81], [85], [137] and [254].

Ranking among the literature	GA / Literature 100 MW solutions	Technology / Configuration	Solar field and TES	LCOE (c/kWh)	CF (%)	Water consumption (m^3/y)
1st	**GA solution number 5**	**50 – 12 – 17.8 SPT-WT-NGCC**	**3.4 SM – 14 h TES**	**10.4**	**70.2**	**60,771.4**
2nd	GA solution number 60	50 – 10 – 8.6 SPT-WT-NGCC	3.4 SM – 18 h TES	10.8	70.4	60,879.1
3rd	GA solution number 80	50 – 4 – 17.8 SPT-WT-NGCC	2.2 SM – 11 h TES	10.7	62.9	51,752.8
4th	GA solution number 17	65 – 2 – 17.8 SPT-WT-NGCC	1 SM – 6 h TES	10.5	78.1	68,216.6
5th	GA solution number 21	50 – 4 – 13.9 SPT-WT-NGCC	1 SM – 5 h TES	10.4	77.3	67,993.3
6th	GA solution number 41	50 – 6 – 13.9 SPT-WT-NGCC	1 SM – 5 h TES	10.8	61.4	51,752.8
7th	GA solution number 68	50 – 8 – 17.8 SPT-WT-NGCC	1.4 SM – 9 h TES	11.3	66.4	60,771.4
8th	GA solution number 59	50 – 4 – 17.8 SPT-WT-NGCC	2.6 SM – 11 h TES	11.1	56.4	52,030.1
..						
127th	[254]	**Standalone SPT**	**1.9 SM - 6 h**	**11.71**	**43.2**	**59,273**
..						
165th	[85]	Standalone SPT (air-cooled)	2.8 SM – 12 h	12.5	44	100,000
185th	[81]	Standalone PTC	1.5 SM – 6 h	13.1	47.5	124,727
186th	[137]	Standalone PTC (Pishin)	2 SM – 6 h	14.7	33.6	95,092
190th	[66]	Standalone SPT (air-cooled)	3 SM – 14 h	11.3	85.1	156,400
191st	[137]	Standalone PTC (Quetta)	2 SM – 6 h	15.3	31.7	94,388
..						
204th	[85]	Standalone SPT (wet-cooled)	2.8 SM - 12 h	11.6	44	1100,000
208th	[66]	Standalone SPT (wet-cooled)	3 SM – 15 h	11	86.4	234,730,0

The breakthrough that the GA solutions possess over those solutions of the literature is noticeably seen in both the CF and the water consumption. All the solutions that have been acquired from the literature have got a way much elevated water consumption quantities than those elected by the GA in this work, i.e. a further proof that the newly top ranked solution (Section 4.3.4) is indeed with an acceptable water consumption level. These elevated water consumption quantities found in the literature are mostly due to the employment of a wet-cooled condenser in these solutions. If not, these solutions are all of a single objective optimization which uniquely targets the lowest LCOE and for the vast majority of this kind of studies the lowest LCOE occurs when employing the largest solar field with the largest TES both of which are the main reasons for water consumption.

Also, after adopting the new weighting criteria with the assistance of the TOPSIS, all the 8 top ranked solutions of the GA elected solutions dominate those of the literature in terms of having a higher CF percentage. The highest CF percentage among all solutions is found in the wet and dry options presented by [66] as these have a CF of 86.4% and 85.1 %, respectively. However, these solutions also have a way larger water consumption which places them among the bottom of the overall ranking at 208^{th} and 190^{th} places, respectively. This occurs even with giving the water consumption the lowest importance weight by the TOPSIS, which signifies how large the water consumption of these solutions and its negative impact on the overall judgment. According to the weights that have been assigned to the objective functions to fit the harsh environmental conditions in arid regions, outperforming all other solutions in AEG and CF has not been enough to be ranked among the top optimal solutions.

4.4 Conclusions

This chapter started off by acquiring the performance indicators result of the proposed hybrid system of SPT-WT-NGCC that has been carried out in the previous chapter. It has been first noticed that the key performance indicators of interest are of a conflictive nature, which makes the optimal solution's finding process a nonlinear process. This work's main goal is to promote a system configuration that fit the following through its performance indicators: the worldwide CO_2 emissions' mitigation policies, are indicative with regards to the techno-economic efficiency, ensure energy provision and commitment to the end user, contribute in the limitation of water consumption and finally exploit both renewable and

fossil fuel existing natural resources that happen to exist in the case study location. As a result, this work has specifically chosen the performance indicators of LCOE, CF, CO_2 emissions and the water consumption among many other that exist in the literature. These performance indicators are assigned as objective functions that are either to be minimized or maximized in the optimization problem, from where both the contradiction and the complexity originate.

This work has used a multi-objective optimization approach to solve such a complex problem with multiple objectives, namely the Genetic Algorithm (GA). This is because of the great ability of such a tool to solve such a problem while including a large number of variables and objective functions. Once the various solutions are assessed, the GA elects a set of optimal solutions that satisfy, to the best of its ability, all the objective functions. For this to be properly carried out in terms of inclusivity and accuracy, the number of solutions from the previous chapter had to be substantially increased. Despite the fact that the in-house developed algorithm that has enabled this work of hybridizing the proposed configuration of SPT-WT-NGCC and has been illustrated in detail in the previous chapter is very reliable, however, it is associated with a very time-consuming process. In order to address these two issues, a surrogate model has been built. The surrogate model is able to take in the outputs from the in house developed algorithm with their corresponding variables, interpolate new outputs, however within smaller step sizes of these variables with great precision and very little time.

With the assistance of the surrogate model, this work has been able to deliver a total of 76,608 solutions which correspond to an equivalent number of system's possible configurations to the GA. From here, the GA is able to assess each configurations based on their respective performance indictors and thus elect a set of optimal solutions. The GA in this work has been set to elect 200 optimal solutions while applying specific constraints that are appropriate to the optimization problem and the case study location. As the GA variant of this work is the NSGA-II, these elected optimal solutions dominate all other unselected ones. Despite its ability of electing a set of optimal solutions, the GA still lacks two things; it is unable to rank the solutions in the set of optimal solutions and it is unable to prioritize an objective function over the others.

This is addressed by the usage of a multi criteria decision making tool (MCDMT) that is able to fulfill these two tasks, i.e. the TOPSIS. This MCDMT is able not only to rank the

optimal solutions from best to worst, but also to assign different importance criteria weights to the various objective functions. The TOPSIS has initially ranked the solution number 141 at the top of the set of optimal solutions while having a LCOE of 8.9 c/kWh, a water consumption of 19,436.4 m^3/y, 68.5 g of CO_2 eq. / kWh and a CF of 35.6 %. Despite having acceptable LCOE, water consumption and CO_2 figures, the top ranked solution's CF percentage has been a serious concern. This is because, first, it contradicts one of the main objectives of this work of having a high CF percentage, and secondly, some standalone mature technologies such as the WT can also achieve this CF and with even lower LCOE.

Thus, the CF has been assigned a more important weighting criteria and has been placed immediately after the LCOE and that made the TOPSIS alter the ranking and place the solution number 38 at the top of the set of optimal solutions. This had substantial returns on the top ranked solution which has had improvements in the LCOE (10.4 c/kWh), the CF (70.2 %) and the CO_2 emissions (77.1 g of CO_2 eq. / kWh), however on the account of the water consumption which drastically increased (60,771.4 m^3/y). This still stood solid as an optimal solution as it outperformed both its counterpart of the standalone SPT simulated in this work and other CSP configurations that have been found in the literature.

Chapter 5 – Conclusion & Future Work

Abstract

In this chapter, a conclusive summary is drawn with regards to what has been carried out and accomplished in the entire thesis. This summary interprets the results obtained in the three core chapters (Chapters 2-4) and hence highlights how the work presented by this thesis is significant, different from what already exists in the literature, contributes to existing knowledge and furtherly extends it. In addition, this chapter sheds further light on the limitations encountered in this thesis, the reasons and consequences of these limitations and lastly proposes some new research scopes that have a potential to step beyond these limitations.

The main aim of this work is to propose a novel energy system that manages to optimally exploit the solar energy resources in arid regions where harsh climates represent a threat to the feasibility of solar energy applications. In addition, this work sheds more light on other renewable as well as fossil fuel based technologies' ability to improve the performance of the proposed solar energy technology. This goal originates from the fact that multiple regions worldwide are rich in both fossil fuel and renewable resources with serious intentions to switch from the former to the latter. In line with that, this work has promoted a renewable-fossil fuel based system that will have a great potential to be a corner stone in the soft transitioning policy towards total renewable energy usage and carbon neutrality that is being increasingly adopted worldwide. This is extremely important and realistic for developing economies that are totally based on fossil fuel energy generation as it can make use of the already existing knowledge and infrastructure in the fossil fuel industry before totally abandoning it for renewable replacements.

5.1 Conclusive Summery of the Aerosols Affected SPT

With the breakthrough performance of the increasingly adopted CSP, this work has identified two different major risks to the feasibility of this solar energy applications in arid regions, i.e. aerosols density and water scarcity. Regarding the aerosols effect on the CSP, this effect is usually captured within the weather file that is used for the simulation as the latter describes the incoming irradiance intensity as well as other important metrological parameters. However, since CSP is based on refocusing the sun irradiance with the assistance

of solar reflectors, the effect of the aerosols on the reflected sun irradiance in the solar field cannot be captured with the help of a conventional weather file. This is extremely important in arid regions as aerosols are the most affecting factor in the mitigation of the DNI in cloud free conditions. The literature confirms the importance of such phenomena on the CSP and especially the SPT, which differs among other CSP types in having much larger slant ranges (distances between solar reflector and the receiver). This fact jeopardizes the many advantages that the SPT has over all other CSP types, e.g. higher solar concentration rates and higher solar to electricity conversion rates.

To accurately assess the solar field with regards to aerosols, a new multiple temporal resolutions aerosols techno-economic assessment of a SPT in arid regions has been proposed in the second chapter of this thesis. This has been based on an arid remote region in Kuwait, where the irradiation levels are elevated, however these may be heavily attenuated by the frequent sandstorms. Thus, this work has quantified the aerosols effect and included it as a probable factor in the attenuation of the main key design parameter in such technology, i.e. the DNI. Likewise, the DNI is more accurately measured and only then has the parametric analysis of the TES-SM sizing strategy been implemented. Conversely, in the case that the aerosols are excluded from the assessment, and this is usually the situation in the literature, the DNI, which is the main design parameter of the technology is often amplified and eventually this leads to probable incorrect evaluations of the DNI resource. Thus, this leads to an inappropriate solar field size. A too big/small solar field size translates into what appears to be a higher/lower capital cost, which drives the LCOE higher/lower than it is actually. Often, this leads to wrong, or misleading estimations for the decision makers.

For this reason, the most reliable, yet short-term ground measurement of aerosols data has been acquired in order to site adapt the longer-term MERRA-2 reanalysis data. The site adaptation, which has been realized by the employment of a quantile mapping technique, has managed to minimally reduce the bias that exists between the short and long-term sets of data. The bias corrected new long-term data has been employed in the Finkelstein-Schafer statistics in order to assemble a TAY. As a result, a year of the annually averaged AOD values from the site adapted TAY has been found to be 0.3205 and this has been integrated into the solar field attenuation extinction function in the SAM simulation tool with the assistance of

the Polo model [60]. From here, a parametric analysis that varies both the TES and the SM has been carried out to locate the optimal SPT configuration post the aerosols effect.

Further, the same parametric analysis has been performed but with four different cooling options: wet, dry and two hybrid scenarios in a trial to optimize the SPT water consumption. This has been considered as it is firstly, another threat to the feasibility of CSP in arid regions, and secondly, it is found that the cooling type contributes to the amount of energy generated, which is only clearly observed when there is a variation in both the TES and SM. In addition, the cooling type variation comes with an impact on both the LCOE, and thus it has to be also assessed and presented. The aerosols are just an attenuation factor of the DNI which, along with the cooling type, are directly related to the energy generation; the DNI is a thermal energy input in the solar field, while the cooling type is an efficiency enhancement factor in the power block.

Two dry bulb temperatures of reference have been observed and these have been used in order to optimize the hybrid scenarios set ups, namely 32 °C and 37 °C. This resulted in the first hybrid set up being with a 30% wet side activation and the other with only 19% wet side activation. Both hybrid set-ups have managed to reduce drastically the water consumption by 55.1 and 68.7%, respectively. In addition, both hybrid set ups surpassed the AEG of the air-cooled scenario by 4.6 and 4.4%, respectively. Due to the minor improvement offered by the 30% hybrid scenario in the AEG compared to that of the 19% scenario, in addition to the much larger water saving that the latter offers, the 19% hybrid set up can be suggested as an appropriate good candidate in the case where the wet-cooled condenser is not an option.

Consequently, the parametric analysis of the SPT model based on the annually averaged AOD value has been performed by varying the TES capacity from 0h to 18h and the SM value from 1 to 4, aiming to identify the TES-SM combination that results in the lowest LCOE. The lowest LCOE among all the configurations based on the annually averaged AOD has been found to be 12.78 ¢/kWh in the wet-cooled configuration and that is at a TES of 16h and a SM of 3.2, while a LCOE of 12.06 ¢/kWh has been found for the no aerosols scenario. Further, since aerosols are characterized by their high spatiotemporal variability, the LCOE of each optimal TES-SM combination of the parametric analysis has been observed based on the

daily AOD resolution and found to be 12.87 ¢/kWh, which is 6.7% from the no aerosols scenario and 0.7% from the annually averaged AOD scenario.

The variation of the slant range through solar field's optimization that has been in the current work along with the variation of TES capacity and this resulted in different aerosols effect on the solar field, and thus different reduction percentages of the AEG ranging from 0.6 - 6.7% (for the wet-cooled scenario). This signifies how sensitive the AEG is to the solar field size with one specific location's aerosols levels despite the gradual contribution of the TES in the compensation of the reduced AEG along with the increasing size of the solar field. The maximum obtained reduction of the current work is considered as low/intermediate compared to the results found in [49] (20 %) which examined different aerosols density levels of multiple locations based on only two fixed configurations.

In line with the work of Polo et al. [49] which has confirmed a non-negligible effect of the aerosols on the reflected irradiance of the SPT solar field, the current work made use of similar tools to first evaluate the aerosols effects. In addition, this work then presented a general SPT sizing strategy methodology with which the user can define the appropriate TES-SM configuration given the effect of aerosols on each solar field size and the role of TES in the compensation of the reduced AEG (due to the aerosols attenuation). The methodology also detailed how the LCOE has been affected by both the reduction of the AEG and the variation of the capital costs (by varying the TES capacity).

Also, in order to furtherly test the aerosols effects and not to be limited to a single tested SPT capacity, the third chapter of this work extended the aerosols effect assessment to include higher SPT capacities. This has been done by testing this effect on an incremental ascending basis of the SPT capacities up to 100 MW. The results show an increasing effect of the aerosols density on the SPT solar field and the AEG as the losses of the latter reach up to 9.1%. With the increasing SPT capacity range, the obtained results of the aerosols effect on the solar field show an almost linear trend. This is most probably because of the methodology used by the simulation tool's strategy in the process of new heliostats addition in the solar field which adds new heliostats at the outer circumference of the already existing ones at each time a larger solar field is adopted. Also, this has been found to be projected at the LCOE, which also deviates by 9% compared to the LCOE of the no aerosols scenario.

Despite being affected by aerosols as a result of being located in an arid remote region, the SPT application in the case study location of SREP in Kuwait is a totally feasible option in the large scale as the SPT with 100 MW capacity yields a LCOE of 12.4 c/kWh, i.e. an outperforming LCOE compared to other CSP that has been simulated at the same location (15.1 c/kWh for a 50 MW PTC [61]). However, there exists a chance of aerosols disruptions that causes an AEG deviation of up to 9.1% compared to its hypothetical no aerosols scenario. It is worth mentioning that in this chapter, only the annually averaged AOD value of the TAY (assembled in the previous chapter) has been used in the simulation process for larger SPT capacities. This has been unwillingly carried out despite the fact that the daily AOD resolution resulted in more accurate results than the yearly averaged AOD value and even has shown extensive losses on the daily basis energy generation. This is because, as seen in the previous chapter, the computational effort for the daily AOD temporal resolution application is a very time-consuming process.

5.2 Conclusive Summery of the Hybridization

In order to compensate any lost energy in the SPT due to the aerosols' density effect on the reflected irradiance of the solar field, two different technologies have been proposed as the hybridization options in this work, i.e. WT and NGCC. The WT has been chosen because it has a great potential in the same case study location that has been confirmed by other studies. In addition, the WT is considered as one of the most mature RE technologies that can enhance the hybrid configuration's performance. The competitive CAPEX prices of the WT enables it of the provision of energy for relatively lower prices, thus makes it with a great outlook to improve the hybrid plant's economic performance by lowering the LCOE. Similarly, the NGCC has been selected because of the positive economic returns that this technology can bring to the hybridization due to its ability to provide constant energy levels.

Despite the various advantages that the SAM offers, the ability of integrating multiple renewable energy technologies that this tool is capable of is very limited. To step beyond this issue and still benefit from the advantages offered by the SAM, an in-house developed algorithm has been created to integrate multiple renewable energy technology in the SAM. This in-house developed algorithm is able to break down the main figures that are considered in the calculation of the performance indicators of interest (AEG, CF, water consumption and LCOE) and calculate a corresponding total value for each performance indicator that

represents the hybrid configuration. This has enabled this work to automate the hybrid configuration of the existing performance models of SPT and WT in the SAM; a typically non existing feature in the conventional set up of the SAM. The latter is only able to hybridize two of its fixed RE models without the ability of automating them. In addition, the SAM does not possess any fossil fuel options, which represented an ambiguity for this work general aim and has been overcome through the developed algorithm. It is worth mentioning that for the NGCC performance simulation, the Aspen Plus simulation tool has been used. Then, the outputs of the NGCC in its selected different configurations, including/excluding a CCS unit, have been integrated into the developed algorithm in the SAM.

Prior to the hybridization, both the WT and the NGCC have been simulated and validated against commercial and published data from the literature in a similar manner for the SPT which has been validated in the second chapter. Then, the in-house developed algorithm has been used in order to hybridize the system's three components (SPT, WT and NGCC) and output the performance indicators of LCOE, CF and water consumption, while the CO_2 emissions have been calculated using SimaPro LCA tool.

The system preliminary performance has been evaluated based on a coarse range of variables for each of the three technologies. This step has been carried out in order to better understand the components contribution in the evolution of the performance indicators that have been assigned in this work, i.e. LCOE, CF, CO_2 emissions and water consumption. While the water consumption and the CF calculation are quite straight forward and the LCOE has been calculated by the developed algorithm, the CO_2 emissions is treated differently. This is because the CO_2 emissions of this work is a result of the GWP normalized values of the LCA that has been scaled based on the only three available, yet reliable LCA inventory data for the SPT. The different values of the GWP that correspond to different SPT configurations has been aggregated to averaged values of each the WT and the NGCC which exist in the literature. The reliance on these three reference SPT LCA inventories has assisted this work to obtain a more accurate and realistic normalized GWP values / kWh. Based on the three SPT LCA inventory, the averaged normalized GWP has been found to be equal to 30.1 g of CO_2 per kWh which falls in the mid-low range of the approved range by the United Nations Economic Commission for Europe [193] and that is from 14 to 87 g of CO_2 per kWh for the SPT technology.

The preliminary results of the system's performance depict that the hybrid configuration with larger NGCC capacity results in an increased AEG and thus the CF, which reaches up to 95%. On the other hand, this inclusion of larger NGCC capacities drastically increases the CO_2 emissions in the no CCS scenario. This has been avoided in the CCS scenario; however, the latter comes with a penalty on the AEG as energy is needed in the CCS process. This energy penalty is typically projected at the LCOE, which is also furtherly affected by the CAPEX of the CCS unit besides that of the energy penalty. Lastly, the WT has a positive effect on the LCOE because of its low CAPEX. Also, the WT has typically negligible effect on the CO_2 emissions compared to the SPT and the NGCC.

Post the preliminary evaluation of the system performance, it has been concluded that a further analysis with finer step sizes of the variables is needed. However, this can hardly be carried out with the developed algorithm as the latter has one drawback, i.e. it is very expensive in simulation time. This has been overcome by the development of a surrogate model, which has the ability of interpolating the performance indicators that correspond to different configurations of the hybrid system with ease and great speed. The surrogate model has shortcut immense periods of the needed time for the simulation with minimally deviated values from those originally simulation in the SAM by the developed algorithm. With the assistance of the surrogate model this work has managed to increase the number of possible solutions by more than 10 folds, which increases this work's inclusivity and accuracy.

5.3 Conclusive Summery of the Optimization

Post the extensive and detailed parametric analysis of the hybrid system, the four performance indicators of LCOE, CF, CO_2 emissions and water consumption have been assigned as objective functions in a multi-objective optimization process. A evolutionary algorithm namely the GA has been used in this optimization problem due to its great ability to solve such a problem while including a large number of variables and objective functions. Once the various solutions are assessed, the GA elects a set of optimal solutions that satisfy, to the best of its ability, all the objective functions.

From here, the GA is able to assess each configuration based on its respective performance indictors and thus elect a set of optimal solutions that outperform all other solutions. Prior to the election of the set of optimal solutions, the GA permits an application

of constraints. This has been found as very beneficial for the optimization because it eliminates all unfulfilling solutions before the optimization process begins, which avoids the elimination of a dominant solution/s that would have been elected on the set of optimal solutions if it weren't for the presence of an unfulfilling one/s. On the other hand, the GA has got two drawbacks, first; it has not the ability of ranking the individual solutions among the set of optimal solutions. Secondly, the GA has not got any preference criteria that can be assigned to different objective functions, which assumes all objective functions are of the same importance while this is not necessarily true.

This is addressed by the employment of a MCDMT (here the TOPSIS), which is able to solve both issues simultaneously. This has been initially thought as a perfect fit for this work's aim as prioritizing the reduction of water consumption has been an important objective function to fit arid region requirements. However, it has been found that assigning a top importance criterion to an objective function can be really critical and turn out the optimal solutions with mediocre performance indicators. This has occurred in this work because initially the water consumption has been assigned the top importance weight, but because this objective function is totally dependent on the solar field size, the GA has been totally biased towards the reduction of solar field size and thus heavily affect all other objective functions.

This work has successfully managed to obtain an outperforming plant configuration that is represented by having a very competitive CF, lowered water consumption and above all, a lowered LCOE that is even lower than the actual price of electricity generation in Kuwait (14 c/kWh [142], [143]) which is mainly achieved by fossil fuel power plants. On the other hand, even the obtained lowered LCOE of this work needs to be heavily subsidized in order for it to be sellable for most of the consumer sectors in the country. This is because the selling price of the unit of electricity in Kuwait is equal to 0.7 c/kWh [255]. Consequently, the proposed plant configuration and its competitive LCOE will only slightly mitigate the subsidy burden on the government responsibility, as it will be reduced from approximately 95% to only to 93.3%. However, according to the International Renewable Energy Agency (IRENA), the commitment of the GCC countries to their RE plans would save up 2.5 billion barrels and thus mitigate up to 155 megatons of CO_2 emission by the year 2030 [255].

5.4 Generalizability of the Conclusions

It can be safe to report that the results of this work's first chapter can and must be generalized to all SPT applications in arid region, e.g. all countries across the MENA region. This is because of the risk of having inaccurate assessment of the aerosols effect on the SPT's solar field and thus, inaccurate optimal solar field size, inaccurate techno-economic assessment. This work has revealed up to 9% of less AEG when the aerosols effect is adopted on the reflected irradiance of the SPT solar field, which is subject to even being higher in case applied in a more aerosols dense arid region. On the other hand, the inclusion of aerosols effect on the reflected irradiance of other CSP types such as PTC and LFR is less relevant as the slant range of these types is much less than that of the SPT and thus, the aerosols effect on the reflected irradiance is expected to be of a much less impact.

The application of CSP-WT hybridization can also be adopted on a wide span of regions, however, to a lesser extent than the stand-alone CSP. This is clear, because the standalone CSP only require high levels of beam irradiance, while a CSP-WT would require a collocation of this high solar irradiance with certain levels of wind power. This work has given an image of how such a hybridization can be techno-economically viable. This has been accomplished by firstly assessing the resources of both technologies, then assessing the performance of each technology in standalone configuration and lastly both technologies as a hybrid system. From here, future researchers can easily take this work's techno-economic figures as a reference and expect similar resources to achieve similar or close by techno-economic figures.

Regarding the NGCC integration, it is true that some regions are more privileged than others by having natural gas resources and it makes more sense for them to adopt NGCC or other similar technologies. For instance, this work has not included any natural gas related costs (other than purchase price, e.g. extraction, transport and storage) because the infrastructure for these already exist in the case study location. However, NGCC application worldwide is also a viable option but with associated costs attributed to the seller and subject to market fluctuations. This will affect the techno-economic performance of the NGCC as higher CAPEX are required. As for the environmental performance, this will impose a higher number of materials and processes in the LCA of the NGCC, i.e. a typical factor for raising GWP among other environmental indicators. The latter can be crucial for decision makers for

whether NGCC or other similar technologies are to be adopted in the case that natural gas is not available in the study case location.

5.5 The Novel Contributions of the Thesis

A novel method for carrying out a techno-economic assessment has been illustrated in the second chapter of this thesis. This method integrated the aerosols effect on the reflected irradiance of the SPT's solar field, a typically left out effect in the literature. With the assistance of the proposed method, this work has been able to find up to 9% reduction in the AEG. This reduction in the AEG is projected at the LCOE, which is elevated as a result. This method's adoption is very important in arid regions, especially because some more aerosols dense locations must have further aerosols effects, and thus more uncertainties about the viability of the SPT. Any policy that is considering the implementation of a SPT in an arid region must take into account this work's findings. This work's findings might change the application policies in this context from a direct implementation to a pilot plant, for example.

In addition, a novel approach of assessing the environmental and LCA perspective has been presented in the third chapter of this thesis. Prior to the proposed method of this work, many environmental research works have been found inflexible as it only assess fixed system configurations and capacities. With the assistance of the proposed method, a very wide range of system's configurations can be allocated a specific environmental indicator and likewise it can be assessed and compared to other similar set ups or configurations. The method also went further by the inclusion of this environmental indicator in addition to other important techno-economic performance indicators in a multi-objective optimization process, i.e. a typically non-existing method before. The fact of being able to weight the importance of the environmental indicator in addition to other techno-economic performance indicators has great potential to change the policies of decision makers.

5.6 Future Work Recommendations

The aerosols data of this work has been limited to only one year of ground measured data that has been acquired from the AERONET station in the SREP. This is because no longer data set has been found available for this station. Thus, this has been overcome by the

acquirement of the 5 years MERRA-2 data as seen in chapter, however, the longer is the ground measured data used, the better for the site adaptation process and thus better aerosols representation. With regards to that, the AERONET station at the case study location of SREP has just made publicly available a very high-quality type of AOD data for 3 consecutive years, i.e. 2017-2019. This long ground measured aerosols data was not available in the time when this work was being carried out, however, these data can drastically increase the aerosols data behavior understanding and thus, its effect on the SPT.

In addition, it is true that this work has assessed all the possible aerosols effects on the SPT, however, these effects are of the suspended aerosols in the air, wither those which obstruct the incoming sun light from the atmosphere or these which mitigate the reflected irradiance in the solar field. This work could have interpreted these site adapted aerosols data into soiling rates data, which can clarify how affected the reflectivity of the solar reflectors would be from the heliostats' reflectivity prospective. This has not been done due to the lack of a proper model that translates aerosols data in addition to data such as wind speed, humidity and reflectors adhesively into soiling rates data. Such model can be of massive benefit for obtaining accurate solar field outputs in arid regions and based on these soiling rates the CSP water consumption process can be systematically optimized rather than being based on a fixed periodic schedule.

Also, despite the fact that the daily AOD temporal resolution is more accurate and yields more effects of the aerosols than other more coarse temporal resolutions, this work has only adopted an annually averaged AOD from chapter three onwards and that is because the daily AOD temporal resolution is very expensive in computational time. However, the daily temporal assessment revealed some serious reductions in the solar field optical efficiency of the SPT and thus on the daily energy generation scale, which highlights the importance of the adoption of such methodology in the day-to-day SPT energy generation forecast. This is very important for the operation of the plant as it might present an issue in the commitment of energy delivery to the grid. The operation of the fossil fuel back up of proposed in this work (NGCC) can be scheduled based on both the solar irradiance intensity and the daily aerosols resolution to better optimize the grid energy provision process

References

[1] BP Statistical Review of World Energy Statistical Review of World. 2019.

[2] Wright VP. World Energy Outlook. 2023.

[3] BRITISH PETROLEUM COMPANY. (1981). BP statistical review of world energy. London BPC. 67 th edition Contents is one of the most widely respected. Stat Rev World Energy 2018:1–56.

[4] Ramanathan V, Feng Y. Air pollution, greenhouse gases and climate change: Global and regional perspectives. Atmos Environ 2009;43:37–50. https://doi.org/10.1016/j.atmosenv.2008.09.063.

[5] Stroeve JC, Serreze MC, Holland MM, Kay JE, Malanik J, Barrett AP. The Arctic's rapidly shrinking sea ice cover: A research synthesis. Clim Change 2012;110:1005–27. https://doi.org/10.1007/s10584-011-0101-1.

[6] world ocean network 2013. https://www.worldoceannetwork.org/won-part-6/carem-wod-2014-4/thematic-resources-coastal-management/facts-figures-coastal-management/%0D.

[7] Tsao J, Lewis N, Crabtree G. Solar FAQs. US Dep Energy 2006:1–24.

[8] Capuano L. International Energy Outlook 2020 2020. https://www.eia.gov/outlooks/ieo/pdf/ieo2020.pdf (accessed December 11, 2023).

[9] Windows M, Corporation M, Hori K, Sakajiri A. An Evaluation of Molten-Salt Power Towers Including Results of the Solar Two Project n.d.

[10] Wang Z, Yang W, Qiu F, Zhang X, Zhao X. Solar water heating: From theory, application, marketing and research. Renew Sustain Energy Rev 2015;41:68–84. https://doi.org/10.1016/j.rser.2014.08.026.

[11] Hite KA, Seitz JL. Global Issues: An Introduction. 4th ed. John Wiley & Sons; 2012.

[12] McCann K. 10,000 sq km of Solar in the Sahara could provide all the world's energy needs 2020. https://energypost.eu/10000-sq-km-of-solar-in-the-sahara-could-provide-all-the-worlds-energy-needs/ (accessed December 13, 2023).

[13] Madaeni SH, Sioshansi R, Denholm P. How Thermal Energy Storage Enhances the Economic Viability of Concentrating Solar Power 2012;100:335–47.

[14] Dincer I, Zamfirescu C. Advanced Power Generation Systems. Elsevier Science; 2014.

[15] L'Orange Seigo S, Dohle S, Siegrist M. Public perception of carbon capture and storage (CCS): A review. Renew Sustain Energy Rev 2014;38:848–63. https://doi.org/10.1016/j.rser.2014.07.017.

[16] Bui M, Adjiman CS, Bardow A, Anthony EJ, Boston A, Brown S, et al. Carbon capture

and storage (CCS): The way forward. Energy Environ Sci 2018;11:1062–176. https://doi.org/10.1039/c7ee02342a.

[17] Owebor K, Diemuodeke EO, Briggs TA. Thermo-economic and environmental analysis of integrated power plant with carbon capture and storage technology. Energy 2022;240:122748. https://doi.org/10.1016/j.energy.2021.122748.

[18] Jordán PS, Javier Eduardo AM, Zdzislaw MC, Alan Martín ZG, Liborio HP, Jesús Antonio FZ, et al. Techno-economic analysis of solar-assisted post-combustion carbon capture to a pilot cogeneration system in Mexico. Energy 2019;167:1107–19. https://doi.org/10.1016/j.energy.2018.11.010.

[19] Xiaoxing Wang, Song C. Capture of CO2 from Concentrated Sources and the Atmosphere. An Econ. Based Carbon Dioxide Water, Springer International Publishing; 2019.

[20] Trieb F, Schillings C, O'Sullivan M, Pregger T, Hoyer-Klick C. Global Potential of Concentrating Solar Power. Conf. Proc., Berlin: 2009, p. 1–11.

[21] Islam MT, Huda N, Abdullah AB, Saidur R. A comprehensive review of state-of-the-art concentrating solar power (CSP) technologies: Current status and research trends. Renew Sustain Energy Rev 2018;91:987–1018. https://doi.org/10.1016/j.rser.2018.04.097.

[22] Binamer AO. Al-Abdaliya integrated solar combined cycle power plant: Case study of Kuwait, part I. Renew Energy 2019;131:923–37. https://doi.org/10.1016/j.renene.2018.07.076.

[23] Al-Hajraf S. Feasibility Study of Renewable Energy Technologies for Power Generation in the State of Kuwait. 2010.

[24] Atalay Y, Biermann F, Kalfagianni A. Adoption of renewable energy technologies in oil-rich countries: Explaining policy variation in the Gulf Cooperation Council states. Renew Energy 2016;85:206–14. https://doi.org/10.1016/j.renene.2015.06.045.

[25] Lins C, Chair R, Galán EM, Wetstone G, Junfeng L, Thornton K, et al. REN21 STEERING COMMITTEE EXECUTIVE SECRETARY INDUSTRY ASSOCIATIONS Chinese Renewable Energy Industries Association (CREIA) Irene Giner-Reichl Global Forum on Sustainable Energy (GFSE) Mali Folkecenter (MFC) / Citizens United for Renewable Energy and Susta. 2016.

[26] Khatti SS. Techno-Economic Optimization and Market Potential Study of Small-Scale Particle Heating Receiver Based Central Receiver Power Tower Plants in MENA Region. Georgia Institute of Technology, 2021.

[27] IRENA. Renewable Energy Market Analysis TH GCC. 2015.

[28] Krane J. Reversing the trend in domestic energy consumption in the GCC: Consequences of success and failure? 2015. https://m.gulf-

times.com/story/460223/Reversing-the-trend-in-domestic-energy-consumption-in-the-GCC-Consequences-of-success-and-failure (accessed April 8, 2020).

[29] Griffiths S. Renewable energy policy trends and recommendations for GCC countries. Energy Transitions 2017;1:1–15. https://doi.org/10.1007/s41825-017-0003-6.

[30] Krane J. Energy Kingdoms: Oil and Political Survival in the Persian Gulf. New York: Columbia University Press; 2019.

[31] Solar ME. Solar Outlook Report 2020 2020.

[32] Wogan D, Pradhan S. GCC Energy System Overview – 2017 2017:1–36.

[33] Energy M of E& W& R. Electrical energy stastical year book. Kuwait: 2023. https://doi.org/10.1201/b11786-6.

[34] Marful AB. MASTER PLANNING TO HARNESS THE SUN AND WIND ENERGY: The Case of Shagaya Renewable Energy Master Plan Project, Kuwait. MIPALCON 2014 Clim Chang – A Glob Challenge Contrib Infrastruct Plan 2016:105–15. https://www.researchgate.net/publication/305627794_MASTER_PLANNING_TO_HARNESS_THE_SUN_AND_WIND_ENERGY_The_Case_of_Shagaya_Renewable_Energy_Master_Plan_Project_Kuwait (accessed December 18, 2022).

[35] Lude S, Fluri TP, Alhajraf S, Jülch V, Kühn P, Marful A, et al. Optimization of the Technology Mix for the Shagaya 2 GW Renewable Energy Park in Kuwait. Energy Procedia 2015;69:1633–42. https://doi.org/10.1016/j.egypro.2015.03.120.

[36] NREL. SAM Case Study: Gemasolar 2013:1–10.

[37] Pacheco JE, Bradshaw RW, Dawson DB, De la Rosa W, Gilbert R, Goods SH, et al. Final Test and Evaluation Results from the Solar Two Project. Contract 2002:294. https://doi.org/10.2172/793226.

[38] Whitaker MB, Heath GA, Burkhardt JJ, Turchi CS. Life cycle assessment of a power tower concentrating solar plant and the impacts of key design alternatives. Environ Sci Technol 2013;47:5896–903. https://doi.org/10.1021/es400821x.

[39] Qu W, Wang R, Hong H, Sun J, Jin H. Test of a solar parabolic trough collector with rotatable axis tracking. Appl Energy 2017;207:7–17. https://doi.org/10.1016/j.apenergy.2017.05.114.

[40] Siva Reddy V, Kaushik SC, Ranjan KR, Tyagi SK. State-of-the-art of solar thermal power plants - A review. Renew Sustain Energy Rev 2013;27:258–73. https://doi.org/10.1016/j.rser.2013.06.037.

[41] Behar O, Khellaf A, Mohammedi K. A review of studies on central receiver solar thermal power plants. Renew Sustain Energy Rev 2013;23:12–39. https://doi.org/10.1016/j.rser.2013.02.017.

[42] Aboelwafa O, Fateen SEK, Soliman A, Ismail IM. A review on solar Rankine cycles:

Working fluids, applications, and cycle modifications. Renew Sustain Energy Rev 2018;82:868–85. https://doi.org/10.1016/j.rser.2017.09.097.

[43] N.R.E.L. Website with the collaboration of Solar Paces n.d. https://solarpaces.nrel.gov/ (accessed December 15, 2021).

[44] Report GS. Http://Www.Ren21.Net/Gsr-2017/. 2017.

[45] Shahabuddin M, Alim MA, Alam T, Mofijur M, Ahmed SF, Perkins G. A critical review on the development and challenges of concentrated solar power technologies. Sustain Energy Technol Assessments 2021;47:101434. https://doi.org/10.1016/j.seta.2021.101434.

[46] Samaan Ladkany, William Culbreth, Nathan Loyd. Molten Salts and Applications III: Worldwide Molten Salt Technology Developments in Energy Production and Storage. J Energy Power Eng 2018;12:533–44. https://doi.org/10.17265/1934-8975/2018.11.003.

[47] Rhodes J. Nuclear and wind power estimated to have lowest levelized CO2 emissions 2017. https://energy.utexas.edu/news/nuclear-and-wind-power-estimated-have-lowest-levelized-co2-emissions (accessed July 17, 2023).

[48] Khalil SA, Shaffie AM. Attenuation of the solar energy by aerosol particles: A review and case study. Renew Sustain Energy Rev 2016;54:363–75. https://doi.org/10.1016/j.rser.2015.09.085.

[49] Polo J, Ballestrín J, Alonso-Montesinos J, López-Rodriguez G, Barbero J, Carra E, et al. Analysis of solar tower plant performance influenced by atmospheric attenuation at different temporal resolutions related to aerosol optical depth. Sol Energy 2017;157:803–10. https://doi.org/10.1016/j.solener.2017.09.003.

[50] Burgaleta JI, Arias S, Ramirez D. Gemasolar, the first tower thermosolar commercial plant with molten salt storage. Solarpaces, 2011, p. 1–8.

[51] Dunn RI, Hearps PJ, Wright MN. Molten-salt power towers: Newly commercial concentrating solar storage. Proc IEEE 2012;100:504–15. https://doi.org/10.1109/JPROC.2011.2163739.

[52] Balghouthi M, Trabelsi SE, Amara M Ben, Ali ABH, Guizani A. Potential of concentrating solar power (CSP) technology in Tunisia and the possibility of interconnection with Europe. Renew Sustain Energy Rev 2016;56:1227–48. https://doi.org/10.1016/j.rser.2015.12.052.

[53] Zhang HL, Baeyens J, Degrève J, Cacères G. Concentrated solar power plants: Review and design methodology. Renew Sustain Energy Rev 2013;22:466–81. https://doi.org/10.1016/j.rser.2013.01.032.

[54] Gueymard CA. Uncertainties in modeled direct irradiance around the sahara as affected by aerosols: Are current datasets of bankable quality. J Sol Energy Eng Trans

ASME 2011;133:1–13. https://doi.org/10.1115/1.4004386.

[55] Gueymard CA. Impact of on-site atmospheric water vapor estimation methods on the accuracy of local solar irradiance predictions. Sol Energy 2014;101:74–82. https://doi.org/10.1016/j.solener.2013.12.027.

[56] Gueymard CA. Temporal variability in direct and global irradiance at various time scales as affected by aerosols. Sol Energy 2012;86:3544–53. https://doi.org/10.1016/j.solener.2012.01.013.

[57] Gueymard CA. Visibility, aerosol conditions, and irradiance attenuation close to the ground-Comments on "Solar radiation attenuation in solar tower plants" by J. Ballestrin and A. Marzo, Solar Energy (2012). Sol Energy 2012;86:1667–8. https://doi.org/10.1016/j.solener.2011.12.027.

[58] Mohammadi K, Saghafifar M, Ellingwood K, Powell K. Hybrid concentrated solar power (CSP)-desalination systems: A review. Desalination 2019;468:114083. https://doi.org/10.1016/j.desal.2019.114083.

[59] Ruiz-Arias JA, Gueymard CA, Santos-Alamillos FJ, Pozo-Vázquez D. Worldwide impact of aerosol's time scale on the predicted long-term concentrating solar power potential. Sci Rep 2016;6. https://doi.org/10.1038/srep30546.

[60] Polo J, Ballestrín J, Carra E. Sensitivity study for modelling atmospheric attenuation of solar radiation with radiative transfer models and the impact in solar tower plant production. Sol Energy 2016;134:219–27. https://doi.org/10.1016/j.solener.2016.04.050.

[61] Sultan AJ, Hughes KJ, Ingham DB, Ma L, Pourkashanian M. Techno-economic competitiveness of 50 MW concentrating solar power plants for electricity generation under Kuwait climatic conditions. Renew Sustain Energy Rev 2020;134. https://doi.org/10.1016/j.rser.2020.110342.

[62] Rouibah A, Benazzouz D, Kouider R, Al-Kassir A, García-Sanz-Calcedo J, Maghzili K. Solar tower power plants of molten salt external receivers in Algeria: Analysis of direct normal irradiation on performance. Appl Sci 2018;8. https://doi.org/10.3390/app8081221.

[63] Boudaoud S, Khellaf A, Mohammedi K, Behar O. Thermal performance prediction and sensitivity analysis for future deployment of molten salt cavity receiver solar power plants in Algeria. Energy Convers Manag 2015;89:655–64. https://doi.org/10.1016/j.enconman.2014.10.033.

[64] Mihoub S, Chermiti A, Beltagy H. Methodology of determining the optimum performances of future concentrating solar thermal power plants in Algeria. Energy 2017;122:801–10. https://doi.org/10.1016/j.energy.2016.12.056.

[65] Murat Cekirge H. A Comparison of Solar Power Systems (CSP): Solar Tower (ST) Systems versus Parabolic Trough (PT) Systems. Am J Energy Eng 2015;3:29.

https://doi.org/10.11648/j.ajee.20150303.11.

[66] Hirbodi K, Enjavi-Arsanjani M, Yaghoubi M. Techno-economic assessment and environmental impact of concentrating solar power plants in Iran. Renew Sustain Energy Rev 2020;120. https://doi.org/10.1016/j.rser.2019.109642.

[67] Agyekum EB, Velkin VI. Optimization and techno-economic assessment of concentrated solar power (CSP) in South-Western Africa: A case study on Ghana. Sustain Energy Technol Assessments 2020;40:100763. https://doi.org/10.1016/j.seta.2020.100763.

[68] Izquierdo S, Montañs C, Dopazo C, Fueyo N. Analysis of CSP plants for the definition of energy policies: The influence on electricity cost of solar multiples, capacity factors and energy storage. Energy Policy 2010;38:6215–21. https://doi.org/10.1016/j.enpol.2010.06.009.

[69] Coelho B, Varga S, Oliveira A, Mendes A. Optimization of an atmospheric air volumetric central receiver system: Impact of solar multiple, storage capacity and control strategy. Renew Energy 2014;63:392–401. https://doi.org/10.1016/j.renene.2013.09.026.

[70] Casati E, Casella F, Colonna P. Design of CSP plants with optimally operated thermal storage. Sol Energy 2015;116:371–87. https://doi.org/10.1016/j.solener.2015.03.048.

[71] Chen R, Rao Z, Liao S. Determination of key parameters for sizing the heliostat field and thermal energy storage in solar tower power plants. Energy Convers Manag 2018;177:385–94. https://doi.org/10.1016/j.enconman.2018.09.065.

[72] Hanrieder N, Wilbert S, Mancera-Guevara D, Buck R, Giuliano S, Pitz-Paal R. Atmospheric extinction in solar tower plants – A review. Sol Energy 2017;152:193–207. https://doi.org/10.1016/j.solener.2017.01.013.

[73] Carra E, Ballestrín J, Polo J, Barbero J, Fernández-Reche J. Atmospheric extinction levels of solar radiation at Plataforma Solar de Almería. Application to solar thermal electric plants. Energy 2018;145:400–7. https://doi.org/10.1016/j.energy.2017.12.111.

[74] Muñoz J, Martínez-Val JM, Abbas R, Abánades A. Dry cooling with night cool storage to enhance solar power plants performance in extreme conditions areas. Appl Energy 2012;92:429–36. https://doi.org/10.1016/j.apenergy.2011.11.030.

[75] Marugán-Cruz C, Sánchez-Delgado S, Gómez-Hernández J, Santana D. Towards zero water consumption in solar tower power plants. Appl Therm Eng 2020;178:115505. https://doi.org/10.1016/j.applthermaleng.2020.115505.

[76] U.S. Department of Energy. Concentrating solar power commercial application study: Reducing water consumption of concentrating solar power electricity generation. vol. 2001. 2010. https://doi.org/https://doi.org/10.2172/1218186.

[77] Poullikkas A, Hadjipaschalis I, Kourtis G. A comparative overview of wet and dry cooling systems for Rankine cycle based CSP plants. Trends Heat Mass Transf 2013;13:27–50.

[78] Wagner MJ, Kutscher C. THE IMPACT OF HYBRID WET / DRY COOLING ON CONCENTRATING SOLAR POWER PLANT PERFORMANCE. Proc. ASME 2010 4th Int. Conf. Energy Sustain., 2010, p. 1–8. https://doi.org/https://doi.org/10.1115/ES2010-90442.

[79] Duvenhage DF, Brent AC, Stafford WHL. The need to strategically manage CSP fleet development and water resources: A structured review and way forward. Renew Energy 2019;132:813–25. https://doi.org/10.1016/j.renene.2018.08.033.

[80] Rutberg MJ (Michael J. Modeling water use at thermoelectric power plants 2012:77.

[81] Qoaider L, Liqreina A. Optimization of dry cooled parabolic trough (CSP) plants for the desert regions of the Middle East and North Africa (MENA). Sol Energy 2015;122:976–85. https://doi.org/10.1016/j.solener.2015.10.021.

[82] Fares MS Ben, Abderafi S. Water consumption analysis of Moroccan concentrating solar power station. Sol Energy 2018;172:146–51. https://doi.org/10.1016/j.solener.2018.06.003.

[83] Blanco-Marigorta AM, Victoria Sanchez-Henríquez M, Peña-Quintana JA. Exergetic comparison of two different cooling technologies for the power cycle of a thermal power plant. Energy 2011;36:1966–72. https://doi.org/10.1016/j.energy.2010.09.033.

[84] Yilmazoglu MZ. Effects of the selection of heat transfer fluid and condenser type on the performance of a solar thermal power plant with technoeconomic approach. Energy Convers Manag 2016;111:271–8. https://doi.org/10.1016/j.enconman.2015.12.068.

[85] Aly A, Bernardos A, Fernandez-Peruchena CM, Jensen SS, Pedersen AB. Is Concentrated Solar Power (CSP) a feasible option for Sub-Saharan Africa?: Investigating the techno-economic feasibility of CSP in Tanzania. Renew Energy 2019;135:1224–40. https://doi.org/10.1016/j.renene.2018.09.065.

[86] Asfand F, Palenzuela P, Roca L, Caron A, Lemarié CA, Gillard J, et al. Thermodynamic performance and water consumption of hybrid cooling system configurations for concentrated solar power plants. Sustain 2020;12. https://doi.org/10.3390/su12114739.

[87] Gueymard CA, Al-Rasheedi M, Ismail A, Hussain T. Long-Term variability of aerosol optical depth, dust episodes, and direct normal irradiance over Kuwait for CSP Applications. ISES Sol World Congr 2017 - IEA SHC Int Conf Sol Heat Cool Build Ind 2017, Proc 2017:75–84. https://doi.org/10.18086/swc.2017.04.04.

[88] Al-Rasheedi M, Gueymard C, Al-Hajraf S, Ismail A. Solar Resource Assessment over Kuwait: Validation of Satellite-derived Data and Reanalysis Modeling 2015:1–10. https://doi.org/10.18086/eurosun.2014.08.01.

[89] Alshawaf M, Poudineh R, Alhajeri NS. Solar PV in Kuwait: The effect of ambient temperature and sandstorms on output variability and uncertainty. Renew Sustain Energy Rev 2020;134:110346. https://doi.org/10.1016/j.rser.2020.110346.

[90] SolarGIS IMAPS n.d. https://solargis.info/imaps/#tl=GeoModel:lc&loc=29.792422,49.088559&c=29.403148,49.393429&z=8 (accessed March 3, 2020).

[91] Steensma G, Román R, Marshall C, Bermejo J, Iyer K, Al-Hajraf S, et al. Shagaya renewable energy park project. AIP Conf. Proc., vol. 2126, 2019. https://doi.org/10.1063/1.5117583.

[92] Polo J, Wilbert S, Ruiz-arias JA, Meyer R, Gueymard C, Su M, et al. ScienceDirect Preliminary survey on site-adaptation techniques for satellite-derived and reanalysis solar radiation datasets 2016;132:25–37. https://doi.org/10.1016/j.solener.2016.03.001.

[93] Cebecauer T, Suri M. Site-adaptation of satellite-based DNI and GHI time series: Overview and SolarGIS approach. AIP Conf Proc 2016;1734. https://doi.org/10.1063/1.4949234.

[94] Holben BN, Eck TF, Slutsker I, Tanré D, Buis JP, Setzer A, et al. AERONET - A federated instrument network and data archive for aerosol characterization. Remote Sens Environ 1998;66:1–16. https://doi.org/10.1016/S0034-4257(98)00031-5.

[95] NASA. The Modern-Era Retrospective analysis for Research and Applications Version 2 (MERRA-2) n.d. https://gmao.gsfc.nasa.gov/reanalysis/%0AMERRA-2/ (accessed November 20, 2020).

[96] Feigenwinter I, Kotlarski S, Casanueva A, Fischer A, Schwierz C, Liniger MA. Exploring quantile mapping as a tool to produce user tailored climate scenarios for Switzerland. Tech Rep MeteoSwiss 2018.

[97] Fernández-Peruchena CM, Polo J, Martín L, Mazorra L. Site-adaptation of modeled solar radiation data: The SiteAdapt procedure. Remote Sens 2020;12:1–17. https://doi.org/10.3390/rs12132127.

[98] Vamvakas I, Salamalikis V, Benitez D, Al-Salaymeh A, Bouaichaoui S, Yassaa N, et al. Estimation of global horizontal irradiance using satellite-derived data across Middle East-North Africa: The role of aerosol optical properties and site-adaptation methodologies. Renew Energy 2020;157:312–31. https://doi.org/10.1016/j.renene.2020.05.004.

[99] Festa R, Ratto CF. Proposal of a numerical procedure to select Reference Years. Sol Energy 1993;50:9–17. https://doi.org/10.1016/0038-092X(93)90003-7.

[100] Carra E, Marzo A, Ballestrín J, Polo J, Barbero J, Alonso-Montesinos J, et al. Atmospheric extinction levels of solar radiation using aerosol optical thickness satellite data. Validation methodology with measurement system. Renew Energy 2020;149:1120–32. https://doi.org/10.1016/j.renene.2019.10.106.

[101] EC HIPRAHB. GENERATION OF TYPICAL METEOROLOGICAL YEARS FOR 26 SOLMET STATIONS. ASHRAE TRANS 1979;85:507–18.

[102] Wilcox S, Marion W. Users manual for TMY3 data sets. Renew Energy 2008:51.

[103] Polo J, Fernández-Peruchena C, Gastón M. Analysis on the long-term relationship between DNI and CSP yield production for different technologies. Sol Energy 2017;155:1121–9. https://doi.org/10.1016/j.solener.2017.07.059.

[104] Kalamees T, Kurnitski J. Estonian test reference year for energy calculations, 2006, p. 40–58.

[105] Beccali M, Bertini I, Ciulla G, Di Pietra B, and Lo Brano V. SOFTWARE FOR WEATHER DATABASES MANAGEMENT AND CONSTRUCTION OF REFERENCE YEARS Department of Energy , University of Palermo , Palermo , Italy THE ISO 15927-4 METHODOLOGY. Proc. Build. Simul. 2011, Sydney: 2011.

[106] Gueymard CA. REST2: High-performance solar radiation model for cloudless-sky irradiance, illuminance, and photosynthetically active radiation - Validation with a benchmark dataset. Sol Energy 2008;82:272–85. https://doi.org/10.1016/j.solener.2007.04.008.

[107] Ångström A. On the atmospheric transmission of sun radiation and on dust in the air. Geogr Ann 1929;11:156–66.

[108] Polo J, Zarzalejo LF, Salvador P, Ramírez L. Angstrom turbidity and ozone column estimations from spectral solar irradiance in a semi-desertic environment in Spain. Sol Energy 2009;83:257–63. https://doi.org/10.1016/j.solener.2008.06.011.

[109] Measuring Aerosols n.d. https://earthobservatory.nasa.gov/features/Aerosols/page5.php (accessed January 30, 2020).

[110] Blair N, Diorio N, Freeman J, Gilman P, Janzou S, Neises T, et al. System Advisor Model (SAM) General Description (Version 2017.9.5). 2018. https://doi.org/https://doi.org/10.2172/1440404.

[111] Cruz NC, Redondo JL, Berenguel M, Álvarez JD, Ortigosa PM. Review of software for optical analyzing and optimizing heliostat fields 2017;72:1001–18. https://doi.org/10.1016/j.rser.2017.01.032.

[112] University of Wisconsin Madison. TRNSYS. TRNSYS, a Transient Simul Progr 1975. http://trnsys.com/index.html (accessed August 15, 2020).

[113] Wagner MJ, Wendelin T. SolarPILOT : A power tower solar fi eld layout and characterization tool 2018;171:185–96. https://doi.org/10.1016/j.solener.2018.06.063.

[114] Gamil A, Gilani SIU, Al-kayiem HH. Simulation of Incident Solar Power Input to Fixed Target of Central Receiver System in Malaysia. 2013 IEEE Conf Sustain Util Dev Eng Technol 2013:92–7. https://doi.org/10.1109/CSUDET.2013.6739506.

[115] Benammar S, Khellaf A, Mohammedi K. Contribution to the modeling and simulation of solar power tower plants using energy analysis. Energy Convers Manag 2014;78:923–30. https://doi.org/10.1016/j.enconman.2013.08.066.

[116] Mutuberria A, Pascual J, Guisado M V, Mallor F. Comparison of heliostat field layout design methodologies and impact on power plant efficiency. Energy Procedia 2015;69:1360–70. https://doi.org/10.1016/j.egypro.2015.03.135.

[117] Sastry A, Duvenhage DF, Hoffmann JE. A Parametric Study of Heliostat Size for Reductions in Levelized Cost of Electricity. South African Sol Energy Conf 2016 2016:1–8.

[118] Gueymard CA. Irradiance Variability and Its Dependence on Aerosols. SolarPACES 2011.

[119] Awan AB, Zubair M, Chandra Mouli KVV. Design, optimization and performance comparison of solar tower and photovoltaic power plants. Energy 2020;199:117450. https://doi.org/10.1016/j.energy.2020.117450.

[120] Zhao Z, Arif MT, Oo AMT. Solar Thermal Energy with Molten-salt Storage for Residential Heating Application. Energy Procedia 2017;110:243–9. https://doi.org/10.1016/j.egypro.2017.03.134.

[121] Mokheimer EMA, Dabwan YN, Habib MA. Optimal integration of solar energy with fossil fuel gas turbine cogeneration plants using three different CSP technologies in Saudi Arabia. Appl Energy 2017;185:1268–80. https://doi.org/10.1016/j.apenergy.2015.12.029.

[122] Srilakshmi G, Suresh NS, Thirumalai NC, Ramaswamy MA. A novel approach to determine the non-dimensional heliostat field boundary for solar tower plants. Sustain Energy Technol Assessments 2016;17:26–37. https://doi.org/10.1016/j.seta.2016.08.001.

[123] Blair N, Dobos AP, Freeman J, Neises T, Wagner M, Ferguson T, et al. System Advisor Model, SAM 2014 .1.14 : General Description. 2014. https://doi.org/https://doi.org/10.2172/1126294.

[124] Chaanaoui M, Vaudreuil S, Bounahmidi T. Benchmark of Concentrating Solar Power Plants: Historical, Current and Future Technical and Economic Development. Procedia Comput Sci 2016;83:782–9. https://doi.org/10.1016/j.procs.2016.04.167.

[125] Qaisrani MA, Wei J, Khan LA. Potential and transition of concentrated solar power: A case study of China. Sustain Energy Technol Assessments 2021;44:101052. https://doi.org/10.1016/j.seta.2021.101052.

[126] Water's High Heat Capacity n.d. https://bio.libretexts.org/Bookshelves/Introductory_and_General_Biology/Book%3A_General_Biology_(Boundless)/2%3A_The_Chemical_Foundation_of_Life/2.2%3A_Water/2.2C%3A_Water's_High_Heat_Capacity (accessed September 2, 2020).

[127] The Heat Capacity of Air is too Low to Heat Oceans of Melt Polar Ice n.d. http://nov79.com/gbwm/htcap.html (accessed September 2, 2020).

[128] Cohen G, Kearney D, Kolb G. Final report on the operation and maintenance improvement program for concentrating solar power plants 1999:1–44.

[129] ToolBox E. Thermal Conductivity of selected Materials and Gases 2003. https://www.engineeringtoolbox.com/thermal-conductivity-d_429.html (accessed September 9, 2020).

[130] Deng H, Boehm RF. An estimation of the performance limits and improvement of dry cooling on trough solar thermal plants. Appl Energy 2011;88:216–23. https://doi.org/10.1016/j.apenergy.2010.05.027.

[131] Turchi CS, Wagner MJ, Kutscher CF. Water Use in Parabolic Trough CSP- Summary Results from Worley Parsons' Analyses. vol. Task No. S. 2010. https://doi.org/https://doi.org/10.2172/1001357.

[132] Gilman P, Dobos A. System Advisor Model, SAM 2011.12.2: General Description. 2012. https://doi.org/https://dx.doi.org/10.2172/1046896.

[133] Soomro, Mengal, Memon, Khan, Shafiq, Mirjat. Performance and Economic Analysis of Concentrated Solar Power Generation for Pakistan. Processes 2019;7:575. https://doi.org/10.3390/pr7090575.

[134] Torresol Energy n.d. https://torresolenergy.com/en/gemasolar/ (accessed April 24, 2023).

[135] Quaschning V, Kistner R, Ortmanns W. Influence of direct normal irradiance variation on the optimal parabolic trough field size: A problem solved with technical and economical simulations. J Sol Energy Eng Trans ASME 2002;124:160–4. https://doi.org/10.1115/1.1465432.

[136] Musi R, Grange B, Sgouridis S, Guedez R, Armstrong P, Slocum A, et al. Techno-economic analysis of concentrated solar power plants in terms of levelized cost of electricity. AIP Conf Proc 2017;1850. https://doi.org/10.1063/1.4984552.

[137] Tahir S, Ahmad M, Abd-ur-Rehman HM, Shakir S. Techno-economic assessment of concentrated solar thermal power generation and potential barriers in its deployment in Pakistan. J Clean Prod 2021;293. https://doi.org/10.1016/j.jclepro.2021.126125.

[138] CSP Focus n.d. http://www.cspfocus.cn/en/ (accessed December 15, 2021).

[139] Dersch J, Schwarzbözl P, Richert T. Annual yield analysis of solar tower power plants With GREENIUS. J Sol Energy Eng Trans ASME 2011;133:1–9. https://doi.org/10.1115/1.4004355.

[140] Li X, Jin J, Yang D, Xu N, Wang Y, Mi X. Comparison of tower and trough solar thermal power plant efficiencies in different regions of China based on SAM simulation. AIP

Conf Proc 2019;2126. https://doi.org/10.1063/1.5117545.

[141] Ouali HAL, Merrouni AA, Moussaoui MA, Mezrhab A. Electricity yield analysis of a 50 MW solar tower plant under Moroccan climate. Proc 2015 Int Conf Electr Inf Technol ICEIT 2015 2015:252–6. https://doi.org/10.1109/EITech.2015.7162978.

[142] Ali H, Alsabbagh M. Residential Electricity Consumption in the State of Kuwait. Environ Pollut Clim Chang 2018;02:1–7. https://doi.org/10.4172/2573-458x.1000153.

[143] Ansari M. Kuwait Utilities Sector. Ind Res 2013:1–15.

[144] Hinkley JT, Hayward JA, Curtin B, Wonhas A, Boyd R, Grima C, et al. An analysis of the costs and opportunities for concentrating solar power in Australia. Renew Energy 2013;57:653–61. https://doi.org/10.1016/j.renene.2013.02.020.

[145] Alfailakawi MS, Michailos S, Ingham DB, Hughes KJ, Ma L, Pourkashanian M. Multi-temporal resolution aerosols impacted techno-economic assessment of concentrated solar power in arid regions: Case study of solar power tower in Kuwait. Sustain Energy Technol Assessments 2022;52:102324. https://doi.org/10.1016/j.seta.2022.102324.

[146] Benda V, Černá L. PV cells and modules – State of the art, limits and trends. Heliyon 2020;6. https://doi.org/10.1016/j.heliyon.2020.e05666.

[147] U.S. Energy Information Administration. Levelized Cost of New Generation Resources in the Annual Energy Outlook 2022. 2022.

[148] Kost C. Levelized Cost of Electricity - Renewable Energy Technologies. 2016.

[149] Yang J, Yang Z, Duan Y. Optimal capacity and operation strategy of a solar-wind hybrid renewable energy system. Energy Convers Manag 2021;244. https://doi.org/10.1016/j.enconman.2021.114519.

[150] Al-Nassar W, Alhajraf S, Al-Enizi A, Al-Awadhi L. Potential wind power generation in the State of Kuwait. Renew Energy 2005;30:2149–61. https://doi.org/10.1016/j.renene.2005.01.002.

[151] Al-Hajraf S, Heil O. Feasibility study of renewable energy technologies for power generation in the state of Kuwait. Kuwait City: 2011.

[152] Al-Khayat M, Al-Rasheedi M, Gueymard CA, Haupt SE, Kosović B, Al-Qattan A, et al. Performance analysis of a 10-MW wind farm in a hot and dusty desert environment. Part 2: Combined dust and high-temperature effects on the operation of wind turbines. Sustain Energy Technol Assessments 2021;47. https://doi.org/10.1016/j.seta.2021.101461.

[153] Al-Dousari A, Al-Nassar W, Al-Hemoud A, Alsaleh A, Ramadan A, Al-Dousari N, et al. Solar and wind energy: Challenges and solutions in desert regions. Energy 2019;176:184–94. https://doi.org/10.1016/j.energy.2019.03.180.

[154] Al-Dousari AM, Ibrahim MI, Al-Dousari N, Ahmed M, Al-Awadhi S. Pollen in aeolian dust

with relation to allergy and asthma in Kuwait. Aerobiologia (Bologna) 2018;34:325–36. https://doi.org/10.1007/s10453-018-9516-8.

[155] Kost C, Pfluger B, Eichhammer W, Ragwitz M. Fruitful symbiosis: Why an export bundled with wind energy is the most feasible option for North African concentrated solar power. Energy Policy 2011;39:7136–45. https://doi.org/10.1016/j.enpol.2011.08.032.

[156] Sioshansi R, Denholm P. Benefits of colocating concentrating solar power and wind. IEEE Trans Sustain Energy 2013;4:877–85. https://doi.org/10.1109/TSTE.2013.2253619.

[157] Vick BD, Moss TA. Adding concentrated solar power plants to wind farms to achieve a good utility electrical load match. Sol Energy 2013;92:298–312. https://doi.org/10.1016/j.solener.2013.03.007.

[158] Sahin AZ. Applicability of wind-solar thermal hybrid power systems in the northeastern part of the Arabian Peninsula. Energy Sources 2000;22:845–50. https://doi.org/10.1080/009083100300001645.

[159] Mohammed S. Alfailakawi, Stavros Michailos, Derek B. Ingham, Ismail AL-Arfi, Kevin J. Hughes, Lin Ma MP. Performance Improvement of Aerosols Impacted Concentrated Solar Power in Arid Regions: Case Study of Solar Power Tower Hybridization With Wind Turbines in Kuwait, 2022. https://doi.org/https://doi.org/10.46855/energy-proceedings-10201.

[160] IEA. Projected Costs of Generating Electricity 2020 Edition. 2020.

[161] Zoelle A, Turner M, Woods M, James III PhD R, Fout T, Shultz T. Cost and Performance Baseline for Fossil Energy Plants, Volume 1: Bituminous Coal and Natural Gas to Electricity, Revision 4. vol. 1. 2022. https://doi.org/10.2172/1574764.

[162] Mabrouk MT, Kheiri A, Feidt M. A systematic procedure to optimize Integrated Solar Combined Cycle power plants (ISCCs). Appl Therm Eng 2018;136:97–107. https://doi.org/10.1016/j.applthermaleng.2018.02.098.

[163] San Miguel G, Corona B. Economic viability of concentrated solar power under different regulatory frameworks in Spain. Renew Sustain Energy Rev 2018;91:205–18. https://doi.org/10.1016/j.rser.2018.03.017.

[164] Busch C, Gimon E. Natural Gas versus Coal: Is Natural Gas Better for the Climate? Electr J 2014;27:97–111. https://doi.org/10.1016/j.tej.2014.07.007.

[165] Gould T, McGlade C. The environmental case for natural gas 2017. https://www.iea.org/commentaries/the-environmental-case-for-natural-gas (accessed December 26, 2023).

[166] Adeoye JT, Amha YM, Poghosyan VH, Torchyan K, Arafat HA. Comparative LCA of Two Thermal Energy Storage Systems for Shams1 Concentrated Solar Power Plant: Molten

Salt vs. Concrete. J Clean Energy Technol 2014;2:274–81. https://doi.org/10.7763/jocet.2014.v2.139.

[167] Corona B, Ruiz D, San Miguel G. Life cycle assessment of a HYSOL concentrated solar power plant: Analyzing the effect of geographic location. Energies 2016;9:0–14. https://doi.org/10.3390/en9060413.

[168] Corona B, San Miguel G, Cerrajero E. Life cycle assessment of concentrated solar power (CSP) and the influence of hybridising with natural gas. Int J Life Cycle Assess 2014;19:1264–75. https://doi.org/10.1007/s11367-014-0728-z.

[169] Ameri M, Mohammadzadeh M. Thermodynamic, thermoeconomic and life cycle assessment of a novel integrated solar combined cycle (ISCC) power plant. Sustain Energy Technol Assessments 2018;27:192–205. https://doi.org/10.1016/j.seta.2018.04.011.

[170] Batuecas E, Mayo C, Díaz R, Pérez FJ. Life Cycle Assessment of heat transfer fluids in parabolic trough concentrating solar power technology. Sol Energy Mater Sol Cells 2017;171:91–7. https://doi.org/10.1016/j.solmat.2017.06.032.

[171] Pelay U, Azzaro-Pantel C, Fan Y, Luo L. Life cycle assessment of thermochemical energy storage integration concepts for a concentrating solar power plant. Environ Prog Sustain Energy 2020;39. https://doi.org/10.1002/ep.13388.

[172] Gasa G, Prieto C, Lopez-Roman A, Cabeza LF. Life cycle assessment (LCA) of a concentrating solar power (CSP) plant in tower configuration with different storage capacity in molten salts. J Energy Storage 2022;53:105219. https://doi.org/10.1016/j.est.2022.105219.

[173] Abdulrahim AH, Chung JN. Comparative thermodynamic performance study for the design of power and desalting cogeneration technologies in Kuwait. Energy Convers Manag 2019;185:654–65. https://doi.org/10.1016/j.enconman.2019.02.027.

[174] Udeh GT, Michailos S, Ingham D, Hughes KJ, Ma L, Pourkashanian M. Optimal sizing of a hybrid PV-WT-battery storage system: Effects of split-ST and combined ST + ORC back-ups in circuit charging and load following. Energy Convers Manag 2022;256:115370. https://doi.org/10.1016/j.enconman.2022.115370.

[175] Al-Rasheedi M, Al-Khayat M, Gueymard CA, Ellen Haupt S, Kosović B, Al-Qattan A, et al. Performance analysis of a 10-MW wind farm in a hot and dusty desert environment. Part 1: Wind resource and power generation evaluation. Sustain Energy Technol Assessments 2021;47. https://doi.org/10.1016/j.seta.2021.101487.

[176] PVGIS PHOTOVOLTAIC GEOGRAPHICAL INFORMATION SYSTEM n.d. https://re.jrc.ec.europa.eu/pvg_tools/en/.

[177] MANWELL JF, MCGOWAN JG, ROGERS AL. WIND ENERGY EXPLAINED THEORY, DESIGN AND APPLICATION. 2nd ed. WILEY; 2009. https://doi.org/10.1002/9781119994367.

[178] Bacci A. Kuwait’s Petroleum Sector: What is the Right Strategy? 2018. https://www.alessandrobacci.com/2018/04/kuwaits-petroleum-sector-what-is-the-right-strategy.html (accessed December 22, 2023).

[179] Energy S. Siemens Energy gas turbine portfolio n.d. siemens-energy.com/gasturbines Gas turbines from 2 to 593 MW (accessed April 13, 2023).

[180] The Engineering ToolBox. Power Plants - Perform Effic n.d. https://www.engineeringtoolbox.com/power-plant-efficiency-d_960.html (accessed January 10, 2024).

[181] Kakaee AH, Paykani A, Ghajar M. The influence of fuel composition on the combustion and emission characteristics of natural gas fueled engines. Renew Sustain Energy Rev 2014;38:64–78. https://doi.org/10.1016/j.rser.2014.05.080.

[182] The Engineering ToolBox. Fuels - High Low Calorific Values n.d. https://www.engineeringtoolbox.com/fuels-higher-calorific-values-d_169.html (accessed January 10, 2024).

[183] U.S. Energy Information Administration. Carbon Dioxide Emissions Coefficients. US Energy Inf Adm 2023. https://www.eia.gov/environment/emissions/co2_vol_mass.php (accessed January 10, 2024).

[184] Baumann H, Tillman A-M. The Hitch Hiker´s Guide to LCA - An orientation in LCA methodology and application 2004.

[185] Gasa G, Lopez-Roman A, Prieto C, Cabeza LF. Life cycle assessment (LCA) of a concentrating solar power (CSP) plant in tower configuration with aqnd without thermal energy storage (TES). Sustain 2021. https://doi.org/https://doi.org/10.3390/su13073672.

[186] Klein SJW, Rubin ES. Life cycle assessment of greenhouse gas emissions, water and land use for concentrated solar power plants with different energy backup systems. Energy Policy 2013;63:935–50. https://doi.org/10.1016/j.enpol.2013.08.057.

[187] Hertwich EG, Gibon T, Bouman EA, Arvesen A, Suh S, Heath GA, et al. Integrated life-cycle assessment of electricity-supply scenarios confirms global environmental benefit of low-carbon technologies. Proc Natl Acad Sci U S A 2015;112:6277–82. https://doi.org/10.1073/pnas.1312753111.

[188] Lata JM, Rodríguez M, Álvarez De Lara M. High flux central receivers of molten salts for the new generation of commercial stand-alone solar power plants. J Sol Energy Eng Trans ASME 2008;130:0210021–5. https://doi.org/10.1115/1.2884576.

[189] Kuenlin A, Augsburger G, Gerber L, Maréchal F. Life cycle assessment and environomic optimization of concentrating solar thermal power plants. Proc. 26th Int. Conf. Effic. Cost, Optim. Simul. Environ. Impact Energy Syst. ECOS 2013, Guilin: 2013.

[190] Turchi CS, Heath GA. Molten Salt Power Tower Cost Model for the System Advisor Model (SAM). Technical Report: NREL/TP-5500-57625. Natl Renew Energy Lab USA 2013;5500–57625:1–53.

[191] Telsnig T, Weinrebe G, Finkbeiner J, Eltrop L. Life cycle assessment of a future central receiver solar power plant and autonomous operated heliostat concepts. Sol Energy 2017;157:187–200. https://doi.org/10.1016/j.solener.2017.08.018.

[192] Rojas-Michaga MF, Michailos S, Cardozo E, Akram M, Hughes KJ, Ingham D, et al. Sustainable aviation fuel (SAF) production through power-to-liquid (PtL): A combined techno-economic and life cycle assessment. Energy Convers Manag 2023;292:117427. https://doi.org/10.1016/j.enconman.2023.117427.

[193] United Nations Economic Commission for Europe. Carbon Neutrality in the UNECE Region: Integrated Life-cycle Assessment of Electricity Sources UNITED NATIONS ECONOMIC COMMISSION FOR EUROPE. 2021.

[194] Rinaldi G, Garcia-Teruel A, Jeffrey H, Thies PR, Johanning L. Incorporating stochastic operation and maintenance models into the techno-economic analysis of floating offshore wind farms. Appl Energy 2021;301:117420. https://doi.org/10.1016/j.apenergy.2021.117420.

[195] NREL. System Advisor Model Help System. 2019.

[196] Shawki S. Kuwait Corporate - Taxes on corporate income n.d. https://taxsummaries.pwc.com/kuwait/corporate/taxes-on-corporate-income (accessed January 26, 2023).

[197] de la Hoz J, Martín H, Miret J, Castilla M, Guzman R. Evaluating the 2014 retroactive regulatory framework applied to the grid connected PV systems in Spain. Appl Energy 2016;170:329–44. https://doi.org/10.1016/j.apenergy.2016.02.092.

[198] Turchi CS, Boyd M, Kesseli D, Kurup P, Mehos M, Neises T, et al. CSP Systems Analysis - Final Project. 2019. https://doi.org/https://doi.org/10.2172/1513197.

[199] U.S. Department of Energy. 2013 Distributed wind market report. 2014. https://doi.org/https://doi.org/10.2172/1220282.

[200] Report A. Annual Report of the fiscal year 2020/2021 2021. https://www.cbk.gov.kw/en/statistics-and-publication/publications/annual-reports (accessed January 24, 2023).

[201] Central Bank of Kuwait. CBK Raises the Discount Rate by a Half Percentage Point 2022. https://www.cbk.gov.kw/en/cbk-news/announcements-and-press-releases/press-releases/2022/12/202212061624-cbk-raises-the-discount-rate-by-a-half-percentage-point#:~:text=The Board of Directors of,%25 effective December 7%2C 2022. (accessed January 24, 2023).

[202] Kuwait Short Term Interest Rate 2022.

https://www.ceicdata.com/en/indicator/kuwait/short-term-interest-rate#:~:text=Kuwait Short Term Interest Rate%3A Month End%3A KIBOR%3A 3,Nov 2001 to Dec 2022. (accessed January 18, 2023).

[203] Michailos S, Gibbins J. A Modelling Study of Post-Combustion Capture Plant Process Conditions to Facilitate 95–99% CO2 Capture Levels From Gas Turbine Flue Gases. Front Energy Res 2022;10:1–17. https://doi.org/10.3389/fenrg.2022.866838.

[204] Ali U, Font-Palma C, Akram M, Agbonghae EO, Ingham DB, Pourkashanian M. Comparative potential of natural gas, coal and biomass fired power plant with post - combustion CO2 capture and compression. Int J Greenh Gas Control 2017;63:184–93. https://doi.org/10.1016/j.ijggc.2017.05.022.

[205] Hu Y, Xu G, Xu C, Yang Y. Thermodynamic analysis and techno-economic evaluation of an integrated natural gas combined cycle (NGCC) power plant with post-combustion CO2 capture. Appl Therm Eng 2017;111:308–16. https://doi.org/10.1016/j.applthermaleng.2016.09.094.

[206] Rojas-Zerpa JC, Yusta JM. Application of multicriteria decision methods for electric supply planning in rural and remote areas. Renew Sustain Energy Rev 2015;52:557–71. https://doi.org/10.1016/j.rser.2015.07.139.

[207] Allouhi H, Allouhi A, Jamil A. Multi-objective optimization of a CSP-based dish Stirling field layout using Genetic Algorithm and TOPSIS method: Case studies in Ouarzazate and Madrid. Energy Convers Manag 2022;254. https://doi.org/10.1016/j.enconman.2022.115220.

[208] Spelling J, Favrat D, Martin A, Augsburger G. Thermoeconomic optimization of a combined-cycle solar tower power plant. Energy 2012;41:113–20. https://doi.org/10.1016/j.energy.2011.03.073.

[209] Guédez R, Topel M, Spelling J, Laumert B. Enhancing the Profitability of Solar Tower Power Plants through Thermoeconomic Analysis Based on Multi-objective Optimization. Energy Procedia 2015;69:1277–86. https://doi.org/10.1016/j.egypro.2015.03.155.

[210] Awan AB, Chandra Mouli KVV, Zubair M. Performance enhancement of solar tower power plant: A multi-objective optimization approach. Energy Convers Manag 2020;225:113378. https://doi.org/10.1016/j.enconman.2020.113378.

[211] Singh S, Singh M, Kaushik SC. A review on optimization techniques for sizing of solar-wind hybrid energy systems. Int J Green Energy 2016;13:1564–78. https://doi.org/10.1080/15435075.2016.1207079.

[212] Polat ME, Cadirci S. Artificial neural network model and multi-objective optimization of microchannel heat sinks with diamond-shaped pin fins. Int J Heat Mass Transf 2022;194:123015. https://doi.org/10.1016/j.ijheatmasstransfer.2022.123015.

[213] Karimi N, Feylizadeh MR, Govindan K, Bagherpour M. Fuzzy multi-objective

programming: A systematic literature review. Expert Syst Appl 2022;196. https://doi.org/10.1016/j.eswa.2022.116663.

[214] Al Busaidi AS, Kazem HA, Al-Badi AH, Farooq Khan M. A review of optimum sizing of hybrid PV-Wind renewable energy systems in oman. Renew Sustain Energy Rev 2016;53:185–93. https://doi.org/10.1016/j.rser.2015.08.039.

[215] Sinha S, Chandel SS. Review of recent trends in optimization techniques for solar photovoltaic-wind based hybrid energy systems. Renew Sustain Energy Rev 2015;50:755–69. https://doi.org/10.1016/j.rser.2015.05.040.

[216] Al-arfi I, Shboul B, Michailos S, Alfailakawi M, Udeh GT, Ingham D, et al. Multi-objective optimal sizing of a hybrid concentrated solar power-biogas for desalination and power generation, Bochum: International Conference on Applioed Energy; 2022. https://doi.org/https://doi.org/10.46855/energy-proceedings-10209.

[217] Bousselamti L, Ahouar W, Cherkaoui M. Multi-objective optimization of PV-CSP system in different dispatch strategies, case of study: Midelt city. J Renew Sustain Energy 2021;13. https://doi.org/10.1063/5.0025928.

[218] Liang Y, Chen J, Yang Z, Chen J, Luo X, Chen Y. Economic-environmental evaluation and multi-objective optimization of supercritical CO2 based-central tower concentrated solar power system with thermal storage. Energy Convers Manag 2021;238:114140. https://doi.org/10.1016/j.enconman.2021.114140.

[219] Luna-Rubio R, Trejo-Perea M, Vargas-Vázquez D, Ríos-Moreno GJ. Optimal sizing of renewable hybrids energy systems: A review of methodologies. Sol Energy 2012;86:1077–88. https://doi.org/10.1016/j.solener.2011.10.016.

[220] Shidhani T Al, Ioannou A, Falcone G. Multi-objective optimisation for power system planning integrating sustainability indicators. Energies 2020;13. https://doi.org/10.3390/en13092199.

[221] Cristóbal-Monreal IR, Dufo-López R. Optimisation of photovoltaic-diesel-battery stand-alone systems minimising system weight. Energy Convers Manag 2016;119:279–88. https://doi.org/10.1016/j.enconman.2016.04.050.

[222] Giudici F, Castelletti A, Garofalo E, Giuliani M, Maier HR. Dynamic, multi-objective optimal design and operation of water-energy systems for small, off-grid islands. Appl Energy 2019;250:605–16. https://doi.org/10.1016/j.apenergy.2019.05.084.

[223] Starke AR, Cardemil JM, Escobar R, Colle S. Multi-objective optimization of hybrid CSP+PV system using genetic algorithm. Energy 2018;147:490–503. https://doi.org/10.1016/j.energy.2017.12.116.

[224] Moura PS, de Almeida AT. Multi-objective optimization of a mixed renewable system with demand-side management. Renew Sustain Energy Rev 2010;14:1461–8. https://doi.org/10.1016/j.rser.2010.01.004.

[225] Chen Z, Chen Y, He R, Liu J, Gao M, Zhang L. Multi-objective residential load scheduling approach for demand response in smart grid. Sustain Cities Soc 2022;76. https://doi.org/10.1016/j.scs.2021.103530.

[226] Shakouri G. H, Kazemi A. Multi-objective cost-load optimization for demand side management of a residential area in smart grids. Sustain Cities Soc 2017;32:171–80. https://doi.org/10.1016/j.scs.2017.03.018.

[227] Diaf S, Belhamel M, Haddadi M, Louche A. Technical and economic assessment of hybrid photovoltaic/wind system with battery storage in Corsica island. Energy Policy 2008;36:743–54. https://doi.org/10.1016/j.enpol.2007.10.028.

[228] Zurita A, Mata-Torres C, Cardemil JM, Guédez R, Escobar RA. Multi-objective optimal design of solar power plants with storage systems according to dispatch strategy. Energy 2021;237. https://doi.org/10.1016/j.energy.2021.121627.

[229] Al-arfi I, Shboul B, Michailos S, Alfailakawi M, Udeh GT, Ingham D, et al. Multi-objective optimal sizing of a hybrid concentrated solar power-biogas for desalination and power generation. vol. 2, 2022, p. 2–6. https://doi.org/https://doi.org/10.46855/energy-proceedings-10209.

[230] Mata-Torres C, Palenzuela P, Alarcón-Padilla DC, Zurita A, Cardemil JM, Escobar RA. Multi-objective optimization of a Concentrating Solar Power + Photovoltaic + Multi-Effect Distillation plant: Understanding the impact of the solar irradiation and the plant location. Energy Convers Manag X 2021;11. https://doi.org/10.1016/j.ecmx.2021.100088.

[231] Bravo R, Ortiz C, Chacartegui R, Friedrich D. Multi-objective optimisation and guidelines for the design of dispatchable hybrid solar power plants with thermochemical energy storage. Appl Energy 2021;282:116257. https://doi.org/10.1016/j.apenergy.2020.116257.

[232] Sharma R, Kodamana H, Ramteke M. Multi-objective dynamic optimization of hybrid renewable energy systems. Chem Eng Process - Process Intensif 2022;170. https://doi.org/10.1016/j.cep.2021.108663.

[233] Pourrajabian A, Ebrahimi R, Mirzaei M, Shams M. Applying genetic algorithms for solving nonlinear algebraic equations. Appl Math Comput 2013;219:11483–94. https://doi.org/10.1016/j.amc.2013.05.057.

[234] Westermann P, Evins R. Surrogate modelling for sustainable building design – A review. Energy Build 2019;198:170–86. https://doi.org/10.1016/j.enbuild.2019.05.057.

[235] Elsakka MM. The Aerodynamics of Fixed and Variable Pitch Vertical Axis Wind Turbines. The University of Sheffield, 2020.

[236] Wang K, He YL, Xue XD, Du BC. Multi-objective optimization of the aiming strategy for the solar power tower with a cavity receiver by using the non-dominated sorting genetic algorithm. Appl Energy 2017;205:399–416.

https://doi.org/10.1016/j.apenergy.2017.07.096.

[237] Ellingwood K, Mohammadi K, Powell K. Dynamic optimization and economic evaluation of flexible heat integration in a hybrid concentrated solar power plant. Appl Energy 2020;276:115513. https://doi.org/10.1016/j.apenergy.2020.115513.

[238] Lazzari F, Mor G, Cipriano J, Solsona F, Chemisana D, Guericke D. Optimizing planning and operation of renewable energy communities with genetic algorithms. Appl Energy 2023;338. https://doi.org/10.1016/j.apenergy.2023.120906.

[239] Tsoumalis GI, Bampos ZN, Chatzis G V., Biskas PN, Keranidis SD. Minimization of natural gas consumption of domestic boilers with convolutional, long-short term memory neural networks and genetic algorithm. Appl Energy 2021;299. https://doi.org/10.1016/j.apenergy.2021.117256.

[240] Reddy MJ, Kumar DN. Optimal reservoir operation using multi-objective evolutionary algorithm. Water Resour Manag 2006;20:861–78. https://doi.org/10.1007/s11269-005-9011-1.

[241] Udeh GT, Michailos S, Ingham D, Hughes KJ, Ma L, Pourkashanian M. A modified rule-based energy management scheme for optimal operation of a hybrid PV-wind-Stirling engine integrated multi-carrier energy system. Appl Energy 2022;312:118763. https://doi.org/10.1016/j.apenergy.2022.118763.

[242] Ishizaka A, Labib A. Analytic Hierarchy Process and Expert Choice: Benefits and limitations. OR Insight 2009;22:201–20. https://doi.org/https://doi.org/10.1057/ori.2009.10.

[243] Rezaei J. Best-worst multi-criteria decision-making method. Omega (United Kingdom) 2015;53:49–57. https://doi.org/10.1016/j.omega.2014.11.009.

[244] Brans J-P, Smet Y De. PROMETHEE MEthods. Mult. Criteria Decis. Anal. Int. Ser. Oper. Res. Manag. Sci., Springer, New York, NY; n.d., p. 187–219. https://doi.org/https://doi.org/10.1007/978-1-4939-3094-4_6.

[245] Kumar A, Sah B, Singh AR, Deng Y, He X, Kumar P, et al. A review of multi criteria decision making (MCDM) towards sustainable renewable energy development. Renew Sustain Energy Rev 2017;69:596–609. https://doi.org/10.1016/j.rser.2016.11.191.

[246] Baumann M, Weil M, Peters JF, Chibeles-Martins N, Moniz AB. A review of multi-criteria decision making approaches for evaluating energy storage systems for grid applications. Renew Sustain Energy Rev 2019;107:516–34. https://doi.org/10.1016/j.rser.2019.02.016.

[247] Vo TTQ, Xia A, Rogan F, Wall DM, Murphy JD. Sustainability assessment of large-scale storage technologies for surplus electricity using group multi-criteria decision analysis. Clean Technol Environ Policy 2017;19:689–703. https://doi.org/10.1007/s10098-016-1250-8.

[248] Balali A, Yunusa-Kaltungo A, Edwards R. A systematic review of passive energy consumption optimisation strategy selection for buildings through multiple criteria decision-making techniques. Renew Sustain Energy Rev 2023;171:113013. https://doi.org/10.1016/j.rser.2022.113013.

[249] Cavallaro F. Fuzzy TOPSIS approach for assessing thermal-energy storage in concentrated solar power (CSP) systems. Appl Energy 2010;87:496–503. https://doi.org/10.1016/j.apenergy.2009.07.009.

[250] Li B, Miao H, Li J. Multiple hydrogen-based hybrid storage systems operation for microgrids: A combined TOPSIS and model predictive control methodology. Appl Energy 2021;283:116303. https://doi.org/10.1016/j.apenergy.2020.116303.

[251] Guo X, Guo Q, Nojavan S. Optimal offering of wind-photovoltaic-thermal generation company in energy and reserve markets in the presence of environmental and risk analysis. Sustain Energy Technol Assessments 2021;47:101567. https://doi.org/10.1016/j.seta.2021.101567.

[252] Rezk H, Mukhametzyanov IZ, Abdelkareem MA, Salameh T, Sayed ET, Maghrabie HM, et al. Multi-criteria decision making for different concentrated solar thermal power technologies. Sustain Energy Technol Assessments 2022;52:102118. https://doi.org/10.1016/j.seta.2022.102118.

[253] Saaty TL. A scaling method for priorities in hierarchical structures. J Math Psychol 1977;15:234–81. https://doi.org/10.1016/0022-2496(77)90033-5.

[254] Abbas M, Belgroun Z, Merzouk NK. Techno economic performances of a dry cooling solar power tower plant under Algerian climate. Int J Energy Technol Policy 2014;10:109–24. https://doi.org/10.1504/IJETP.2014.066325.

[255] Frroukhi R, Khalid A, Diala H, Divyam N, El-Katiri L, Fthenakis V, et al. Renewable Energy Market Analysis The GCC Region. 2016.

[256] Schuster GL, Dubovik O, Holben BN. Angstrom exponent and bimodal aerosol size distributions. J Geophys Res Atmos 2006;111:1–14. https://doi.org/10.1029/2005JD006328.

[257] Models W turbine. Gamesa G97 n.d. https://en.wind-turbine-models.com/turbines/764-gamesa-g97 (accessed February 22, 2023).

[258] Bornemisza G. Life Cycle Assessment of a Concentrated Solar Power Plant. BUDAPEST UNIVERSITY OF TECHNOLOGY AND ECONOMICS, 2018.

[259] Mazzaferro CA. Life Cycle Assessment of Electricity Production from Concentrating Solar Thermal Power Plants. University of Padua, n.d.

Appendices

Appendix A - Site Adaptation

The site adaptation by quantile mapping has shown deviation improvement between the long and short terms AOD data sets which has been seen in Figure 2-6 on a scale of 5 years. Here, a closer look on the improvement done by the site adaptation for the same year of the short term data, i.e. 2015-2016:

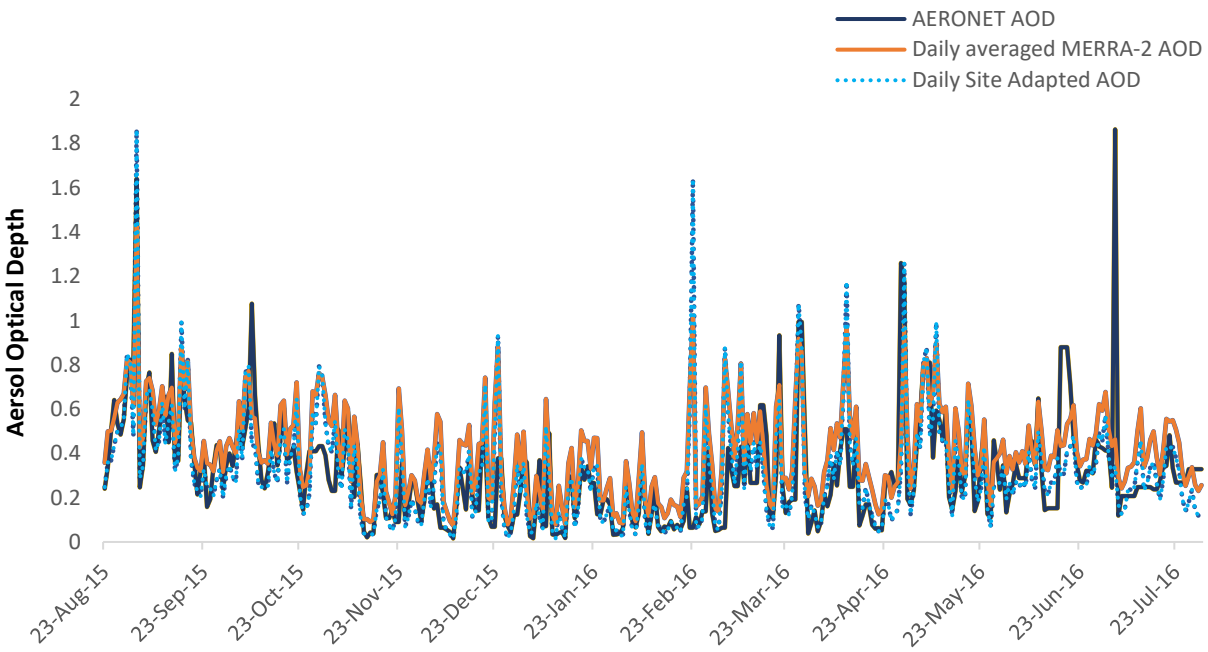

Fig. A.1 The site adaptation **on a** year scale by quantile mapping for the MERRA-2 AOD product in Shagaya, Kuwait.

This improvement has also been confirmed by the usual data deviation measurements techniques, i.e. MBD and RMSD which can be applied as follows:

$$\text{MBD}=\frac{1}{N}\sum_{i=1}^{N}(ci-mi) \tag{A.1}$$

$$\text{RMSD}=\sqrt{\frac{1}{N}\sum_{i=1}^{N}(ci-mi)^2} \tag{A.2}$$

Appendix B - AERONET AOD Data

Although AERONET AOD data is available at 7 different wavelengths, between 340 and 1020 nm, the most commonly used wavelength worldwide is 550nm (because the satellites sensors report the AOD at this wavelength [54]) is not among them [94]. This creates an issue as even the Polo model which introduces the aerosols effect in SAM is built based on AOD at

550 nm wavelength. Thus, this issue can be addressed through the interpolation method as given by [256]:

$$\ln(\tau_\lambda) = \alpha_0 + \alpha_1 \ln(\lambda) + \alpha_2 [\ln(\lambda)]^2 \quad \text{(B.1)}$$

where α is the variation that is observed along the different wavelengths (λ).

Appendix C - Polo Model Validation

The validation of the Polo model [60] has been performed by demonstrating the linearity of the AEG with an increasing theoretical range of AOD values after the integration of Polo model into the SAM. This step has been taken in order to ensure that the Polo model is well integrated into the SAM simulation environment and this can be seen as the AOD value increases, the AEG of the model decreases which agrees with physical nature of aerosols and their ability to attenuate the key parameter in the thermal energy received by the solar field, i.e. the DNI. The linearity of the model is mainly dependent on the RTM.

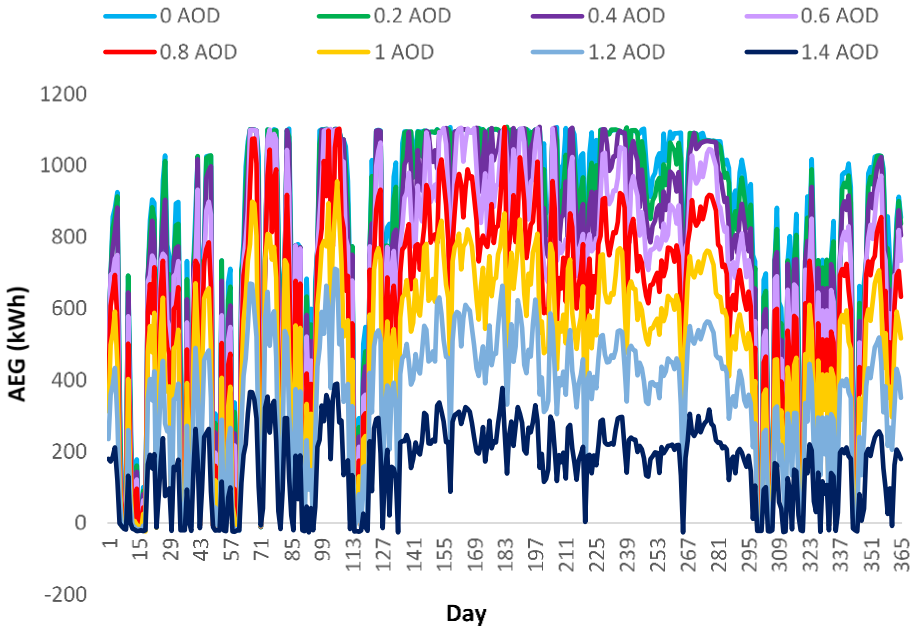

0 AOD	301568286
0.1 AOD	296625619
0.2 AOD	291166949
0.3 AOD	291166949
0.4 AOD	275647671
0.5 AOD	265712431
0.6 AOD	253209123
0.7 AOD	238104369
0.8 AOD	220460897
0.9 AOD	200916682
1 AOD	178881407
1.1 AOD	154039934
1.2 AOD	126386052
1.3 AOD	94947081
1.4 AOD	58980902

(a) (b)

Fig. C.1 Polo model linearity based on a range of AOD values: (a) daily energy generation and (b) annual energy generation sum.

Appendix D - Condenser Scenarios Performance

The outputs of the parametric analysis have been observed in detail and are illustrated in Tables D.1, D.2 and D.3, which correspond to the air-cooled, 30% hybrid and 19% hybrid

scenarios, respectively. These tables the techno-economic outputs for each TES-SM configuration. Once an optimal SM value is located for each TES capacity based on the lowest LCOE, each SM-TES configuration is observed in detail over the range of 0-18h. This has been primarily done based on an annually averaged AOD value and then compared to both non-aerosols and daily aerosols scenarios.

Differences between each scenario outputs are first seen in the solar field thermal energy output (the incident thermal energy on the receiver) and this is projected to the thermal energy transferred to the HTF which also translates into a variation on the AEG. Since the latter affects the economics, the LCOE varies too. A quite similar trend has been found in all configurations, where thermal energy of the solar field is mainly affected when the aerosols scheme is adopted compared to no aerosols scheme. The maximum reduction observed in this work for the capacity of 50 MW is 6.7% and this results in an increase of the LCOE by 6.3%.

Table D. 1

50 MW air-cooled condenser SPT technical outputs for each optimal SM over the TES range based on different aerosols scenarios.

TES (h)	LCOE ($/kWh)			SM (-)	Gross to net conversion factor (%)	CF (%)	No. of heliostats	Aperture Area (m^2)	Total power incident on the SF (MWh_{th})	Thermal power from SF (MWh_{th})		Total absorbed energy (MWh_{th})		Thermal energy to the PB (MWh_{th})	Thermal energy into the TES (MWh_{th})	Total water consumption (m^3/α)	AEG (kWh)			Overall efficiency (%)
	No aerosols	Annually averaged AOD	Daily AOD							Annually averaged AOD	Daily AOD	Annually averaged AOD	Daily AOD				No aerosols	Annually averaged AOD	Daily AOD	
0	23.15	23.94	24.07	1.2	88	19.8	2725	393,421.3	655,820.1	301,837.9	300,425.9	286,169.9	283,949.7	269,372.2	0	22,917	80,689,840	77,973,672	77,485,870.1	11.8
1	20.76	21.71	21.83	1.2	88.2	22.2	2756	397,896.9	663,576.5	328,280.7	326,641.9	285,114.5	282,921.7	295,660.4	32,238.1	23,705	91,459,096	87,369,864	86,819,887.7	13.1
2	19.34	20.1	20.22	1.4	88.5	26.2	3190	435,005.5	768,140.1	380,946.9	378,730.2	335,177.5	332,311	342,028.1	68,550	27,510	107,342,456	103,186,736	102,444,262.9	13.4
3	18.32	18.97	19.09	1.6	88.7	30	3633	524,513.6	874,896.2	429,546.7	426,828.7	384,335.4	380,761.3	385,700	106,053.7	31,313	122,496736	118,167,792	117,281,784.1	13.5
4	17.29	18.17	18.26	1.6	88.8	31.7	3625	523,358.7	872,783.9	450,605.2	448,157.8	384,936.3	381,397.9	405,613	128,037.9	31,710	131,611,176	125,127,712	124,328,816	14.3
5	17	17.6	17.72	2	89	37.3	4569	659,648.5	1,100,520	521,937.2	518,253.2	480,200.8	475,260.9	469,632.1	182,409.8	39,159	151,927,904	147,080,752	145,864,345.7	13.4
6	16.2	16.9	17	2	89.1	39.4	4557	657,916	1,097,684	547,908.5	544,554.3	482,072.9	477,173.5	493,613.4	270,886.5	39,4	162,448,896	155,419,840	154,307,145.9	14.2
7	15.52	16.41	16.5	2	89.2	40.9	4597	663,691	1,107,327	561,812.1	558,728.4	480,920.2	475,946.3	509,120.1	224,249.2	40,226	170,453,760	161,061,376	160,006,596.6	14.5
8	15.17	15.97	16.06	2.2	89.2	44.7	5054	758,218.3	1,217,546	611,309.4	607,495.2	528,998.4	523,322.7	553,848.6	266,359	44,142	185,969,040	176,371,296	175,114,873.3	14.5
9	14.75	15.72	15.81	2.2	89.3	45.8	5057	730,103.4	1,218,414	623,149.8	619,065.9	529,194.7	523,522.4	565,663.5	278,907.6	44,427	192,704,016	180,574,816	179,184,666.2	14.8
10	14.65	15.33	15.43	2.6	89.2	52.5	6050	873,467.5	1,457,914	706,969	701,869.7	627,006.3	619,309.1	641,642.2	350,044.3	52,458	216,538,000	206,769,168	205,101,589.7	14.2
11	14.2	14.99	15.08	2.6	89.2	53.9	5964	861,051.3	1,436,385	726,712	722,172.5	628,380.8	621,188.4	658,472.9	368,462.4	52,290	224,754,400	212,520,656	210,857,084.4	14.8
12	14	14.75	14.85	2.8	89.1	57.6	6474	934,682.5	1,559,481	771,164.8	765,878.9	674,296.1	666,412.9	700,788.8	409,396	56,487	239,553,568	226,962,432	224,929,458	14.6
13	13.85	14.56	14.66	3	89.1	61.3	6935	1,001,239.2	1,670,722	817,758.1	812,186.7	722,532.7	713,712	743,509	451,219.2	60,383	254,266,880	241,586,096	239,403,346.3	14.5
14	13.79	14.46	14.56	3.2	89.1	64.8	7489	1,081,222.9	1,805,276	861,856.8	855,359.6	769,118.3	759,310.2	785,262.4	491,904.1	64,89	268,445,888	255,618,832	253,331,285.9	14.2
15	13.41	14.2	14.3	3.2	89.2	66.6	7485	1,081,222.9	1,804,000	880,473.6	873,839.6	770,707.4	760,514.1	802,759.6	510,165.8	65,270	278,542,144	262,613,456	260,236,704	14.6
16	13.18	14	14.1	3.2	89.1	67.7	7358	1,062,309.8	1,773,422	893,052.1	887,488.8	773,352.8	763,449.2	811,922.1	520,013	64,753	284,120,032	267,066,848	264,479,448.4	15.1
17	13.2	14.05	14.15	3.2	89.2	67.9	7429	1,072,560.4	1,790,605	891,398.2	886,264.9	771,066.7	760,971.9	812,830.8	520,961.7	65,244	285,436,160	267,769,456	264,975,087.4	15.5
18	13.23	14.08	14.2	3.2	89.2	68	7431	1,072,849.1	1,791,183	891,740.2	886,457.9	770,273.5	760,508.4	813,926.5	522,233	65,290	285,879,488	268,181,840	265,202,800.9	15

Table D. 2

50 MW 30% hybrid condenser SPT technical outputs for each optimal SM over the TES range based on different aerosols scenarios.

TES (h)	LCOE ($/kWh)			SM (-)	Gross to net conversion factor (%)	CF (%)	No. of heliostats	Aperture Area (m^2)	Total power incident on the SF (MWh_{th})	Thermal power from SF (MWh_{th})		Total absorbed energy (MWh_{th})		Thermal energy to the PB (MWh_{th})	Thermal energy into the TES (MWh_{th})	Total water consumption (m^3/α)	AEG (kWh)			Overall efficiency (%)
	No aerosols	Annually averaged AOD	Daily AOD							Annually averaged AOD	Daily AOD	Annually averaged AOD	Daily AOD				No aerosols	Annually averaged AOD	Daily AOD	
0	21.56	22.3	22.42	1.2	86.8	21.4	2763	398,907.6	664,945.6	301,544.6	300,031.9	285,009.6	282,670.5	269,916	0	225,832	87,126,400	84,162,232	83,626,070.2	12.7
1	19.29	20.14	20.26	1.2	87	24	2727	393,710.1	656,636.6	331,196.6	329,252.3	286,801.2	284,529.4	297,011.8	32,900.6	241,805	98,652,096	94,419,344	93,728,639.5	14.4
2	18.06	18.76	18.88	1.4	87.4	28.2	3210	463,443.1	773,002.1	381,354.3	379,053.4	335,580.6	332,637.9	342,713.3	68,615.33	268,526	115,417,608	111,015,976	110,176,887.8	14.4
3	17.17	17.78	17.89	1.6	87.7	32.1	3636	524,946.8	875,207.6	430,311	427,596.9	384,424.2	380,845.9	386,068	106,256.9	289,575	131,169,400	126,598,112	125,629,527.4	14.5
4	16.2	17.02	17.11	1.6	87.8	33.9	3640	525,524.3	876,525.5	450,322.4	447,902	384,761	381,176.5	405,754.3	127,537.9	297,365	140,605,136	133,683,264	132,811,700.1	15.3
5	15.64	16.38	16.46	1.8	88	38	4123	595,257.3	993,005.5	498,845.8	495,897.9	433,148.1	428,894.9	450,409.7	167,493.5	315,823	156,967,104	149,719,744	148,745,145.6	15.1
6	15.2	15.87	15.96	2	88.1	41.9	4571	659,937.2	1,101,057	545,962.9	542,615.2	480,924.9	475,996.2	493,189.8	506,957.7	328,929	172,454,672	164,997,024	163,795,065.9	15
7	14.64	15.48	15.56	2	88.1	43.2	4590	662,680.3	1,105,794	560,390.3	557,336.1	480,124	475,137.5	508,455.9	223,095.9	330,988	180,540,800	170,454,608	169,342,204.6	15.4
8	14.35	15.11	15.19	2.2	88.2	47.4	5055	729,814.6	1,217,709	611,702.5	607,960.7	529,176.4	523,467.2	554,230.8	266,227.1	343,245	196,798,560	186,738,144	185,414,933.9	15.3
9	14.08	14.76	14.85	2.4	88.3	51.5	5548	800,991.4	1,336,948	661,415.5	656,957.2	579,455.9	572,903.4	599,733	309,390.2	352,314	213,085,600	203,059,888	201,518,162.9	15.2
10	13.69	14.51	14.59	2.4	88.4	52.8	5542	800,125.1	1,335,504	676,703.2	672,605.8	579,936.4	573,380.5	614,391.8	324,818.3	352,269	221,140,016	208,319,152	206,872,569.8	15.6
11	13.5	14.24	14.33	2.6	88.3	56.8	5942	857,8750.1	1,430,800	727,583	722,905.5	628,730.4	621,319.1	659,172.7	368,530.5	358,004	236,638,672	223,932,832	222,123,311.7	15.7
12	13.35	14.03	14.13	2.8	88.3	60.7	6413	925,875.6	1,545,466	774,543.5	769,242.9	676,682	668,486	702,581.2	410,584.7	363,323	251,812,272	239,171,824	236,965,672.1	15.5
13	13.03	13.84	13.94	2.8	88.3	61.7	6440	929,773.7	1,552,026	784,272.9	779,152.2	674,862.4	666,624.8	714,130.7	422,607.2	365,517	258,760,464	243,211,232	240,843,104.3	15.7
14	12.86	13.79	13.9	2.8	88.4	62.6	6487	936,559.3	1,563,347	793,476.9	786,752.9	674,547.7	666,370.2	723,529.5	432,221.8	371,862	265,213,664	246,788,048	244,074,238.9	15.8
15	12.82	13.54	13.64	3.2	88.2	69.8	7404	1,068,951	1,784,501	884,091.8	877,771.5	772,371.2	762,361.4	804,064.7	511,081.1	401,719	291,219,296	275,243,936	272,549,318.9	15.4
16	12.79	13.46	13.55	3.4	88.2	73.6	7934	1,145,469.7	1,912,492	922,270.1	915,951.5	820,133.1	809,412.5	839,278.8	545,513.4	421.682	305,696,000	290,020,672	287,557,248.3	15.2
17	12.7	13.39	13.48	3.4	88.3	74.2	7897	1,140,127.8	1,903,559	927,150.7	921,258.5	821,228.8	810,536.1	843,549.1	550,104.6	424,402	308,950,336	292,518,624	289,893,503.6	15.4
18	12.77	13.47	13.64	3.4	88.3	74.5	7965	1,149,945.3	1,920,270	928,866.4	923,609.4	820,867	810,018.7	845,997.6	552,487.8	426,181	310,436,608	293,677,120	290,597,172.3	15.3

Table D. 1

50 MW 19% hybrid condenser SPT technical outputs for each optimal SM over the TES range based on different aerosols scenarios.

TES (h)	LCOE ($/kWh)			SM (-)	Gross to net conversion factor (%)	CF (%)	No. of heliostats	Aperture Area (m^2)	Total power incident on the SF (MWh_{th})	Thermal power from SF (MWh_{th})		Total absorbed energy (MWh_{th})		Thermal energy to the PB (MWh_{th})	Thermal energy into the TES (MWh_{th})	Total water consumption (m^3/α)	AEG (kWh)			Overall efficiency (%)
	No aerosols	Annually averaged AOD	Daily AOD							Annually averaged AOD	Daily AOD	Annually averaged AOD	Daily AOD				No aerosols	Annually averaged AOD	Daily AOD	
0	21.68	22.43	22.55	1.2	86.9	21.2	2763	398,907.6	664,945.6	301,544.4	300,031.7	285,023.1	282,681.6	269,920.5	0	183,912	86,619,136	83,670,040	83,146,461.4	12.6
1	19.4	20.26	20.38	1.2	87.1	23.8	2727	409,113.8	656,636.9	331,200.5	329,255.5	286,815.4	284,542.1	297,020.9	32,905.4	198,396	98,096,392	93,871,552	93,200,835.4	14.3
2	18.18	18.9	19.05	1.4	87.6	28	3234	466,908.1	778,829.6	380,188	377,889.2	334,851	331,875.3	342,361.8	68,271.8	218,561	114,727,680	110,529,264	109,443,403.8	14.2
3	17.35	17.97	18.08	1.6	87.8	31.9	3679	531,154.9	885,975.4	429,640	426,937	383,837.1	380,220.6	385,933.7	105,907.8	226,307	130,346,728	125,726,240	124,760,861.1	14.2
4	16.35	17.17	17.26	1.6	87.9	33.7	3619	522,492.4	871,283	452,029.6	449,596	385,435	381,859.2	406,155.9	128,228	225,710	139,697,344	132,905,976	132,051,140.9	15.2
5	15.73	16.48	16.56	1.8	88.1	37.7	4099	591,792.3	987,230.3	498,617.6	495,671	432,774.9	428,533.8	449,965.3	167,262.7	231,137	155,650,224	148,452,576	147,516,535.3	15
6	15.3	15.97	16.06	2	88.3	41.6	4585	661,958.5	1,104,417	545,922.4	542,556.1	481,120.3	476,166.1	493,507.9	207,137.9	235,965	171,480,928	164,052,704	162,853,087.2	14.9
7	14.74	15.58	15.66	2	88.3	43.1	4585	661,958.5	1,104,426	562,145.1	559,119.6	481,120.3	476,166.1	509,419.1	224,047.5	236,021	179,706,512	169,757,248	168,653,074.3	15.4
8	14.41	15.16	15.24	2.2	88.4	47.2	5028	725,916.5	1,211,043	614,346.3	610,660.8	531,137.1	525,324.1	555,666.1	267,725.6	240,373	195,906,832	186,069,440	184,762,198.3	15.4
9	14.17	14.86	14.95	2.4	88.5	51.2	5564	803,301.4	1,340,797	660,863.1	656,335.1	579,169.3	572,573.3	599,598.7	309,220.9	245,192	211,817,664	201,813,984	200,249,319.7	15.1
10	13.77	14.6	14.68	2.4	88.5	52.5	5550	801,280.1	1,337,428	675,829.6	671,686.9	579,410.5	572,859.7	614,000.4	324,385.9	245,213	219,694,720	206,878,064	205,416,024.9	15.5
11	13.58	14.33	14.42	2.6	88.5	56.6	5957	860,040.7	1,435,037	728,895.6	724,192.6	629,818.1	622,412.3	660,102.	369,272.6	249,132	235,758,320	223,109,664	221,331,383	15.5
12	13.44	14.14	14.24	2.8	88.6	60.5	6539	944,066.8	1,576,054	773,061.8	767,433.8	676,246.4	667,963.2	703,332.4	410,737.2	254,218	251,276,896	238,553,872	236,299,966.9	14.9
13	13.14	13.96	14.06	2.8	88.6	61.7	6539	944,066.8	1,576,054	786,493.8	781,181.5	676,246.4	667,963.2	716,529.2	424,518.3	256,067	258,762,704	243,200,896	240,796,238.7	15.4
14	12.93	13.87	13.99	2.8	88.6	62.5	6539	944,066.8	1,576,054	795,982.4	789,231.9	676,246.4	667,963.2	725,796.3	434,203.4	261,333	264,874,064	246,559,504	243,799,485.8	15.6
15	12.83	13.56	13.65	3.2	88.5	69.7	7464	1,077,613.5	1,798,635	882,903.5	876,542.6	773,038.9	763,173.7	805,118.9	511,944.2	284,339	290,868,864	274,776,384	272,225,042.1	15.3
16	12.82	13.49	13.57	3.4	88.4	73.4	7901	1,140,705.3	1,904,525	924,355.5	918,062.9	821,911.4	811,199.7	840,567.2	546,811	298,862	304,701,824	289,224,512	286,854,976.1	15.2
17	12.77	13.47	13.56	3.4	88.4	73.9	7901	1,140,705.3	1,904,525	928,142.1	922,237	821,911.4	811,199.7	844,163.3	550,698.9	300,334	307,682,368	291,232,096	288,613,427.8	15.3
18	12.8	13.5	13.6	3.4	88.4	74.1	7901	1,140,705.3	1,904,525	930,466.7	925,445.8	821,911.5	811,199.7	846,304.1	553,110.4	301,211	308,833,344	292,192,768	289,295,779	15.3

Appendix E – Siemens Gamesa WT Power Curve

The Siemens Gamesa G97 wind turbines used in this research as they have been already deployed in the case study location in Kuwait. The 2 MW wind turbine's power curve obtained from the manufacturer [257] is illustrated in Figure E.1 and shows the a 3m/s and 25 m/s as cut in and cut out speeds, respectively.

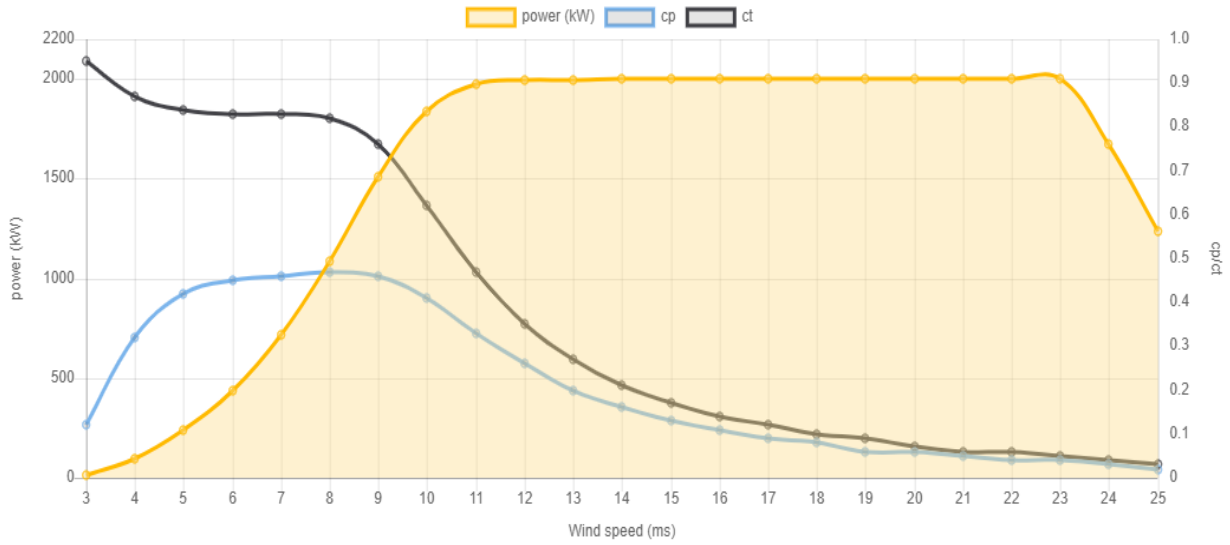

Fig. E.1. Siemens Gamesa G97 wind turbine power curve [246].

Appendix F – WT Different Alignments Configurations

This work has adopted the same WT alignment of the existing 5 WT in the pilot plant in SREP for the sake of validation. Then, other alignment configurations had to be studied in order to examine whether exists a better arrangement in the case study location or not. To this extent, this work has examined a variety of alignments, none of which seem to be better performing than the already operating 5 WT in SREP. The examined WT alignments are illustrated in Figure F. 1.

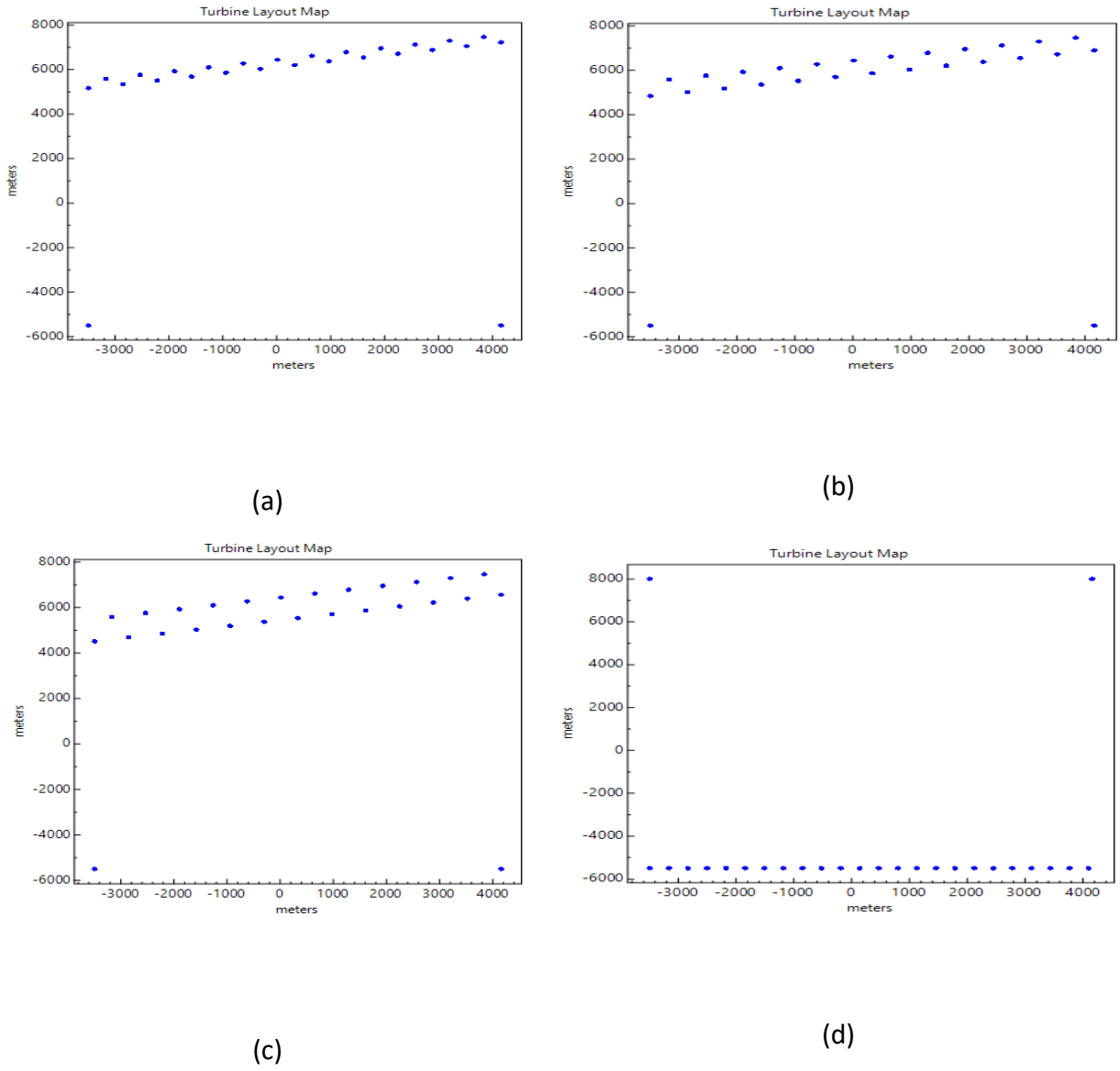

Fig. F.1. Different WT alignments in SREP (a) 330m apart WT, (b) 660m apart WT, (c) 990m apart WT and a straight line of 330m apart WT.

Appendix G – NGCC Wet-Cooled Condenser Scenario

In the NGCC alternative simulation scenario, it has been noticed that the water quantities that are required at the heat exchanger to cool off the water out of the ST are of huge amounts

even when assuming that only 5% of these quantities is really consumed while the rest is recirculated. The water quantities for the three different NGCC configurations are as follows:

- 8.6 MW NGCC: 9,753,589.9 m^3/y of which 487,679.5 is consumed.
- 13.9 MW NGCC: 17,416,119.5 m^3/y of which 870,805.9 is consumed.
- 17.8 MW NGCC: 24,725,336.5 m^3/y of which 1,236,266.8 is consumed.

In return, no substantial increase in the CAPEX of the air-cooled condenser which is to replace the wet-cooled one. Also, a negligible amount of energy penalty has been found to be consumed in order for the fans of the air-cooled condenser to cool off the steam out of the ST turbine of the NGCC. The required amounts of energy for the fans for all NGCC scenarios are listed in Table G.1 and have been included in the AEG and thus, the LCOE calculations.

Table G.1
The air cooled condenser simulation for the NGCC different configurations.

		Steam mass flow rate (kg/h)	Required air quantity for cooling (kg/h)	Required energy for the air condenser fans (kWh)
NGCC	**8.6 MW**	10,513	350,000	33
	13.9 MW	17,525	550,000	52
	17.8 MW	24,880	750,000	71

Appendix H – NGCC CO_2 Emissions

Based on the natural gas hourly consumption quantities from the Aspen Plus simulation tool, the CO_2 emissions of the three different NGCC can be calculated. The heat that is supplied to the system H can be obtained through the multiplication of the natural gas quantity by the natural gas calorific value. Then, the result is multiplied by 947.817 to convert the MJ/h into BTU/h. Then, the heat rate can be obtained by equation (3-6), however, in BTU/kWh and this must transferred into MMBTU/kWh. Thus, the amount of heat that is consumed in order to produce each kWh is known and with knowing the amount of the kWh/y produced by the system

from Aspen Plus, the amount of MMBTU/y can be known. Lastly, the natural gas is assumed to emit 52.91 kg of CO_2 per MMBTU [183], thus the CO_2 in kg/y is obtained.

Table H-1
The CO_2 emissions for all three NGCC scenarios with conversion details.

		NGCC		
		8.5 MW	**13.9 MW**	**17.8 MW**
System's Hourly fuel consumption (kg/h)		1190	2080	2900
The natural gas heat input to the system	**(MJ/h)**	59,500	104,000	145,000
	(BTU/h)	56,395,290	98,573,280	137,433,900
Electricity energy generation (kW)		7,773	13,796	17,695
System heat rate	**(BTU/kWh)**	7,255.3	7,145.1	7,766.8
	(MMBTU/kWh)	0.00725	0.00714	0.00776
	(MMBTU/y)	419,613.7	733,456.6	1,022,434.1
The CO_2 emissions (kg/y)		22,201,760.9	38,807,188.7	54,096,988.2

Appendix I – LCA Inventory

Here, all the raw materials inventory for the SPT sub components are listed in Table I.1. It is worth mentioning that other SPT references could have been used here in the LCA inventory (such as Abengoa [38] and other plants from the literature [171]), however, the published LCA inventory of these elsewhere existing SPT references drastically differ from the considered categories here in this study. This has an immense effect of the final product of GWP and thus other SPT references are not considered here. Table I.1 contains a sub category named

''replacement materials'' in each LCA category of the SPT which is dedicated for the needed maintenance for this category all along the plant's lifetime.

Table I.1.
The SPT sub components categories LCA inventory (all weights are in tons, concrete + excavation + tap water in m^3 and transport distances are in tkm).

SPT sub component	LCA raw material category	Gemasolar SPT [37], [187], [188], [189], [36], [258]	115 MW SPT [190], [189], [258], [259]	220 MW SPT [191], [258]
site preparation	reinforcing steel	99.1	103	36.4
	copper production, primary	1.13	1	3
	polyvinylchloride, bulk polymerized	84	399	103.382
	excavation, hydraulic digger	519	2997	5734
	transport, freight, lorry > 32 metric ton	212000	1225126	2343719
replacement materials	reinforcing steel	0.966	5.552	10.621
	copper production, primary	0.203	1.167	2.233
O & M	electricity, high voltage, production mix	2095452	12571683	23958000
	occupation, industrial area	1424494	7345044	16021505
	tap water	432720	2587890	5199240
Receiver & tower	reinforcing steel	552.874	3195	5242.6
	copper production, primary	7.268	42	49.95
	rock wool	66.8	128	908.55
	chromium steel 18/8	211	234	157.15
	concrete, normal	3824	22097	21074
	transport, freight, lorry > 32 metric ton	2455300	15515282.5	29950000
replacement materials	reinforcing steel	10.136	58.576	112.058
	copper production, primary	2.643	15.274	29.22
Solar field	reinforcing steel	27800	34434.472	41767.311
	copper production, primary	33.685	194.664	372.401
	flat glass, coated	10000	21855.443	34958.827
	concrete, normal	30084	61042	95259
	excavation, hydraulic digger	30084	61042	95259
	transport, freight, lorry > 32 metric ton	30300000	52066783	76124806
replacement materials	reinforcing steel	69.5	414.474	104.418
	flat glass, coated	95.342	548.218	1048.765
TES	steel, low-alloyed	2.578	14.898	285
	reinforcing steel	88.275	524	975.9

	copper production, primary	1	10	8.7
	rock wool	298	411.05	536
	potassium nitrate	15000	6967.2	21240
	sodium nitrate	2400	10450.8	33276
	chromium steel 18/8	79.374	452	877.5
	concrete, normal	18	105	207
	transport, freight, lorry > 32 metric ton	1200000	6900000	13200000
replacement materials	KNO3	45	209.016	637.2
	NaNO3	72	313.524	998.28
Molten salt/steam generation	steel, low-alloyed	2	8	8.45
	reinforcing steel	27	133	340.45
	copper production, primary	35	68	100
	rock wool	5	27	62
	chromium steel 18/8	143	254	485
	concrete, normal	7	42	74
	transport, freight, lorry > 32 metric ton	18682	107420	205500
replacement materials	reinforcing steel	4.61	7.072	10
	copper production, primary	5	10.887	15
Power Cycle	steel, low-alloyed	50	249	452.4
	aluminum, primary	60	366	524.3
	reinforcing steel	500	4907	5075.1
	copper production, primary	32.174	185	353.913
	rock wool	13	53	187.15
	lubricating oil	69.667	95	104.716
	polyvinylchloride, bulk polymerized	55	115	536
	chromium steel 18/8	34.1	67	142.7
	concrete, normal	5126	8210	19480
	transport, freight, lorry > 32 metric ton	423884	2331364	4460000
replacement materials	reinforcing steel	7.266	36.329	69.025
	copper production, primary	2.646	13.23	25.137
	lubricating oil	25	137	98.3

In addition, since this work is integrating different sizes and heights of both the SPT receiver and tower, it has been a must to separate the materials in the LCA of these categories, i.e. receiver and tower. Inconveniently, most of the previously cited references in Table I.1 combine these two categories and thus this work has estimated the materials based on each

category's usual materials usage in the literature. For example, all the required concrete quantities are assigned to the tower newly separated category as there is no concrete usage in the receiver. Also, one of the few references that already separated both the receiver and tower LCA inventories is [190] which has helped this work in the splitting process of the LCA inventories for the other two SPT plants. Table I.2 lists the LCA inventory of the newly separated two SPT categories of receiver and tower.

Table I.2
The LCA inventory of the newly separated receiver and tower components.

SPT sub component	LCA raw material category	Gemasolar	115 MW	220 MW
Receiver	reinforcing steel	66.4	384	630.1
	copper production, primary	0.36	40	2.5
	rock wool	30.4	88	412.9
	chromium steel 18/8	15.07	70	11.225
	transport, freight, lorry > 32 metric ton	2455300	15515282.5	29950000
Tower	reinforcing steel	486.4	2811	4612.5
	copper production, primary	6.9	2	47.5
	rock wool	36.4	40	495.5
	chromium steel 18/8	195.9	5	145.9
	concrete, normal	3824	22097	21074
	transport, freight, lorry > 32 metric ton	2455300	15515282.5	29950000

Appendix J – Aerosols Effect on SPT Performance

Figure J.1 illustrates a performance analysis of the ascending SPT capacity within the range of 50-100 MW with a step size of 10 MW. The comparison has been carried out between the aerosols affected and the hypothetical non-aerosols standalone scenarios. It is clear from Figure J.1 that there is a proportional relation between the capacity and the aerosols effect as the latter increases as the former does.

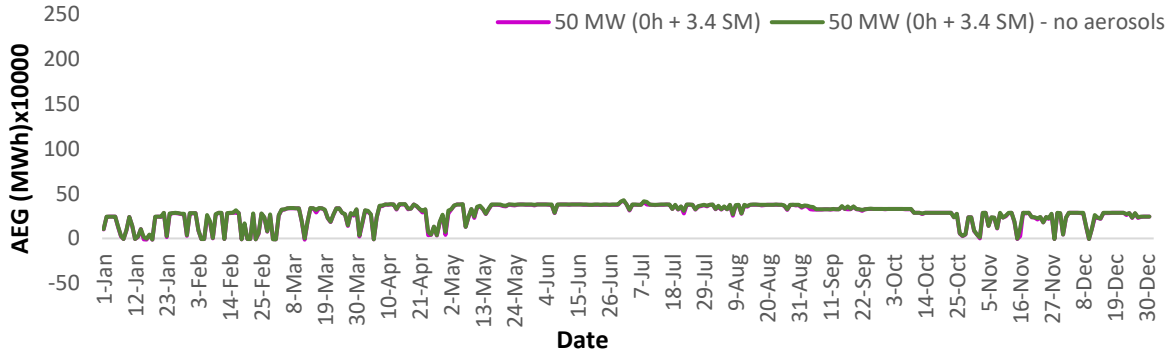
50 MW (0h + 3.4 SM)
50 MW (0h + 3.4 SM) - no aerosols
AEG (MWh)x10000
250
200
150
100
50
0
-50
1-Jan
12-Jan
23-Jan
3-Feb
14-Feb
25-Feb
8-Mar
19-Mar
30-Mar
10-Apr
21-Apr
2-May
13-May
24-May
4-Jun
15-Jun
26-Jun
7-Jul
18-Jul
29-Jul
9-Aug
20-Aug
31-Aug
11-Sep
22-Sep
3-Oct
14-Oct
25-Oct
5-Nov
16-Nov
27-Nov
8-Dec
19-Dec
30-Dec
Date

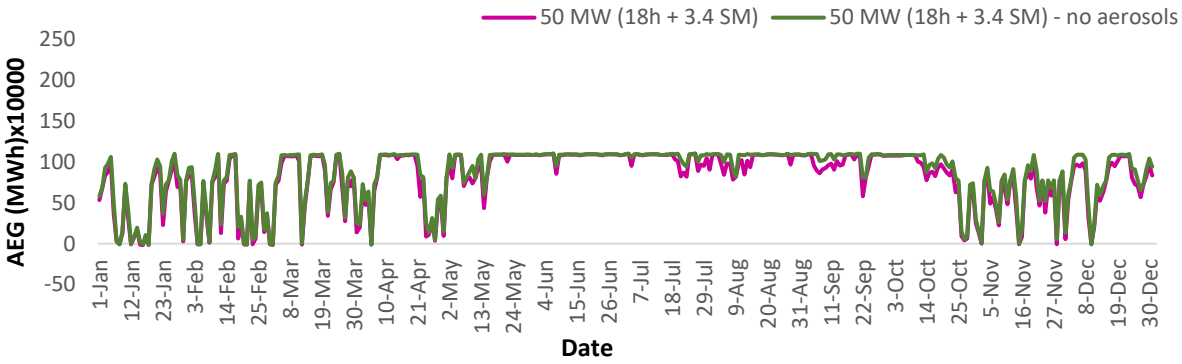
50 MW (18h + 3.4 SM)
50 MW (18h + 3.4 SM) - no aerosols
AEG (MWh)x10000
250
200
150
100
50
0
-50
1-Jan
12-Jan
23-Jan
3-Feb
14-Feb
25-Feb
8-Mar
19-Mar
30-Mar
10-Apr
21-Apr
2-May
13-May
24-May
4-Jun
15-Jun
26-Jun
7-Jul
18-Jul
29-Jul
9-Aug
20-Aug
31-Aug
11-Sep
22-Sep
3-Oct
14-Oct
25-Oct
5-Nov
16-Nov
27-Nov
8-Dec
19-Dec
30-Dec
Date

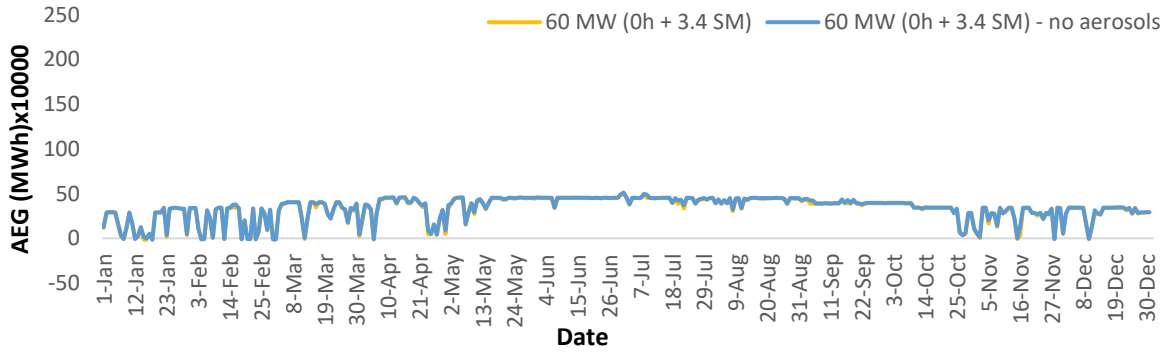
60 MW (0h + 3.4 SM)
60 MW (0h + 3.4 SM) - no aerosols
AEG (MWh)x10000
250
200
150
100
50
0
-50
1-Jan
12-Jan
23-Jan
3-Feb
14-Feb
25-Feb
8-Mar
19-Mar
30-Mar
10-Apr
21-Apr
2-May
13-May
24-May
4-Jun
15-Jun
26-Jun
7-Jul
18-Jul
29-Jul
9-Aug
20-Aug
31-Aug
11-Sep
22-Sep
3-Oct
14-Oct
25-Oct
5-Nov
16-Nov
27-Nov
8-Dec
19-Dec
30-Dec
Date

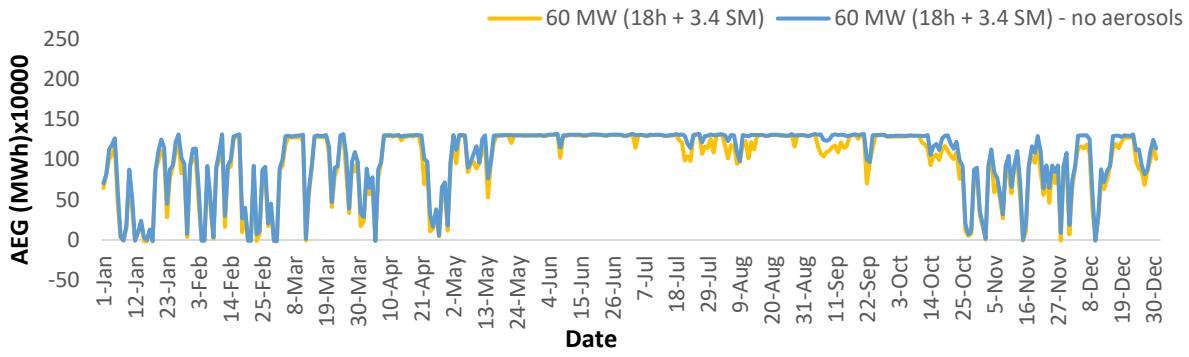
60 MW (18h + 3.4 SM)
60 MW (18h + 3.4 SM) - no aerosols
AEG (MWh)x10000
250
200
150
100
50
0
-50
1-Jan
12-Jan
23-Jan
3-Feb
14-Feb
25-Feb
8-Mar
19-Mar
30-Mar
10-Apr
21-Apr
2-May
13-May
24-May
4-Jun
15-Jun
26-Jun
7-Jul
18-Jul
29-Jul
9-Aug
20-Aug
31-Aug
11-Sep
22-Sep
3-Oct
14-Oct
25-Oct
5-Nov
16-Nov
27-Nov
8-Dec
19-Dec
30-Dec
Date

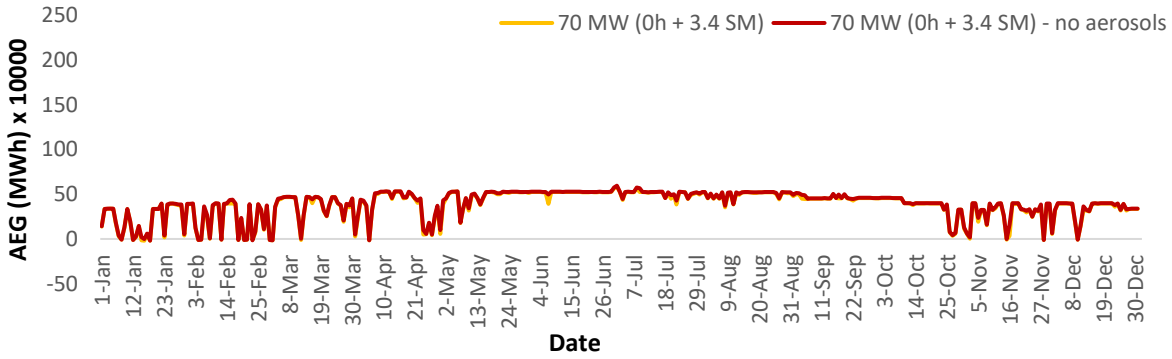
70 MW (0h + 3.4 SM)
70 MW (0h + 3.4 SM) - no aerosols
AEG (MWh) x 10000
250
200
150
100
50
0
-50
1-Jan
12-Jan
23-Jan
3-Feb
14-Feb
25-Feb
8-Mar
19-Mar
30-Mar
10-Apr
21-Apr
2-May
13-May
24-May
4-Jun
15-Jun
26-Jun
7-Jul
18-Jul
29-Jul
9-Aug
20-Aug
31-Aug
11-Sep
22-Sep
3-Oct
14-Oct
25-Oct
5-Nov
16-Nov
27-Nov
8-Dec
19-Dec
30-Dec
Date

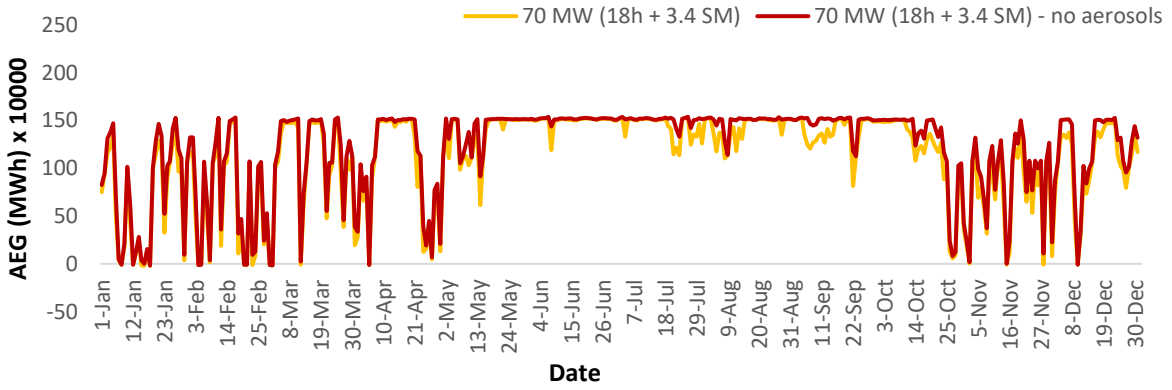
70 MW (18h + 3.4 SM)
70 MW (18h + 3.4 SM) - no aerosols
AEG (MWh) x 10000
250
200
150
100
50
0
-50
1-Jan
12-Jan
23-Jan
3-Feb
14-Feb
25-Feb
8-Mar
19-Mar
30-Mar
10-Apr
21-Apr
2-May
13-May
24-May
4-Jun
15-Jun
26-Jun
7-Jul
18-Jul
29-Jul
9-Aug
20-Aug
31-Aug
11-Sep
22-Sep
3-Oct
14-Oct
25-Oct
5-Nov
16-Nov
27-Nov
8-Dec
19-Dec
30-Dec
Date

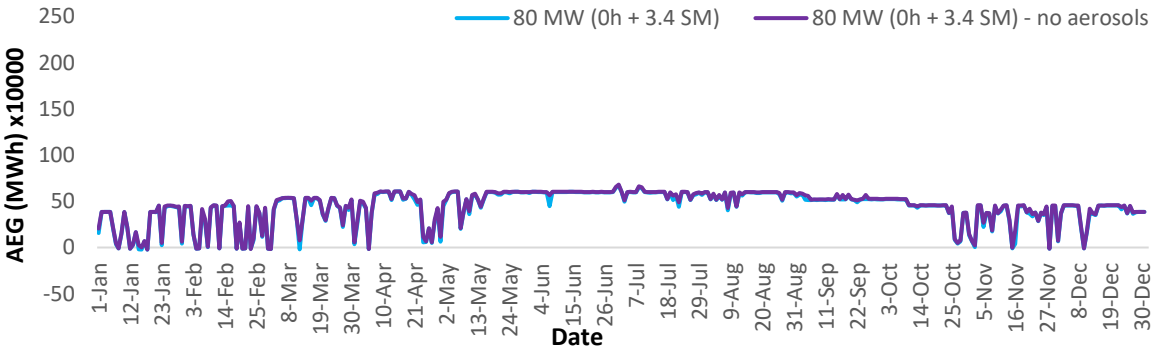
80 MW (0h + 3.4 SM)
80 MW (0h + 3.4 SM) - no aerosols
AEG (MWh) x10000
250
200
150
100
50
0
-50
1-Jan
12-Jan
23-Jan
3-Feb
14-Feb
25-Feb
8-Mar
19-Mar
30-Mar
10-Apr
21-Apr
2-May
13-May
24-May
4-Jun
15-Jun
26-Jun
7-Jul
18-Jul
29-Jul
9-Aug
20-Aug
31-Aug
11-Sep
22-Sep
3-Oct
14-Oct
25-Oct
5-Nov
16-Nov
27-Nov
8-Dec
19-Dec
30-Dec
Date

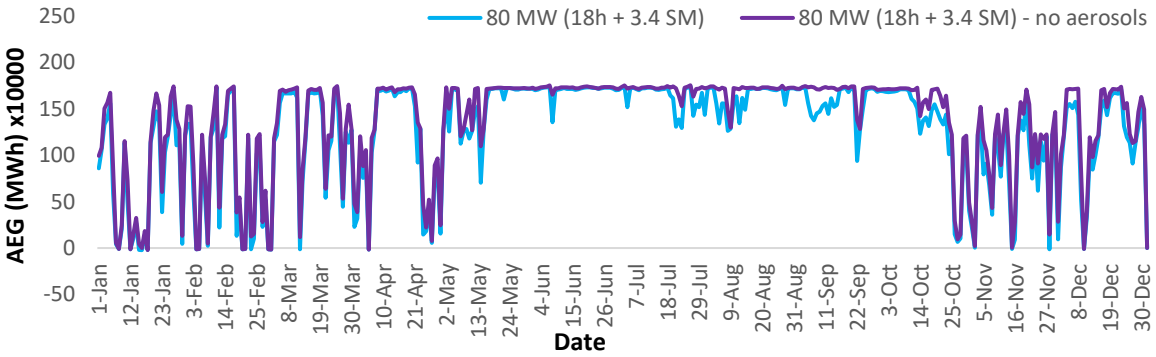
80 MW (18h + 3.4 SM)
80 MW (18h + 3.4 SM) - no aerosols
AEG (MWh) x10000
250
200
150
100
50
0
-50
1-Jan
12-Jan
23-Jan
3-Feb
14-Feb
25-Feb
8-Mar
19-Mar
30-Mar
10-Apr
21-Apr
2-May
13-May
24-May
4-Jun
15-Jun
26-Jun
7-Jul
18-Jul
29-Jul
9-Aug
20-Aug
31-Aug
11-Sep
22-Sep
3-Oct
14-Oct
25-Oct
5-Nov
16-Nov
27-Nov
8-Dec
19-Dec
30-Dec
Date

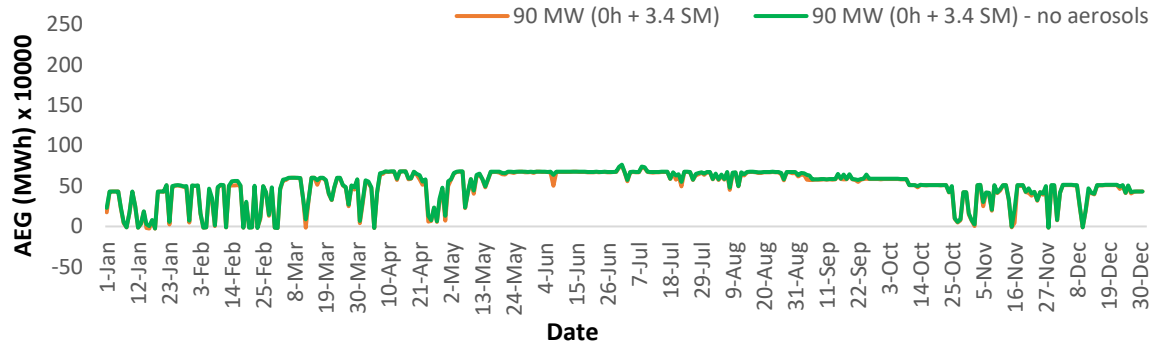
90 MW (0h + 3.4 SM)
90 MW (0h + 3.4 SM) - no aerosols
AEG (MWh) x 10000
250
200
150
100
50
0
-50
1-Jan
12-Jan
23-Jan
3-Feb
14-Feb
25-Feb
8-Mar
19-Mar
30-Mar
10-Apr
21-Apr
2-May
13-May
24-May
4-Jun
15-Jun
26-Jun
7-Jul
18-Jul
29-Jul
9-Aug
20-Aug
31-Aug
11-Sep
22-Sep
3-Oct
14-Oct
25-Oct
5-Nov
16-Nov
27-Nov
8-Dec
19-Dec
30-Dec
Date

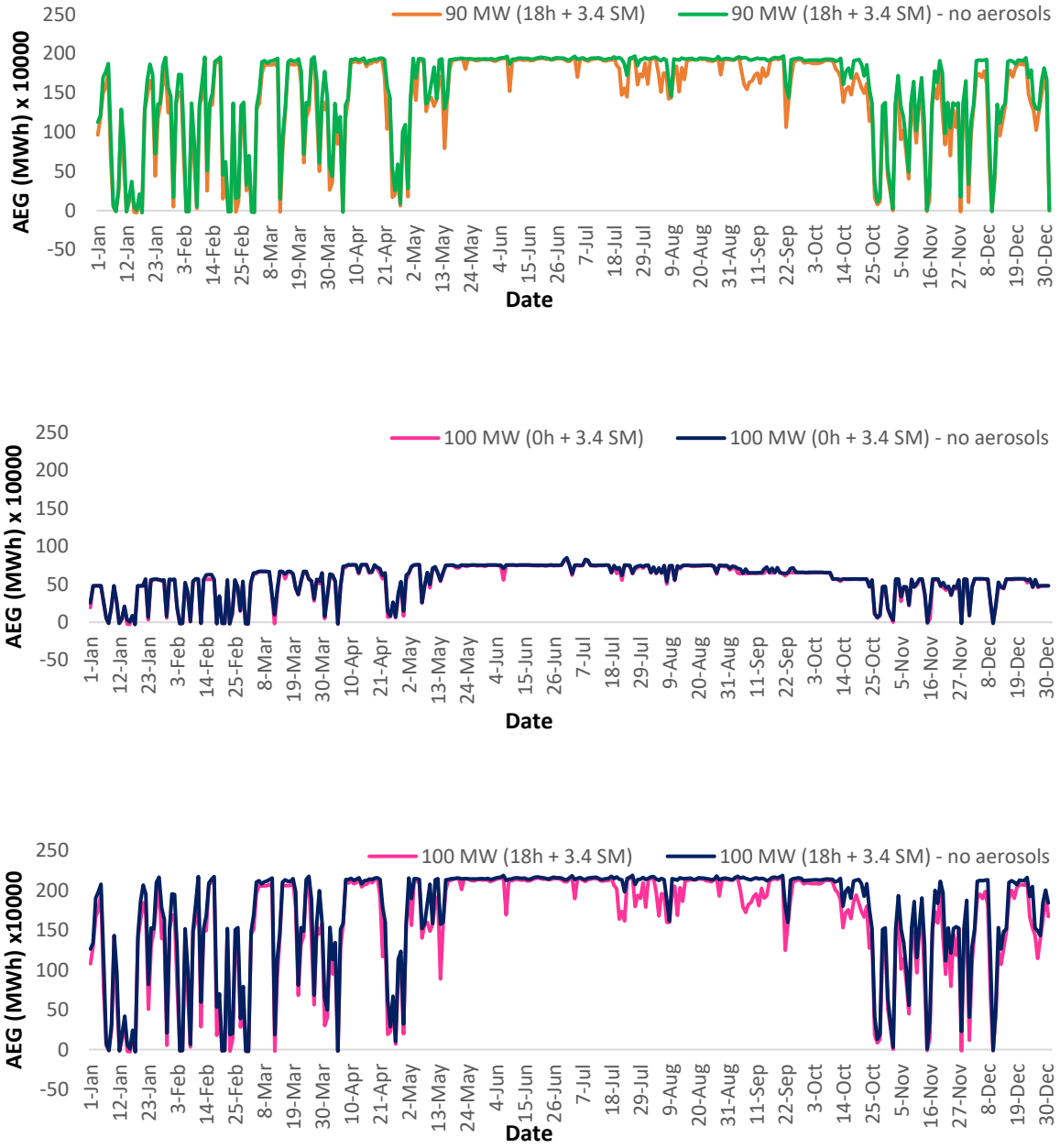

Fig. J. 1. Different SPT capacities AEG comparison of aerosols and non-aerosols scenarios.

It is also clear from Figure J.1 that the relation between the SPT capacity and the aerosols effect gets amplified with the bigger employed TES. This is because the TES increases the AEG and by increasing the AEG the effect of aerosols becomes more obvious.

Appendix K – CCS Energy Penalty

From the calculations carried out in Table 3-8, this work has been able to calculate CO_2 emissions in kg/y. Also, the used CCS of [203] is able to capture 99% of this CO_2, however for an energy penalty of 3.7 MJ/kg, which is considered as low grade thermal energy (at 135 °C) and thus needs to be converted. The conversion rate can be obtained by the following equation:

$$B = Q\ (1 - \frac{T_0}{T_{source}}) \tag{K-1}$$

where B is the exergy (here the electrical energy), is Q the thermal energy, T_0 is the considered surrounding temperature (31.65 °C as it is assumed in all previous simulation in SAM and Aspen Plus) and T_{source} is the temperature at which the low grade thermal energy is obtained (135 °C). Temperatures in equation (K-1) are converted to Kelvin for the calculation. The conversion factor of the required heat to electricity has been calculated as 0.253.

Appendix L - Carbon Capture and Storage Unit

Here, the Aspen Plus model of the acquired CCS model from [203] is illustrated in Figure L.1.

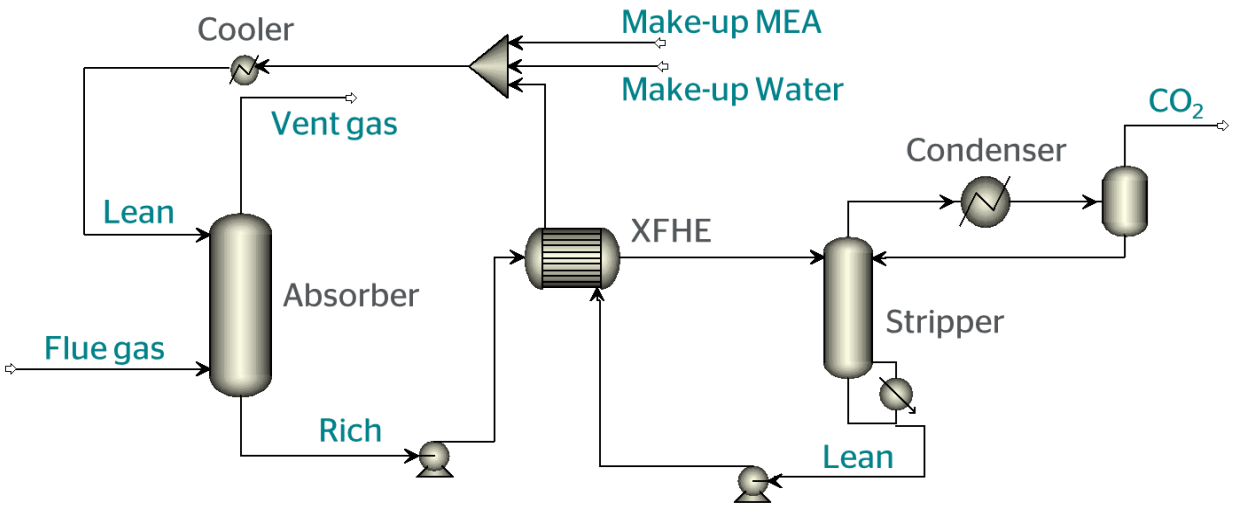

Fig. L.1 The flow diagram of the CCS as implemented in Aspen Plus (from [203]).

Appendix M - Quantile Mapping Algorithm (Matlab)

```
function y_corr=QuantileMappingBR(y_obs,y_mod)
% Function for Bias Removal in modeled data y_mod by Quantile Mapping
% over a smaller smaple of observations y_obs
% INPUT:
%        y_obs    :   observational data
%        y_mod    :   modeled data
%
% OUTPUT:
%        y_corr   :  Vector of corrected data
%
% ******************************************************
% This function provides a vector y_corr of corrected data with the same
% lenght as y_mod (modeled data that shoudl be corrected) based upon
% Quantile mapping technique over the empirical CDF calculated for the observational
values y_obs
% NOTE: all vectors should provide positive values since they are intended
% for solar radiation data, nevertheless the function ensures it.
% SINTAXIS: y_corr=QuantileMappingBR(y_obs,y_mod)
% ******************************************************************

y_obs = xlsread('23aug2015 to 29jul2016.xlsx','B2:B344');              %AERONET DATA
y_mod = xlsread('23aug2015 to 29jul2016.xlsx','C2:C344');              %MERRA-2 DATA

% J Polo, Sep 2019  CIEMAT Solar PV Unit
y_corr=y_mod;

% Empirical CDF for observational values
indo=find(y_obs>0);
[cdf_emp,x_emp]=ecdf(y_obs(indo));

% Empirical CFD for modeled values
indm=find(y_mod>0);
[cdf_mod,x_mod]=ecdf(y_mod(indm));

% We must ensure uniqueness in x_mod
[C,ia,ic]=unique(x_mod);
x_mod=C;
cdf_mod=cdf_mod(ia);

% Estimation of quantile for y_mod(indm), i.e.
% Translate the data to the quantile domain
quantile=interp1(x_mod,cdf_mod,y_mod(indm),'next');

% Quantile mapping using the empirical CDF
```

Appendix N - AOD Temporal Resolution Variation Algorithm (LK script)

```
a = csvread('C:/Users/Mohammed/Desktop/SAM trials/Kuwait/techno-economic/evaporative/evaporative 14/SAM coupling only a.csv', {'skip'=1, 'numeric'=true});
b = csvread('C:/Users/Mohammed/Desktop/SAM trials/Kuwait/techno-economic/evaporative/evaporative 14/SAM coupling only b.csv', {'skip'=1, 'numeric'=true});
c = csvread('C:/Users/Mohammed/Desktop/SAM trials/Kuwait/techno-economic/evaporative/evaporative 14/SAM coupling only c.csv', {'skip'=1, 'numeric'=true});
d = csvread('C:/Users/Mohammed/Desktop/SAM trials/Kuwait/techno-economic/evaporative/evaporative 14/SAM coupling only d.csv', {'skip'=1, 'numeric'=true});

active_case = ('untitled');

for (i=0; i<#a; i++)
{
    R = a[i][0];
    set ('c_atm_3', R);
    //simulate ();

        S = b[i][0];
    set ('c_atm_2', S);
    //simulate ();

    T = c[i][0];
    set ('c_atm_1', T);
    //simulate ();

    Q = d[i][0];
    set ('c_atm_0', Q);

    simulate ();

    Annualgen = get('system_pre_curtailment_kwac');
    RecPowHTF = get('q_dot_est_cr_on');
    RECINC = get('q_dot_rec_inc');

    outln(Annualgen);
    outln(RecPowHTF);
    outln(RECINC);

}
```

Appendix O – SPT Parametric Analysis Algorithm (LK script)

```
a = csvread(cwd()+'/Design TES range - Copy.csv', {'skip'=1,
'numeric'=true});
b = csvread(cwd()+'/Design SM range - Copy.csv', {'skip'=1,
'numeric'=true});

active_case = ('untitled');

for (i=0; i<8; i++)
{
     for (k=0; k<7; k++)
     {

     R = b[i][0];
     set ('solarm', R);

     R = a[k][0];
     set ('tshours', R);

     simulate ();

     Annualgen = get('annual_energy_pre_curtailment_ac');
     LCOE = get('lcoe_real');
     WaterUse = get('annual_total_water_use');
     NetCapCost = get ('cost_installed');
     Helio = get ('N_hel');

     outln(LCOE);
     outln(Annualgen);
     outln(WaterUse);
     outln(NetCapCost);
     outln(Helio);

     }
}
```

Appendix P – SAM Performance Models Hybridization Algorithm (LK script)

```
//2 Wind turbine + SPT + NGCC + CCS

path = '//stfdata07/home/ME/Mep19ma/ManW10/Desktop/SPT + GT + CC' + '/';

    SPT_variable_costs = csvread (path + 'SPT variable M&O costs basemodel with equations.csv', {'numeric' = true});
    GT_variable_costs = csvread (path + 'GT variable M&O costs basemodel with equations.csv', {'numeric' = true});
    operating_year = csvread (path + 'operating year.csv', {'numeric' = true,'table' = false});

    WT_AEG = [ 0, 13680774, 13680774,13680774,13680774,13680774,13680774,13680774,13680774,13680774,13680774,13680774,13680774,13680774,13680774,13680774,13680774,13680774,13680774,13680774,13680774,13680774,13680774,13680774,13680774,13680774,13680774];
WT_capacity = 4000;
    WT_PPA_price = [ 0, 4, 4.04, 4.0804, 4.1212, 4.16242, 4.20404, 4.24608, 4.28854, 4.33143, 4.37474, 4.41849, 4.46267, 4.5073, 4.55237, 4.5979, 4.64388, 4.69031, 4.73722, 4.78459, 4.83244, 4.88076, 4.92957, 4.97886, 5.02865, 5.07894];        //0.24 cent/kW/h
    WT_total_installed_cost = 5400000;
    WT_net_capital_cost = 6153597;
    WT_total_revenue = [ 0, 547231, 552703, 558230, 563813, 569451, 575145, 580897, 586706, 592573, 598498, 604483, 610528, 616634, 622800, 629028, 635318, 641671, 648088, 654569, 661115, 667726, 674403, 681147, 687959, 694838];     //PPA rvenue = total revenue   //cell No. 28

    GT_AEG = [ 0, 34315114.38, 34315114.38,34315114.38,34315114.38,34315114.38,34315114.38,34315114.38,34315114.38,34315114.38,34315114.38,34315114.38,34315114.38,34315114.38,34315114.38,34315114.38,34315114.38,34315114.38,34315114.38,34315114.38,34315114.38,34315114.38,34315114.38,34315114.38,34315114.38,34315114.38,34315114.38];
GT_capacity = 8600;      //kW net
```

```
GT_PPA_price = [ 0, 5.0000, 5.0500, 5.1005, 5.1515, 5.2030, 5.2551, 5.3076, 5.3607, 5.4143, 5.4684, 5.5231, 5.5783, 5.6341, 5.6905, 5.7474, 5.8048, 5.8629, 5.9215, 5.9807, 6.0405, 6.1010, 6.1620, 6.2236, 6.2858, 6.3487]; // 43.3 * 100 (for transfer from dollar to cent) / 1000 (from MW to kW) =  4.33 c/kWh. THUS, 5 to cover the LCOE.

GT_total_installed_cost =  22095166.97;         //  1727 * ( CEPCI2022 / CEPCI 2018 ) == 1727 * ( 816 / 603.1 ) == 2336.65 * 8600 == 22095166.97 $       //1727$ (NGCC from NETL) * 8600(capacity from Siemens SGT 100 + D-R SST NGCC)

GT_net_capital_cost = 26681075.78;              //  2293 * (CEPCI2022 / CEPCI 2018)  ==  2293 * ( 816 / 603.1 ) ==  3102.45 * 8600 == 26681075.78 $          //2293$ (NGCC from NETL)*8600(capacity from Siemens SGT 100 + D-R SST NGCC)

GT_total_revenue = [0, 1715755.719, 1732913.276, 1750242.409, 1767743.117, 1785415.401, 1803293.576, 1821309.011, 1839530.337, 1857923.238, 1876487.715, 1895258.082, 1914200.025, 1933347.859, 1952701.584, 1972226.884, 1991923.76, 2011860.841, 2031969.498, 2052284.046, 2072804.484, 2093565.128, 2114497.348, 2135635.459, 2156979.46, 2178563.667];    //PPA rvenue = total revenue   //cell No. 28



inflation_rate = 2.4;

a = csvread(cwd()+'/Design TES range.csv', {'skip'=1, 'numeric'=true});
b = csvread(cwd()+'/Design SM range.csv', {'skip'=1, 'numeric'=true});

//
active_case( 'AC SPT' );
//

SPT_capacity = get ('P_ref');


 for (w=0; w<8; w++)
{
        S = b[w][0];
        set ('solarm', S);

   for (y=0; y<7; y++)
```

```
{
        R = a[y][0];
        set ('tshours', R);


        SPT_WT_GT_fixed_costs_1st = 66 * (0.9 * SPT_capacity/(0.9 * SPT_capacity + (WT_capacity/1000))) + 42 * ((WT_capacity/1000)/((0.9 * SPT_capacity) + (WT_capacity/1000))) + 0.076 * ((GT_capacity/1000)/((0.9 * SPT_capacity) + (GT_capacity/1000)));  //3.6 $/MWh is the GT fixed costs (NETL GTCC)

        inflation_per_operating_year[0] = SPT_WT_GT_fixed_costs_1st * ( 1 + inflation_rate/100 + 0/100)^ 1;
        inflation_per_operating_year[1] = SPT_WT_GT_fixed_costs_1st * ( 1 + inflation_rate/100 + 0/100)^ 2;
        inflation_per_operating_year[2] = SPT_WT_GT_fixed_costs_1st * ( 1 + inflation_rate/100 + 0/100)^ 3;
        inflation_per_operating_year[3] = SPT_WT_GT_fixed_costs_1st * ( 1 + inflation_rate/100 + 0/100)^ 4;
        inflation_per_operating_year[4] = SPT_WT_GT_fixed_costs_1st * ( 1 + inflation_rate/100 + 0/100)^ 5;
        inflation_per_operating_year[5] = SPT_WT_GT_fixed_costs_1st * ( 1 + inflation_rate/100 + 0/100)^ 6;
        inflation_per_operating_year[6] = SPT_WT_GT_fixed_costs_1st * ( 1 + inflation_rate/100 + 0/100)^ 7;
        inflation_per_operating_year[7] = SPT_WT_GT_fixed_costs_1st * ( 1 + inflation_rate/100 + 0/100)^ 8;
        inflation_per_operating_year[8] = SPT_WT_GT_fixed_costs_1st * ( 1 + inflation_rate/100 + 0/100)^ 9;
        inflation_per_operating_year[9] = SPT_WT_GT_fixed_costs_1st * ( 1 + inflation_rate/100 + 0/100)^ 10;
        inflation_per_operating_year[10] = SPT_WT_GT_fixed_costs_1st * ( 1 + inflation_rate/100 + 0/100)^ 11;
        inflation_per_operating_year[11] = SPT_WT_GT_fixed_costs_1st * ( 1 + inflation_rate/100 + 0/100)^ 12;
```

```
inflation_per_operating_year[12] = SPT_WT_GT_fixed_costs_1st * ( 1 + inflation_rate/100 +
0/100)^ 13;
inflation_per_operating_year[13] = SPT_WT_GT_fixed_costs_1st * ( 1 + inflation_rate/100 +
0/100)^ 14;
inflation_per_operating_year[14] = SPT_WT_GT_fixed_costs_1st * ( 1 + inflation_rate/100 +
0/100)^ 15;
inflation_per_operating_year[15] = SPT_WT_GT_fixed_costs_1st * ( 1 + inflation_rate/100 +
0/100)^ 16;
inflation_per_operating_year[16] = SPT_WT_GT_fixed_costs_1st * ( 1 + inflation_rate/100 +
0/100)^ 17;
inflation_per_operating_year[17] = SPT_WT_GT_fixed_costs_1st * ( 1 + inflation_rate/100 +
0/100)^ 18;
inflation_per_operating_year[18] = SPT_WT_GT_fixed_costs_1st * ( 1 + inflation_rate/100 +
0/100)^ 19;
inflation_per_operating_year[19] = SPT_WT_GT_fixed_costs_1st * ( 1 + inflation_rate/100 +
0/100)^ 20;
inflation_per_operating_year[20] = SPT_WT_GT_fixed_costs_1st * ( 1 + inflation_rate/100 +
0/100)^ 21;
inflation_per_operating_year[21] = SPT_WT_GT_fixed_costs_1st * ( 1 + inflation_rate/100 +
0/100)^ 22;
inflation_per_operating_year[22] = SPT_WT_GT_fixed_costs_1st * ( 1 + inflation_rate/100 +
0/100)^ 23;
inflation_per_operating_year[23] = SPT_WT_GT_fixed_costs_1st * ( 1 + inflation_rate/100 +
0/100)^ 24;


        for   (i = 0 ; i<26; i++)

                { SPT_WT_GT_fixed_costs = [0,SPT_WT_GT_fixed_costs_1st, inflation_per_operating_year[0],
inflation_per_operating_year[1], inflation_per_operating_year[ 2], inflation_per_operating_year[ 3],
inflation_per_operating_year[4 ], inflation_per_operating_year[5 ], inflation_per_operating_year[ 6],
inflation_per_operating_year[ 7], inflation_per_operating_year[ 8], inflation_per_operating_year[9 ],
inflation_per_operating_year[ 10], inflation_per_operating_year[11 ], inflation_per_operating_year[12 ],
inflation_per_operating_year[13 ], inflation_per_operating_year[ 14], inflation_per_operating_year[15 ],
```

```
inflation_per_operating_year[16 ], inflation_per_operating_year[ 17], inflation_per_operating_year[ 18],
inflation_per_operating_year[19 ], inflation_per_operating_year[20 ], inflation_per_operating_year[ 21],
inflation_per_operating_year[22 ], inflation_per_operating_year[ 23]];


                }

            simulate ();

        SPT_AEG = get ('cf_energy_sales');
        SPT_electricity_from_grid = get ('cf_energy_purchases');
        SPT_PPA_price = get ('cf_ppa_price');              //14 cent/kW/h (price of electricity production in Kuwait)
        SPT_net_capital_cost = get('cost_installed');
        SPT_total_installed_cost = get('cost_prefinancing');
        SPT_total_revenue = get ('cf_total_revenue');        //PPA rvenue = total revenue
        Nominal_discount_rate = get ('nominal_discount_rate');
        Real_discount_rate = get ('real_discount_rate');
        SPT_debt_closing_cost = get ('cost_debt_closing');
        N_heliostats = get('N_hel');


        capacity = WT_capacity + GT_capacity + (0.9 * SPT_capacity * 1000);   //kW capacity
        MW_capacity = capacity / 1000;
        insurance_rate = 0.5;
        net_capital_cost = SPT_net_capital_cost + WT_net_capital_cost + GT_net_capital_cost;
        total_installed_cost = SPT_total_installed_cost + WT_total_installed_cost + GT_total_installed_cost;
        size_of_debt = 0.5 * net_capital_cost;                          //only for 50% debt percent
        term_interest_rate = 4;

        //

        for  (i = 0 ; i<26; i++)

        {
```

```
SPT_WT_GT_AEG [i] = WT_AEG[i] + SPT_AEG[i] + GT_AEG[i];

OM_production_based_expenses[i] = (SPT_variable_costs[i][0] * SPT_AEG[i]/1000) + (GT_variable_costs[i][0] * GT_AEG[i]/1000);  // Generation AC/MWh

OM_capacity_based_expenses[i] = capacity * SPT_WT_GT_fixed_costs[i];

PPA_price [i] = (SPT_PPA_price[i]*((0.9*SPT_capacity)/MW_capacity)) + (WT_PPA_price[i]*((WT_capacity/1000)/MW_capacity)) + (GT_PPA_price[i]*((GT_capacity/1000)/MW_capacity));
electricity_purchase_price [i] = - SPT_electricity_from_grid [i] * (PPA_price [i]/100);  //only SPT gets electricity from the grid

for (j =0; j<25; j++)

  {

insurance[0] = 0;
insurance[j+1] = total_installed_cost * insurance_rate /100 * (1 + inflation_rate/100) ^ ((operating_year[0][j])-1);  // cell No. 61

 total_used_fuel = 1190;  //(kg/hr from Aspen STG100 NGCC mode)
 Annual_fuel_usage = total_used_fuel * 0.0447 * 8760 * 0.85;  // (MMBTU/y) A typical value for natural gas is 44,700 BTU/kg, which means 1 Kilogram = 0.0447 MMBTU (online)
 methane_calorific_value = 50;  //from online (50-55 MJ/kg)
 fuel_cost_escalation = 1;
 fuel_cost = 4.42;  // $/MMBTU (from NETL report fro NGCC)

 GT_input_energy_MJ = total_used_fuel * methane_calorific_value;  //MJ/hr = kg/h * MJ/kg

 GT_input_energy = GT_input_energy_MJ * 947.82;  //transfer from MJ/h to BTU/h

 GT_heat_rate_BTU = GT_input_energy / (5354 + 2244);  //BTU/kWh = (BTU/hr) / kW  // (5354 + 2244) ==> hourly output in kW from Aspen model
```

```
GT_heat_rate_MMBTU = GT_heat_rate_BTU / 1000000;

//GT_heat_rate = GT_heat_rate_BTU * 0.000293;                    // BTU/kWH == 1055 J / kWh == 1055 J / 3600 kJ/h * h == 1055 J / 3600 kJ == 1055 J / 3600 * 1000 J == 0.000293
Annual_fuel_usage = (GT_input_energy * 8760 ) / 1000000;

Fuel[0] = 0;
//Fuel[j+1] = fuel_cost * GT_AEG [1] * GT_heat_rate_MMBTU * (1 + fuel_cost_escalation / 100 + inflation_rate / 100) ^ ((operating_year[0][j])-1);          //modified equation based on unit analysis (fuel $/year)
//Fuel[j+1] = (fuel_cost * Annual_fuel_usage/1000) * GT_heat_rate * (1 + fuel_cost_escalation / 100 + inflation_rate / 100) ^ ((operating_year[0][j])-1);          //equation from SAM
Fuel[j+1] = fuel_cost * Annual_fuel_usage * (1 + fuel_cost_escalation / 100 + inflation_rate / 100) ^ ((operating_year[0][j])-1);          // suugested from Stavros


}

total_expenses[i] = insurance[i] + electricity_purchase_price[i] + OM_production_based_expenses[i] + OM_capacity_based_expenses[i] + Fuel[i];          //cell No. 62

total_revenue [i] = (SPT_WT_GT_AEG [i]/100) * PPA_price [i];
//cell No. 28
EBITDA[i] = total_revenue[i] - total_expenses[i];                    //cell NO. 64

}

for  (i = 0 ;i<25 ; i++)

{
months_working_reserve = 6;                    //input to reserves page in SAM
working_capital_reserve_ending_balance [25] = 0;                    //cell No. 609
working_capital_reserve_ending_balance [i] = total_expenses[i+1] * months_working_reserve/12;
```

```
working_capital_reserve_beginning_balance [0] = 0;
working_capital_reserve_beginning_balance [i+1] = working_capital_reserve_ending_balance [i];
}


term_tenor = 18;

for (i=0; i<26; i++)

{

PMT =   12  *  (size_of_debt  *((term_interest_rate/100)/12))  /  (1  -  (1+(term_interest_rate/100)/12)^(-
term_tenor*12)) ;

PMT_arr                                                                                          =
[0,PMT,PMT,PMT,PMT,PMT,PMT,PMT,PMT,PMT,PMT,PMT,PMT,PMT,PMT,PMT,PMT,PMT,PMT,0,0,0,0,0,0,0];

}

debt_ending_balance[0] = size_of_debt;
debt_principal_payement[0] = 0;
debt_interest_payement[0] = 0;

debt_interest_payement[1] = debt_ending_balance[0] * term_interest_rate / 100;

debt_principal_payement[1] = PMT_arr [1] - debt_interest_payement[1];

debt_ending_balance[1] = debt_ending_balance[0] - debt_principal_payement[1];

//

debt_interest_payement[2] = debt_ending_balance[1] * term_interest_rate / 100;

debt_principal_payement[2] = PMT_arr [2] - debt_interest_payement[2];
```

```
debt_ending_balance[2] = debt_ending_balance[1] - debt_principal_payement[2];

//

debt_interest_payement[3] = debt_ending_balance[2] * term_interest_rate / 100;

debt_principal_payement[3] = PMT_arr [3] - debt_interest_payement[3];

debt_ending_balance[3] = debt_ending_balance[2] - debt_principal_payement[3];
 //

debt_interest_payement[4] = debt_ending_balance[3] * term_interest_rate / 100;

debt_principal_payement[4] = PMT_arr [4] - debt_interest_payement[4];

debt_ending_balance[4] = debt_ending_balance[3] - debt_principal_payement[4];
 //

debt_interest_payement[5] = debt_ending_balance[4] * term_interest_rate / 100;

debt_principal_payement[5] = PMT_arr [5] - debt_interest_payement[5];

debt_ending_balance[5] = debt_ending_balance[4] - debt_principal_payement[5];

//

debt_interest_payement[6] = debt_ending_balance[5] * term_interest_rate / 100;

debt_principal_payement[6] = PMT_arr [6] - debt_interest_payement[6];

debt_ending_balance[6] = debt_ending_balance[5] - debt_principal_payement[6];

//
```

```
debt_interest_payement[7] = debt_ending_balance[6] * term_interest_rate / 100;

debt_principal_payement[7] = PMT_arr [7] - debt_interest_payement[7];

debt_ending_balance[7] = debt_ending_balance[6] - debt_principal_payement[7];

//

debt_interest_payement[8] = debt_ending_balance[7] * term_interest_rate / 100;

debt_principal_payement[8] = PMT_arr [8] - debt_interest_payement[8];

debt_ending_balance[8] = debt_ending_balance[7] - debt_principal_payement[8];

 //
debt_interest_payement[9] = debt_ending_balance[8] * term_interest_rate / 100;

debt_principal_payement[9] = PMT_arr [9] - debt_interest_payement[9];

debt_ending_balance[9] = debt_ending_balance[8] - debt_principal_payement[9];

 //
debt_interest_payement[10] = debt_ending_balance[9] * term_interest_rate / 100;

debt_principal_payement[10] = PMT_arr [10] - debt_interest_payement[10];

debt_ending_balance[10] = debt_ending_balance[9] - debt_principal_payement[10];

 //
debt_interest_payement[11] = debt_ending_balance[10] * term_interest_rate / 100;

debt_principal_payement[11] = PMT_arr [11] - debt_interest_payement[11];
```

```
debt_ending_balance[11] = debt_ending_balance[10] - debt_principal_payement[11];

//
debt_interest_payement[12] = debt_ending_balance[11] * term_interest_rate / 100;

debt_principal_payement[12] = PMT_arr [12] - debt_interest_payement[12];

debt_ending_balance[12] = debt_ending_balance[11] - debt_principal_payement[12];

//
debt_interest_payement[13] = debt_ending_balance[12] * term_interest_rate / 100;

debt_principal_payement[13] = PMT_arr [13] - debt_interest_payement[13];

debt_ending_balance[13] = debt_ending_balance[12] - debt_principal_payement[13];

//
debt_interest_payement[14] = debt_ending_balance[13] * term_interest_rate / 100;

debt_principal_payement[14] = PMT_arr [14] - debt_interest_payement[14];

debt_ending_balance[14] = debt_ending_balance[13] - debt_principal_payement[14];

//
debt_interest_payement[15] = debt_ending_balance[14] * term_interest_rate / 100;

debt_principal_payement[15] = PMT_arr [15] - debt_interest_payement[15];

debt_ending_balance[15] = debt_ending_balance[14] - debt_principal_payement[15];

//
debt_interest_payement[16] = debt_ending_balance[15] * term_interest_rate / 100;

debt_principal_payement[16] = PMT_arr [16] - debt_interest_payement[16];
```

```
debt_ending_balance[16] = debt_ending_balance[15] - debt_principal_payement[16];

 //
debt_interest_payement[17] = debt_ending_balance[16] * term_interest_rate / 100;

debt_principal_payement[17] = PMT_arr [17] - debt_interest_payement[17];

debt_ending_balance[17] = debt_ending_balance[16] - debt_principal_payement[17];

 //
debt_interest_payement[18] = debt_ending_balance[17] * term_interest_rate / 100;

debt_principal_payement[18] = PMT_arr [18] - debt_interest_payement[18];

debt_ending_balance[18] = debt_ending_balance[17] - debt_principal_payement[18];

 //
debt_interest_payement[19] = 0;
debt_principal_payement[19] = 0;
debt_ending_balance[19] = 0;

//
debt_interest_payement[20] = 0;
debt_principal_payement[20] = 0;
debt_ending_balance[20] = 0;

//
debt_interest_payement[21] = 0;
debt_principal_payement[21] = 0;
debt_ending_balance[21] = 0;

//
debt_interest_payement[22] = 0;
```

```
debt_principal_payement[22] = 0;
debt_ending_balance[22] = 0;

//
debt_interest_payement[23] = 0;
debt_principal_payement[23] = 0;
debt_ending_balance[23] = 0;

//
debt_interest_payement[24] = 0;
debt_principal_payement[24] = 0;
debt_ending_balance[24] = 0;
//
debt_interest_payement[25] = 0;
debt_principal_payement[25] = 0;
debt_ending_balance[25] = 0;



for  (i = 0 ;i<26 ; i++)

{

DSR = (debt_interest_payement [1] + debt_principal_payement [1]) / 2;      //over 2 becasue only 6 months of the year (SAM inputs)

debt_service_reserve_ending_balance = [DSR,DSR,DSR,DSR,DSR,DSR,DSR,DSR,DSR,DSR,DSR,DSR,DSR,DSR,DSR,DSR,DSR,DSR,0,0,0,0,0,0,0,0];
working_capital_reserve_release_of_funds = [0,0,0,0,0,0,0,0,0,0,0,0,0,0,0,0,0,0,0,0,0,0,0,0,0, -working_capital_reserve_beginning_balance [25]];      //cell No. 608

}

for  (i = 0 ;i<26 ; i++)
```

```
{

working_capital_reserve_funding [i] = working_capital_reserve_ending_balance [i] - working_capital_reserve_beginning_balance [i] - working_capital_reserve_release_of_funds[i];

total_reserve [i] =  working_capital_reserve_ending_balance [i] + debt_service_reserve_ending_balance [i];  //cell No. 714 ==> Cell No. 609

}

for  (i = 0 ;i<25 ; i++)

{
reserve_interest = 1.75 ;
interest_on_reserve [0] = 0;
interest_on_reserve [i+1] = total_reserve[i] * reserve_interest / 100;

}


//state_tax_depreciation [i] = five_yr_MACRS [i] + fifteen_yr_MACRS [i] + fiteen_SL [i] + twenty_SL [i];

for  (i = 0 ;i<26 ; i++)

{

taxable_income_after_benefit_state [i] = EBITDA[i] + interest_on_reserve[i] - debt_interest_payement[i]; //  - state_tax_depreciation[i];        //cell No. 198-167-168

state_tax_rate = 0;
state_tax_benefit[i] = (taxable_income_after_benefit_state[i] * state_tax_rate/100);

federal_tax_rate = 17;
```

```
taxable_income_after_benefit_federal[i] = EBITDA[i] + interest_on_reserve[i] - debt_interest_payement[i] - state_tax_benefit[i];    // - federal_tax_depreciation[i]

federal_tax_benefit[i] = taxable_income_after_benefit_federal[i] * (federal_tax_rate/100);            //cell No. 240

total_debt_closing_cost = SPT_debt_closing_cost;              // + WT_debt_closing_cost; only one of them in the combined case by generic system
debt_upfront_fee = size_of_debt * 2.75/100;
total_purchase_of_property = total_installed_cost + total_debt_closing_cost + debt_upfront_fee; //cell No. 88


//five_yr_MACRS = 90;                                                    //SAM inputs
//ITC_qualifying_cost [i] = - total_cash_from_investing_activities [i] * five_yr_MACRS / 100;          //cell No. I+K 389

//itc_fed_percent = 0;                                                   //cell No. H382 (SPT 22%)
// federal_investment_tax_credit = itc_fed_percent / 100 * ITC_qualifying_cost[0];              //cell No. G 382
//                                  federal_investment_tax_credit_arr                                  = [0,federal_investment_tax_credit,0,0,0,0,0,0,0,0,0,0,0,0,0,0,0,0,0,0,0,0,0,0,0];          //cell No 128


debt_service_reserve_funding = [ DSR,0,0,0,0,0,0,0,0,0,0,0,0,0,0,0,0,0,0,0,0,0,0,0,0];
debt_service_reserve_release_of_funds      =      [0,0,0,0,0,0,0,0,0,0,0,0,0,0,0,0,0,0,0,0,-DSR,0,0,0,0,0,0,0]; //year 18 (SAM inputs)

}

for  (i = 0 ;i<25 ; i++)

{
```

```
        Annual_costs[i] = state_tax_benefit[i+1] + federal_tax_benefit[i+1] - total_expenses[i+1] - working_capital_reserve_funding[i+1] - working_capital_reserve_release_of_funds [i+1] - debt_service_reserve_funding [i+1] - debt_service_reserve_release_of_funds [i+1] - debt_interest_payement[i+1] - debt_principal_payement[i+1] + interest_on_reserve [i+1];                //+ federal_investment_tax_credit_arr[i]//debt_interest_payment + debt_pricipal_payment          //cell No. C200 + C240 - C62 + C124 - C607

        issuance_of_equity = total_purchase_of_property + working_capital_reserve_ending_balance[0] + DSR - size_of_debt;

   NPV_Annual_costs [i] = ((Annual_costs[i]) / ((1 + Nominal_discount_rate)^i)) ;

        NPV_AEG [i] = ((SPT_WT_GT_AEG[i+1]) / ((1 + (Real_discount_rate/100))^i)) ;

        Calc_LCOE = -( (- issuance_of_equity + sum(NPV_Annual_costs)) / (sum(NPV_AEG))) * 100;

   }

   NPV = sum(NPV_Annual_costs);
   SPT_Water_Use = get ('annual_total_water_use');
   SPT_GT_Water_Use = SPT_Water_Use + 1.30991e+06;          //from the 100 SGT + D-R SST model in Aspen

   Capacity_factor = ( SPT_WT_GT_AEG[1] / (8760*(capacity))) * 100;

        CAPACITY = get ('P_ref');
   // outln('CAPACITY');

   TES = get ('tshours');
   //outln('TES');

   SM = get ('solarm');
   //outln('SM');
```

```
        //outln('LCOE');
outln(Calc_LCOE);


//outln('AEG');
outln(SPT_WT_GT_AEG[1]);


//outln(Capacity_factor);

//outln('Water_Use');
outln(SPT_GT_Water_Use);


//outln('Net capital costs');
//outln(net_capital_cost);


//outln('Number of heliostats');
//outln(N_heliostats);


        //area = get('csp.pt.sf.total_land_area');
        //outln(area);

    }
        }
```

Appendix Q - Surrogate Model Main Function Algorithm (Matlab)

```
clear all;clc;

table = xlsread('all scenarios.xlsx','sheet1');    %prior to interpolation

WT = table(:,1);
GT = table(:,2);
CAP = table(:,3);
TES = table(:,4);
SM = table(:,5);
LCOE = table(:,6);
AEG = table(:,7);
WC = table(:,8);
CF = table(:,9);
AREA = table(:,10);

[U,W,X,Y,Z] = ndgrid (0:2:6, 0:1:3, 40:10:110, 0:3:18, 1:0.4:3.8);

XI = [U(:) W(:) X(:) Y(:) Z(:)];
YI = [WT(:) GT(:) CAP(:) TES(:) SM(:)];

%%                                                                  Leveliezed
Cost of Energy
Vq_LCOE = griddatan(YI,LCOE,XI,"linear");

[U1,W1,X1,Y1,Z1] = ndgrid (0:1:6, 1:1:3, 50:5:100, 0:1:18, 1:0.4:3.8);

XII = [U1(:) W1(:) X1(:) Y1(:) Z1(:)];

Vq1_LCOE = reshape(Vq_LCOE, size(U));
Vq2_LCOE = griddatan(YI, LCOE, XII, "linear");
Vq3_LCOE = reshape(Vq2_LCOE, size(U1));

global G Gf
G = griddedInterpolant(U,W,X,Y,Z,Vq1_LCOE, 'linear','none');
Gf = griddedInterpolant(U1, W1, X1, Y1, Z1, Vq3_LCOE, 'linear','none');

%%                                                                  Annual
Energy Generation
Vq_AEG = griddatan(YI,AEG,XI,"linear");

Vq1_AEG = reshape(Vq_AEG, size(U));
Vq2_AEG = griddatan(YI, AEG, XII, "linear");
Vq3_AEG = reshape(Vq2_AEG, size(U1));

global G1 Gf1
G1 = griddedInterpolant(U,W,X,Y,Z,Vq1_AEG, 'linear','none');
Gf1 = griddedInterpolant(U1, W1, X1, Y1, Z1, Vq3_AEG, 'linear','none');

%%                                                                  Carbon
Emissions
table = xlsread('SPT + WT + GT results.xlsx','gridded interpolant');
CO = table(:,27);
```

```
Vq_CO = griddatan(XII,CO,XII,"linear");

Vq1_CO = reshape(Vq_CO, size(U1));
% Vq2_CO = griddatan(XII, CO, XII, "linear");
% Vq3_CO = reshape(Vq2_CO, size(U1));

global Gf2
% G2 = griddedInterpolant(U,W,X,Y,Z,Vq1_CO, 'linear','none');
Gf2 = griddedInterpolant(U1, W1, X1, Y1, Z1, Vq1_CO, 'linear','none');

% Gf2 = Vq1_CO;

%%                                                                  Capacity
Factor
Vq_CF = griddatan(YI,CF,XI,"linear");

Vq1_CF = reshape(Vq_CF, size(U));
Vq2_CF = griddatan(YI, CF, XII, "linear");
Vq3_CF = reshape(Vq2_CF, size(U1));

global G3 Gf3
G3 = griddedInterpolant(U,W,X,Y,Z,Vq1_CF, 'linear','none');
Gf3 = griddedInterpolant(U1, W1, X1, Y1, Z1, Vq3_CF, 'linear','none');

%%                                                                  Water
Consumption
Vq_WC = griddatan(YI,WC,XI,"linear");

Vq1_WC = reshape(Vq_WC, size(U));
Vq2_WC = griddatan(YI, WC, XII, "linear");
Vq3_WC = reshape(Vq2_WC, size(U1));

global G4 Gf4
G4 = griddedInterpolant(U,W,X,Y,Z,Vq1_WC, 'linear','none');
Gf4 = griddedInterpolant(U1, W1, X1, Y1, Z1, Vq3_WC, 'linear','none');

%%                                                                  AREA
% Vq_AREA = griddatan(YI,AREA,XI,"linear");
%
% Vq1_AREA = reshape(Vq_AREA, size(U));
% Vq2_AREA = griddatan(YI, AREA, XII, "linear");
% Vq3_AREA = reshape(Vq2_AREA, size(U1));
%
% global G4 Gf4
% G4 = griddedInterpolant(U,W,X,Y,Z,Vq1_AREA, 'linear','none');
% Gf4 = griddedInterpolant(U1, W1, X1, Y1, Z1, Vq3_AREA, 'linear','none');
```

Appendix R - Surrogate Model Multi-Objective Functions Algorithm (Matlab)

```
function Output = GA_objective_function(Input)

U1 = Input(1);
W1 = Input(2);
X1 = Input(3);
Y1 = Input(4);
Z1 = Input(5);

WTi  = [0:1:6]';
GTi  = [1:1:3]';
CAPi = [40:5:110]';
TESi = [0:1:18]';
SMi  = [1:0.4:3.8]';


%%

global Gf
LCOE_q  =   Gf([WTi(U1) GTi(W1) CAPi(X1) TESi(Y1) SMi(Z1)]);

%%

% global Gf1
% AEG_q   = - Gf1([WTi(U1) GTi(W1) CAPi(X1) TESi(Y1) SMi(Z1)]);

%%

global Gf2
CO_q    =   Gf2([WTi(U1) GTi(W1) CAPi(X1) TESi(Y1) SMi(Z1)]);

%%

global Gf3
CF_q    = - Gf3([WTi(U1) GTi(W1) CAPi(X1) TESi(Y1) SMi(Z1)]);

%%
global Gf4
WC_q  =  Gf4([WTi(U1) GTi(W1) CAPi(X1) TESi(Y1) SMi(Z1)]);

%%
% global Gf5
% AREA_q  =  Gf4([WTi(U1) GTi(W1) CAPi(X1) TESi(Y1) SMi(Z1)]);

%%

Output   = [LCOE_q WC_q CO_q CF_q];

end
```

Appendix S - GA Algorithm (Matlab)

```
Var_N = 5;
LB = [1 1 1 1 1];
UB = [7 3 12 19 8];

intg=[1 2 3 4 5];

% Set nondefault solver options
options5 = optimoptions("gamultiobj","PopulationSize",200,"CrossoverFcn",...
    "crossoverintermediate","MaxGenerations",1000,"ParetoFraction",0.5,...
    "HybridFcn","fgoalattain","Display","iter","PlotFcn","gaplotpareto");

% Solve
[solution,objectiveValue] = gamultiobj(@GA_objective_function,Var_N,[],[],[],...
    [],LB,UB,@constraintFcn,intg,options5);

solution
objectiveValue

LCOE = objectiveValue(:,1);
Water_Consumption = objectiveValue(:,2);
Carbon_Emission = objectiveValue(:,3);
Capacity_Factor = - objectiveValue(:,4);

scatter3(LCOE,Water_Consumption,Capacity_Factor,35,Carbon_Emission,'filled')
grid on
hold on

%xlim([8 16])
ylim([0 1*10^5])
%zlim([0 80])

xlabel('LCOE (c/kWh)')
ylabel('Water Consumption (m^3)')
zlabel('CF (%)')
hold on

cb = colorbar;
cb.Label.String = ('Carbon Emissions (kg CO_2 / kWh)');

%water consumption in color map (mini = 0, max = 1872399), color map type = turbo.
```

Appendix T - Manuscript Revision Certificate

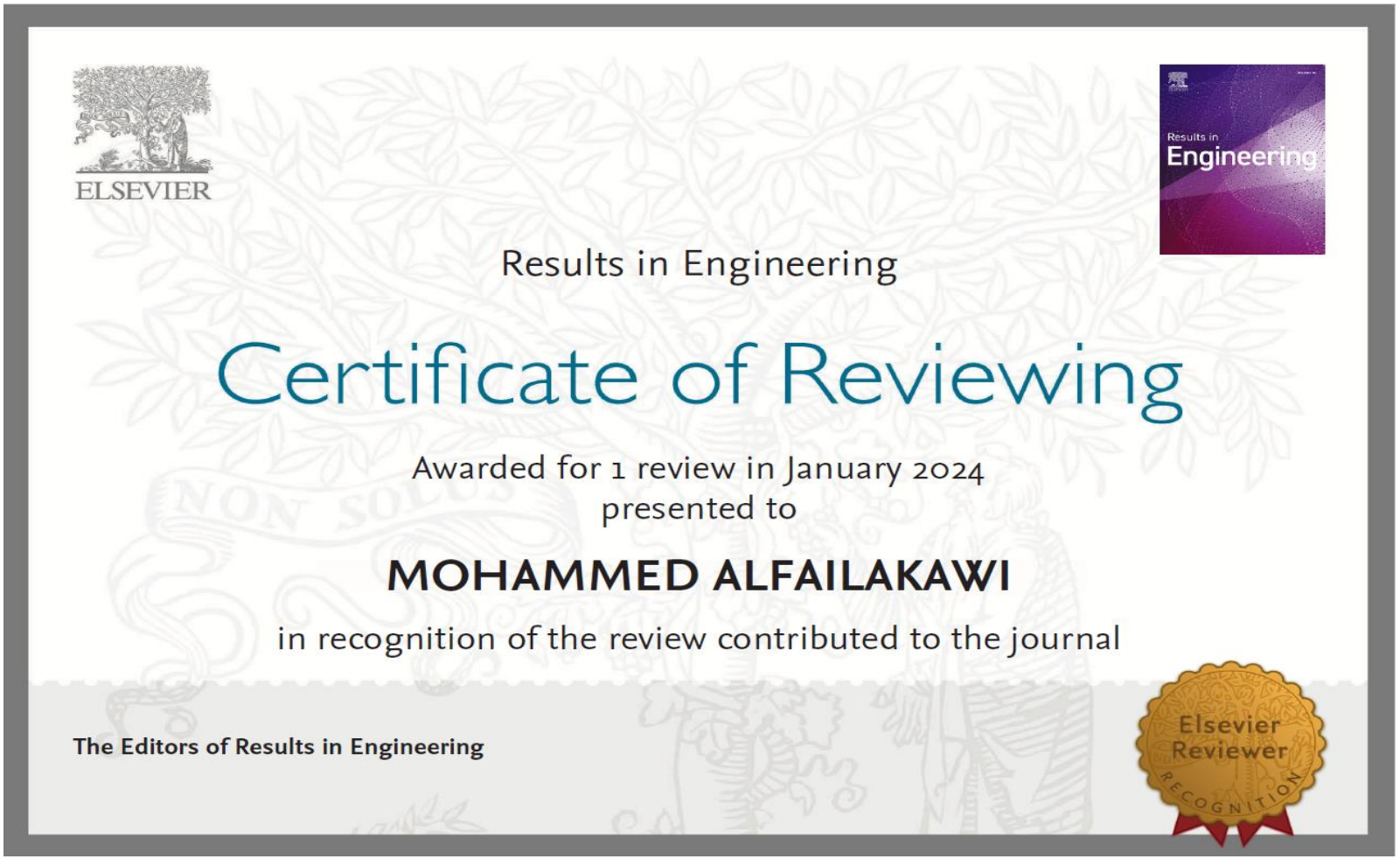

Fig. T.1. Certificate of reviewing of a manuscripts submitted at ''Results in Engineering'' journal.

Appendix U - Conference Committee Recommendation

University of Sheffield

Mohammed Alfailakawi <malfailakawi2@sheffield.ac.uk>

ICAE2022: Recommendation to the special issue of ICAE2022

1 message

14th International Conference on Applied Energy (ICAE2022) <noreply@xcdsystem.com>
Reply-To: icae2022@applied-energy.org
To: Malfailakawi2@sheffield.ac.uk, moha.slman@gmail.com

13 September 2022 at 20:24

Dear Mohammed Alfailakawi,

Based on the evaluations of the session chairs and the scientific committee of ICAE2022, we are pleased to inform you that your paper:

83: Performance improvement of aerosols impacted concentrated solar power in arid regions: Case study of solar power tower hybridization with wind turbines in Kuwait

presented at the 14th International Conference on Applied Energy, (ICAE2022), Aug 8-11, 2022 has been selected for the further consideration in Applied Energy and Advances in Applied Energy.

The submission will be open from Nov 1, 2022 and the DEADLINE for the submission to the Special Issue is May 31, 2023. You are free to choose the target journal, but we may transfer your paper depending on, for example, the scope and other plans. Please pay attention to the DEADLINE and carefully check the following issues when preparing your manuscript:

(1) Prepare the full paper following the Guide for Authors (APEN: https://www.elsevier.com/journals/applied-energy/0306-2619/guide-for-authors; ADAPEN: https://www.elsevier.com/journals/advances-in-applied-energy/2666-7924/guide-for-authors). The template of ICAE2022 shall NOT be used anymore.

(2) Carefully address originality and the relevance to applied energy issues. You are suggested to read previous published papers in Applied Energy and Advances in Applied Energy to understand the readership and scope of the journals. A proof reading by a native English speaker is suggested.

(3) Please clearly indicate your paper ID in the cover letter and mention that this paper is recommended to the SI:ICAE2022. Your submission will be returned to you if this is NOT added.

(4) A footnote should be added in the manuscript, indicating "The short version of the paper was presented at ICAE2022, Bochum, Germany, Aug 8-11, 2022. This paper is a substantial extension of the short version of the conference paper."

(5) To avoid the potential conflict in indexing system, a modified title and significant extension (**adding at least 50%**) of the text and content shall be conducted based on the conference paper.

(6) The final decision of the acceptance/rejection of the manuscript will be decided by Applied Energy and Advances in Applied Energy after review organized by the Journal.

(7) Please choose VSI:ICAE2022 when you submit your paper at https://www.editorialmanager.com/APEN/default.aspx and https://www.editorialmanager.com/adapen/default1.aspx

If you have any question, please contact us at icae2022@applied-energy.org.

Sincerely,

Prof J. Yan and Prof R. Span

Conference Chair of ICAE2022

Fig. U.1. The 14th ICAE recommendation for further journal publication at Applied Energy and Advances in Applied Energy.